Dissertation ETH Nr.17177

Synthesis, PGSE Diffusion and Multidimensional NMR Studies on Transition Metal Organometallic Species: Applications in Coordination Chemistry and Homogeneous Catalysis

A Dissertation submitted to the

SWISS FEDERAL INSTITUTE OF TECHNOLOGY ZURICH

For the degree of

Doctor of Sciences

Presented by

Devendra Babu Nama

M.Sc., Bangalore University, India

Born October 05th 1977

Citizen of India

Accepted on the recommendation of

Prof. Dr. P. S. Pregosin, Examiner

Prof. Dr. W. H. Koppenol, Co-examiner

Zurich, 2007

Acknowledgements

First and foremost I offer my sincerest gratitude to my supervisor, Professor Paul S. Pregosin, for guiding and supporting me throughout my PhD time with his fruitful discussions, patience and knowledge.

I am also grateful to Dr. Heinz Rügger, for sharing with me his wealth of knowledge in NMR and Chemistry.

Professor Dr. Willem H. Koppenol for having accepted to be my co-examiner.

Professors Mike Whittlessey, Alberto Albinati, Paul J Dyson, L F Veiros, M J Calhorda and their coworkers for their worthwhile and interesting collaborations.

A special thanks to Pietro Butti and Professor Frank Breher for X-ray structure determination.

I would like to thank my Indian professors Prof. N. M. Nange Gowda, Prof. K. V. Ramanathan and Prof. N. Suryaprakash for their encouragement and kind help.

I thank all my present and former lab colleagues: Anil, Nacho, Daniele, Rene, Serena, Helen, Stefan, Alexey, Aitor and Nicole (PSP secretary) for their kind help and for maintaining a lively working atmosphere.

To all my Indian friends, specifically, Ravi, Sai, Jagan, Shiva, Vishwa, Trishool, Srinivas, Shravan, and all InSaz memebrs who made my stay so enjoyable.

To all members of the Institute of Inorganic Chemistry at ETH who made a comfortable and pleasant working atmosphere.

Finally, and most importantly, I wish to thank my family and friends, particularly my parents Rajamma and Janardhana Chetty. They raised me, supported me, taught me, and loved me. To them I dedicate this thesis.

Publications

^{195}Pt, ^{1}H and ^{31}P PGSE diffusion studies on platinum complexes. Nama, D; Kumar, P. G. A; Pregosin, P S. Magnetic Resonance in Chemistry (**2005**), 43(3), 246-250.

^{1}H, ^{19}F-HOESY and PGSE diffusion studies on ionic liquids: The effect of co-solvent on structure.
Nama, D; Kumar, P. G. A; Pregosin, P S.; Geldbach, T J.; Dyson, P J. Inorganica Chimica Acta (**2006**), 359(6), 1907-1911.

Cationic Tris N-Heterocyclic Carbene Rhodium Carbonyl Complexes: Molecular Structures and Solution NMR Studies.
Burling, S; Douglas, S; Mahon, M F.; Nama, D; Pregosin, P S.; Whittlesey, M K. Organometallics (**2006**), 25(10), 2642-2648.

Diffusion and Overhauser NMR studies on dicationic palladium complexes of BINAP.
Nama, D; Schott, D; Pregosin, P S.; Veiros, L. F.; Calhorda, M. J. Organometallics (**2006**), 25(19), 4596-4604.

C-H Activation Reactions of Ruthenium N-Heterocyclic Carbene Complexes: Application in a Catalytic Tandem Reaction Involving C-C Bond Formation from Alcohols.
Burling, S; Paine, B M.; Nama, D; Brown, V S.; Mahon, M F.; Prior, T J.; Pregosin, P S.; Whittlesey, M K.; Williams, J M. J. Journal of the American Chemical Society (**2007**), 129, 1987.

Synthesis, X-ray, and NMR Studies on Palladium BINAP Complexes Containing Oxazolidinone and Acetylacetone Anions.
Nama, D; Pregosin, P S.; Albinati, A.; Rizzato, S. Veiros, L. F. Organometallics (**2007**), 26, 2111.

Synthesis and Reactivity of $Ru(PPh_3)_3(CO)HF$ and the N-Heterocyclic Carbene Derivatives $Ru(NHC)(PPh_3)_3(CO)HF$
Reade, S P.; Nama, D; Mohan, M F.; Pregosin, P S; Whittlesey, M K. Organometallics (**2007**), 26, 3484.

Conformational Changes and Anion-Cation interactions in Pd-Cyclometallated BINAP and Chiraphos Cationic complexes. A Structural Study via NMR and X-ray Methods.
Nama, D; Butti, P; Pregosin, P S. (**2007**), Submitted.

List of Abbreviations

BINAP	2,2'-bis(diphenylphosphino)-1,1'-binaphthyl
BF_4^-	tetrafluoroborate
BINPHAT	bis(tetrachlorobenzenediolato)mono([1,1′] binaphthalenyl-2,2′ diolato)-phosphate(V)
BArF$^-$ or BAr^{F-}	tetrakis(3,5-bis(trifluoromethyl)phenyl)borate
CF_3SO_3-	trifluoromethanesulfonate
Chiraphos	butane-2,3-diylbis(diphenylphosphine)
COSY	Correlation Spectroscopy
Cy	Cyclohexane
DOSY	Diffusion-ordered spectroscopy
DMSO	Dimethyl Sulfoxide
DFT	Density Functional theory
DNMR	Dynamic Nuclear Magnetic Resonance
HMBC	Heteronuclear Multiple Bond Coherence
HMQC	Heteronuclear Multiple Quantum Coherence
HOESY	Heteronuclear Overhauser Spectroscopy
ICy	1,3-bis(cyclohexnyl)imidazol-2-ylidene
IMes	1,3-bis(2,4,6-trimethylphenyl)imidazole-2-ylidene
I^{t}Bu	1,3-bis(*tert*-butyl)imidazol-2-ylidene
IEt_2Me_2	1,3-bis(ethyl)-4,5-dimethylimidazol-2-ylidene
IPr_2Me_2	1,3-bis-isopropyl-4,5-dimethlyimidazol-2-ylidene
i-Pr	iso-propyl
LED	Longitudinal eddy-current delay
NHC	N-heterocyclic carbene
NMR	Nuclear Magnetic Resonance
NOESY	Nuclear Overhauser Spectroscopy
NPA	Natural Population Analysis
ORTEP	Oak Ridge Thermal Ellipsoid Plot
Oxazolidinone	(E)-3-but-2-enoyloxazolidin-2-one
PF_6^-	hexafluorophosphate(V)

PGSE	Pulsed Gradient Spin Echo
picoline	methylpyridine
ROESY	Rotational Overhauser Spectroscopy
TRISPHAT	tris(tetrachlorobenzenediolato)phosphate(V)
THF	Tetrahydrofuran
TMVS	trimethyl vinylsilane

Contents

Summary

The applications of Pulsed Gradient Spin Echo (PGSE) diffusion, exchange and multidimensional NMR techniques to the study of organometallic complexes relevant to coordination and homogeneous catalysis are described in this thesis.

Chapter 1 describes the basic principles of NMR spectroscopy, and specifically, PGSE NMR and its applications to organometallic/ coordination chemistry.

Chapter 2 focuses on diffusion studies on a modest number of mono and dicationic Pd(II) complexes and neutral Pt(II) complexes, plus ^{195}Pt as a diffusion probe for PGSE diffusion measurements. Thus, studies are related to molecular volumes, solvent and / or anion effects on ion pairing, hydrogen bonding and aggregation effects.

A series of mono-cationic palladium BINAP complexes, [Pd(*rac*-BINAP)(an acetylacetonate anion)][X], (X = **a**, $CF_3SO_3^-$, **b**, BF_4^-), have been synthesized and characterized. These salts are believed to be intermediates in catalytic hydroamination or Michael reaction.

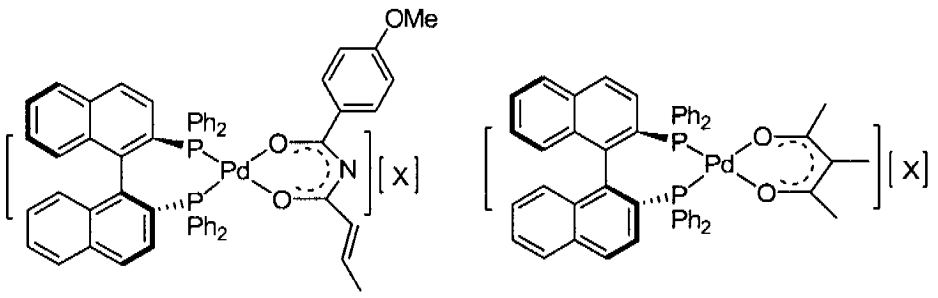

Chapter 3 deals with structure, exchange and dynamics (restricted rotation) of Ru(II) and Rh(I) N-heterocyclic carbene complexes.

The phosphine (PPh_3) exchange and dissociation have been studied via variable temperature and 2D NMR methods. Restricted rotation of the bulky carbene ligand in Ru(II) and Rh(I) carbene complexes is discussed based on line shape and exchange NMR studies.

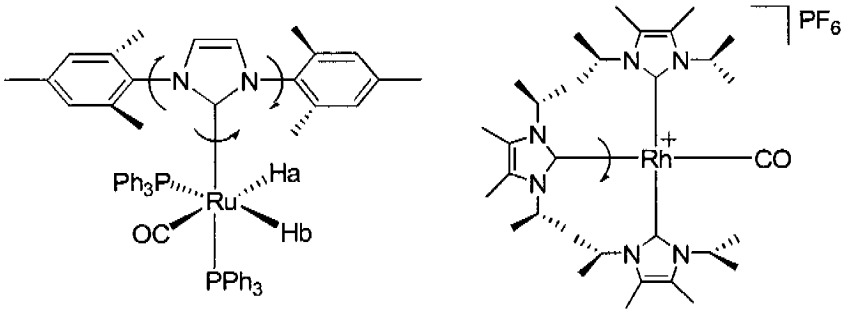

Zusammenfassung

Diese Dissertation beschreibt die Anwendung von Pulsed Gradient Spin Echo (PGSE) Diffusionen, Austausch und multidimensionalen NMR Methoden zur Untersuchung von organometallischen Komplexen in Bezug auf die Koordination und die Anwendung in homogener Katalyse.

Kapitel 1 beschreibt die Grundprinzipien der NMR-Spektroskopie, speziell die PGSE NMR-Methode und ihre Anwendung in der Koordinations-Chemie.

Kapitel 2 betrachtet Diffusionsuntersuchungen einer Anzahl mono- und dikationischer Pd(II)-Komplexe und neutraler Pt(II)-Komplexe, mit ^{195}Pt als Nukleon für die PGSE Diffusionsmessungen. Diese Untersuchungen stehen in Verbindung mit Wasserstoffbindungen, Aggregationseffekten, Lösungsmittel und Ionenpaar-Effekten.

Es wurde eine Serie von mono-kationischen Palladium-BINAP-Komplexen, [Pd(*rac*-BINAP)(Acetylacetonat-Anion)[X], (X = **a**, $CF_3SO_3^-$, **b**, BF_4^-), synthetisiert und charakterisiert. Man glaubt dass diese Salze Intermediate in katalysierten Hydroaminierungen und Michale Reaktionen sind.

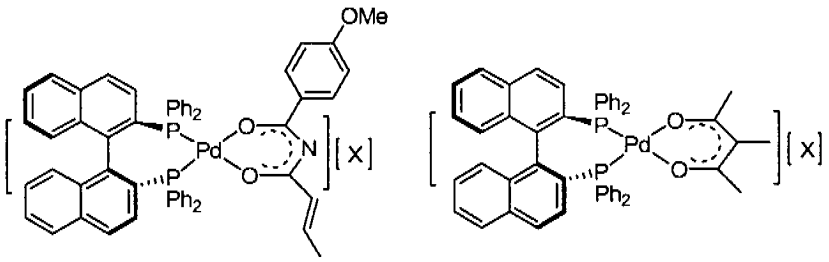

Kapitel 3 handelt von Strukturen, Austausch und dynamischen Prozessen (eingeschränkte Rotationen) von Ru(II) und Rh(I) N-heterocyclischen Carben-Komplexen.

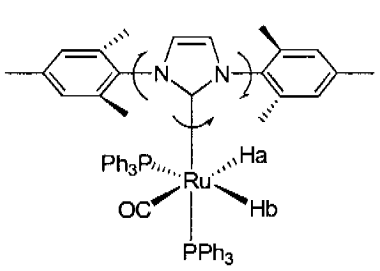

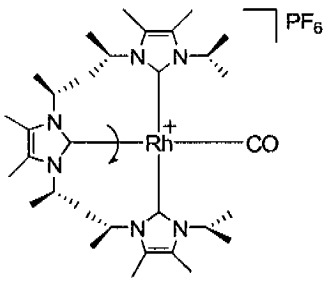

Die Dissoziation und der Austausch von Phosphanen (PPh_3) wurde mit verschiedenen Temperaturen und 2D NMR Methoden untersucht. Auf der Basis von Linienbreiten und NMR-Austausch-Experimenten wurde die eingeschränkte Rotation der sterisch anspruchsvollen Carben-Liganden der Ru(II)- und Rh(I)-Carben-Komplexen diskutiert.

Chapter 1

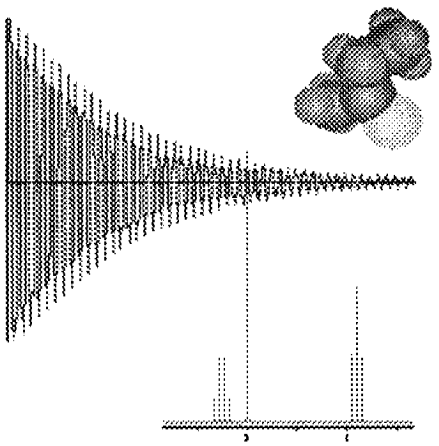

NMR Spectroscopy

1.1 General Introduction to NMR Spectroscopy

Since the first observations of the phenomenon in bulk materials[1, 2], NMR has played a key and rapidly expanding role in chemistry, biochemistry, polymer chemistry and materials research. NMR has become one of the most important techniques for determining organic structure despite its extreme insensitivity (it is the least sensitive of the spectroscopic techniques). Its strengths come from the wealth of chemical shift and spin-spin coupling contained in NMR spectra and the ability to relate these to specific molecular structure and motional features. Given that researchers have had to work with smaller quantities of increasingly complex molecular structures, it appeared that NMR would not keep pace with the requirements of science. However, major developments in methodology, software and hardware have always become available just as it appeared that the chemical and biological challenges were going to exceed the limits of NMR's capabilities.

Continuous developments in the applications of high field superconducting magnet technology have provided further sensitivity gains as well as improvements in the ability to disperse and resolve the spectral detail necessary to analyze complex NMR data. Developments in the electronics industry have also provided reliable, low-noise components that have resulted in sensitivity gains; and have provided fast computers that enhance the ability to work with both large data sets, and to provide software-based image processing methods. The recent availability of commercial cryogenically cooled probes and electronic components is already having a significant impact on the ability to study small quantities of material and promises to greatly expand the utility of NMR methods that have been previously considered too difficult to be broadly applicable[3]. Microprobes also play a key role in improving the

sensitivity of NMR when the applications involve limited sample quantity[4]. Over the past 40 years, these cumulative contributions have resulted in an overall improvement in detection limit of four orders of magnitude.

1.2 NMR in Organometallic Chemistry

NMR (Nuclear Magnetic Resonance) has become the preeminent technique for determining the structure of organic compounds. It is one of the fastest ways to screen reactions and, at the same time, provides insights into molecular structure and solution dynamics. At a more sophisticated level, the analysis of subtle 2- and 3-D measurements resulted in the solution of hundreds of complicated organic and biological structures.

Historically, inorganic co-ordination chemists still rely heavily on X-ray crystallography. This community tends to shy away from 'sporting methods' and some extent, this tradition has been carried forward into organometallic chemistry. Homogeneous catalysis, and particularly enantioselective catalysis, combines fundamental aspects of inorganic transition-metal chemistry with the mature elegance of organic carbon architecture[5, 6]. The former discipline provides the template for bringing the correct pieces together, *via* complexation, and the latter, the necessary chiral frame work, frequently *via* a bidentate ligand auxiliary. Subtle steric effects[7], arising from the interaction of the chiral pocket with the co-ordinated substrate, together with electronic effects[8], induced by different donor atoms, can determine whether a given auxiliary will be successful for any one substrate.

In both principle and practice, NMR spectroscopy offers unique opportunities for monitoring solution structures in chiral organometallics, and specifically, in the recognition of the subtle

interplay between auxiliary and substrate[9]. However since the proton spectra of mixtures of diastereomers containing for example, complexed bis phosphine BINAP [2,2′ –bis(diphenylphosphino)-1,1′-binaphthyl], are often not readily amenable to interpretation, it is

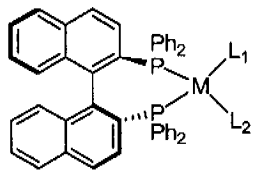

Complexed BINAP

useful to have a plan of attack: (1) Assign the ^{1}H resonances by correlating these to other spins, for example, ^{31}P, ^{13}C, metals (such as ^{195}Pt or ^{103}Rh or ^{183}W), or other protons. (2) Determine the solution 3-D structure, using ^{1}H NOE spectroscopy. (3) determine if and which exchange process occur (phase sensitive NOESY or ROESY data). In addition to (1)-(3) there are always the usual empirical coupling constant and chemical shift correlations which function as supplementary aids.

The following sections describe these methods and several simple applications related, primarily, to structural problems of chiral complexes.

1.2.1 Multidimensional NMR

In the late 1960's chemists were predicting that NMR would soon reach its limits and that its utility would diminish with time. However, about that time, the concept of two dimensional (2D) NMR was introduced, and later demonstrated[10, 11]. In 2D FT-NMR, the experiments are generally composed of four periods: preparation, evolution, mixing and detection; as illustrated in Fig. 1.1.

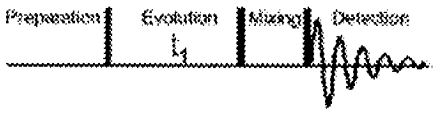

Fig. 1.1. Representative pulse sequences for acquiring 2D- NMR

The preparation can be a simple relaxation delay, as is used in a simple one-pulse 1D experiment, or it can be a more complicated series of events that moves coherence between atoms and selectively destroys NMR coherence components that would produce undesired signals in the final spectrum. During the variable evolution period (t_1) one or more NMR interactions are allowed to occur. This interaction can be chemical shift precession of a second nucleus (not detected during t_2), J-coupling, or any of a number of other possible interactions. The mixing period provides coherence transfer from the nuclei whose signals are modulated during t_1 to those detected during t_2. Thus the signals of those nuclei detected during t_2 are modulated by the NMR interactions that occurred during t_1. Many separate FID's (typically 100–1000) are collected (Fig. 1.2a), each with a different value of t_1. These FID's are individually Fourier transformed to produce a series of 1D NMR spectra (Fig. 1.2b), which can be similar to normal 1D NMR of the detected nuclei, *i.e.* peaks (in this example at frequencies *a* and *b*) in f_2 are seen corresponding to those normally observed in the spectrum of the nucleus detected in the f_2 dimension. However, the intensities of these peaks are modulated as a function of the length of t_1 and the NMR interactions that occurred during that period. Fig. 1.2c represents plots of the *a* and *b* signal intensities as a function of t_1. A second FT is performed with respect to the t_1 dimension to provide the final 2D-NMR spectrum (Fig. 1.2d).

The NMR parameters plotted along the f_2 axis are those of the detected nucleus. For example, if ^{13}C is detected, then the ^{13}C chemical shifts are plotted; if ^{1}H is detected, then the ^{1}H chemical

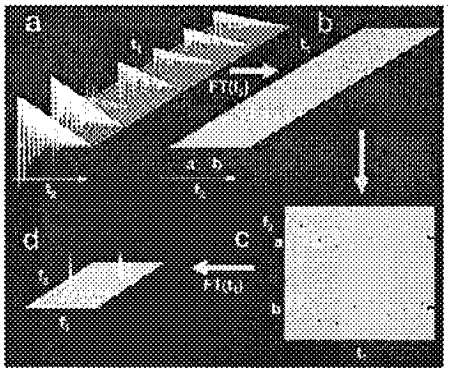

Fig. 1.2. Diagram illustrating the sequence used to produce a 2D-NMR spectrum;

shifts and coupling constants are plotted along f_2. The NMR parameter plotted along the f_1 axis is determined by the preparation period and the interaction in effect during t_1. For example, if the preparation period places coherence on ^{13}C and ^{13}C chemical shift is active during t_1, then the ^{13}C chemical shift would be plotted along the f_1 axis. Correlations between these frequencies would be observed based on the method of coherence transfer between nuclei during the mixing period.

1.2.1.1 Homo and Hetero Nuclear Correlations

The simplest 2D-NMR experiment is named COSY (Correlation Spectroscopy)[11] and contains a t_1 period flanked by two 90 degree pulses (Fig. 1.3). The second 90 degree pulse serves as a mixing period, exchanging coherence between different proton spins. The resulting spectrum contains the shifts and J-couplings along both the f_1 and f_2 axis. The spectrum contains peaks along a diagonal, corresponding to the resonances in the normal 1D spectrum, and off diagonal cross-peaks connecting these frequencies if the nuclei are J-coupled to each other.

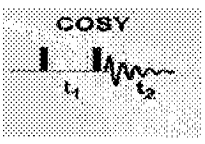

Fig. 1.3. Representative pulse sequences for acquiring COSY

The $^{1}H,^{1}H$ COSY spectrum for the complex [Pd(μ-OH)(*p*-tol-BINAP)]$_2$[OTf]$_2$, below (Fig. 1.4) helps to assign the phenyl groups in the BINAP system.

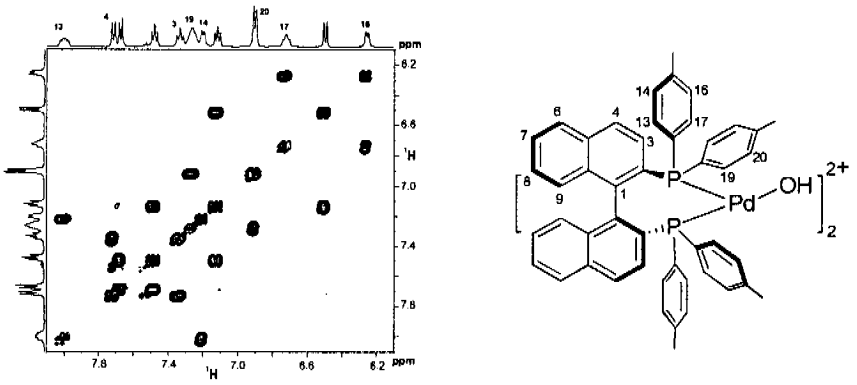

Fig. 1.4. Section of the ^{1}H, ^{1}H COSY spectrum of [Pd(μ-OH)(*p*-tol-BINAP)]$_2$[OTf]$_2$ at 203 K (CD_2Cl_2, 500 MHz).

A second commonly used sequence is the 2D-HMQC (Heteronuclear Multiple Quantum Coherence) experiment[12](Fig. 1.5). The spectrum from this sequence contains ^{1}H chemical shift data along the f_2 axis and the chemical shift of some other nucleus (usually ^{13}C or ^{15}N) along the f_1 axis. Coherence is transferred between the heteronucleus and the protons using one-bond H–X couplings. Resonances are observed at the intersection of the chemical shifts of directly bound H and X nuclei. When the NMR observable isotope of the X nucleus has low natural abundance (*e.g.* ^{13}C, 1.1%), the pulse sequence eliminates the signals of ^{1}H atoms not bound to the NMR-active X isotope (*e.g.* ^{1}H-^{12}C which accounts for 99% of the ^{1}H NMR signal). Fig. 1.6 shows the $^{15}N,^{1}H$ HMQC spectrum of W carbene complex. The separation of the signals corresponds to $^{1}J(^{15}N,^{1}H)$.

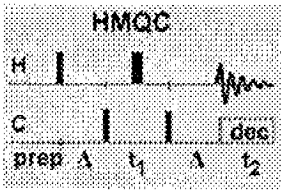

Fig. 1.5. Representative pulse sequences for acquiring HMQC.

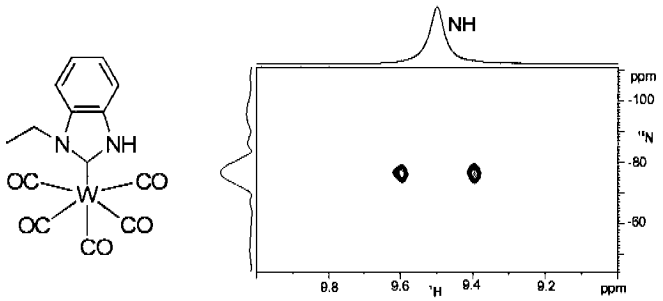

Fig. 1.6. Section of ^{15}N, ^{1}H HMQC spectra showing one bond coupling ($^{1}J_{NH}$ = 103 Hz) for W carbene complex (CD_2Cl_2, 50.7 MHz, 298 K).

1.2.1.2 NOE and HOESY Spectroscopy

The nuclear Overhauser effect (NOE) represents the manifestation of cross-relaxation between two nuclear spins which are close to each other in space[13]. The NOE has become increasingly important for the characterization of the spatial relationship between nuclei. Today, NOE measurements represent an essential part of the "routine NMR spectroscopy" used for the assignment, structure elucidation and conformational analysis of complex molecules. It is also one of the most important experimental methods for the structural analysis of biological macromolecules[13].

The basic sequence for a 2D NOESY experiment is shown in Fig. 1.7. The pulse sequence involves a 90 degree pulse followed by a delay, which is incremented to provide the second dimension, a second 90 pulse followed by a mixing time, τ_m, and a final 90 degree pulse followed by collection of the free induction decay. The mixing time is a delay which allows the NOE to build up due to relaxation effects. Cross-peaks are observed in the 2D spectra

where a significant NOE is induced between nearby nuclei. The spectrum from this sequence contains ^1H chemical shift along both the f_2 and f_1 axis.

Fig. 1.7. Representative pulse sequences for acquiring 2D-NOESY.

Since the observation of an NOE depends on the spatial relationship of two nuclei it is a tool for studying intermolecular interactions[14]. When the two spins are of the same species, i.e. $\gamma_I = \gamma_S$, then the steady state homo nuclear NOE, η_{max} is:

$$\eta_{max} = (5 + \omega^2\tau_c^{\,2} - 4\omega^4\tau_c^{\,4})/(10 + 23\omega^2\tau_c^{\,2} + 4\omega^4\tau_c^{\,4})$$

Where ω is frequency, τ_c is correlation time

In a routine NOESY spectrum, the phase of the NOE cross-peaks are usually opposite to those of the diagonal[15, 16]. However, when chemical change takes place, the exchange cross-peaks appear with the same phase as diagonal, thus providing an often unexpected bonus.

For example, reaction of ligand **1** with the aquo-complex, $[Pd(H_2O)_2(BINAP)]_2(CF_3SO_3)_2$, **2**, in dichloromethane solution, affords a mixture which, via integration, contains ca 16% of **3**. Both the ^1H and $^{31}P\{^1H\}$ spectra at room temperature gave broad resonances suggesting dynamic behaviour. From a phase sensitive $^1H,^1H$ NOESY spectrum at 203 K, one finds exchange cross peaks arising from the free oxazolidinone, **1** and the chelated ligand in complex **3** (see Fig. 1.8).

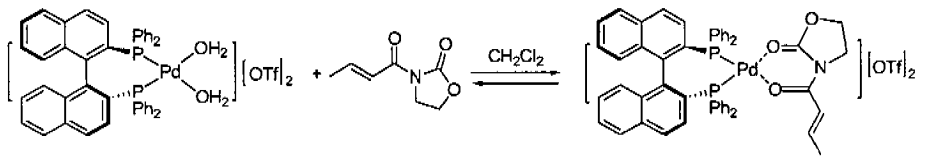

2 **1** **3**

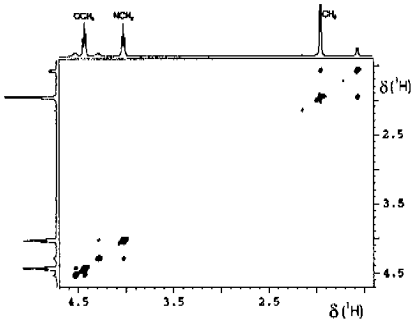

Fig. 1.8. Section of $^{1}H,^{1}H$ NOESY spectra of complex **3**, showing cross-peaks due to exchange between free ligand **1** and chelated ligand in complex **3** (CD_2Cl_2, 500 MHz, 203 K).

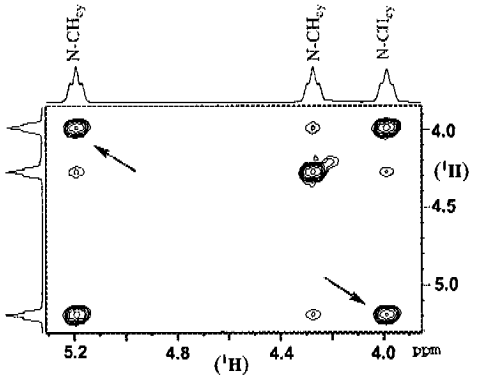

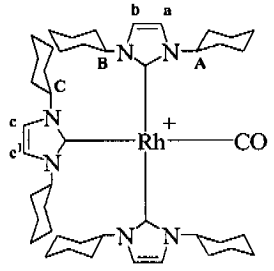

4[PF_6]

Fig. 1.9. Sections of the ROESY spectra at 203 K for the methine region of **4**[PF_6], the cross-peaks due to the exchange between the two sides of the *trans* carbene ligands are indicated with arrows and rest of the cross-peaks indicates noe (CD_2Cl_2, 500 MHz).

As a second example, we consider the Rh-carbene complex **4**[PF_6]. At low temperature the three different Cy-methine proton sites are assigned as A-C and the three NCH=CHN protons as **a-c**, as indicated in the structure, Fig. 1.9, above. A section of the ROESY spectra[15] for **4**[PF_6] is shown above and reveals that, even at 203 K, there is slow exchange between sites A and B due to restricted rotation around the Rh-C bonds.

HOESY Spectroscopy

The heteronuclear version of NOESY (often called HOESY) was developed by Rinaldi[17] as well as by Yu and Levy[18, 19]. In these experiments, using the pulse sequence shown in Fig. 1.10, relaxation between the heteronuclei is detected directly.

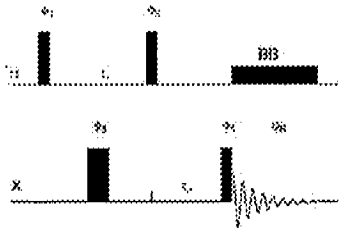

Fig. 1.10. Pulse sequence for the 2D HOESY experiment. Narrow and wide filled bars correspond to 90 and 180 hard pulses, respectively. X refers to any heteronucleus.

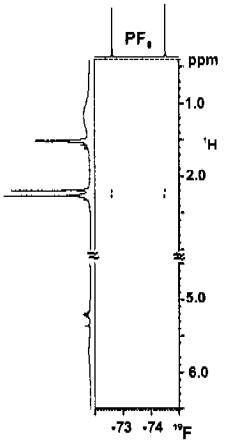

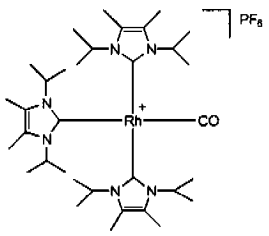

5

Fig. 1.11. HOESY spectra for **5** in THF-d_8, showing selective contacts to the methyl groups of carbene (400 MHz, 298 K).

In the example of Fig. 1.11, the ^1H, ^{19}F HOESY spectra for the $[Rh(IPr_2Me_2)_3(CO)](PF_6)$ carbene salt, **5,** in THF-d_8 solvent is shown. The PF_6 anion reveals selective contacts to the olefin methyl groups but not the i-pr methyl groups of the carbene ligand.

1.3 PGSE Diffusion NMR

1.3.1 Concepts of Diffusion

Self-diffusion concerns the random translational motion of molecules driven by their internal kinetic energy[20]. Translational diffusion and rotational diffusion can be distinguished from each other[20].

The Diffusion is related to molecular size, as becomes apparent from the Stokes-Einstein equation

$$D = k_B T / f \qquad (1)$$

Where D is the diffusion coefficient, k_B is the Boltzmann constant, T is the temperature, and f is the friction coefficient. If the solute is considered to be a spherical particle with an effective hydrodynamic radius (i.e Stokes radius) r_s in a solution of viscosity η, then the friction coefficient is given by

$$f = 6\pi\eta r_s \qquad (2)$$

Gierer and Wirtz[21] derived an expression for the friction coefficient of a solute in a solvent considering the solvent molecules as spheres with radius $r_{solvent}$ (and not as a continuous medium as in Eq. (2)):

$$f = \frac{6\pi\eta r_s}{\frac{3r_{solvent}}{2r_s} + \frac{1}{1+\frac{r_{solvent}}{r_s}}} \qquad (3)$$

A semiempirical improvement of Eq. (3) has been reported[22]:

$$f = \frac{6\pi\eta r_s}{1+0.695\left(\frac{r_{solvent}}{r_s}\right)^{2.234}} \qquad (4)$$

In eqs. (3) and (4) r_s represents the radius of the solute.

Translational diffusion is the most fundamental form of transport and is a prerequisite for chemical reactions, since the reacting species have first to collide[20].

1.3.2 PGSE Diffusion and Experimental Methods

The determination of molecular size in solution remains a subject of considerable interest to the coordination chemistry community, in particular with respect to the formation of polynuclear complexes, ion pairs and otherwise aggregated species. Apart from classical methods such as mass spectrometry[23] and those based on colligative properties[24] - boiling point elevation, freezing point depression, vapor and osmotic pressure - the Pulsed Field Gradient Spin-Echo (PGSE) methodology[25, 26] has recently resurged as a promising technique. PGSE measurements make use of the translational properties, that is, diffusion, of molecules and ions in solution and thus are directly responsive to molecular size and shape. Since one can measure several components of a mixture simultaneously[27, 28] PGSE methods are particularly valuable where the material in question is not readily isolable and/or the mixture is of especial interest, as for equilibria mixtures.

PGSE methods were introduced in 1965 by Stejskal and Tanner[29] and, since then, have been widely used. In the 1970's, this approach was used to determine diffusion coefficients of organic molecules[26]. In the following decade, variants of this technique have been applied to problems in polymer chemistry[30]. Recently, diffusion data on dendrimers[31] and peptides[32] as well as on molecules in various environments, for example, in porous silica[33], and zeolites[34], have been obtained. Recent applications of PGSE methods in coordination and/or organometallic chemistry have emerged[35, 36].

Measuring Diffusion by NMR

Diffusion can be investigated either by analysis of relaxation data[37, 38] or by pulsed field gradient (PFG) NMR measurements. While relaxation measurements are sensitive to motions occurring in the pico to nano second time scale, in PFG experiments motion on the millisecond to seconds time scale is measured.

Analysis of relaxation data yields the rotational correlation time, τ_c, of the molecule which can be related to the solvent viscosity, η. The viscosity in turn can be used for the calculation of the translational diffusion coefficient (D) by using the Debye equation (Eq. (5)) and the Stokes–Einstein equation (Eq. (6)).

$$\tau_c = 4\pi\eta r_s^3/(3k_BT) \qquad (5)$$

$$D = \frac{k_BT}{6\pi\eta r_H} \qquad (6)$$

r_H = hydrodynamic radius (Which includes both solvent (hydro) and shape (dynamic) effects.

However, far-reaching assumptions are necessary when performing this analysis, and Stokes radius r_S needs to be known. For this reason only PFG NMR methods are considered.

Using the PFG method, the diffusion coefficient (D) is measured by evaluating the attenuation of a spin-echo signal[39]. The attenuation is achieved by the dephasing of nuclear spins due to the combination of the translational motion and the imposition of gradient pulses. In contrast to the previously mentioned relaxation methods, no assumptions concerning the relaxation mechanism(s) are necessary.

The basic element of an NMR diffusion measurement consists of a spin-echo sequence[40], in combination with the application of static

or pulsed field gradients[29, 41]. Several common sequences are shown in Fig. 1.12,

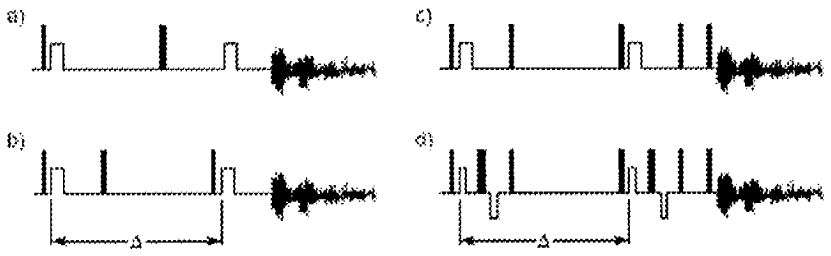

Fig. 1.12. Pulse sequences commonly used for PGSE measurements. Sequences with a) Spin-Echo, b) Stimulated Echo, c) Stimulated Echo and longitudinal eddy-current delay (LED), and d) Stimulated Echo with bipolar pulsed field gradients and LED. Narrow and wide black rectangles represent $\pi/2$ and π radio frequency pulses, respectively. Narrow and broader open rectangles represents field gradient pulses of duration δ/2 and δ, respectively and strength G.

1.3.2.1 Spin-Echo Method or Stejskal-Tanner Experiment

The Stejskal-Tanner experiment[29], Fig. 1.12a, is the simplest sequence for measuring diffusion. The transverse magnetization is generated by the initial $\pi/2$ pulse which, in the absence of the static or pulsed field gradients, dephases due to chemical shift, hetero- and homonuclear coupling evolution, and spin-spin (T_2) relaxation. After application of an intermediate π pulse, the magnetization refocuses, generating an echo. At this point the sampling (signal intensity measurement) of the echo decay starts. Fourier transformation of these data results in a conventional NMR spectrum, in which the signal amplitudes are weighted by their individual T_2's and the signal phases of the multiplets due to homonuclear coupling are distorted. Both effects are present in the

diffusion experiment; however, due to the fixed timing, these are kept constant within the experiment. The application of the first pulsed linear field gradient results in an additional (strong) dephasing of the magnetization with a phase angle proportional to the length (δ) and the amplitude (G) of the gradient. Because the strength of the gradient varies linearly along, e.g., the z-axis, only spins contained within a narrow slice of the sample acquire the same phase angle. In other words, the spins (and therefore the molecules in which they reside) are phase encoded in one-dimensional space. The second gradient pulse, which must be exactly equal to the first, reverses the respective phases and the echo forms in the usual way. If, however, spins move out of their slice into neighboring slices via Brownian motion, the phase they acquire in the refocusing gradient will not be the one they experienced in the preparation step. This leads to incomplete refocusing, as in the T_2 dephasing, and thus to an attenuation of the echo amplitude. As smaller molecules move faster, they translate during the time interval Δ into slices further apart from the original, thus giving rise to smaller echo intensities for a given product of length and strength of the gradient.

1.3.2.2 Stimulated Echo Method

The second experiment, shown in Fig. 1.12b[41], works quite the same way with the difference that the phase angles which encode the position of the spins are stored along the z-axis in the rotating frame of reference by the action of the second $\pi/2$ pulse. Transverse magnetization and the respective phases are restored by the third $\pi/2$ pulse. This method is advantageous in that during time Δ, T_1 as opposed to T_2 is the effective relaxation path. Since T_1 is often longer than T_2 a better signal/noise ratio is obtained.

Furthermore, phase distortion in multiplets due to homonuclear coupling is attenuated.

1.3.2.3 Derived Sequences

The accurate determination of diffusion coefficients for large, slow moving species requires strong gradient amplitudes. The resulting eddy-current fields can cause severe errors in the spatial phase encoding. The sequences shown in Fig. 1.12c[42] and 1.12d[43] contain, in addition, the so-called longitudinal eddy-current delay (LED) element, i.e., magnetization is again stored along the z-axis during the decay time of the eddy-currents. Disturbance of the field-frequency lock system can be minimized by the use of bipolar field gradient pulses, Fig. 1.12d.

Technically, all of above experiments are performed by repeating the sequence while systematically changing either the time allowed for diffusion (Δ), the length (δ) or the strength (G)

The diffusion coefficient D is obtained from the slope of the regression line by plotting $\ln(I/I_0)$ (I/Io = observed spin echo intensity/intensity without gradients) vs. either $\Delta-\delta/3$, $\delta^2(\Delta-\delta/3)$ or G^2, depending on the parameter varied in the course of the experiment, respectively.

$$\ln\left(\frac{I}{I_o}\right) = -(\gamma\delta)^2 G^2 \left(\Delta - \frac{\delta}{3}\right) D$$

G = gradient strength, Δ = delay between the midpoints of the gradients, D = diffusion coefficient, δ = gradient length

The diffusion constant D can be related to the hydrodynamic radii of the molecules *via* the Stokes - Einstein equation (6).

General Considerations

For a routine PGSE measurement, there are no major instrumental or sample requirements, apart from gradients. Indeed, the PGSE methodology presents several advantages. It is relatively fast for ^{1}H and ^{19}F (normally about 1–2 h, but longer for other nuclei such as ^{31}P), non-invasive, and requires modest quantities of the compound (usually 1–2 mM solutions). It is possible to work with the signal intensities from a spin–spin multiplet structure, but sharp lines are usually preferred. Several components of a mixture can be measured simultaneously (as long as they afford resolvable NMR signals), which makes the technique especially valuable for materials which are either not readily isolable, or for solutions containing a mixture of materials, for example, diastereomeric compounds[44], or perhaps several species in equilibrium[45].

Although variable temperature 1- and 2-D NMR studies are now routine, there is an additional problem with variable temperature diffusion measurements. Convection currents are caused by small temperature gradients within the sample, which are difficult to eliminate. For a given sample with a particular set of properties

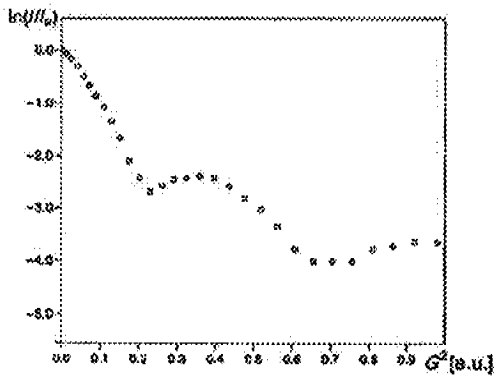

Fig. 1.13. Plot of ln (I/I_0) vs. G^2 (arbitrary units), the square of the gradient amplitude for the neutral platinum complex $Pt(Cl)(H_2O)(PMe_3)(p\text{-}Me\text{-}C_6H_4)$ at 228 K in toluene-d_8 solution in a 5 mm NMR tube. The ^{1}H PGSE diffusion data stem from the p-tolyl methyl group[46]. The lack of linearity arises due to convection (Δ = 68 ms, d = 2 ms).

(viscosity, thermal diffusivity, thermal expansion coefficient) convection appears if the temperature gradient within the solution exceeds a certain value[47]. The general diffusion curve for a sample showing convection is illustrated in Fig. 1.13.

A sensitive test for the onset of convection involves a comparison of D-values measured with different diffusion delays, d, as convection shows up as Δ-dependent (apparent) diffusion coefficient[46]. One solution to the convection problem involves the use of a coaxial insert inside a normal 5 mm NMR tube[46]. The inner and outer tubes are separated by a pyrex spacer suitable for variable temperature experiments. A space of ca. 2 mm is left between both tubes at the bottom.

1.3.3 Applications of Diffusion NMR

Diffusion coefficients and the structural properties of a molecule are connected by the dependence of the diffusion coefficients on molecular size and shape, it is not surprising that the determination of molecular diffusion coefficients by pulsed gradient spin-echo (PGSE) NMR experiments has become a valuable methodology for studies of molecular interaction in solution. In recent years, with the availability of gradient technology, the use of PGSE NMR experiments for determination of translational diffusion in studies related to molecular size, aggregation and binding has become a field of increasing interest.

The following sections describe selected applications of PGSE NMR studies in organometallic chemistry.

1.3.3.1 Molecular Volume

The use of PGSE experiments, which can measure the diffusion coefficients of molecules and thus provide information on molecular size (r_H) from the Stokes–Einstein equation. As the molecules become larger, they move (diffuse) slower. The more phenyl groups one has in the molecule, the slower will be the observed translation. In Fig. 1.14[48], PGSE results (from left to right) for H_2O, $CHCl_3$, and four arsine complexes of Pd(II) in $CDCl_3$. $PdCl_2L_2$, (L = $AsMe_xPh_{3-x}$, x = 3, 2, 1, 0), are reported. One can see that the smaller $AsMe_3$ complex moves faster than the analogous, and all four of these are slower than H_2O and solvent, which move relatively quickly. This is also made clearer in Fig. 1.15 which gives results for three different ferrocene phosphine dendrimers. It is clearly observable that as the size of the ferrocene phosphine dendrimer increases, the r_H value increases.

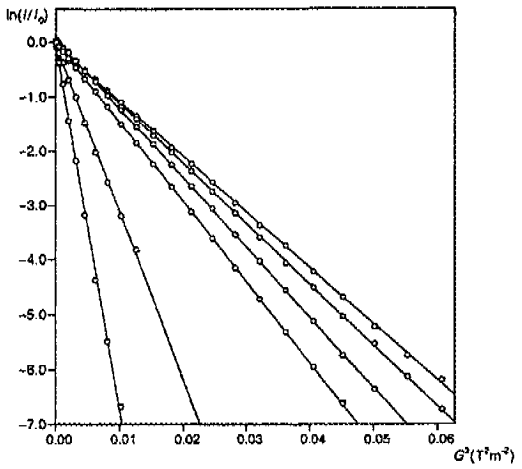

Fig. 1.14. Plot of ln (I/I_o) vs. the square of the gradient amplitude. The slopes of the lines are related to the diffusion coefficients, D. The six lines stem from H_2O, $CHCl_3$, and the four Pd-arsine complexes $PdCl_2L_2$ (L = $AsMe_xPh_{3-x}$, x = 3, 2, 1, 0, increasing molecular volume from left to right). The absolute value of the slope decreases with increasing molecular volume.

Fig. 1.15. Phosphine Dendrimers

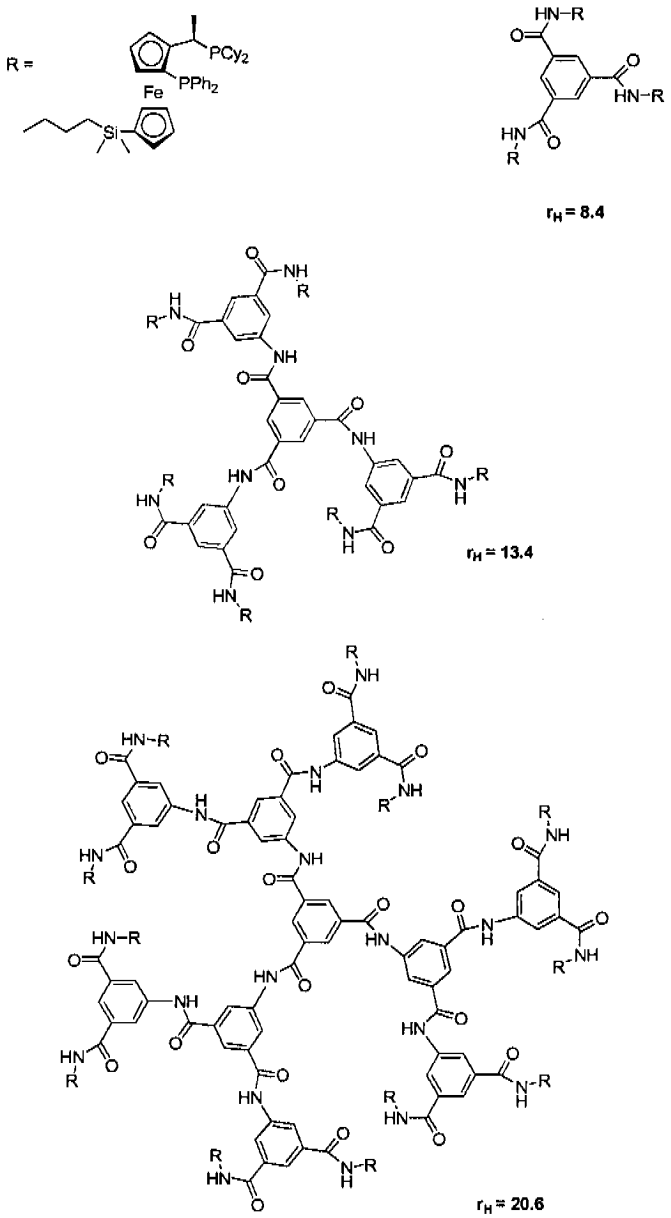

1.3.3.2 Hydrogen Bonding

Another interesting area concerns H-bonding in metal complexes. There are a number of ways in which the D-value for a small molecule (or small anion) can be influenced by the presence of another species: (a) hydrogen bonding (b) host/guest encapsulation and (c) ion pairing. As an example of H-bonding, ^{19}F-PGSE diffusion data for both triflate moieties of the cationic compound **6** suggesting that both triflates are moving at the same rate[48]. Although one could imagine tight ion-pairing as an explanation for the observed identical diffusion coefficients, the reported solid-state structure of **6** suggests an H-bond from the $P(OH)Ph_2$ fragment to the anionic (not to the complexed) triflate. Consequently, the anionic triflate (which might also be involved in ion-pairing) is most likely associated with the cation via the OH group.

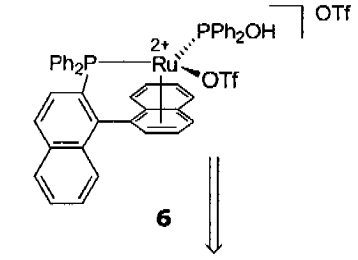

6

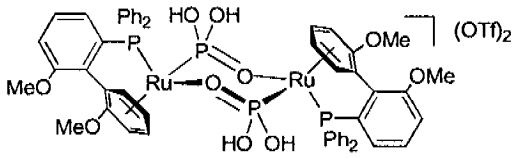

7

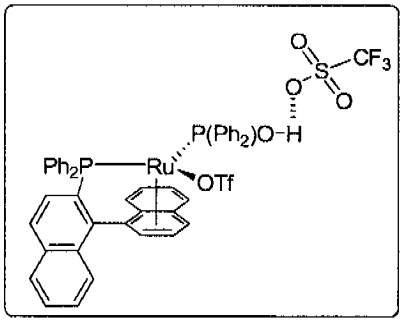

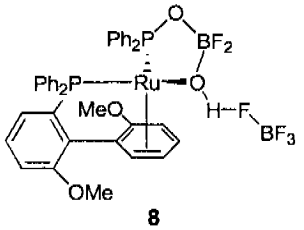

8

Interestingly, for complex **7**, a similar situation exists, that is from the ^{19}F diffusion data the triflate diffuses at the same rate as the

large dication. Again based on the X-ray data, H-bonding to be important. Another H-bonding situation exists for the complex **8**[49] of the Ph_2POBF_2OH bidentate ligand. ^1H- and ^{19}F- PGSE measurements reveal the same diffusion coefficients for both the complex and H-bonded BF_4.

1.3.3.3 Host-Guest Interactions

The diffusion coefficient should be a powerful tool for detecting and probing encapsulation[50], since the encapsulated guests are generally much smaller molecular species than the host itself and, therefore, should have a much higher diffusion coefficient in its free state. Moreover, the encapsulated molecules (guest), which are in slow exchange with the bulk, should have the same diffusion coefficient as the host itself since the host and the encapsulated molecules (guest) diffuse as a single molecular entity[50].The host guest interaction studies using diffusion-based argument was used to probe benzene encapsulation in the tetraureacalix arene dimmer. **9**.

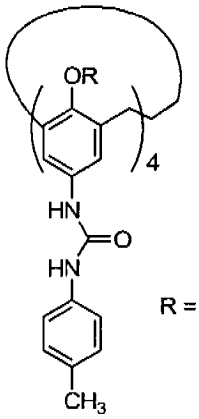

R = $C_{10}H_{21}$

9

Fig. 1.16 shows part of the ^1H NMR spectrum of dimer **9** prepared in a 80:20 mixture of C_6H_6 and C_6D_6. The signal at about δ 4.4 was suspected to be that of the encapsulated benzene. Fig. 1.16b shows the decay of this signal, the signal of "free" benzene (at δ 7.15), and one representative signal of the dimer (at δ 1.95) as a function of the diffusion gradient strength G. This figure demonstrates that the signal at δ 4.4 has a much lower diffusion coefficient than that of the free benzene, and that the extracted diffusion coefficient for this signal ($0.34\pm0.01 \times 10^{-5}$ cm^2s^{-1}) was exactly the same as the one determined for the dimer[50] and

illustrates that, as expected, the encapsulated benzene and the dimer diffuse as a single molecular entity.

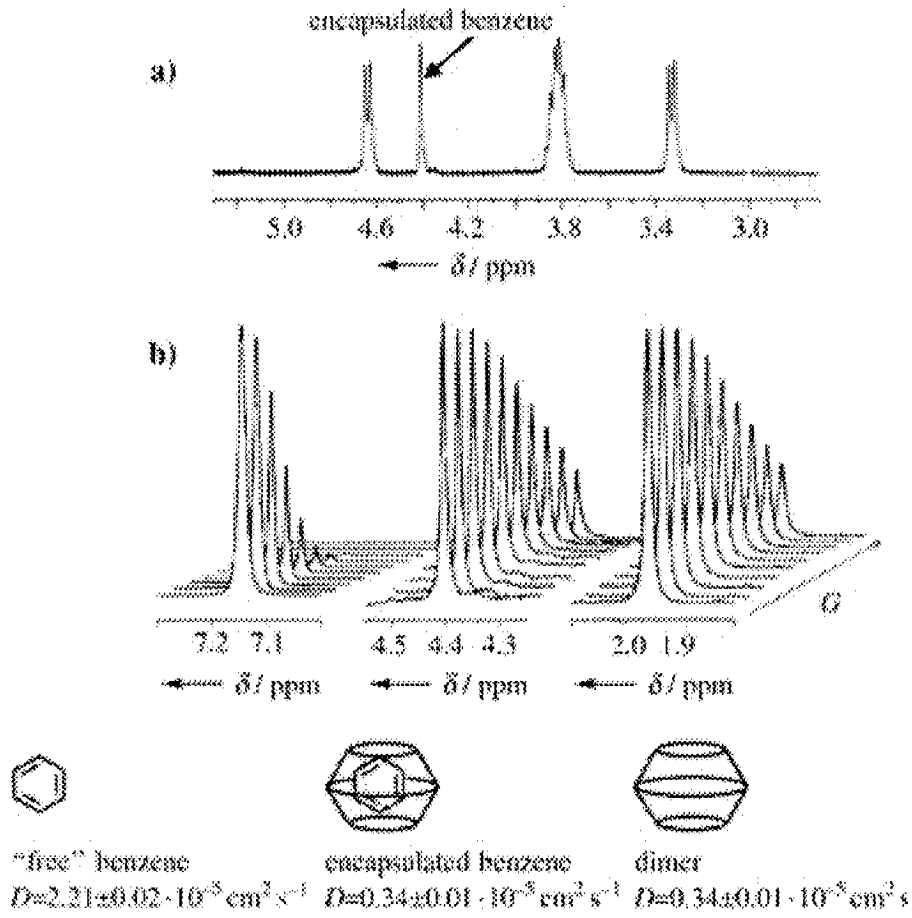

Fig. 1.16. a) Section of the ^{1}H NMR spectrum (500 MHz) of **9** in an 80/20 (v/v) solution of benzene and C_6D_6. b) ^{1}H NMR spectra (500 MHz) of the same sample (recorded with a Stejskal–Tanner diffusion experiment). The figure shows the decay of the signal intensity as a function of G. For clarity, only the signal of **9** at δ = 1.95 ppm and the signals attributed to the "free" and encapsulated benzene at δ = 7.15 and 4.4 ppm, respectively, are shown[50].

1.3.3.4 Ion Pairing

PGSE diffusion studies have shown the potential for recognizing ion pairing[48, 51, 52]. Recent use of PGSE methods shadows conductivity measurements although it is an accepted method of measuring how ions interact[48, 53]. The individual D-values obtained from PGSE diffusion for the ions (usually ^{1}H of cation, ^{19}F of anion) of a given salt can provide a translational properties of the cation and anion, thereby affording insight into whether these species move independently or as a single unit[54]. If the two ions are large enough - and tightly ion-paired - the resulting increase in the molecular volume will be reflected in the observed D values. Cation/anion interactions can therefore be explored in a more direct fashion. In selected cases, with the help of ^{1}H-^{19}F-HOESY data, one can also recognize where the two charged species interact[55-57].

PGSE studies revealed marked solvent and concentration effects on D values in selected transition salts[48, 53]. As expected, there are solvents in which the cation/anion interaction is minimal (e.g., methanol) and others (e.g., dichloromethane or Chloroform) in which there is a significant amount of ion pairing[48, 55, 58, 59].

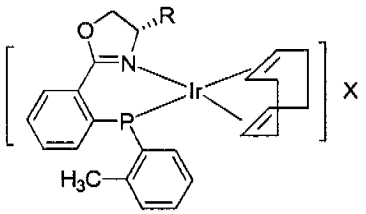

R = t-butyl

X = BF_4, PF_6, OTf, $B(C_6H_5)_4$, BArF

10

The solvent dependence of the ^{1}H and ^{19}F D-values for the Ir(I) salt, **10** having different anions (BF_4^-, PF_6^-, OTf^-, $B(C_6F_5)_4^-$ and $BAr^F{}_4^-$) in methanol, chloroform, dichloromethane, and 1,2-dichloroethane are described below. In methanol, the strongest solvating and most polar of the three solvents, the observed D values for the cation, with all five anions are found to be the same within the experimental error, indicating independent movement of the cation in this solvent. In chloroform solution, the anions and cations of **10** are moving at about the same rate, based on their respective D-values, suggesting strong ion pairing.

However, in dichloromethane solution, the diffusion data suggest mixed picture for the five anions. The results for the cation (**10**) of the BF_4^-, PF_6^- and OTf^- salts reveal radii and molecular volumes which are essentially identical to those calculated in methanol. Clearly, these anions seem unimportant for the translation of the cation in this solvent, giving the impression of little or no ion-pairing. However, relative to the methanol data, the BF_4^-, PF_6^-, and OTf^- anions have larger radii. Possibly, there may be a small amount of ion-pairing. On the other hand, the larger boron-based anions $B(C_6H_5)_4^-$ and $BArF^-$ increases modestly for both cation and anion, relative to the methanol data, indicating some -but not complete ion -pairing. In 1,2-dichloroethane D and r_H values shows similar results to those reported for dichloromethane.

This type of solvent dependence of the ion pairing is not limited to salts of transition metals. The D and r_H values for diasteromers formed between two organic cations, dimethoxyquinacridinium (**11**) and 5,5',7,7'-tetrahydro-6,6'-spirobi[dibenzo[c,e]azepin]-6-ium (**12**) with relatively large chiral tris(tetrachlorobenzenediolato)phosphate(V) (TRISPHAT) and bis(tetrachlorobenzenediolato)mono([1,1']binaphthalenyl-2,2'

diolato)-phosphate(V) BINPHAT anions[60], **13** and **14**, respectively (see Scheme 1.1). In chloroform solution, strong ion pairing is favored. For the BINPHAT salt, (**12**)(**14**), the ^{1}H, ^{19}F and ^{31}P PGSE diffusion studies reveal the first example of the dependence of a diffusion value on diastereomeric structure.

Scheme 1.1.

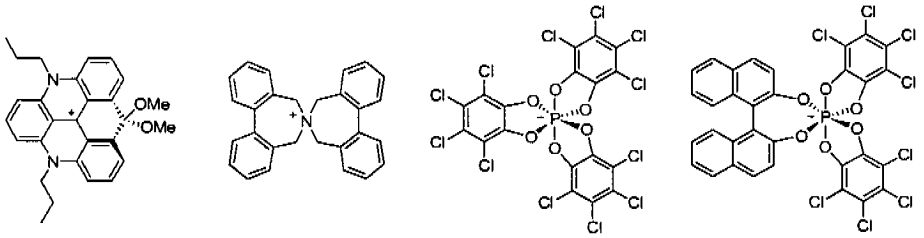

cation **11** cation **12** TRISPHAT anion, **13** BINPHAT anion, **14**

Clearly, the ability to measure the diffusion rates for the cation and anion, separately, that is, multinuclear PGSE studies, represents a powerful tool, and readily affords a qualitative view of the ion pairing.

1.3.4 Homogeneous Catalysis

It is well known from the literature[61-63] that several processes, mediated by charged organometallic complexes, are strongly dependent on the nature of the counterion. The source of these effects is often completely unknown and may be related to coordination and/or ion pairing effects, amongst other explanations. The possibility of directly observing the anion-cation interactions in solution could lead to a better understanding of the role of the anion in the catalytic processes.

In terms of the catalyst activity, as a function of the counterion, it has been found that the weaker the coordinating power of the anion, the higher the reactivity for a given cation[64, 65].

As an example, the anion dependence was first reported[66] by Evans in 1995 for C_2-symmetric cationic copper(II) Lewis acids used in catalysed enantioselective Diels-Alder reaction shown in Scheme 1.2.

Scheme 1.2

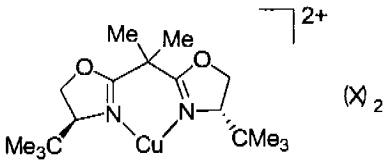

Cu(t-Bu-box)

Evans investigated the enantioselective Diels-Alder reaction of imide-derived dienophiles with dienes catalyzed by (*t*-Bu-box)Cu(X)$_2$ reported in Scheme 1.3, obtaining results for the reaction rate that was about 20 times faster for SbF_6^- than OTf^- [67] (Fig. 1.17). In addition, the cationic Cu(II) complexes with SbF_6^- afforded higher levels of asymmetric induction than the analogous triflate complex. Interestingly, the endo/exo ratio was found to be dependent on the counterion. The lower the coordinating tendency of the counterion, the less diastereoselective the Diels-Alder reaction.

Scheme 1.3

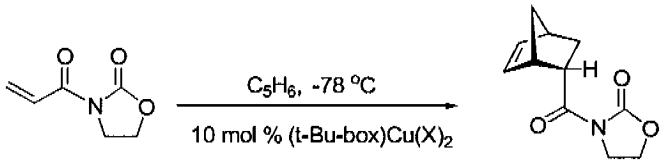

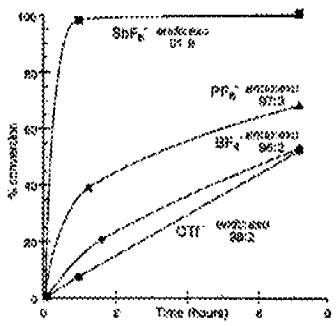

Fig. 1.17. Conversion of reaction reported in Scheme **1.3** catalyzed by complexes (t-Bu-box)Cu(X)$_2$ at -78 °C as a function of time. The endo ee was >98% in all case.[67]

In the case of R-box ligand-containing copper(II) catalysts, it seems certain that the reaction proceeds with the formation of the slightly distorted square-planar adduct reported in Scheme 1.4 with a twopoint catalyst-dienophile binding. Characterization of such an intermediate in solution through NMR experiments was prevented by the d^9 paramagnetic Cu center. Spectroscopic investigations demonstrated that an unsymmetric square-pyramidal geometry exists in solution for a catalyst bearing C_2-symmetric bis(sulfoximines) ligand and the dienophile where one triflate anion occupies the fifth coordination site[68]. In the solid state several X-ray structures of $[(t\text{-Bu-box})CuL_2](X)_2$ complexes (L = H_2O, halogen or L_2 = substrate or substrate-like compounds) were determined[69, 70] that support a distorted square-planar intermediate for reactions catalyzed by these complexes. As far as the bis(aquo) complexes $[(t\text{-Bu-box})Cu(H_2O)_2](X)_2$ (X^- = OTf^- or SbF_6^-) are concerned[69, 70], in the case of the triflate counterion a distorted square-pyramidal geometry with one triflate counterion weakly bonded to the metal center in the apical position was found. In contrast, for the hexafluoroantimonate complex none of the counterions appeared to be coordinated to the metal center, which assumes a distorted square-planar geometry. Theoretical calculations for the catalyst-substrate two-point complex (Scheme 1.4) suggest a distorted square-planar geometry for the cations analogous to that found in the solid state[67, 71, 72].

Scheme 1.4

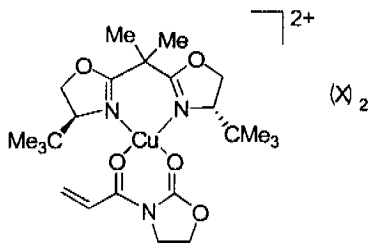

Two factors seem to be responsible for the counterion effect on the catalyst activity. First, the entering substrates must first displace the counterion from the two equatorial coordination sites. Second, the fifth coordination site on copper(II) is required for catalyst turnover through the associative displacement of the bound neutral oxygen ligands by additional dienophile[67]. Both factors are facilitated by the least coordinating anions, and this explains the correlation between the catalytic activity and the "non-coordinating" tendency of the counterions. The understanding of the counterion effect on the diastereoselectivity and on the asymmetric induction is less trivial and is still a matter of debate. The moderately lower enantioselectivity observed in some cases with OTf^- instead of SbF_6^- might be due to intervention of a competing cycloaddition by a less highly organized one-point catalyst dienophile complex. The possibility that the catalyst geometry could be affected by changing the counterion must also be taken into account.

Even in more recent and efficient, N-heterocyclic carbene complexes, the counterion plays a crucial role in deciding the coordination mode of an N-heterocyclic carbene to the metal center. Crabtree and Faller recently showed that besides the normal C-2 coordination mode, N-heterocyclic carbene ligands can bind to the metal center in an "abnormal" C-5 coordination mode (Scheme 1.5)[73, 74].

Scheme 1.5

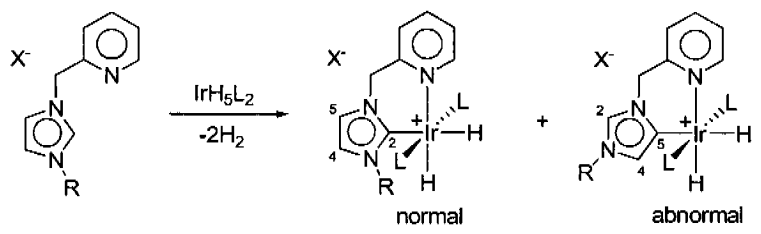

For example, the metalation reaction reported in Scheme 1.5 afforded a 45:55 ratio of C-2- and C-5- bound carbenes when X^- = BF_4^- and R = Me.[75] QM/ MM ONIOM calculations on the cationic anion-free models indicated that the abnormal carbene was 42.3 kJ/mol higher in energy than the normal one. When the anion (BF_4^-) was included in the calculations, the difference in energy between the normal and abnormal carbenes was reduced to 6.7 kJ/mol. In addition, the choice of the anion was found to bias the experimental kinetic product of the reaction to give either normal or abnormal binding[75]. The former was by far the major product with strongly coordinating anions (as Br-), while with weakly coordinating anions (as SbF_6^-), the latter was formed. Theoretical calculations and $^{19}F,^{1}H$-HOESY NMR experiments[76] indicate that ion pairing occurs at the H-5 and CH_2 protons in the normal carbene and at the H-2 and CH_2 protons in the abnormal carbene. The acidity of the CH-2 moiety of imidazolium salts[77] and, in general, of a CH moiety between two nitrogen atoms is well known and may give rise to selective ion pairing[78-80]. The reason for the ion-pairing effect on the normal/abnormal product ratio is not yet understood, but it seems to be connected with the influence of the anion on the relative energies of the transition state vs the ground state of the ion pair.

Conclusion: It would appear that diffusion data provide a unique, relatively rapid way of recognizing and evaluating the general problem of ion pairing. Further, the use of PGSE methods, together with Overhauser data (be they from HOESY or NOESY spectra), to qualitatively investigate problems involving ion-paring and hydrogen bonding. The observed anion effect in selected homogeneously catalyzed reactions represents a nice example of this type of application.

1.4 Concluding Remarks

Diffusion and multidimensional NMR methods, in particular NOE-measurements provide an enormous amount of experimental information about chemical structure. By making use of these NMR methods, the following chapter describes the effect of solvent or anion on the ion pairing and cation/anion interactions in catalytically relevant transition organometallic complexes.

1.5 Bibliography

[1] F. Bloch, W. W. Hansen and M. Packard, *Physical Review* **1946**, *69*, 127-127.

[2] E. M. Purcell, H. C. Torrey and R. V. Pound, *Physical Review* **1946**, *69*, 37-38.

[3] P. Styles, N. F. Soffe, C. A. Scott, D. A. Cragg, F. Row, D. J. White and P. C. J. White, *J. Mag. Res.* **1984**, *60*, 397-404.

[4] A. G. Webb, *Prog. Nucl. Magn. Reson. Spectrosc.* **1997**, *31*, 1-42.

[5] B. M. Trost and R. I. Higuchi, *J. Am.Chem. Soc.* **1996**, *118*, 10094-10105.

[6] B. M. Trost and Y. Li, *J. Am.Chem. Soc.* **1996**, *118*, 6625-6633.

[7] A. Pfaltz, *Acc. Chem.Res.* **1993**, *26*, 339.

[8] P. Vonmatt, O. Loiseleur, G. Koch, A. Pfaltz, C. Lefeber, T. Feucht and G. Helmchen, *Tetrahedron: Asymmetry* **1994**, *5*, 573-584.

[9] P. von Matt, G. C. Lloyd-Jones, A. B. E. Minidis, A. Pfaltz, L. Macko, M. Neuburger, M. Zehnder, H. Rüegger and P. S. Pregosin, *Helv. Chim. Acta* **1995**, *78*, 265.

[10] L. Muller, A. Kumar and R. R. Ernst, *J. Chem. Phys.* **1975**, *63*, 5490-5491.

[11] W. P. Aue, E. Bartholdi and R. R. Ernst, *J. Chem. Phys.* **1976**, *64*, 2229-2246.

[12] A. Bax and M. F. Summers, *J. Am.Chem. Soc.* **1986**, *108*, 2093-2094.

[13] H. P. Mo and T. C. Pochapsky, *Prog. Nucl. Magn. Reson. Spectrosc.* **1997**, *30*, 1-38.

[14] B. Binotti, A. Macchioni, C. Zuccaccia and D. Zuccaccia, *Comments Inorganic Chem.* **2002**, *23*, 417-450.

[15] W. E. Hull, *Two-Dimensional NMR Spectroscopy. Applications for Chemists and Biochemists.*, VCH, New York, **1987**, p. 153.

[16] R. R. Ernst, *Chemia* **1987**, *41*, 323.

[17] P. L. Rinaldi, *J. Am.Chem. Soc.* **1983**, *105*, 5167-5168.

[18] C. Yu and G. C. Levy, *J. Am.Chem. Soc.* **1983**, *105*, 6994-6996.

[19] C. Yu and G. C. Levy, *J. Am.Chem. Soc.* **1984**, *106*, 6533-6537.

[20] W. S. Price, *Concepts Magn. Resonance* **1997**, *9*, 299-336.

[21] A. Gierer and K. Wirtz, *Zeitschrift Fur Naturforschung Section a-a Journal of Physical Sciences* **1953**, *8*, 532-538.

[22] H. C. Chen and S. H. Chen, *J. Phys. Chem.* **1984**, *88*, 5118-5121.

[23] R. Colton, A. Dagostino and J. C. Traeger, *Mass Spectrometry Reviews* **1995**, *14*, 79-106.

[24] A. Weissberger and B. W. Rossiter, *Physical Methods of Chemistry*, John Wiley & Sons, **1971**, p.

[25] C. S. Johnson, *Prog. Nucl. Magn. Reson. Spectrosc.* **1999**, *34*, 203-256.

[26] P. Stilbs, *Prog. Nucl. Magn. Reson. Spectrosc.* **1987**, *19*, 1.

[27] K. F. Morris and C. S. Johnson, *J. Am.Chem. Soc.* **1992**, *114*, 3139-3141.

[28] M. D. Pelta, H. Barjat, G. A. Morris, A. L. Davis and S. J. Hammond, *Magn. Reson. Chem.* **1998**, *36*, 706-714.

[29] E. O. Stejskal and J. E. Tanner, *J. Chem. Phys.* **1965**, *42*, 288.

[30] W. Brown and P. Stilbs, *Polymer* **1982**, *23*, 1780-1789.

[31] I. B. Rietveld and D. Bedeaux, *Macromolecules* **2000**, *33*, 7912-7917.

[32] S. G. Yao, G. J. Howlett and R. S. Norton, *Journal of Biomolecular Nmr* **2000**, *16*, 109-119.

[33] C. Forste, W. Heink, J. Karger, H. Pfeifer, N. N. Feokistova and S. P. Zhdanov, *Zeolites* **1989**, *9*, 299-302.

[34] G. H. Sorland, D. Aksnes and L. Gjerdaker, *J. Mag. Res.* **1999**, *137*, 397-401.

[35] R. Romeo, L. Fenech, L. M. Scolaro, A. Albinati, A. Macchioni and C. Zuccaccia, *Inorg. Chem.* **2001**, *40*, 3293-3302.

[36] P. S. Pregosin, P. G. A. Kumar and I. Fernandez, *Chem. Revs.* **2005**, *105*, 2977-2998.

[37] W. S. Price, P. W. Kuchel and B. A. Cornell, *Biophysical Chemistry* **1989**, *33*, 205-215.

[38] W. S. Price and L. P. Hwang, *Journal of the Chinese Chemical Society* **1992**, *39*, 479-496.

[39] W. S. Price, *Concepts Magn. Resonance* **1998**, *10*, 197-237.

[40] E. L. Hahn, *Physical Review* **1950**, *80*, 580-594.

[41] J. E. Tanner, *J. Chem. Phys.* **1970**, *52*, 2523-&.

[42] S. J. Gibbs and C. S. Johnson, *J. Mag. Res.* **1991**, *93*, 395-402.

[43] A. Jerschow and N. Muller, *J. Mag. Res.* **1997**, *125*, 372-375.

[44] E. Martinez-Viviente, P. S. Pregosin, L. Vial, C. Herse and J. Lacour, *Chem. Eur. J.* **2004**, *10*, 2912-2918.

[45] J. L. Yan, A. D. Kline, H. P. Mo, E. R. Zartler and M. J. Shapiro, *J. Am.Chem. Soc.* **2002**, *124*, 9984-9985.

[46] E. Martinez-Viviente and P. S. Pregosin, *Helv. Chim. Acta* **2003**, *86*, 2364-2378.

[47] M. M. Britton, *J. Phys. Chem. A* **2006**, *110*, 5075-5080.

[48] M. Valentini, H. Ruegger and P. S. Pregosin, *Helv. Chim. Acta* **2001**, *84*, 2833-2853.

[49] C. J. den Reijer, H. Rueger and P. S. Pregosin, *Organometallics* **1998**, *17*, 5213-5215.

[50] L. Frish, S. E. Matthews, V. Bohmer and Y. Cohen, *J. Chem. Soc.Perkin Trans. 2* **1999**, 669-671.

[51] C. Zuccaccia, G. Bellachioma, G. Cardaci and A. Macchioni, *Organometallics* **2000**, *19*, 4663-4665.

[52] M. Valentini, P. S. Pregosin and H. Rüegger, *Organometallics* **2000**, *19*, 2551-2555.

[53] P. S. Pregosin, E. Martinez-Viviente and P. G. A. Kumar, *Dalton Transactions* **2003**, 4007-4014.

[54] Y. Chen, M. Valentini, P. S. Pregosin and A. Albinati, *Inorg. Chim. Acta* **2002**, *327*, 4-14.

[55] P. G. A. Kumar, P. S. Pregosin, J. M. Goicoechea and M. K. Whittlesey, *Organometallics* **2003**, *22*, 2956-2960.

[56] S. P. Smidt, A. Pfaltz, E. Martinez-Viviente, P. S. Pregosin and A. Albinati, *Organometallics* **2003**, *22*, 1000-1009.

[57] D. Zuccaccia, S. Sabatini, G. Bellachiom, G. Cardaci, E. Clot and A. Macchioni, *Inorg. Chem.* **2003**, *42*, 5465-5467.

[58] A. Pichota, P. S. Pregosin, M. Valentini, M. Wörle and D. Seebach, *Angew. Chem.Int. Ed. English* **2000**, *112*, 153-156.

[59] E. Martinez-Viviente, H. Ruegger, P. S. Pregosin and J. Lopez-Serrano, *Organometallics* **2002**, *21*, 5841-5846.

[60] E. Martinez-Viviente, P. S. Pregosin, L. Vial, C. Herse and J. Lacour, *Chem.-Eur. J.* **2004**, *10*, 2912-2918.

[61] P. G. A. Kumar, P. S. Pregosin, M. Vallet, G. Bernardinelli, R. F. Jazzar, F. Viton and E. P. Kundig, *Organometallics* **2004**, *23*, 5410-5418.

[62] K. Fagnou and M. Lautens, *Angew. Chem. Int. Ed. Engl.* **2002**, *41*, 27-47.

[63] T. M. Schmid and G. Consiglio, *Chem. Commun.* **2004**, 2318-2319.

[64] L. Jia, X. M. Yang, C. L. Stern and T. J. Marks, *Organometallics* **1997**, *16*, 842-857.

[65] J. Zhou, S. J. Lancaster, d. A. Walker, S. Beck, M. Thorton-Pett and M. Bochmann, *J. Am.Chem. Soc.* **2001**, *123*, 223-237.

[66] D. A. Evans, J. A. Murry, P. Vonmatt, R. D. Norcross and S. J. Miller, *Angew. chem Int. Ed. Engl.* **1995**, *34*, 798-800.

[67] D. A. Evans, S. J. Miller, T. Lectka and P. von Matt, *J. Am.Chem. Soc.* **1999**, *121*, 7559-7573.

[68] C. Bolm, M. Martin, G. Gescheidt, C. Palivan, D. Neshchadin, H. Bertagnolli, M. Feth, A. Schweiger, G. Mitrikas and J. Harmer, *J. Am.Chem. Soc.* **2003**, *125*, 6222-6227.

[69] D. A. Evans, E. J. Olhava, J. S. Johnson and J. M. Janey, *Angew. Chem.Int.Ed.Engl.* **1998**, *37*, 3372-3375.

[70] J. S. Johnson and D. A. Evans, *Acc. Chem. Res.* **2000**, *33*, 325-335.

[71] J. Thorhauge, M. Roberson, R. G. Hazell and K. A. Jorgensen, *Chem.-Eur. J.* **2002**, *8*, 1888-1898.

[72] R. J. Deeth and N. Fey, *Organometallics* **2004**, *23*, 1042-1054.

[73] S. Grundemann, A. Kovacevic, M. Albrecht, J. W. Faller and R. H. Crabtree, *Chem. Commun.* **2001**, 2274-2275.

[74] S. Grundemann, A. Kovacevic, M. Albrecht, J. W. Faller and R. H. Crabtree, *J. Am.Chem. Soc.* **2002**, *124*, 10473-10481.

[75] A. Kovacevic, S. Grundemann, J. R. Miecznikowski, E. Clot, O. Eisenstein and R. H. Crabtree, *Chem. Commun.* **2002**, 2580-2581.

[76] L. N. Appelhans, D. Zuccaccia, A. Kovacevic, A. R. Chianese, J. R. Miecznikowski, A. Macchioni, E. Clot, O. Eisenstein and R. H. Crabtree, *J. Am.Chem. Soc.* **2005**, *127*, 16299-16311.

[77] J. A. Cowan, J. A. C. Clyburne, M. G. Davidson, R. L. W. Harris, J. A. K. Howard, P. Kupper, M. A. Leech and S. P. Richards, *Angew. Chem. Int. Ed. Engl.* **2002**, *41*, 1432-1434.

[78] C. Zuccaccia, G. Bellachioma, G. Cardaci and A. Macchioni, *J. Am.Chem. Soc.* **2001**, *123*, 11020-11028.

[79] B. Binotti, G. Bellachioma, G. Cardaci, A. Macchioni, C. Zuccaccia, E. Foresti and P. Sabatino, *Organometallics* **2002**, *21*, 346-354.

[80] A. Macchioni, G. Bellachioma, G. Cardaci, G. Cruciani, E. Foresti, S. P/ and C. Zuccaccia, *Organometallics* **1998**, *17*, 5549-5556.

Chapter 2

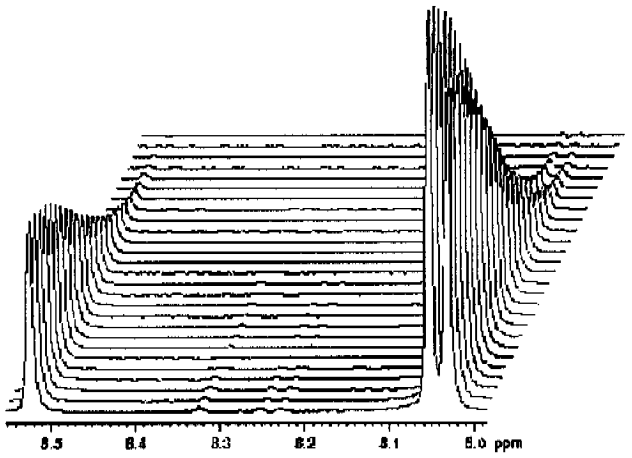

PGSE Diffusion NMR

2. Diffusion Measurements on Organometallic Complexes

Overview:

In this chapter, the sections (**2.1.1** to **2.1.3**) describe the synthesis, solution structure and PGSE NMR diffusion studies of Pd complexes (**1-3**). These salts are known to be catalytically useful in hydroamination[1, 2] (or) ene type reactions[3], amongst others.

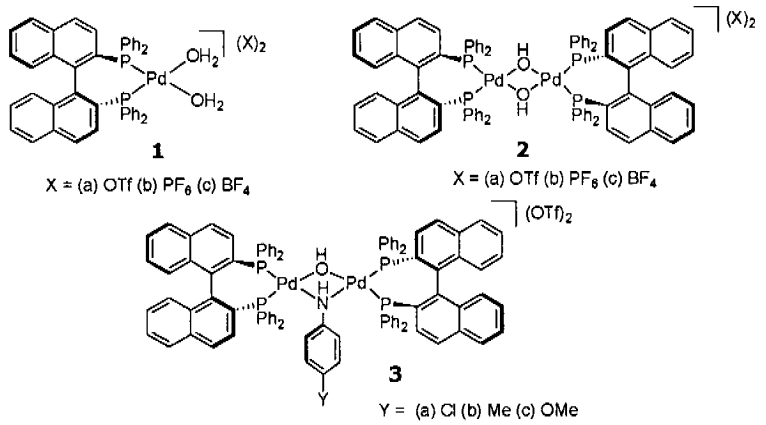

The solvent (e.g., $CHCl_3$, THF, CD_2Cl_2) dependent ion pairing, salt aggregation, and hydrogen bonding are studied using the diffusion constants (D values) obtained from the PGSE measurements. The effect of the different anions ($CF_3SO_3^-$, BF_4^-) and how they interact with different bridged ligands are briefly elaborated and explained in these sections.

Section **2.1.4** describes the synthesis and structural studies of a modest number of mono cationic Pd(BINAP) complexes (**12-16**), which are believed to be intermediates in catalytic hydroamination or the Michael reaction. The acetylacetonate and Oxazolidinone ((E)-3-but-2-enoyloxazolidin-2-one) Pd complexes have been prepared as they are (partially) models for complexes containing a pendant olefin (see **12-14**) which can be attacked by a nucleophile.

The amount of ion pairing in different solvents (e.g., chloroform or CD_2Cl_2) was estimated using PGSE diffusion constants. The position of the anion with respect to the cation was investigated in connection with steric effects in catalysis using HOESY measurements. The complete NMR description is presented in this section.

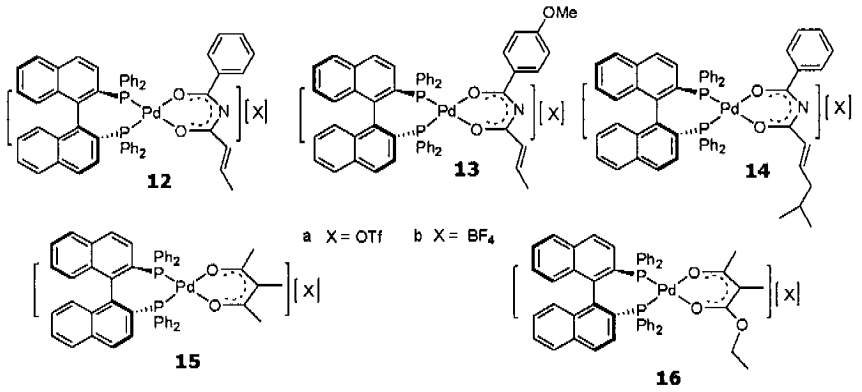

Section **2.1.5** introduces the synthesis and X-ray and NMR structural studies of a imine and chiral amine cyclometallated Pd(II) complexes (**20-27**). These salts are useful in a variety of literature applications e.g., for chiral recognition[4] or in asymmetric synthesis[5].

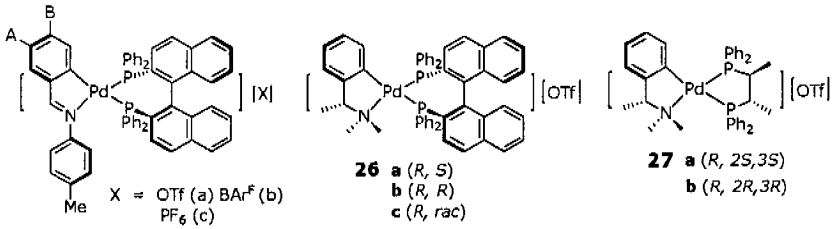

	A	B
20.	Me	H
21.	Cl	H
22.	NO_2	H
23.	OMe	H
24.	H	Me
25.	H	NO_2

The amount of ion pairing and how the nature of a chiral pocket (e.g., (*R*)- or (*S*)- BINAP or Chiraphos) changes the cation/anion interaction was examined using both PGSE diffusion and multidimensional NMR experiments.

Section **2.2**, introduces a series of Rhodium cationic N-heterocyclic carbene complexes (**35** and **36**) (in collaboration with Prof. Whittlesey). These carbene complexes have been used as catalysts in a number of organic transformations[6, 7].

The extent of ion pairing and its dependence on the nature of the anion were investigated using PGSE diffusion data and HOESY measurements.

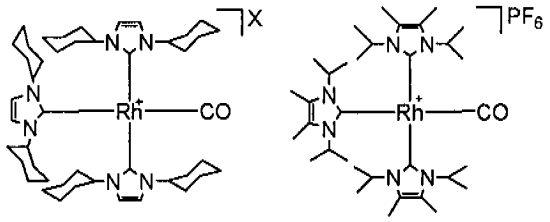

X = **35**[PF_6], **35**[BAr^F] **36**[PF_6]

Finally section **2.3**, offers a discussion on the known Pt(II) complexes (**38-42**). These neutral platinum complexes have been used as model complexes to determine how molecular volumes affect the PGSE diffusion constants (D) and hydrodynamic radii (r_H). Further, it is shown that, the metal nucleus ^{195}Pt can also be used as a diffusion probe (section **2.3.1**) to monitor ion paring or aggregation in special cases.

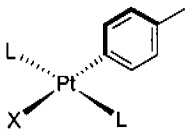

38, L = PEt_3, X = Br
39, L = PEt_3, X = Cl
40, L = PPh_3, X = Cl

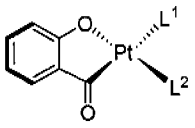

41

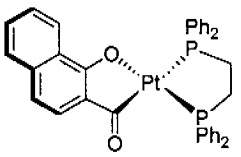

42

The chapter ends with a set of conclusions, with respect to showing how the ion pairing varies with solvent or anion in these catalytically important transition organometallic complexes. The D value, together with HOESY data offers a unique view on the subject of ion pairing.

2.1 Synthesis and Diffusion Studies on Pd(II)-BINAP complexes.

Introduction

Mono and/or dicationic complexes of palladium are widely thought to be involved in a number of catalytic reactions including allylic alkylation[8-10], aldol condensations[11], ene-type Michael additions[3] and hydroamination[1, 2, 12], amongst others. Sodeoka and co-workers[1], and later Hii and co-workers[13-15], have made extensive use of palladium BINAP and *p*-tolyl-BINAP dicationic aquo-complexes, $[Pd(H_2O)_2(BINAP)]^{2+}$ **1**, as catalyst precursors in the enantioselective hydroamination reaction, indicated in eq. 2.1.

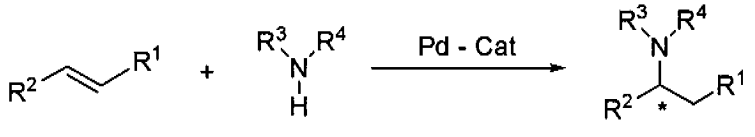

(2.1)

For the enantioselective Michael reaction using 1,3-diketones as substrates, Sodeoka has generated the mono-cationic palladium t-butyl substituted enolate, **A**, shown[1], and found this salt to be a fairly stable and important intermediate.

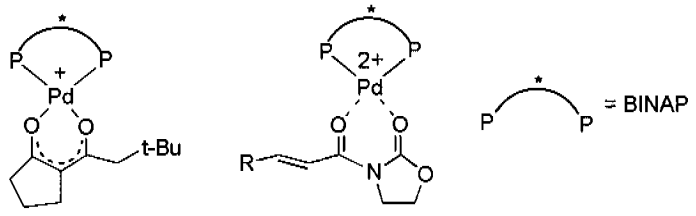

A **B**

This type of chiral palladium complex is also relevant in the area of catalytic enantioselective fluorination. Li and Hii[13], in their studies

on Pd(BINAP) catalysed hydroamination reactions, using unsaturated oxazolidinones as reagents, consider the dicationic chelating intermediate, **B**, shown above, as potentially relevant. Jorgensen and co-workers[16, 17] have proposed a related oxazolidinone complex of nickel.

Occasionally, it has been found to be more convenient to use the hydroxo-bridged dicationic palladium salts, $[Pd(\mu\text{-}OH)(BINAP)]_2^{2+}$, **2**. Sometimes the BF_4^- salts are used as precursors, and on other occasions, the triflate, $CF_3SO_3^-$, analogs. Important differences, in terms of yields and enantioselectivity, between these anions, have been observed[15, 18].

It is now fairly normal to use a number of different anions in cationic palladium chemistry. Occasionally, there are reports suggesting that the anion may play a specific role[19-24], e.g., in determining the nature of the product and/or the reaction kinetics[19]. Generally speaking, the anion may affect the solubility of the catalyst, accelerate or decelerate reactions and occasionally improve reaction selectivity. Presumably the anion is not always "innocent" and may (a) block or actually take up a coordination position (b) affect the cation via ion pairing, or (c) induce aggregation, i.e., significantly change the cation structure.

In the following sections I discuss a series of Pd BINAP (and *p*-tolyl-BINAP) complexes (**1-4**), mono cationic Pd BINAP complexes (**12-17**) containing oxazolidinone and acetylacetonate anions and cyclometallated mono cationic Pd BINAP complexes (**20-26**) (and, lesser extent to Chiraphos (**27**). Finally, using both PGSE and HOESY NMR studies to reveal that how the anions interact.

Synthesis of Complexes (1-4)

The Pd-BINAP aqua and hydroxo complexes were synthesized, as indicated in Scheme 2.1, by preparing the dichloride complex, $PdCl_2$(BINAP or *p*-tolyl-BINAP), and subsequently treating these neutral compounds with the appropriate silver salts to give the bis-aquo-derivatives. The dicationic aquo-complexes, **1**, can be converted to the bridging hydroxo-salts, **2**, by reaction with molecular sieves.[12] The mono-anilide bridged species, **3**, which are intersting in connection with hydroamination catalysis were prepared by addition of an aniline to the bridged hydroxo-complex. The PF_6^- anion is readily hydrolyzed in the presence of the cation to afford the unexpected dicationic salt $[Pd(\mu\text{-}O_2PF_2)(BINAP)]_2(PF_6)_2$, **4**.

Scheme 2.1: Synthesis of the Palladium Complexes[a]

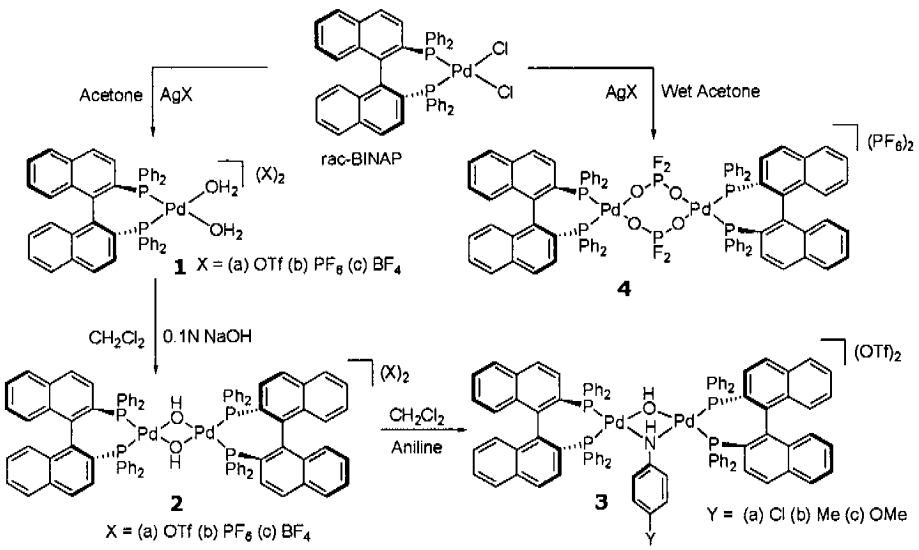

[a] Tha analogous *p*-tolyl-BINAP salts are indiacted in the text by a "prime", e.g., **2a'**

2.1.1 Pd(II)-BINAP Aqua Complexes

The aquo-complexes, **1**, reveal a singlet in their ^{31}P spectra and broad proton resonances at ca δ 3.0 (for the $CF_3SO_3^-$) and ca δ 4.1 (for the BF_4^-) for the two coordinated water molecules.

Diffusion studies. Table 2.1 show PGSE diffusion data for the salts **1**. For the BINAP-cations of the di-aquo-salts, **1**, (and the single Biphemp example), in dichloromethane solution, the corresponding r_H values (calculated from Stokes-Einstein eq, discussed in section **1.3.2.3**) fall in the range 6.2 Å - 6.9 Å (see Table 2.1). These radii are in good agreement with those estimated from Chem3D calculations (shown in the Table 2.1, in parenthesis). The corresponding radii for the $CF_3SO_3^-$ anion, ca 5.8 - 5.9 Å, are much too large for the isolated anion; nevertheless, the anion and cation are not moving at an identical rate. The BF_4^- anion also shows a similar, r_H value[25]. The r_H values for both the $CF_3SO_3^-$ and BF_4^- anions most likely result from a mixture of ion pairing and H-bonding of the anions to the complexed water molecules.

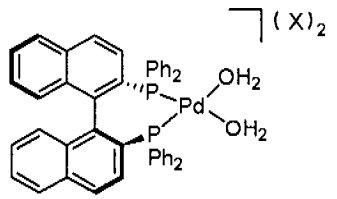

1a, X=OTf; **1b**, X=PF_6; **1c**, X=BF_4
(BINAP)

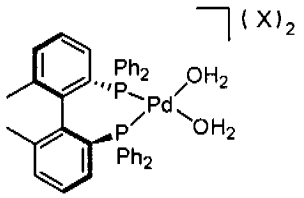

1d, X=OTf
(Biphemp)

In THF solution the values for the cationic radii for **1a** and **1c** are larger and both 7.1 Å, whereas those for the anion are 6.3 Å and 6.8 Å, respectively. Ion pairing is usually more pronounced in THF than in dichloromethane[25]; however, the larger solvent THF

Table 2.1. Diffusion constants, D, and hydrodynamic radii, r_H, for the Pd aquo-complexes.

Compound		CD_2Cl_2		THF	
		D	r_H	D	r_H
1a, OTf	Cation(^{1}H) BINAP	8.22	6.5(6.4)	6.79	7.1
	Anion(^{19}F)	9.26	5.8	7.70	6.3
1a', OTf	Cation(^{1}H) p-Tol-BINAP	7.79	6.9(7.0)		
	Anion(^{19}F)	9.32	5.8		
1b, PF_6	Cation(^{1}H) BINAP			6.99	6.9
	Anion(^{19}F)			10.25	4.7
1c, BF_4	Cation(^{1}H) BINAP	8.33	6.4	6.83	7.1
	Anion(^{19}F)	8.78	6.1	7.04	6.8
1d, OTf	Cation(^{1}H) Biphemp	8.62	6.2		
	Anion(^{19}F)	9.03	5.9		

[a] 400 MHz, 2mM; D values, 10^{-10} m^2 s^{-1} ; r_H values, Å. Numbers in parenthesis are calculated from Chem3D. η (CH_2Cl_2) = 0.410 x 10^{-3} kg m^{-1} s^{-1} at 300 K,η (THF) = 0.456 x 10^{-3} kg m^{-1} s^{-1} at 300 K.

will also contribute to the increase in the cation r_H, relative to dichloromethane solutions. In any case, for **1a**, the percentage increase for cation and anion on going from dichloromethane to THF is ca 9% (7.1/6.5 = 1.09; 6.3/5.8 = 1.08). Taken together, these data for the three salts in THF solution provide a consistent picture for a mononuclear dication strongly, but not completely, associated with the anions.

^{1}H,^{19}F HOESY spectra for the $CF_3SO_3^-$ salt, **1a**, in the two solvents are shown in sections **b** and **c** of Fig. 2.1. The broad resonance for the two bound water molecules is clearly visible. In both solvents the strongest contacts from the fluorine of the anion arise from the *equatorial* P-phenyl aromatic protons. The rather weak contact from the $CF_3SO_3^-$ fluorine to the water is somewhat surprising. Interestingly, in the solid-state structure for $[Pd(H_2O)_2(dppp)](CF_3SO_3)_2$[26] in which the $CF_3SO_3^-$ is clearly hydrogen bonded to a complexed water ligand, the F-H distance is ca 5.9 Å. Consequently, despite the absence of a strong Overhauser effect, we conclude that the anion is relatively strongly H-bonded (and therefore one finds relatively large r_H values) but situated

quite close to one specific P-phenyl group, perhaps as indicated in fragment **C**, thereby explaining the observed relaxation pathway.

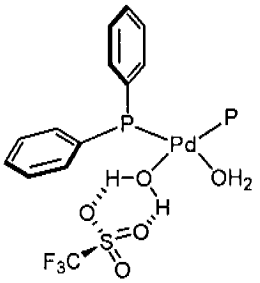

C, fragment showing the proximity of the F-atoms to the *equatorial* P-phenyl.

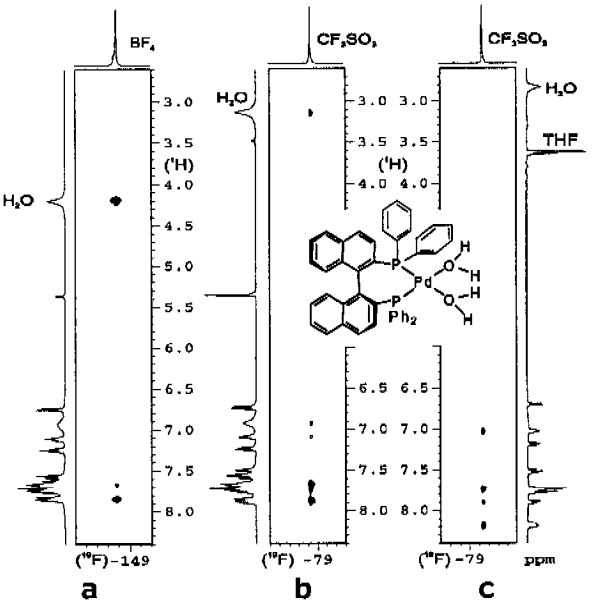

Fig. 2.1. HOESY spectra for (a) **1c** in CD_2Cl_2, (b) **1a** in CD_2Cl_2, and (c) **1a** in THF, all showing selective contacts to the equatorial P-phenyl ring protons. In (a) there is a strong contact to the bound water molecules.

The analogous HOESY spectrum for the BF_4^- salt (Fig. 2.1a) reveals a *strong* contact to the water molecules, and a medium strength contact to the equatorial P-phenyl aromatic protons. Even though the residence time of the BF_4^- anion is not 100%, based on the diffusion data, H-bonding via one of the F atoms (instead of the oxygen in the $CF_3SO_3^-$ anion) brings the anion close enough to the water protons so that this relaxation pathway dominates. In both salts, one finds a selective contact to the equatorial P-phenyl aromatic protons. We conclude that there is not a great deal of

difference between the $CF_3SO_3^-$ and BF_4^- anions in these salts, but this would not be obvious from the Overhauser spectroscopy alone.

2.1.2 Pd(II)-BINAP Bridged Hydroxy Complexes

The characterization of the dinuclear cations, **2**, was assisted by the recognition of the characteristic proton resonance for the μ-OH group at δ ca. -2.9 [12]. Interestingly, all of the BINAP complexes reveal a rather broad aromatic proton resonance between δ 6 and 7. Earlier NMR studies[27-29] have suggested that this signal is associated with restricted rotation of the P-*axial* phenyl (or *p*-tolyl) groups.

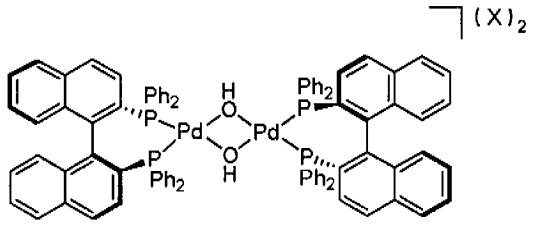

2 X = (a) OTf, (b) PF_6, (c) BF_4

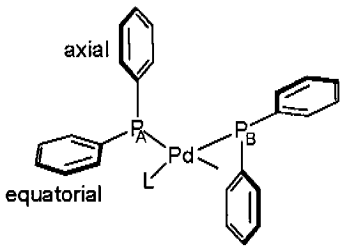

D

L = e.g, H_2O or bridged OH-

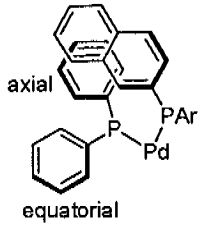

E

stcacking interaction

The axial P_A-aryl group (defined in fragment **D**) experiences a strong steric interaction with the naphthyl moiety associated with P_B (see **E**). In the solid-state these aromatic moieties are usually "stacked"[27, 29, 30]. To confirm the source of the broad line, low

temperature ^{1}H NMR spectra for the bridging hydroxide dinuclear *p*-tolyl salt, **2a'** were measured, and these are shown in Fig. 2.2. The choice of the *p*-tolyl analogs considerably simplifies the ^{1}H spectra and thus helps with the assignments for the conventional BINAP analogues. The broad signal at ca 6.8 ppm disappears as the temperature is lowered and eventually splits into two non-equivalent *ortho* -protons, δ 8.00 and δ 6.72. At the same time two further new *meta* resonances appear, δ 7.21 and δ 6.25. At 213K, the rotation about the P-C(ipso)$_{axial}$ bond is slow and the new broad resonance at δ ca 7.3 corresponds to the equivalent *ortho*-protons of the *equatorial* P(p-tolyl) group. The integration and the various multiplicities are now in agreement with the proposed restricted rotation.

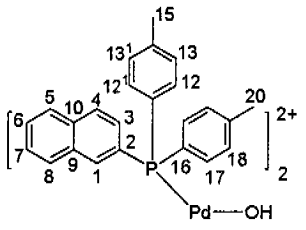

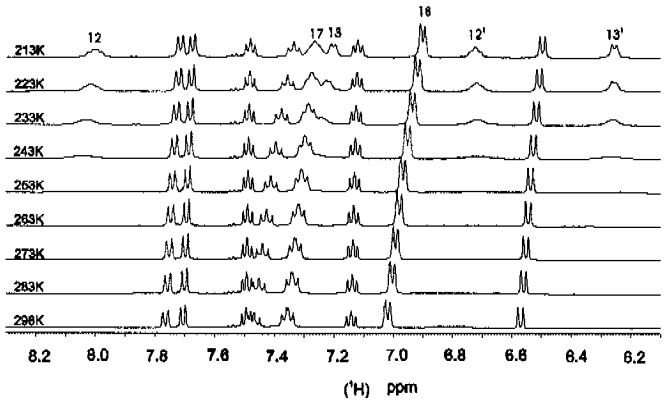

Fig. 2.2. Variable temperature ^{1}H NMR study for **2a'.** There is slow rotation around the P-C(ipso)$_{axial}$ bond at ca. 213K (CD_2Cl_2, 500 MHz).

The ^{31}P,^{1}H correlation for **2a'**, at 213K is given in the lower section of Fig. 2.3 and reveals four sets of cross-peaks: two from the non-equivalent P-axial aryl *ortho* protons, one from the equivalent P-equatorial aryl *ortho*-protons and one set at δ 7.33 for the naphthyl

proton in *ortho* position to the P-atom. The upper trace in Fig. 2.3 shows the same correlation at ambient temperature. The broad resonance at δ ca 6.8 is visible; however only the strong cross-peaks from equivalent P-equatorial aryl *ortho*- protons and those from the *ortho* naphthyl proton are observed. Fig. 2.4 shows a slice of the $^{1}H,^{1}H$ NOESY for **2a'**. The proton from the bridged hydroxide, δ ca -2.9, shows a strong cross-peak only with the equivalent P-equatorial aryl *ortho*-protons, at δ 7.3 (thereby helping to identify these protons), plus a very strong *exchange* cross-peak with ca. 1 equivalent of water, ca δ 1.7. Table 2.2 shows the detailed ^{1}H assignments for this *p*-tolyl salt, **2a'**.

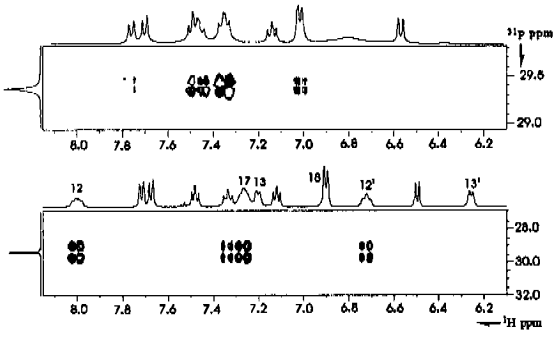

Fig. 2.3. $^{31}P,^{1}H$ correlation for **2a'** at ambient temperature (top) and (below) the same spectrum at 213 K (CD_2Cl_2, 500 MHz).

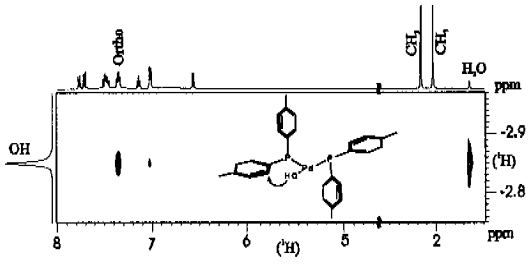

Fig. 2.4. Section of the NOESY spectrum for **2a'** at ambient temperature revealing one strong contact to the *ortho*-protons of the equatorial P-phenyl ring and an exchange cross-peak with water (CD_2Cl_2, 500 MHz).

Crystals of the dinuclear μ-OH salt, **2a,** suitable for diffraction studies were obtained, and a view of this dication is given in Fig. 2.5. The structure of the analogous *p*-tolyl salt has been reported by Sodeoka[2]. The various metric parameters are rather standard

The four-membered Pd-O-Pd-O ring takes on a distorted butterfly shape, that is, the ring is not flat. The dihedral angle between the two tetrahedrally distorted square planar Pd coordination planes is 18.6(1)°.

Table 2.2. ^{1}H NMR data for complex **2a'** (CD_2Cl_2, 500 MHz, 213K)

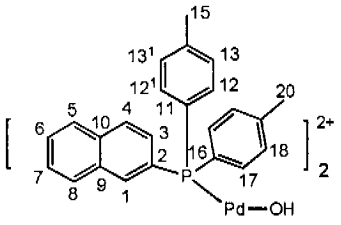

Position	δ ^{1}H
3	7.34
4	7.71
5	6.49
6	7.11
7	7.48
8	7.67
12	6.72
13	6.25
12^1	8.00
13^1	7.20
15	2.11
17	7.26
18	6.90
20	2.03
OH	-2.76

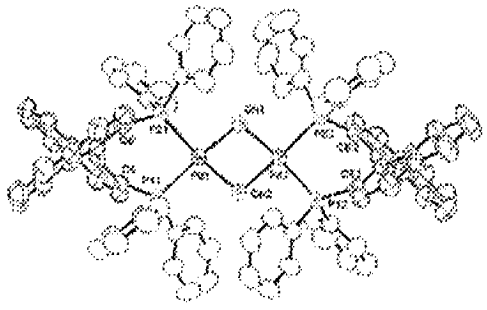

Fig. 2.5. An ORTEP view of the cation of $[Pd(\mu\text{-}OH)(BINAP)]_2(OTf)_2$ **2a** with thermal ellipsoids drawn at the 50% probability level.

Diffusion Studies: For the bridging hydroxide salts, **2a-2c**, in dichloromethane solution, the smaller D-values and thus larger r_H values, relative to **1a-1c** (see Table 2.3). The ratio of D-values (e.g., 8.22/6.63 = 1.24) is in excellent agreement with ca. double the volume of **2a** relative to **1a**[31]. The r_H values of ca 8.0 - 8.4 Å are in good agreement with estimations based on X-ray data. The

few *p*-tolyl-BINAP salts, **2a´** and **2c´** are, as expected, slightly larger due to the added methyl groups. The r_H values for the three anions, $CF_3SO_3^-$, PF_6^- and BF_4^-, are rather similar, and, relative to the r_H values for the cations, modest in size. The r_H value for the $CF_3SO_3^-$ is now much smaller than in **1a**. The cation/anion ratio for **2a** is ca 1.42 whereas this ratio for **1a** is 1.12. Assuming that the anions will prefer to avoid the (formally) negatively charged OH group, attribute these modest anion r_H values to 45-55% ion pairing, that is what one normally finds in dichloromethane solution for a number of different transition metal salts[25]. For **2a** in THF solution the r_H values suggest a much larger percentage of ion pairing. There seems to be no important differentiation between these anions in these salts.

Table 2.3. Diffusion constants, D, and hydrodynamic radii, r_H, for the bridged hydroxy-palladium complexes, **2**.

Compound		CD_2Cl_2		THF	
		D	r_H	D	r_H
2a, OTf	Cation(^{1}H) BINAP	6.63	8.1 (8.1)	5.33	9.0
	Anion(^{19}F)	9.40	5.7	5.94	8.1
2a', OTf	Cation(^{1}H) p-tol-BINAP	6.34	8.5 (8.4)		
	Anion(^{19}F)	9.43	5.7		
2b, PF_6	Cation(^{1}H) BINAP	6.67	8.0		
	Anion(^{19}F)	9.93	5.4		
2c, BF_4	Cation(^{1}H) BINAP	6.67	8.0		
	Anion(^{19}F)	9.76	5.5		
2c', BF_4	Cation(^{1}H) p-tol-BINAP	6.39	8.4		
	Anion(^{19}F)	9.86	5.4		

[a] 400 MHz, 2mM; D values, 10^{-10} m^2 s^{-1} ; r_H values, Å. Numbers in parenthesis are calculated from Chem3D. $\eta(CH_2Cl_2)$ = 0.410 x 10^{-3} kg m^{-1} s^{-1} at 300 K, η(THF) = 0.456 x 10^{-3} kg m^{-1} s^{-1} at 300 K.

^{1}H,^{19}F HOESY spectra for the *p*-tol BINAP $CF_3SO_3^-$ and BF_4^- salts **2a´** and **2c´**are shown in Fig. 2.6. The strongest contacts stem from the aromatic region and these five to six cross-peaks can be assigned to protons from *both* the pseudoaxial and pseudo-equatorial P-aryl groups. Indeed, there are also weak cross-peaks

both *p*-tolyl methyl groups. As expected there is little or no contact to the low-frequency OH proton.

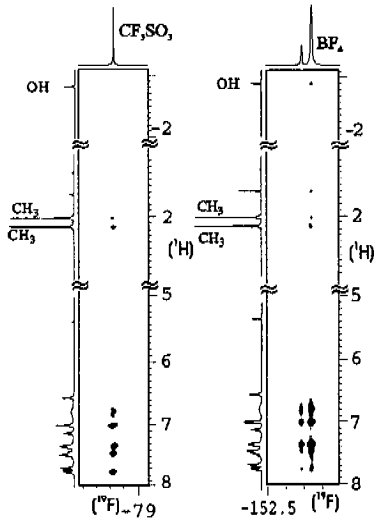

Fig. 2.6. HOESY spectra for **2a'** ($CF_3SO_3^-$) and **2c'** (BF_4^-), The spectra show selective contacts to both the equatorial and axial P-phenyl ring protons.

In collaboration with Prof. L.F Veiros, DFT calculations[32] were performed in order to assist in the interpretation of the HOESY results. The geometries of the two mononuclear complexes, the model cation $[Pd(H_2O)_2(Ph_2CH_2CH_2Ph_2)]^{2+}$, and $[Pd(H_2O)_2(BINAP)]^{2+}$ (**1**), plus one dinuclear species, $[Pd(\mu\text{-}OH)(BINAP)]_2^{2+}$ (**2**), were fully optimized. The optimized structure of **2** is represented in Fig. 2.7. In all cases, the coordination environment around each metal atom is square planar, as expected for Pd(II) complexes. The calculated Pd–P distances (2.29 and 2.30 Å for dppe, and 2.31–2.34 Å for BINAP) are close to the experimental values[33], as are those for Pd–O(H_2O) (2.22–2.25 Å) and Pd–O(OH) (2.09–2.10 Å) separations. Interestingly, the structure optimized for the dinuclear complex **2** confirms the proposed stacking interaction shown in **E**.

The charge distribution on the optimized complexes was evaluated by means of a Natural Population Analysis (NPA)[34-36],

and the atomic charges calculated for the metal and the coordinating atoms were for (a) the dppe complex; O: –0.94/–0.95;

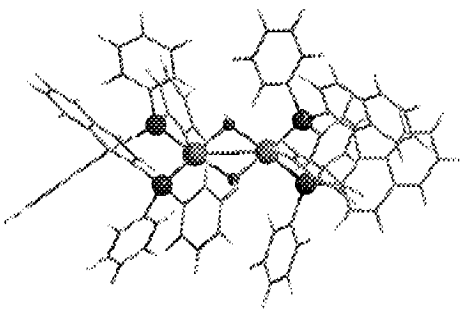

Fig. 2.7. Optimized geometry (B3LYP) for $[Pd(\mu\text{-}OH)(BINAP)]_2^{2+}$. The Pd, P and O atoms are highlighted. (Gas phase analysis)

(b) **8**; Pd: +0.37; P: +1.30; O: –0.95 and (c) **9:** Pd: +0.46/+0.47; P: +1.21 to +1.23 ; O: –1.00. In all three cases, the P-atoms carry the largest amount of positive charge (1.0 – 1.2) and the palladium atoms possess considerably less positive charge, (0.4–0.5). Although these results should not be taken as quantitative, they indicate that the anions are expected to seek out the P-atoms, preferentially. The calculations performed do not account for the H-bonding associated with anions in the aquo-complexes[37, 38], but the NPA charges obtained allow a rationale for the results obtained from the dinuclear dications, **1-4.**

Given the DFT calculations, one can suggest that the anions approach the positive phosphorus and metal centers in such a way as to see both rings, perhaps as suggested by fragment **F**.

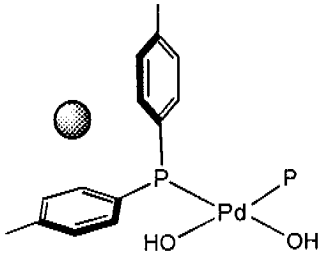

F fragment of the dinuclear complex

2.1.3 Pd(II)-BINAP Bridged Anilide Complexes

The NMR characterization for the bridging hydroxy-anilide dinuclear palladium complexes, **3**, was not trivial. Fig. 2.8 (down) shows a typical ^{31}P NMR spectrum along with a simulation for this ABCD spin system.

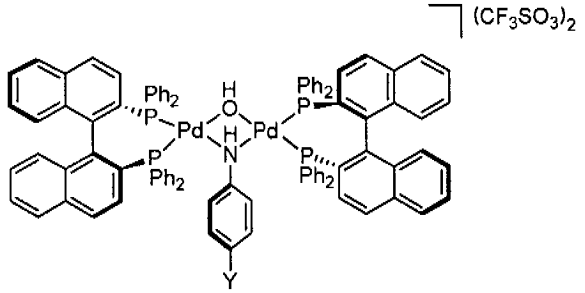

3, Y = (a) Cl, (b) Me, (c) Ome

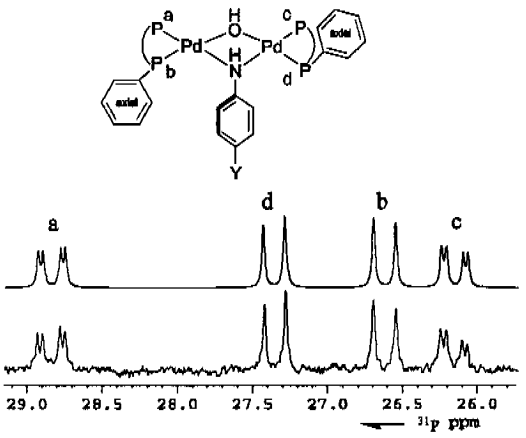

Fig. 2.8. (top) Simulated and (bottom) experimental ^{31}P spectra for salt **3a** in CD_2Cl_2. J_{ab} = 24.07 Hz, J_{ac} = 5.14 Hz, J_{cd}= 23.23 Hz, J_{bd} = 0.5 Hz, J_{bc} = 0.5 Hz, J_{ad} = 0.5 Hz (400 MHz, 298 K).

It is clear that the two ^{31}P-spins in *trans* positions to the μ-OH group are chemically different than the two ^{31}P-spins in *trans* positions to the μ-NH(*p*-RC_6H_4) moiety. The non-equivalence within for example, the two ^{31}P-spins in *trans* positions to the μ-OH group, arises due to the position of the bridging anilide ring with respect to the two axial (or equatorial) rings of the two PPh_2 groups. The solid-state structure for **3b**, shown in Fig. 2.9, confirms that the

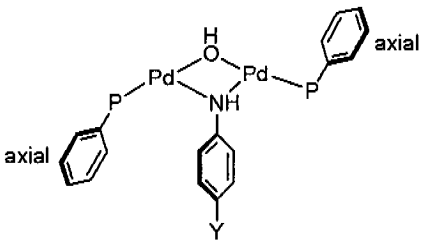

G

anilide ring is proximate to one of these two axial rings, but remote from the second ring, thereby making all four ^{31}P spins chemically non-equivalent (see **G**).

In the solid-state structure of the di-cation, $[Pd_2(\mu\text{-}OH)(\mu\text{-}\{NH(p\text{-}Tol)\})(BINAP)_2](CF_3SO_3)_2$, **3b**, the local coordination geometry about each Pd atom is distorted square planar. The four-membered ring made up by the two Pd atoms and the bridging N and O atoms is not planar; however, the four Pd-P bond lengths, Pd1–P1 223.5(2) pm, Pd1–P2 226.2(1) pm, Pd2–P3, 222.9(1) pm and Pd2–P4 226.9(1) pm, are not very different and relatively standard[39]. Further, the Pd1–O1, 204.9(4) pm, and Pd1–N1, 211.9(4) pm bond lengths are as expected. The two P-Pd-P angles, P1–Pd1–P2 92.32(5)°, and P3–Pd2–P4 90.56(5)° are typical of Pd-BINAP complexes[40-42].

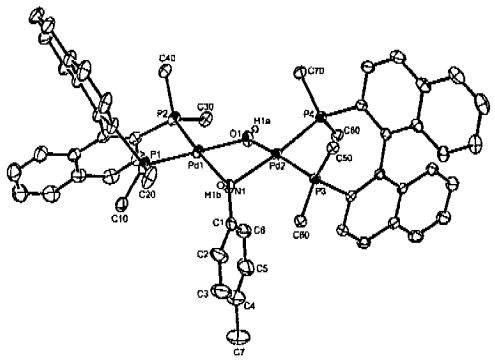

Fig. 2.9. Structure of the dication $[Pd_2(\mu\text{-}OH)(\mu\text{-}\{NH(p\text{-}Tol)\})(BINAP)_2]$ of **3b**. Thermal ellipsoids are drawn at 30% probability; OTf^- anions and solvent molecules have been omitted for clarity; For the BINAP-P phenyl moieties only the *ipso*-carbon atom is shown.

The bridging OH protons appear at slightly lower frequency, ca δ -3.7 to -4.0. Since the NH proton of the anilide does not exchange very rapidly, this signal could be used to detect the nitrogen-15

chemical shift, in **3c**, via an HMQC spectrum (see Fig. 2.10). The ^{15}N chemical shift difference between the uncomplexed aniline and the coordinated $[ArNH]^-$ is 25.1 ppm.

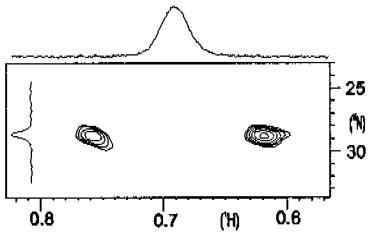

Fig. 2.10. ^{15}N, ^{1}H HMQC spectra for **3c** in CD_2Cl_2 (500 MHz, 213 K, δ ^{15}N = 52.5 for the ligand *p*-MeO-$C_6H_4NH_2$.).

Diffusion Studies: Diffusion data for the $CF_3SO_3^-$ anions of the bridging anilide salts, **3a-3c**, in both dichloromethane and THF, are given in Table 2.4. In dichloromethane solution, the D and r_H values are in good agreement with what one would expect based on the X-ray data for **3b**. The slight increase in size, relative to for example, **2a**, is likely related to the added anilide fragment. The r_H values for the $CF_3SO_3^-$, ca 5.6-5.7 Å, are similar to those found for **2a**. Changing the solvent to THF again results in an increase in the size of the cation due to the change in the ion pairing.

Table 2.4. Diffusion constants[a], D, and hydrodynamic radii, r_H, for the palladium bridged anilide and PO_2F_2 complexes.

Compound		CD_2Cl_2		THF	
		D	r_H	D	r_H
3a	Cation(^{1}H) BINAP	6.46	8.3	5.09	9.5
(Cl)	Anion(^{19}F)	9.49	5.6	5.89	8.2
3b	Cation(^{1}H) BINAP	6.51	8.2 (8.3[b])	5.04	9.5
(Me)	Anion(^{19}F)	9.56	5.6	6.41	7.6
3c	Cation(^{1}H) BINAP	6.38	8.4	5.05	9.5
(OMe)	Anion(^{19}F)	9.32	5.7	5.81	8.3
4	Cation(^{1}H) BINAP	6.06	8.8		
	Anion(^{19}F)	9.81	5.5		

[a] 400 MHz, 2mM; D values, 10^{-10} m^2 s^{-1} ; r_H values, Å. $\eta(CH_2Cl_2)$ = 0.410 x 10^{-3} kg m^{-1} s^{-1} at 300 K, η(THF) = 0.456 x 10^{-3} kg m^{-1} s^{-1} at 300 K. [b] From the X-ray data.

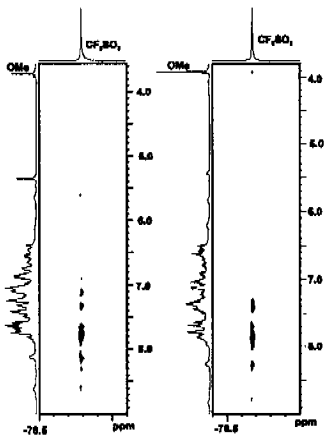

Fig. 2.11. HOESY spectra for **3c** in CD_2Cl_2 (left) and **3c** in THF-d_8 (right) (400 MHz, 298 K).

The $^{1}H,^{19}F$ HOESY spectra for **3c** (Fig. 2.11) in both solvents reveal five to six strong contacts in the aromatic region; however due to the low symmetry of this complex, there is a great deal of overlap and these aromatic protons cannot be readily assigned.

Dinuclear complex **4**, is recognized via the observed multiplicities for the PF_2 moiety in the ^{31}P and ^{19}F spectra. This type of species has been reported on several occasions[43-46] and it is useful to note that it does not readily form in tetrahydrofuran (THF), but rather preferentially in dichloromethane solution. Presumably, occasional weak palladium complexation (and/or H-bonding) of the PF_6 ion will occur in dichloromethane solution, thereby facilitating the hydrolysis, whereas in THF, a solvent which is much stronger ligand relative to dichloromethane, this process is suppressed.

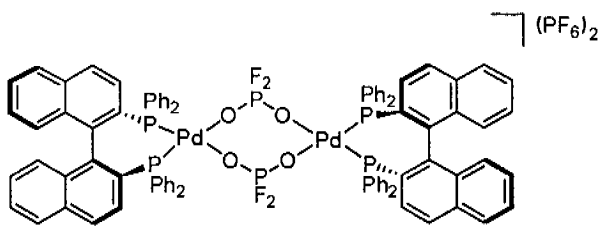

4

Diffusion studies. Table 2.4 also shows diffusion data for the dinuclear salt $[Pd(\mu\text{-}O_2PF_2)(BINAP)]_2(PF_6)_2$, **4**, and the D and r_H values are consistent with the related dinuclear species reported in Tables 2.3 and 2.4.

Yellow crystals of the complex $[Pd(\mu\text{-}O_2PF_2)(BINAP)]_2(PF_6)_2$, **4**, were obtained from dichloromethane / diethyl ether solution at 4° c. Surprisingly, an X-ray diffraction study reveals the product to be neutral $[Pd(O_2PF_2)_2(BINAP)]$, **5** and not to be the more common bridged structure **4**. It is believed that the formation of **5** is due to partial hydrolysis of the PF_6^- anion. The solid state structure of the complex **5**, shown below in Fig. 2.12.

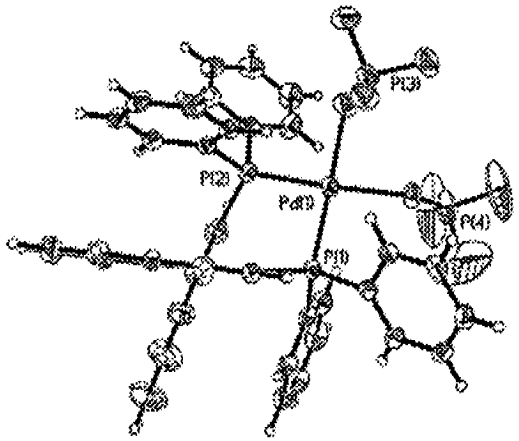

Fig. 2.12. Structure of the neutral $[Pd(O_2PF_2)_2(BINAP)]$, **5**.

2.1.4 Pd (II)-BINAP-Mono Cationic Complexes

Synthesis of Complexes (12-17):

The mono-cationic Pd(II) BINAP complexes, **12** to **16**, are prepared by reacting complex **2a-b** with the unsaturated N-imides **6**, **7** and **8**, or the 1,3-dikeotones **9** and **10** (see Scheme 2.2). The crotonyl oxazolidinone [(E)-3-but-2-enoyloxazolidin-2-one], **11**, coordinates to the Pd(BINAP) fragment via chelation of the two oxygen atoms to form a new complex **17** (see Eq. 2.2).

Scheme2.2

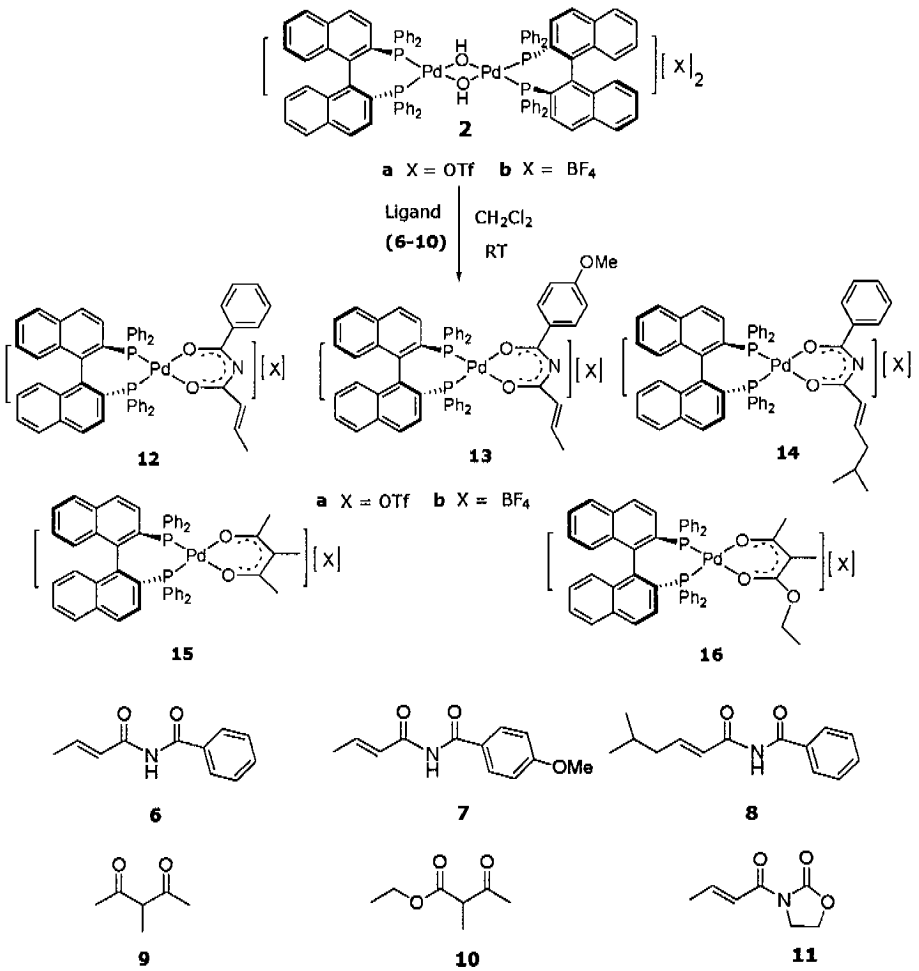

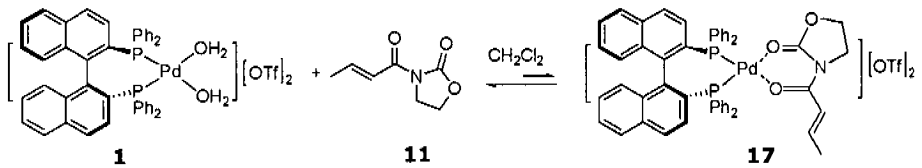

1 **11** **17** (2.2)

Solution structures.

The reaction of **2a-b** (anion = **a**, $CF_3SO_3^-$, **b**, BF_4^-) with ligands (**6-8**) produces one equivalent of water via the deprotonation of the weakly acidic N**H** proton and the generation of Pd(II) salts **12-14.** The new products are readily identified via NMR spectroscopy.

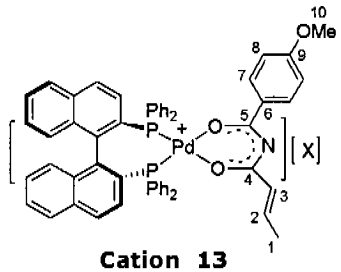

Cation 13

The ^{31}P spectra reveals non-equivalent phosphorus nuclei e.g., for the $CF_3SO_3^-$ complex, **13a**, δ 35.5, and δ 35.1 with $^2J(PP)$ = 33.5 Hz. In the ^1H NMR spectrum, one finds new resonances for the methyl and olefinic protons. Specifically, the C**H**$_3$, is found at δ 1.6, and the two olefinic resonances, $CH_3C\mathbf{H}=C\mathbf{H}$, as a tightly coupled spin system at δ 5.7-5.9. The corresponding ligand positions for **7** are δ 2.0, for the methyl signal, and δ 7.1-7.2 for the $CH_3C\mathbf{H}=C\mathbf{H}$ moiety. We believe that several of these low frequency chemical shifts in **13a** arise from a mixture of anisotropic (P-phenyl on the BINAP proximate to the olefin) and chelation effects.

Continuing, in the $^{13}C\{^1H\}$ NMR spectrum of **13a**, the two olefinic carbons, C2 and C3, are found at δ 145.9 ($CH_3\mathbf{C}H=CH$), and δ 129.6 ($CH_3CH=\mathbf{C}H$). These values do *not* correspond to a coordinated olefin as the coordination chemical shifts, Δδ (= δ for **13a** - δ for **7**), are only -0.7 ppm and 4.9 ppm, respectively. It is useful to note that the deprotonation and complexation of **7** results in a small *low*

frequency (-0.7 ppm) change in the β-olefinic carbon chemical shift. This is not what one expects if this position is to be more electrophilic and thus more readily attacked by an amine nucleophile. A 2D $^{13}C,^{1}H$ long-range correlation reveals the two amide carbonyl carbons at δ 172.8 and δ 173.2. These chemical shift values are consistent with chelation of the anion of **7** to the metal through the oxygen atoms. Similar $^{31}P\{^{1}H\}$, ^{1}H and $^{13}C\{^{1}H\}$ NMR data were found in complexes **12** and **14**.

In a similar fashion, addition of ligands **9** or **10** to a dichloromethane solution of the bridged complexes **2a-b** (anion = **a**, $CF_3SO_3^-$, **b**, BF_4^-) results in the abstraction of the weakly acidic C**H** proton and the generation of Pd(II) enolate complexes **15** and **16**, respectively. For complex **16a**, in dichloromethane solution at room temperature, the $^{31}P\{^{1}H\}$ NMR spectrum shows an AX doublet, $^{2}J(PP)$ = 38 Hz, with the resonances appearing at δ 30.3 and δ 34.8. In the ^{1}H NMR spectrum the absence of doublet multiplicity associated with the central methyl group is consistent with the deprotonated and complexed ligand. Further, the OCH_2 moiety now appears as two diastereotopic CH_2 protons, δ 2.65 and δ 2.90, shifted to low frequency due to the proximate P-phenyl aromatic ring. In the $^{13}C\{^{1}H\}$ NMR spectrum, the central carbon, between the two carbonyl carbons, appears at δ 90.5, Δδ, 29 ppm, and is no longer attached to a proton. The 2D $^{13}C,^{1}H$ long-range correlation reveals the two carbonyl carbons (**C**OMe, **C**OOC_2H_5) at δ 184.2 and δ 169.8, respectively. This same ^{13}C correlation allows one to assign the two, singlet, ^{1}H methyl groups of **16a** in that the signal at δ 1.70 reveals cross-peaks to *both* ^{13}C carbonyl resonances, via the two different $^{3}J(^{13}C,^{1}H)$ pathways.

NMR characterization of dicationic complex, **17**. The addition of ligand **11** to the precursor complex $[Pd(\mu\text{-}OH)(BINAP)]_2(CF_3SO_3)_2$, **2a** in dichloromethane does not yield complex **17**. However, reaction of ligand **11** with the aquo-complex, $[Pd(H_2O)_2(BINAP)]_2(CF_3SO_3)_2$, **1a**, in dichloromethane solution, affords a mixture which, via a low temperature measurement, can be shown to contain ca 16% of **17** plus unreacted starting material (see Fig. 2.13).

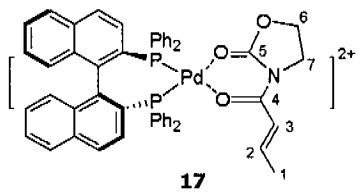

17

Both the ^1H and $^{31}P\{^1H\}$ spectra at room temperature gave broad resonances suggesting dynamic behaviour. The $^{31}P\{^1H\}$ NMR spectrum, which revealed a single broad peak at ca. δ 36.2 at room temperature, sharpens on cooling to 213 K into a sharp singlet along with an AX spin system containing signals at ca. δ 35.5 and ca. δ 37.5, $^2J(PP)$ = 9.5 Hz.

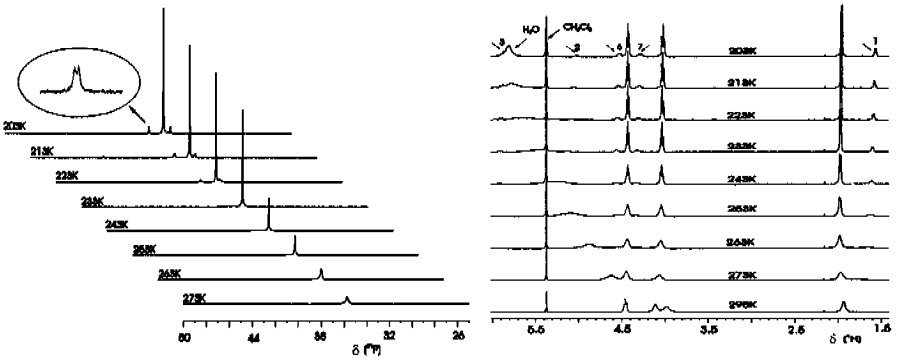

Fig. 2.13. The variable temperature ^{31}P (left) and ^1H (right) NMR spectra showing complex **17**. The AX spin system in $^{31}P\{^1H\}$ spectra is visible (CD_2Cl_2, 20 mM, 500 MHz).

Cooling of the solution to 203 K changes and resolves the broad ^1H NMR spectrum for this solution and reveals new proton resonances

for the minor component, **17** (see Fig. 2.13) and these chemical shift data are given in Table 2.5. It is observed that one of the olefinic resonances of **17** overlaps a water signal. The conventional.$^{13}C\{^1H\}$ NMR spectrum and the 2D $^{13}C,^1H$ long-range correlation both reveal the two **CH** olefin carbons, C2 and C3, at δ 157.3 and δ 119.5, respectively (Table 2.5). These values, once again, are not consistent with olefin complexation. The C2 and C3 coordination chemical shifts, $\Delta\delta$ (= δ for **17** - δ for **11**), are + 9.1 ppm and -1.6 ppm, respectively, that is, complexation of **11** results in a very significant *high frequency* (+ 9.1 ppm) changein the β-olefinic carbon chemical shift. These ^{13}C values are not consistent with direct olefin coordination but the relatively large change for the β-olefinic carbon *is* what one expects if this carbon atom is to become more electrophilic through complexation and thus more readily attacked by a nucleophile. This is in contrast to what one finds for the ^{13}C data for **13**, noted above.

Table.2.5. ^1H and ^{13}C chemical shift data[a] for complex **17** and oxazolidinone, **11.**

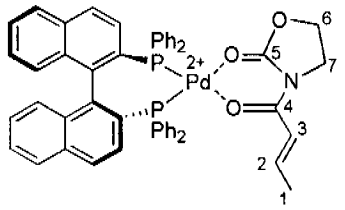

Position	δ ^1H	δ ^{13}C
	11	
1	1.95	19.5
2	7.1-7.2	148.2
3	7.1-7.2	121.1
4	-	165.8
5	-	154.7
6	4.01	63.0
7	4.40	43.5
	17	
1	1.56	19.0
2	5.01	157.3
3	5.86	119.5
4	-	165.4
5	-	158.8
6	4.50	66.2
7	4.28	45.7

[a] δ ^{31}P = 37.4 , δ = 35.6, $^2J(^{31}P,^{31}P)$ = 9.5 Hz. 400 MHz, 203K CD_2Cl_2.

From a phase sensitive $^1H,^1H$ NOESY spectrum at 203 K, one finds exchange cross peaks arising from the free oxazolidinone, **11** and the chelated ligand in complex **17** (see Fig. 2.14).

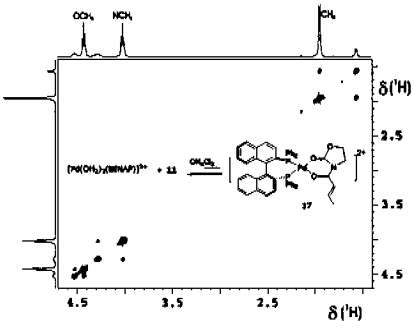

Fig. 2.14. Section of $^1H,^1H$ NOESY spectra of complex **17**, showing exchange between free ligand **11** and chelated ligand in complex **17** (CD_2Cl_2 500 MHz, 203 K).

The ease with which model salt **17** exchanges the complexed chelating ligand is clearly important for the mechanism of a catalytic reaction involving this type of substrate, since the addition product, once formed, must dissociate from the palladium to make room for the new substrate. While **17** represents only a minor component, it is obviously stable enough to be characterized, and is clearly relevant to the palladium catalysed hydroamination chemistry noted in the introduction.

X-ray data. The solid-state structures of *two* separate forms of the BF_4^- complex, **15b** and **15b•CH_2Cl_2** were determined by X-ray diffraction methods. Initially it was thought that two different materials had re-crystallized; however as can been from (Fig. 2.15a), one form of the salt **15b** can be thought of as a tight ion pair whereas the second form (Fig. 2.15b) contains a dichloromethane solvent molecule, packed in approximately a fifth coordination position together with a relatively remote BF_4^- anion. Together these structures represent an unprecedented example of a salt where *both* the structures of the solvent stabilized cation and the tight ion-paired salt can be characterized. This is, admittedly, a

fortunate coincidence, in that the solution diffusion studies reveal only an average D-value for the two ions; nevertheless, these solid-state data help us to envision structural aspects of these two extreme forms.

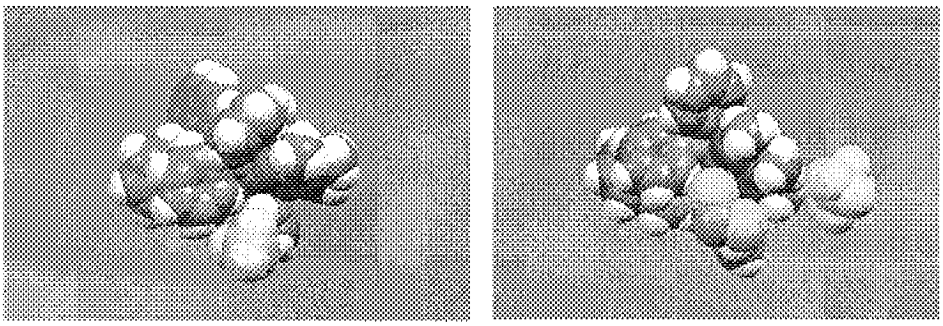

a b

Fig. 2.15. (a) Views of the ion-paired (**15b**) and (b) the solvent separated (**15b**.CH_2Cl_2) salts.

The two-palladium cations are not very different and a view of them are shown in Fig. 2.16. The local coordination geometry about the Pd-atoms is distorted square planar and the metric values for the two cations do not differ significantly (see Table 2.6). The various Pd-donor atoms separations are normal[39] as are the local coordination angles about the palladium atoms. However, we note that, to accommodate the square planar structure, the acetyl acetonate angles, O(1)-C(2L)-C(3L) = 126.1(4)°, and O(2)-C(4L)-C(3L) = 127.1(4)°, in both cations, are larger than the 120° values expected for sp^2 hybridization. As expected, the chiral pocket for the coordinated BINAP ligand reveals pseudo-axial and pseudo-equatorial P-phenyl groups[47-50].

There are two further modest structural differences between these two compounds: (1) The dihedral angle between the complexed

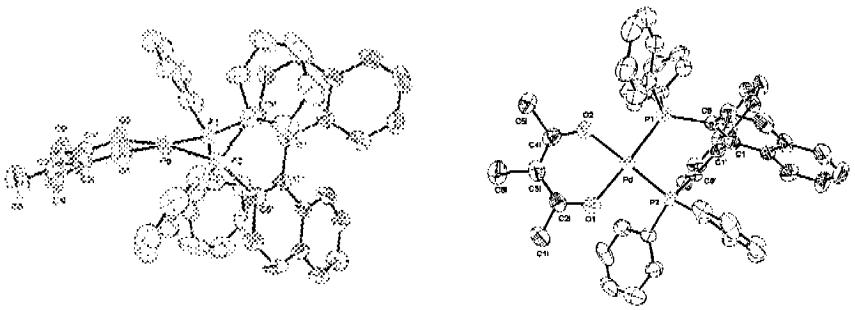

Fig. 2.16. An ORTEP view of the (left) cation of **15b** and (right) **15b**.CH_2Cl_2.

acac ligand and the Pd,O1,O2,P1,P2 plane is 5.3(8)° for the CH_2Cl_2 solvated salt and 23.9° for the tight ion pair. Consequently, the coordinated acac is bent away from the closely positioned BF_4^- anion. (2) The Pd-P distances are slightly longer (>5σ) for the CH_2Cl_2 solvated salt than for the tight ion pair.

These do not represent major structural changes; however, they do indicate that the cation is responding to the two different environments.

Table 2.6. Bond lengths (Å) and bond angles (°) for complex **15b**.

	15b.CH_2Cl_2		
Pd-O(2)	2.026(3)	Pd-O(1)	2.025(3)
Pd-P(1)	2.259(1)	Pd-P(2)	2.264(1)
P(1)-C(111)	1.811(4)	P(1)-C(121)	1.825(4)
P(1)-C(6)	1.838(4)	P(2)-C(221)	1.818(3)
P(2)-C(6')	1.825(4)	P(2)-C(211)	1.822(4)
O(1)-C(2L)	1.292(5)	O(2)-C(4L)	1.281(5)
O(2)-Pd-O(1)	89.0(1)	O(2)-Pd-P(1)	89.23(9)
O(1)-Pd-P(1)	174.2(1)	O(2)-Pd-P(2)	177.3(1)
O(1)-Pd-P(2)	90.42(9)	P(1)-Pd-P(2)	91.57(3)
B-F (av.)	1.4(3)	F-B-F (av)	107(1)

		15b	
Pd-O(2)	2.021(4)	Pd-O(1)	2.032(4)
Pd-P(1)	2.251(2)	Pd-P(2)	2.253(2)
P(1)-C(121)	1.802(6)	P(1)-C(111)	1.823(6)
P(2)-C(221)	1.819(6)	P(2)-C(211)	1.799(5)
P(1)-C(6)	1.834(5)	P(2)-C(6')	1.837(8)
O(1)-C(2L)	1.275(7)	O(2)-C(4L)	1.276(7)
O(2)-Pd-O(1)	88.3(2)	O(2)-Pd-P(1)	88.5(1)
O(1)-Pd-P(1)	176.9(1)	O(2)-Pd-P(2)	171.4(1)
O(1)-Pd-P(2)	90.8(1)	P(1)-Pd-P(2)	92.32(5)
B-F (av.)	1.25(3)	F-B-F (av.)	108(2)

Diffusion studies. PGSE diffusion data for the Pd(BINAP) $CF_3SO_3^-$ and BF_4^- salts, **12-16** in dichloromethane solution are given in Table 2.7. The r_H values for cations fall in the range of 6.2 Å - 7.2 Å (Table 2.7) and are in reasonable agreement with our earlier data on Pd BINAP complexes[51]. For **15b**, the r_H value of 6.2 Å is in excellent agreement with the $r_{x\text{-}ray}$ value of 6.3 Å found for the ion paired structure, and only slightly smaller than the $r_{x\text{-}ray}$ value of 6.5 Å found for the dichloromethane solvated species. The corresponding radii for the $CF_3SO_3^-$ anion, 4.0 Å - 4.5 Å, are somewhat larger than the values estimated for the solvated anion in methanol solution (ca 3 Å [50, 52]). Clearly, the anion and cation are not moving at an identical rate. The BF_4^- anion shows r_H values in the range 3.8 Å - 3.9 Å (Table 2.7), which are also bit larger than for the isolated anion in methanol solution[50, 52]. As in previous studies we assign these results to partial ion pairing in dichloromethane solution.

In THF solution the r_H values for the cations of the $CF_3SO_3^-$ salts, **12a** to **16a,** are larger and fall in the range of 7.0 Å - 7.8 Å (Table 2.8), whereas those for the anion now span the range are 5.0 Å - 5.3 Å. As expected, these increased radii in THF solution indicates

Table 2.7. Diffusion constants [a] and radii[b] for complexes **12** to **16** in CD_2Cl_2.

	CD_2Cl_2											
	a ($CF_3SO_3^-$)						**b** (BF_4^-)					
comp	Cation(^1H)			Anion(^{19}F)			Cation(^1H)			Anion(^{19}F)		
	D	r_H	(r_H)	D	r_H	(r_H)	D	r_H	(r_H)	D	r_H	(r_H)
12	8.11	6.5	(7.1)	13.13	4.0	(5.0)	8.00	6.6	(7.1)	13.70	3.9	(4.8)
13	8.02	6.6	(7.1)	11.86	4.5	(5.2)	7.74	6.8	(7.3)	13.96	3.8	(4.8)
14	7.35	7.2	(7.7)	13.39	4.0	(4.9)	7.79	6.8	(7.3)	14.06	3.8	(4.8)
15	8.27	6.4	(7.0)	12.40	4.3	(5.1)	8.53	6.2	(6.8)	14.02	3.8	(4.8)
16	8.11	6.5	(7.1)	11.70	4.5	(5.3)	8.37	6.3	(6.9)	14.02	3.8	(4.8)

[a] 400 MHz, 2mM; D values, 10^{-10} m^2 s^{-1} ; [b] r_H values, Å; "c" corrected[53] r_H values are in brackets. Estimated radii for the solvents r_{vdw} = 2.49 (CD_2Cl_2), $\eta(CH_2Cl_2)$ = 0.414 x 10^{-3} kg m^{-1} s^{-1} at 299 K.

that the ion pairing is more pronounced in THF than dichloromethane solution. In any case, the r_H values for the cations and anions in THF solution suggest that these mono cations are more strongly, but not completely, associated with the anions.

Table 2.8. Diffusion constants [a] and radii[b] for **12a-16a** in THF-d_8, $CDCl_3$ and, for **15**, in CD_3CN.

	a ($CF_3SO_3^-$)											
	THF						$CDCl_3$					
comp	Cation(^1H)			Anion(^{19}F)			Cation(^1H)			Anion(^{19}F)		
	D	r_H	(r_H)	D	r_H	(r_H)	D	r_H	(r_H)	D	r_H	(r_H)
12	6.43	7.4	(7.9)	9.25	5.1	(6.0)	5.66	7.2	(7.8)	5.96	6.9	(7.4)
13	6.28	7.6	(8.1)	9.30	5.1	(6.0)	5.53	7.4	(7.9)	6.46	6.3	(6.9)
14	6.06	7.8	(8.4)	8.93	5.3	(6.1)	5.26	7.8	(8.2)	6.08	6.7	(7.4)
15	6.78	7.0	(7.6)	9.24	5.1	(6.0)	5.82	7.0	(7.6)	6.30	6.5	(7.1)
16	6.55	7.3	(7.8)	9.43	5.0	(5.9)	5.88	7.0	(7.5)	6.29	6.5	(7.1)

	CD_3CN			
15	10.22	6.2	23.86	2.7

[a] 400 MHz, 2mM; D values, 10^{-10} m^2 s^{-1} ; [b] r_H values, Å; "c" corrected r_H values. are in brackets. Estimated radii for the solvents: r_{vdw} = 2.68 (THF), r_{vdw} =2.60($CDCl_3$), $\eta(CHCl_3)$ = 0.534 x 10^{-3} kg m^{-1} s^{-1} at 299 K, η(THF) = 0.461 x 10^{-3} kg m^{-1} s^{-1} at 299 K. $\eta(CH_3CN)$ = 0.345 x 10^{-3} kg m^{-1} s^{-1} at 299 K.

Continuing with the $CF_3SO_3^-$ salts, using $CDCl_3$ as solvent, the r_H values for cations are even larger and fall in the range of 7.2 Å -

7.8 Å. The corresponding radii for the $CF_3SO_3^-$ anion, ca. 6.3 Å - 6.9 Å (Table 2.8), are now ca 2 Å larger than in dichloromethane. These cation and anion r_H values suggest that the change of solvent from dichloromethane to THF and then to $CDCl_3$ has resulted in an increasingly tight ion pair. To contrast the $CDCl_3$, data we have measured the diffusion for complex **15a** in CD_3CN, a much more polar solvent. As expected, the r_H value for $CF_3SO_3^-$ anion, at 2.7 Å, approaches the value of the solvated anion.

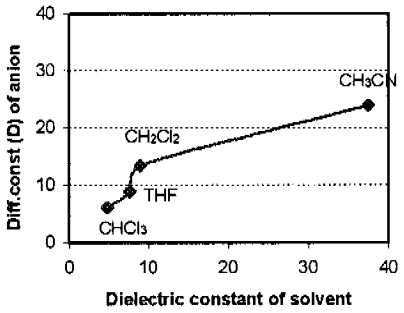

Fig. 2.17. Graph of diffusion constant (D) of CF_3SO_3 anion *vs.* dielectric constant (ε) of solvent in complex **15a.**

A plot of the D-value for the $CF_3SO_3^-$ anion verses with dielectric constant of the solvent at room temperature ($CHCl_3$ (4.8) < THF (7.6) < CH_2Cl_2 (8.9) < CH_3CN (37.5)) is not linear. However, the graph (see Fig. 2.17) clearly shows that the diffusion constant of the anion increases (faster motions, less ion pairing) with an increase in dielectric constant of the solvent.

^{1}H,^{19}F-HOESY NMR experiments. To further explore the ion paring, and to place the cation in three dimensional space, relative to the anion, ^{1}H,^{19}F-HOESY spectra for **12a-16a** in chloroform solution were measured and these are shown in Fig. 2.18.

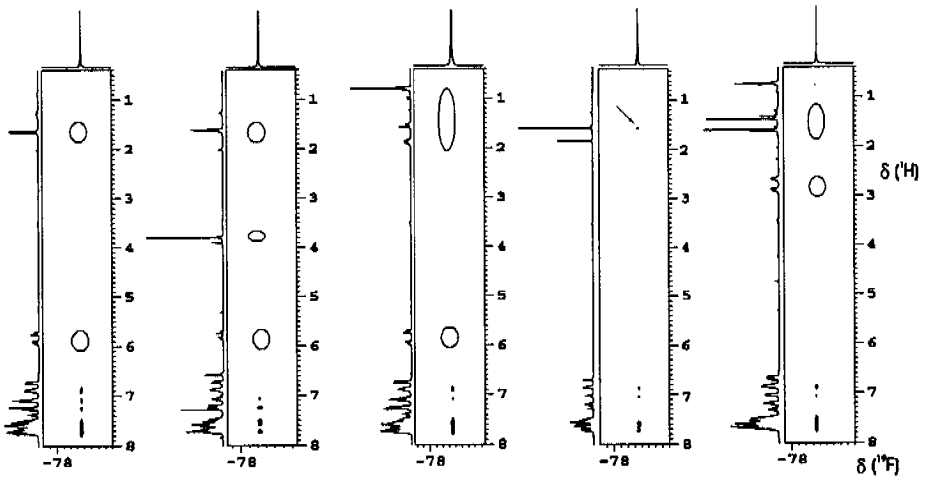

Fig. 2.18. $^{1}H,^{19}F$-HOESY spectra for the complexes (left to right) **12a** to **16a** ($CF_3SO_3^-$ anion) in $CDCl_3$, all showing selective contacts primarily to the P-phenyl ring protons and not to the chelated anionic ligand. In complex **15,** one finds a weak contact (shown by arrow) to the methyl group (six protons). The empty circles indicate the absence of an NOE cross-peak (400 MHz, 298 K).

In all of these spectra the strongest cross-peaks arise due to the fluorine spins of the $CF_3SO_3^-$ anion interacting with P-phenyl (probably *ortho*) aromatic protons of the complexed BINAP. There are almost no contacts to either the chelating N-imide or the acetylacetonate. (There is a weak contact to the strongest methyl signal in **15**). The P-phenyl *ortho* aromatic protons of the complexed BINAP can be partially assigned via a $^{31}P,^{1}H$ COSY correlation.

Consequently, it is believed that the anion is (a) approaching the positive metal and phosphorus centers via a pathway which brings it closest to the P-phenyl groups, and (b) avoiding the region of the negatively charged chelating ligands. The cartoon below offers two possible pathways of approach. It is not necessary that the anion (indicated as ball) approach from a "vertical" position (dotted arrow) as this is not sterically favoured.

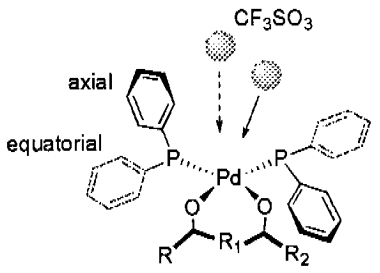

Conclusions: The various cations do not all behave identically towards the anions in this study. The PF_6^- anion is readily hydrolyzed by the cation of **1**, whereas the anions $CF_3SO_3^-$ and BF_4^- hydrogen-bond to the water ligands and are relatively stable. There is not much H-bonding of the anions in the dinuclear μ-OH salts **2**, and the anion selects an approach path towards the P atoms that brings it between the two P-aryl moieties. The bridged dinuclear salts, **3**, form readily from **2** by addition of an aniline, and reveal diffusion characteristics which are similar to **2**. Where measurable, the solvent THF promotes more ion pairing than does dichloromethane.

The Pd(BINAP) dication, **17**, postulated by Hii and co-workers, in connection with the enantioselective Pd-catalysed hydroamination reaction, clearly exists in solution and can be characterized at low temperature. It is not the major component of the mixture; however, its dynamic nature is consistent with the ease with which a possible product could be eliminated from the palladium moiety to allow the next substrate molecule to complex.

The mono cationic Pd-complexes, **12-16**, might be generated in a catalytic solution containing a labile Pd(II)(BINAP) moiety, a diketone such as **9** and a base. These conditions are fulfilled in a number of literature reports. However, their relative stability, and

the ^{13}C data for the olefinic carbons, suggest that these may not be important in the palladium catalyzed reactions, in agreement with a suggestion by Sodeoka[1]. However, a related *Ru-enolate* has recently been suggested as an active intermediate in an asymmetric Michael addition reaction[54].

As expected, the ion pairing in **12-16** is strongly solvent dependent; but, even in chloroform solution, where one finds the largest amount of ion pairing, there is no reason to believe that the ion pair would hinder attack of e.g., of a nucleophile on the double bond of the complexed enolate, since the counter-anion prefers to remain remote from the coordinated chelated anion.

Together, the structures of the two forms of the acetyl acetonate BF_4^- complex, **15b**, provide a rare structural picture of a tight ion pair vs a solvent separated analog. Moving the anion closer to the metal affects the cation structure.

2.1.5 Pd (II)-BINAP-Cyclometallated Complexes

N,C-cyclopalladated compounds of various types are known for more than thirty years[55-58], can be modified to P,C-analogs[59, 60], and have been used in a variety of applications, e.g., as valuable intermediates in synthetic organic reactions, for chiral recognition[4], as a template,[61] or in asymmetric synthesis.[5] Despite the interest in these complexes, little is known concerning (a) electronic effects arising from Schiff base ligands on the ion paring (b) the nature and the position of the anion in cyclometallated Pd complexes having bidentate phosphine ligand.

Synthesis:

The new cyclometallated Pd complexes (**20-27**) were prepared by reaction of the appropriate bidentate phosphine with the known cyclometallated chloro-bridged Pd(II) species (**18 a-f** and **19**), in the presence of AgX as indicated in Scheme 2.3.

Results and discussion

The ^{31}P NMR spectra for the new salts showed AX spin systems with two very different phosphorus chemical shifts, e.g., for **24a**, P1, δ 40.8, and P2, δ 13.3 ($^2J_{PP}$ = 47.8 Hz). The lower frequency resonance, P2, can be assigned to the P-atom *trans* to the sigma bound carbon donor. The ^1H spectra for the Schiff's base complexes showed the imine proton at relatively high frequency, e.g., for **24a**, H7, δ 8.05, whereas the diastereomeric N,N-dimethylamino-salts revealed three well resolved methyl signals in addition to the aliphatic methine CH-absorption.

Scheme 2.3

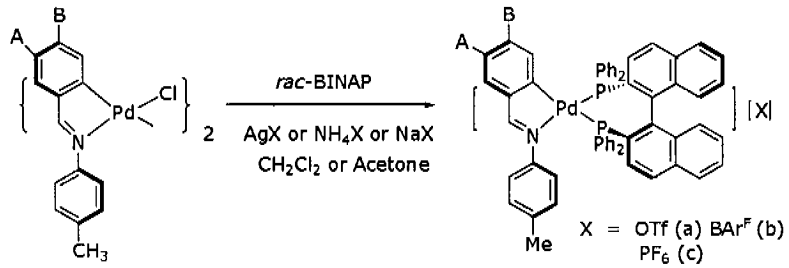

18	**a.**	A = Me	B = H	**20.**	A = Me	B = H
	b.	Cl	H	**21.**	Cl	H
	c.	NO_2	H	**22.**	NO_2	H
	d.	OMe	H	**23.**	OMe	H
	e.	H	Me	**24.**	H	Me
	f.	H	NO_2	**25.**	H	NO_2

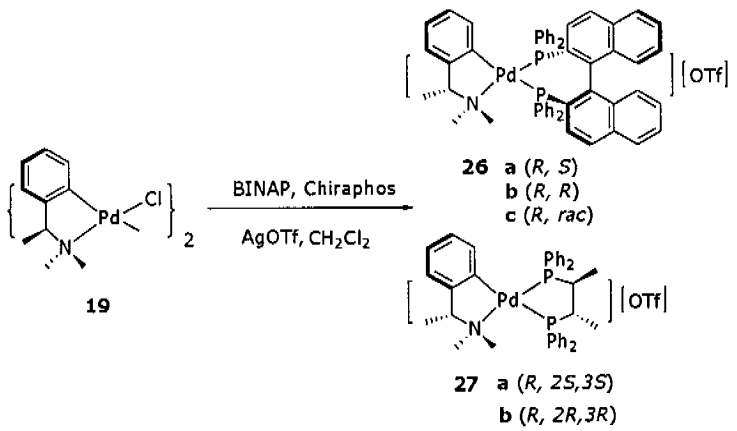

As expected, the ^{13}C chemical shifts for the imine complexes, **20-27**, show that the Pd-bound carbon atom appears at relatively high frequency[62-64] and senses the presence of the A substituent, in that this resonance is shifted markedly to high frequency[64, 65] with A = NO_2 and to lower frequency with A = MeO (see Table 2.9). Interestingly, ^2J(P,C) is not markedly affected by the A or B groups.

Table 2.9. ^{13}C NMR data for bound C-atom, C_1 in the complexes **20a** to **27a.**

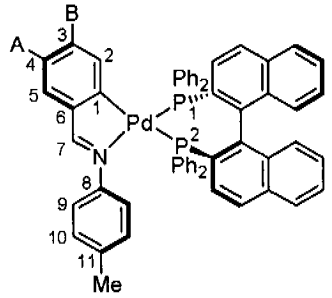

A	B	δ (^{13}C)	$^2J_{CP}$ trans	$^2J_{CP}$ cis
Me	H	164.8	122.0	5.5
Cl	H	166.0	124.0	5.7
NO_2	H	177.2	123.3	4.6
OMe	H	158.6	126.0	5.8
H	Me	168.3	125.0	6.0
H	NO_2	169.2	125.2	4.8

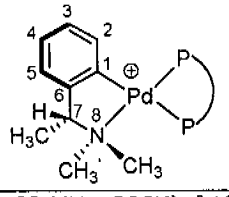

comp			
26a[a]	162.1	108.9	5.0
27a	158.9	111.0	4.8

(CD_2Cl_2, 100 MHz, 298K). [a] 125.8 MHz

Solid-state structures: Table 2.10 gives selected bond lengths (Å) and bond angles (°) for the Pd(*rac*-BINAP) $CF_3SO_3^-$, salts of the imine derivatives, **20a** and **22a**, as well as for the Pd(*R*-cyclometallated amine)((*R*)-BINAP) diastereomer, **26b** and the *R*, *rac* combination, **26c**. The first descriptor refers to the amine (and is always *R*) and the second to the phosphine. Figures 2.19-2.22 show ORTEP views of these salts. The X-ray data for a fifth salt, **27a,** afforded a clear result for the cation, see Fig. 2.23; however, a suitable solution for the disorder in the anion could not be found.

All four cations reveal local distorted square planar geometry about the palladium atom. Within each cation, the two Pd-P separations are quite different. The Pd-P distance *trans* to the carbon, is seen to be ca 0.10-0.15 Å, longer than that found for the Pd-P distance *trans* to the nitrogen atom. We note that for **26b**, the Pd-P separation of ca 2.42 Å lies at the upper end of the range for that type of bond. Moreover, this value is significantly larger than the analogous distance found in **22a**, ca 2.36 Å suggesting a stronger *trans* influence for the aliphatic carbon donor. The Pd-N and Pd-C bond lengths are consistent with the literature[66]. As expected, the N-Pd-C angle from the five-membered ring is relatively small, ca 79-80°, whereas the P-Pd-P angles are all slightly larger than 90°. This latter angle is typical for the BINAP chelate[67, 68]. The Figures 2.21 to 2.23 show views of several of the five membered N,C-chelate rings. As expected, this ring is not planar, and this subject will be extended in the solution discussion.

We note further that the coordinated BINAP ligands demonstrate the usual[47, 67-69] pseudo-axial and pseudo-equatorial P-phenyl rings and that both rings for the Schiff's base do not lie in the same plane. Figs. 2.19-2.22 suggest that the $CF_3SO_3^-$, anion is localized near the nitrogen chelate and we shall address this point via the HOESY results that follow.

Table 2.10 Bond lengths (Å) and bond angles (°) for complexes **20a**, **22a**, **26b** and **26c**.

20a		**22a**		**26b**	
Pd(1)-C(1)	2.065(4)	Pd(1)-C(1)	2.069(2)	Pd(1)-C(1)	2.026(3)
Pd(1)-N(1)	2.124(3)	Pd(1)-N(1)	2.134(2)	Pd(1)-N(1)	2.192(2)
Pd(1)-P(1)	2.2601(10)	Pd(1)-P(2)	2.2670(6)	Pd(1)-P(2)	2.2616(6)
Pd(1)-P(2)	2.3876(10)	Pd(1)-P(1)	2.3643(6)	Pd(1)-P(3)	2.4182(7)
C(1)-Pd(1)-N(1)	80.11(14)	C(1)-Pd(1)-N(1)	80.39(9)	C(1)-Pd(1)-N(1)	78.74(10)
C(1)-Pd(1)-P(1)	92.16(11)	C(1)-Pd(1)-P(2)	92.96(7)	C(1)-Pd(1)-P(2)	90.39(8)
N(1)-Pd(1)-P(1)	166.94(9)	N(1)-Pd(1)-P(2)	167.86(6)	N(1)-Pd(1)-P(2)	162.77(7)
C(1)-Pd(1)-P(2)	160.27(11)	C(1)-Pd(1)-P(1)	166.13(7)	C(1)-Pd(1)-P(3)	171.30(9)
N(1)-Pd(1)-P(2)	98.50(9)	N(1)-Pd(1)-P(1)	96.97(6)	N(1)-Pd(1)-P(3)	101.46(7)
P(1)-Pd(1)-P(2)	92.31(3)	P(2)-Pd(1)-P(1)	91.86(2)	P(2)-Pd(1)-P(3)	91.31(2)

26c (*R*,*S*)		**26c** (*R*,R)	
Pd(1)-C(1)	2.043(4)	Pd(2)-C(55)	2.035(4)
Pd(1)-N(1)	2.181(4)	Pd(2)-N(2)	2.187(3)
Pd(1)-P(2)	2.2653(11)	Pd(2)-P(4)	2.2531(10)
Pd(1)-P(1)	2.4100(11)	Pd(2)-P(3)	2.3968(10)
C(1)-Pd(1)-N(1)	79.38(16)	C(55)-Pd(2)-N(2)	78.69(14)
C(1)-Pd(1)-P(2)	92.82(13)	C(55)-Pd(2)-P(4)	91.36(11)
N(1)-Pd(1)-P(2)	164.42(12)	N(2)-Pd(2)-P(4)	159.46(10)
C(1)-Pd(1)-P(1)	170.72(11)	C(55)-Pd(2)-P(3)	170.27(11)
N(1)-Pd(1)-P(1)	97.97(10)	N(2)-Pd(2)-P(3)	100.29(9)
P(2)-Pd(1)-P(1)	91.75(4)	P(4)-Pd(2)-P(3)	92.48(3)

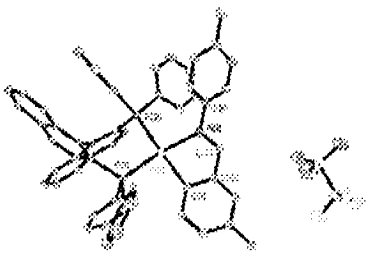

Fig.2.19 An ORTEP view of the cation of **20a** with thermal ellipsoids drawn at the 30% probability level (solvent molecules are not shown for clarity).

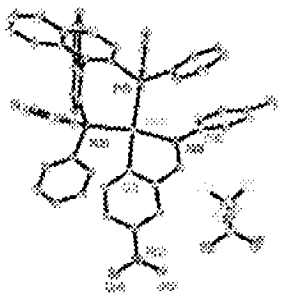

Fig.2.20 An ORTEP view of the cation of **22a** with thermal ellipsoids drawn at the 30% probability level (solvent molecules are not shown for clarity).

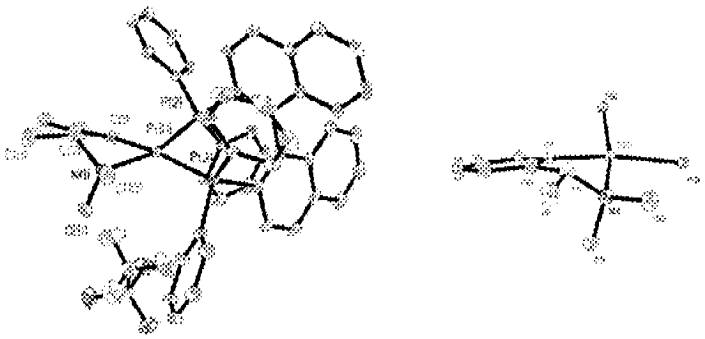

Fig. 2.21 (left) An ORTEP view of the cation of **26b** with thermal ellipsoids drawn at the 30% probability level and (right) a section showing the five-membered cyclometallated ring.

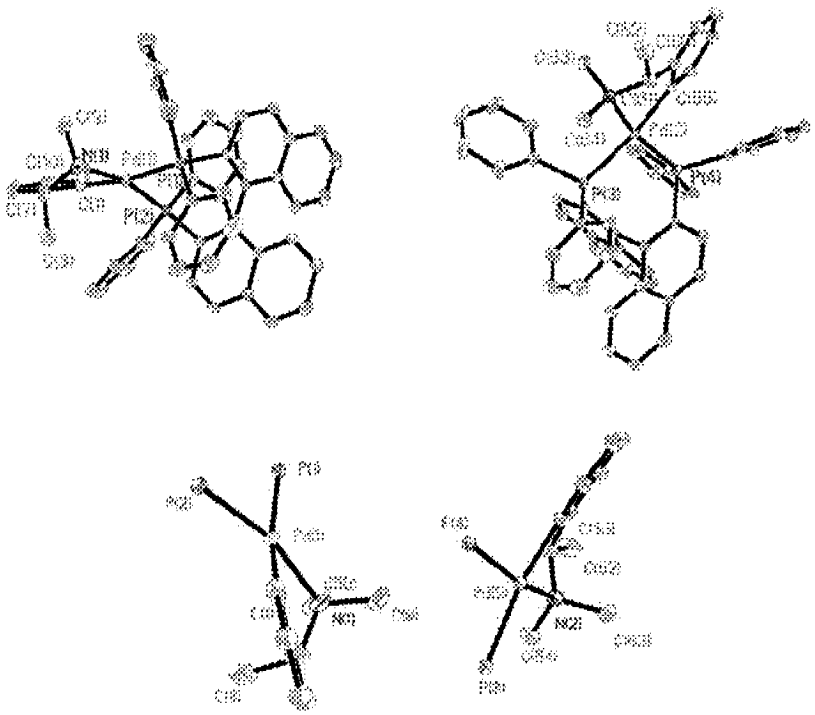

Fig. 2.22 (top) ORTEP views of the cations of **26c** with thermal ellipsoids drawn at the 30% probability level and (bottom) sections showing the five-membered cyclometallated rings for the two cations (the anions are not shown for clarity).

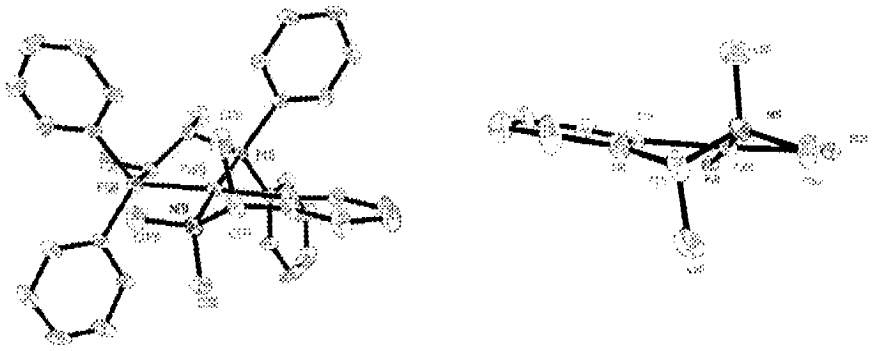

Fig. 2.23 An ORTEP view of the cation of **27a** with thermal ellipsoids drawn at the 30% probability level and section showing the five-membered cyclometallated ring.

Overhauser spectroscopy:

Cyclometallated Imine salts. Fig 2.24 shows $^{1}H,^{19}F$-HOESY results in $CDCl_3$ solution for the model Pd(*rac*-BINAP)(MeO-Schiff's base) salts, **23a-23c**, which contain the $CF_3SO_3^-$, $BAr^F{}_4^-$ and PF_6^- as anions, respectively. For all three salts there are numerous $^{1}H,^{19}F$ contacts, and indeed, these three differ, but not dramatically. The strongest contacts stem from a number of PPh_2 BINAP protons, as previously described (section **2.1.1**). Continuing, the relatively small PF_6^- anion (right trace) "sees" the MeO-group, the Schiff's base ring protons (see Table 2.9 for numbering), H5, H9, H10 and the imine proton, H7. There is no contact to the aromatic methyl group. This suggests that this anion is trying to position itself close to the partial positive charges on the imine N, Pd and P-atoms. For the slightly larger $CF_3SO_3^-$, anion (left trace) we find contacts to the MeO-group, the Schiff's base ring protons, H2, H3, H5, H9, H10 and the imine proton, H7, plus a number of interactions with the PPh_2 BINAP protons. As before, there is no contact to the aromatic methyl group; however as the triflate is a little larger and the F-atoms somewhat remote from the O-atoms bearing the negative charge, we now have contacts to H2 and H3 (see arrow in the figure). These results are consistent with the same type of approach as for the PF_6^- anion. For the even larger $BArF^-$, anion (center trace) we find contacts to the MeO-group, the *para* methyl group, the Schiff's base ring protons, H2, H3, H5, H9, H10 and the usual PPh_2 BINAP protons; however, the contact to the imine proton, H7, is absent. The larger $BArF^-$ anion, with its *meta* CF_3 groups, stretches far enough to approach the *para* methyl group, but is now a little further away from the imine proton, H7. We conclude that, in solution, for **20** and **25**, the anions prefer to be localized close to the partially positive coordinated imine, Pd and P- moieties. These observations do not reflect directly on the amount of ion pairing

(see the diffusion discussion below), but rather that these anions can approach the cation in a similar way.

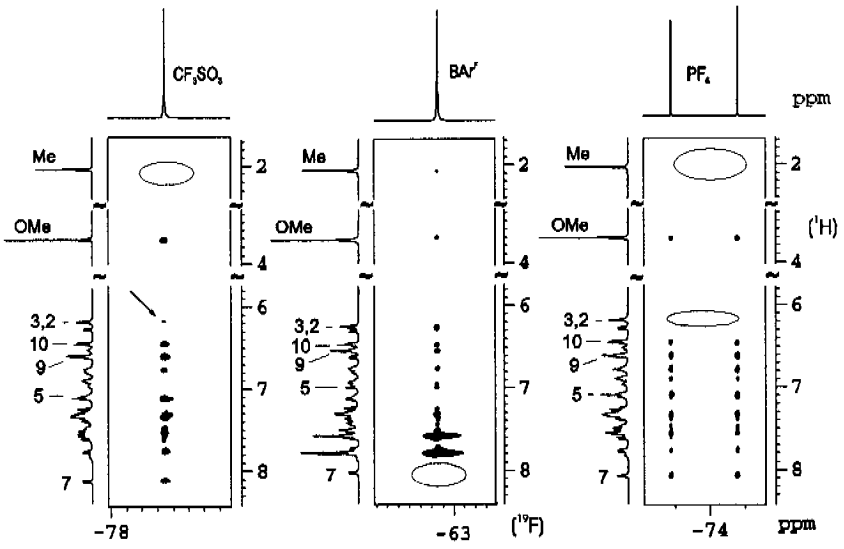

Fig. 2.24. ^{1}H, ^{19}F HOESY spectra for the complexes **23a** (left) **23b** (middle) and **23c** (right) in $CDCl_3$. The spectra show selective strong contacts primarily to the P-phenyl ring protons as well as contacts to the cyclometallated ligand. In complex **23b**, one finds a contact to the para methyl group and not to the imine (H7) proton (400 MHz, 298 K).

Cyclometallated amine salts.

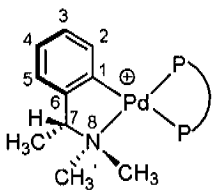

For the chiral amine salts **26a,b** and **27a,b**, the interpretation of the $^{1}H,^{19}F$-HOESY results rests on the assignment of the three methyl resonances. The correct assignment of the two N-methyl groups, CH_3' (somewhat closer to the aliphatic methyl) and CH_3 (proximate to the methine CH) is crucial, since we expect that the anion may approach the cation via the amine moiety, in analogy to the results described above. The assignment of the aliphatic methyl signal is trivial as it is spin-spin coupled to the adjacent methine CH

and appears as a sharp doublet. The differentiation between NCH_3' and NCH_3 was not straightforward and was made primarily using $^1H,^1H$ Overhauser measurements, together with ^{31}P spin coupling data. The two N-methyl groups reveal very different and characteristic line shapes. $^{31}P,^1H$ correlations (see Fig. 2.25) reveal that the broad "triplet" shape associated with an N-methyl group stems from long-range ^{31}P spin-spin coupling to two P-atoms, and this was interesting. The difference in the line shape stems from the dependence of $^4J(P,H)$ on the relative position of the NMe and NMe'-groups. When one of these lies roughly in the P-Pd-P plane, both ^{31}P spins couple sufficiently to be visible in the ^1H spectrum. However, since the change from e.g., *R*-BINAP to *S*-BINAP, changes the amine ring conformation, and consequently the relative positions of these two NMe groups (as detailed in the text), in one diastereomer, the NMe shows the triplet and in the other, the NMe' signal. Fig. 2.26 shows NOE results for the (*R,S*) and (*R,R*) BINAP diastereomers, **26a** and **26b**. The selectivity shown from these NOE data (note the absences indicated by the circles) suggest that the conformation of the five-membered metallocycle ring changes with the chirality of the BINAP. For the *R,S* diastereomer, the N-atom is

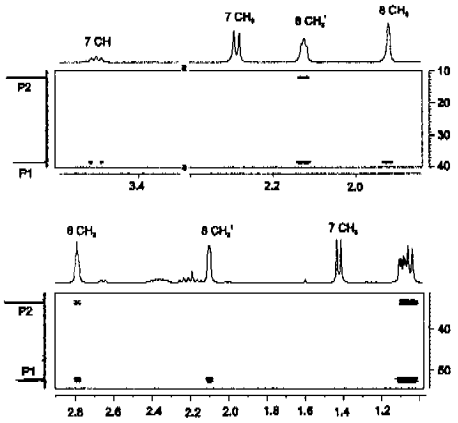

Fig. 2.25 Sections of ^{31}P, ^1H COSY spectra for complex **26a** (CD_2Cl_2, 500 MHz, 298 K) and **27b** ($CDCl_3$, 300 MHz, 298 K) each showing two ^{31}P contacts to the methyl 8 CH_3' and 8 CH_3 respectively, thereby explaining the observed triplet multiplicity.

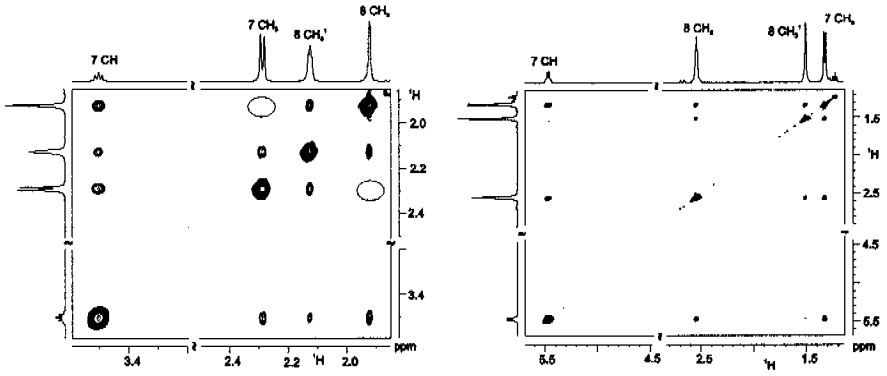

Fig. 2.26 Sections of the ^1H, ^1H NOESY spectra for complex **26a** (CD_2Cl_2, 500 MHz) and **26b** ($CDCl_3$, 400 MHz), showing selective NOE contacts in both cases. Blank circles indicate no contact and suggest a specific conformation.

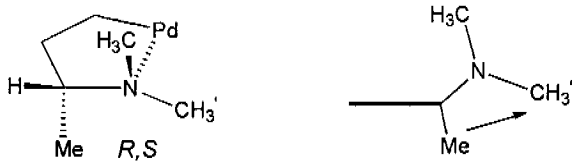

28 structural fragment (left) plus cartoon (right, the bold line in the cartoon represents the plane defined by the Pd and the three carbon atoms)

placed slightly above the plane defined by the Pd and the three carbon atoms, see cartoon in **28**. This places the C-Me group in a pseudo *trans* position relative to the NCH_3 (and thus one finds no NOE between these two groups), but proximate to NCH_3' and the arrow in the cartoon indicates this NOE contact. For the *R,R* diastereomer, the N-atom is placed slightly below the plane defined by the Pd and the three carbon atoms, see cartoon in **29**. This places the C-Me group roughly equidistant from both the NCH_3 and the NCH_3' moieties with the result that two fairly strong interactions(see arrows) are observed. In line with this proposal are the selective NOE's from the methine CH proton: one each to the

NCH_3 and the NCH_3' groups in **28** and only one to the NCH_3 in **29.** Exactly these two specific ring conformations are found in the solid-

29 structural fragment (left) plus cartoon (right)

state structures and we show these in Figs. 2.21-2.23. It is interesting that both amine ring conformations are found for the two diastereomers of the racemic BINAP of **26c** (see Fig. 2.22). Moreover, the solid-state data show-if one defines a plane made up of the metal, the two C-atoms of the metallated ring, C1 and C6, and the methane CH, C7,- that in one diastereomer the N1-atom lies 0.75 Å below this plane, whereas in the second diastereomer, the N2-atom lies 0.87 Å above this plane.

Continuing, the changes in ring conformation are accompanied by selective anisotropic effects from the P-phenyl array on the chemical shifts of the three methyl groups (see Fig. 2.26): e.g., for the *R,R* diastereomer two of these are found at lower frequency. Possibly, this change in amine ring conformation, as a function of the shape of the chiral pocket, relieves unfavourable steric interactions between the PPh_2 groups from P2 (*trans* to the C-donor) and the two proximate N-methyl groups.

The shapes and relative positions of the chiral arrays containing the four P-phenyl groups of complexed (*S*) and (*R*)-BINAP, are shown in **30** and **31**, respectively, and these have been defined both by NMR and X-ray measurements a number of times[42, 51, 67, 69, 70].

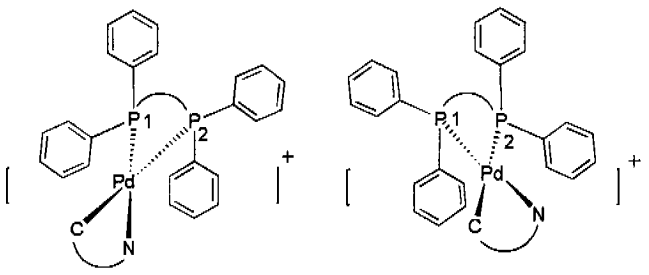

30 *S* BINAP **31** *R* BINAP

Fig. 2.27 gives the $^{1}H,^{19}F$-HOESY results in $CDCl_3$ solution for the BINAP salts **26a-c**. The strongest contacts arise from the protons of the P-phenyl groups, however, there is a great deal of selectivity. The contacts for *R,R*-**26b** are not so numerous and ca twice as strong as for *R,S*-**26a**. The most important contacts for *R,R*-**26b** are shown in the structural fragment, **32**, below.

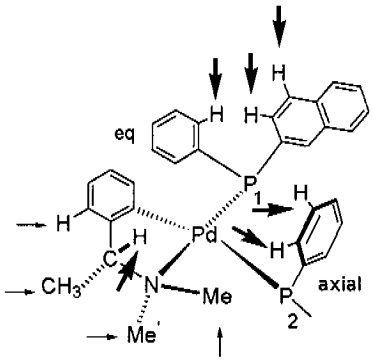

32, R,R BINAP Salt

There are six fairly strong interactions (bolder arrows) stemming from the methine CH and five aromatic protons of the BINAP and four weaker contacts (thinner arrows) from the cyclometallated ring. The analysis of these NOE data leads to a fairly clear preference for the anion on the same side of the coordination plane where one finds the phenyl ring P_2(axial) and the amine ring methine CH proton. The anion is not complexed but hovers over the most open position available that permits it to approach the positive

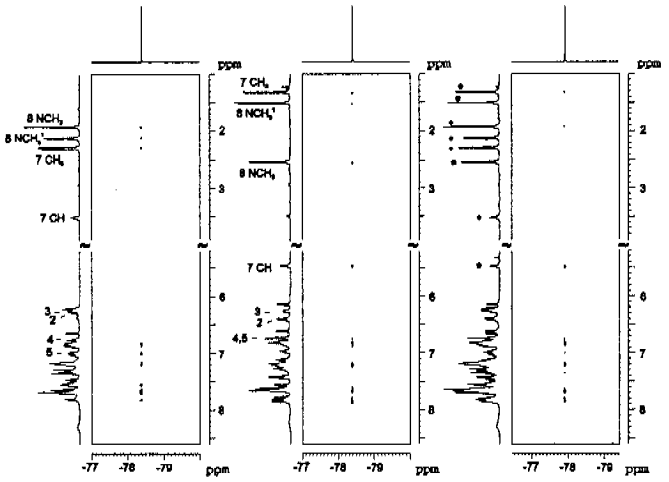

Fig. 2.27 ^{1}H, ^{19}F HOESY spectra for the complexes **26a** (left) **26b** (middle) and **26c** (right, with *rac* BINAP) in $CDCl_3$, all showing selective strong contacts primarily to the BINAP P-phenyl ring protons (400MHz, 298K). The stars and crosses in the spectrum of **26c** indicate the signals from the individual diastereomers.

centers. In the *R,S* diastereomer (we do not show a cartoon as the contacts are too numerous-and unfortunately not always unambiguous), the data suggest that the anion now prefers the opposite side of the coordination plane. In this connection there are two points worthy of mention (a) the contact to the methine CH-bond is now *very* weak (and easily missed) and (b) there is a strong contact to the *ortho* protons of P_2(axial), which now is positioned on the other face of the coordination plane due to the change in chirality (see **30** relative to **31**). We conclude that the change in the shape of the chiral pocket affects not only the cyclometallated ring conformation, but also moves the anion from one side of the metal complex to the other. For the *R,rac* BINAP mixture (far right trace), only the cross peaks from the $CF_3SO_3^-$ anion to those *of the R,R diastereomer CH and the Me* protons are readily observed. This is partly because the strong signals from **26b** mask the weaker ones from **26a**. In any case, the measurement of the racemic mixture, alone, would not have afforded a clear picture of how the triflate anion interacts with the two diastereomeric cations.

For the Chiraphos diastereomeric pair, **27a,b**, the $^{1}H,^{1}H$ NOE's (see Fig. 2.28) indicate that, for these salts as well, the nature of the five-membered metallocycle ring changes with the chirality of the Chiraphos ligand salt, **27a**, *R,2S,3S*, shows the conformation **28**, however, for salt **27b**, *R,2R,3R*, the situation is somewhat different, but in line with the literature[71, 72]. For **27b**, in contrast to **26b**, one finds a somewhat more flexible five-membered ring conformation based on the observed NOE's. This is interesting and suggests that each enantiomer of BINAP can induce a more decisive conformational change, whereas this is not completely true for both forms of the Chiraphos.

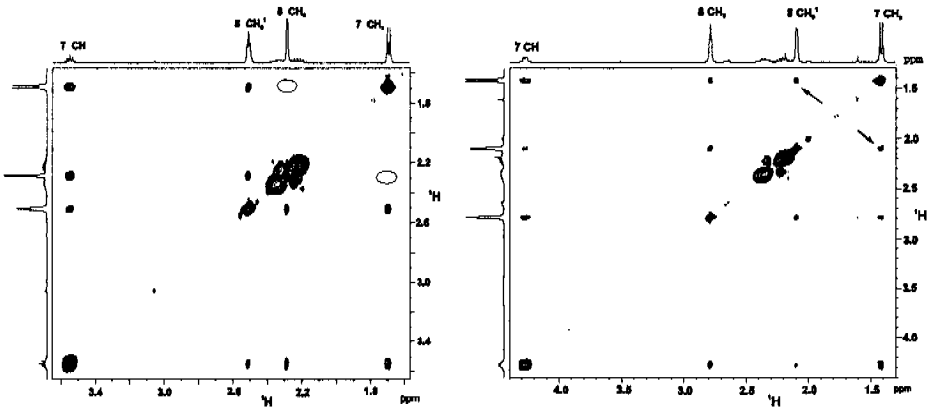

Fig. 2.28 Sections of ^{1}H, ^{1}H NOESY for complex (left) **27a** ($CDCl_3$, 400 MHz) and (right) **27b** ($CDCl_3$, 300 MHz), showing selective NOE contacts in both cases. Blank circles indicate no contact and suggest a specific conformation.

The $^{1}H,^{19}F$-HOESY (Fig.2.29) results for the Chiraphos salts **27a,b,** are simple relative to the BINAP analogues and these are summarized in the fragments **33** and **34**. In the *R,S,S* salt, one finds three major contacts: one to an *ortho* P-phenyl set and one each to the NCH_3' and NCH_3 groups (There is a very weak contact to the Chirapos methyl groups. The chiral array does not show marked

axial or equatorial P-phenyl groups). In the *R,R,R* salt, one finds four major contacts: one to an *ortho* P-phenyl set on the other side

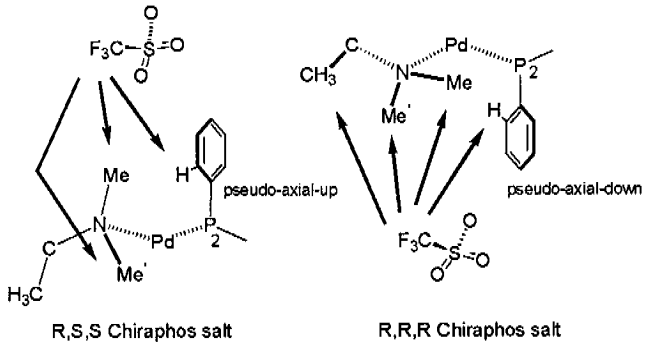

33 (left) and **34** (right). The anion approaches as indicated by the arrows

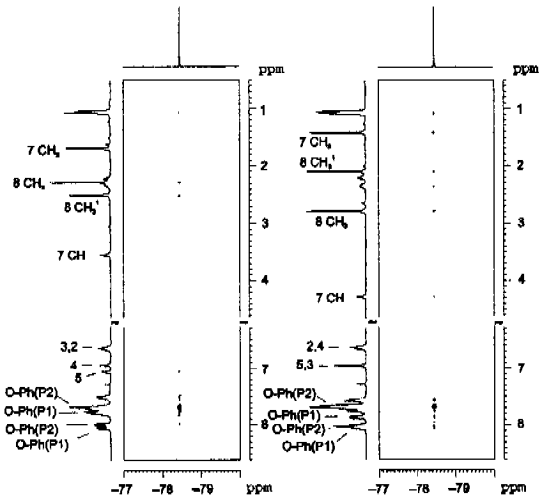

Fig. 2.29 ^{1}H, ^{19}F HOESY spectra for complexes **27a** (left) and **27b** (right) in $CDCl_3$, both showing selective strong contacts primarily to the Chiraphos *ortho* P-phenyl ring protons (400 MHz, 298 K).

of the coordination plane, and one each to the three methyl groups suggesting that the anion has, once again, moved from one side of the complex to the other. The strongest contacts come from a P-phenyl ring from the PPh_2 *trans* to the carbon donor. The interpretation of the ^{1}H spectra is much simpler, relative to the BINAP salts, due to the absence of the naphthyl protons. In no case do we find a contact to the amine methine CH-proton.

Diffusion data. Tables 2.11 and 2.12 give PGSE diffusion data (D-values) for the cations and anions of the complexes **20-25** and **26, 27**, respectively, in CD_2Cl_2 and $CDCl_3$ solutions.

Table 2.11. Diffusion constants [a] and radii [b] for complexes **20** to **25** in CD_2Cl_2.

	CD_2Cl_2													
	CF_3SO_3(a)					BArF(b)				PF_6(c)			
	Cation(^{1}H)			Anion(^{19}F)		Cation(^{1}H)		Anion(^{19}F)		Cation(^{1}H)		Anion(^{19}F)	
Comp	D	r_H (r_H)	r_{Xray}	D	r_H (r_H)	D	r_H (r_H)	D	r_H	D	r_H (r_H)	D	r_H (r_H)
20	7.83	6.8 (7.2)	7.0	12.91	4.1 (5.0)	7.54	7.0	8.14	6.5				
21	7.74	6.8		12.72	4.2	7.42	7.1	8.12	6.5				
22	7.73	6.8 (7.3)	7.1	12.46	4.2 (5.2)	7.48	7.1 (7.5)	8.20	6.5 (7.0)	7.66	6.9 (7.4)	12.65	4.2 (5.1)
23	7.69	6.9		12.84	4.1	7.41	7.1	8.10	6.5	7.71	6.9	14.19	4.0
24	7.94	6.7		12.98	4.1	7.61	7.0	8.20	6.5				
25	7.75	6.8		12.30	4.3	7.69	6.9	8.23	6.4				
	$CDCl_3$												
22	5.49	7.5 (8.0)		5.78	7.1 (7.6)	4.85	8.5 (8.9)	5.00	8.2 (8.6)	5.66	7.2 (7.8)	5.95	6.9 (7.4)
23	5.62	7.3		6.06	6.8	4.95	8.3	5.21	7.9	5.68	7.2	6.15	6.7

[a] 400 MHz, 2mM; D values, 10^{-10} m^2 s^{-1} ; [b] r_H values, Å; "c" corrected r_H values are in the bracket. r_{vdw} = 2.49 (CD_2Cl_2),), r_{vdw} = 2.60 ($CDCl_3$), $\eta(CH_2Cl_2)$ = 0.414 x 10^{-3} kg m^{-1} s^{-1}, $\eta(CHCl_3)$ = 0.534 x 10^{-3} kg m^{-1} s^{-1} at 299 K.

the experimental error (this assumes (a) the absence of other interactions, e.g., hydrogen bonding or anion encapsulation etc which would result in restricted translation of the anion, and (b) that the two ions are markedly different in size). In all cases there is much more ion pairing in $CDCl_3$ solution. Further, for **20-25**, in CD_2Cl_2 solution, the ion pairing seems to be more or less independent of the substituents A and B. For **26** and **27**, we do not find a dependence of the D-values on the sense of the chirality.

Table 2.12: Diffusion constants [a] and radii[b] for complex **26** and **27** in CD_2Cl_2 and in $CDCl_3$.

		CD_2Cl_2					$CDCl_3$			
Comp	**Configuration[c]**	**Cation(^{1}H)**			**Anion(^{19}F)**		**Cation(^{1}H)**		**Anion(^{19}F)**	
		D	**r_H (r_H)**	**r_{Xray}**	**D**	**r_H (r_H)**	**D**	**r_H (r_H)**	**D**	**r_H (r_H)**
26	**a** (*R, S*)	8.24	6.4		13.04	4.1	5.86	7.0	6.27	6.5
	b (*R, R*)	8.16	6.5	6.9	12.58	4.2	5.97	6.9	6.17	6.6
			(7.0)			(5.1)		(7.4)		(7.2)
	c (*R, rac*)	8.11	6.5		13.04	4.1	5.97	6.9	6.24	6.6
		8.18	6.5				5.88	7.0		
27	**a** (*R, 2S,3S*)	8.86	6.0		12.70	4.2	6.30	6.5	6.68	6.1
			(6.5)			(5.1)		(7.1)		(6.8)
	b (*R,2R,3R*)	8.86	6.0		12.65	4.2	6.30	6.5	6.53	6.2

[a] 400 MHz, 2mM; D values, 10^{-10} m^2 s^{-1} ; [b] r_H values, Å; [c] The first configuration refers to the asymmetric carbon in cyclometalated ring and the second configuration refers to the binaphthyl ring.; "c" corrected r_H values are in the bracket. r_{vdw} = 2.49 (CD_2Cl_2), r_{vdw} = 2.60 ($CDCl_3$), $\eta(CH_2Cl_2)$ = 0.414 x 10^{-3} kg m^{-1} s^{-1}, $\eta(CHCl_3)$ = 0.534 x 10^{-3} kg m^{-1} s^{-1} at 299 K.

The calculated hydrodynamic radii, r_H, are in good agreement with the $r_{x\text{-}ray}$ values estimated from the solid-state measurements. From Table 2.11, one finds that the D-values for the $CF_3SO_3^-$, and PF_6^- anions are similar, and from Table 2.12, as expected, it is clear that the complexes **26** are somewhat larger than those from **27**. Assuming an r_H, value of ca 5.9 Å for the solvated $BArF^-$ anion[73], then the ca 6.5 Å r_H, value for the $BArF^-$ anion in **20-25** in CD_2Cl_2 solution, given in Table 2.11, is suggestive of ca 10% ion pairing, i.e., very modest but not zero, ion pairing for this anion. This estimation, when taken with the NOE data, serves as a reminder that the observation of strong HOESY contacts does not imply strong ion pairing, but rather that the anion can approach the cation.

Conclusions. We find that the chiral organometallic amine chelate recognizes the change in the sense of the chirality, both for the

BINAP and the Chiraphos auxiliaries, and responds by a conformational adjustment. Associated with this, is a change in the approach of the $CF_3SO_3^-$ anion towards the positively charged centers. The conformational change of the amine ring was easily detected via intra-molecular proton-proton NOE data; however defining the interplay between the anion and cation required a detailed understanding of the various fairly complex ^1H NMR spectra and involved the interpretation of both strong and modest $^1H,^{19}F$ Overhauser contacts.

We believe that these observations will eventually prove helpful in understanding how chiral auxiliaries affect structural changes and thus influence the outcome of enantioselective reactions. It is now well documented that a prochiral substrate, e.g., an olefin capable of forming a chelate ring, may complex either the *re* or *si* face and that the chiral pocket assists in this selection process. However, it is not obvious that the chiral pocket might be able to induce a change in the conformation of such a chelate ring. Further, from this and earlier studies, it is now becoming clear that non-coordinating anions (a) can be selective in their approach to a metal center and (b) do not all demonstrate the same degree of ion pairing-and this is especially true for the commonly used $BArF^-$ anion.

2.2 Diffusion Studies on Rh(I) N-Heterocyclic Carbene Complexes

There are increasing indications of counter-ion effects on the kinetics of various homogeneously catalysed reactions[19, 24, 74]. Changing the structure of a given cationic complex might well modify how the anion interacts. To probe this possibility we have measured diffusion constants for three Rh(I) carbene complexes and show these data for **35**[PF_6], **36**[PF_6] and **35**[$BArF^-$] in CH_2Cl_2 solution in Table 2.13. Diffusion constants from the individual ions of a salt are now recognized to reflect the degree of ion pairing[52, 75]. As expected, based on the X-ray data[76], the PF_6^- anions reveal very much larger diffusion constants (D-values) than the corresponding cation, so that for both **35**[PF_6] and **36**[PF_6] in CH_2Cl_2, there is not a substantial amount of ion pairing. Strong ion pairing would result in D-values for the PF_6^- anion which are close to-or equal to-that for the larger cation. The hydrodynamic radii, r_H, for the cations, calculated from the Stokes-Einstein equation, are slightly smaller than the radii calculated using the volume data from the crystallographic data.

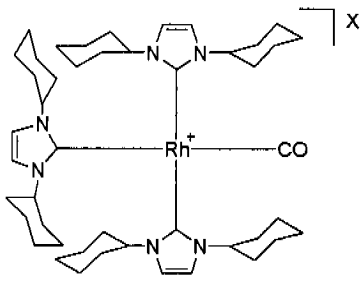

X = **35**[PF_6], **35**[$BArF^-$]

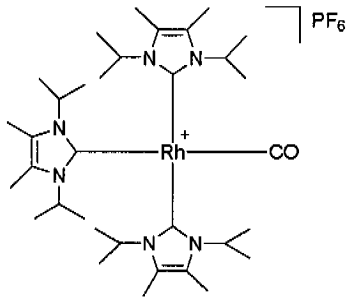

36[PF_6]

The $BArF^-$ salt diffusion data are interesting in that they represent a fairly rare example of measured identical D-values for the two ions

of a salt in the *absence* of strong ion pairing. By coincidence, the two ions in **35**[BArF$^-$] are of similar size and thus afford about the same r_H values. A typical r_H value for BArF$^-$ in a polar solvent would be ca 6 Å[21, 77, 78] and the cation itself has an r_H value of 6.1 Å. Allowing for perhaps 5-10% ion pairing readily explains the 6.4 Å r_H values.

Table 2.13. PGSE diffusion data[a] for the Rh-NHC salts **35**[PF_6], **35**[BAr^F] and **36**[PF_6].

Compound		D	r_H	$r_{x\text{-}ray}$(Å)
35[PF_6]	Cation	8.67	6.1	6.6
	Anion	14.02	3.8	
35[BArF$^-$]	Cation	8.30	6.4	
	Anion	8.32	6.4	
36[PF_6]	Cation	9.33	5.7	6.2
	Anion	14.70	3.6	

[a] Conditions: 400 MHz, 2mM in CH_2Cl_2; D values, 10^{-10} m^2 s^{-1}; r_H values, Å ; η (CH_2Cl_2) = 0.414 x 10^{-3} kg s^{-1} m^{-1} at 299K.

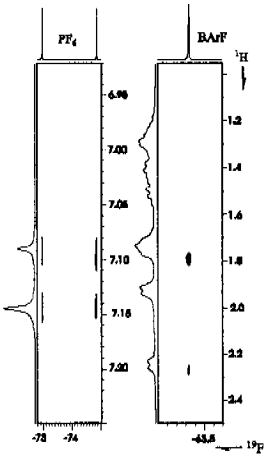

Fig. 2.30. Sections of the ^1H, ^{19}F HOESY results for (left) **35**[PF_6] and (right) **35**[BArF$^-$]. In the PF_6^- salt, there are only modest contacts to the NCH=NCH protons, whereas for the BArF$^-$ salt, the selective contacts are now to CH_2 protons of the Cy-groups (ambient temperature, CD_2Cl_2, 400 MHz).

Fig. 2.30 shows ^1H,^{19}F HOESY results for **35**[PF_6] and **35**[BArF$^-$]. The PF_6 anion, when it approaches the cation, does so via the NCH=CHN protons and avoids the Cy-groups. The BArF$^-$ anion, which is considerably larger than the PF_6^-, cannot easily take the

same pathway and thus reveals only modest contact to the methylene protons of the Cy-substituents. For these two salts the size of the anion determines the proximity to the metal centre.

Conclusions: Pulsed-gradient spin-echo (PGSE) NMR measurements show that there is only a relatively small amount of ion pairing for both **35**, **36** PF_6^- and **35** $BArF^-$ salts in dichloromethane solution. ^1H,^{19}F HOESY data help to place the anions relative to the cations.

2.3 Diffusion Studies of Pt(II) Complexes

Pulsed gradient spin-echo (PGSE) NMR diffusion methods are now currently widely used[79-83]. In many cases the applications are restricted to the use of ^1H PGSE (or DOSY)[25] data in order to estimate the molecular volumes of species generated in situ; however, it has recently been shown that a multinuclear approach, including the use of either ^{19}F[50, 52], ^{31}P[84], ^{35}Cl[84], or ^{7}Li[25, 85-88], provides an alternative methodology to recognizing and characterizing how ions, and, specifically, chiral organic[89] or chiral transition metal ions[90], interact with solvent and their corresponding anions.

To interpret properly the D-and r_H values obtained from PGSE diffusion, it is frequently necessary to have an appropriate model compound since solvation or ion pairing can be rather specific for a given class of material. It would be better to have D-and r_H values for a set of models with varying-but similar-environments; however, this is rare[91].

The following section explains how a variety of ligands within the coordination sphere of Pt(II) can affect the D-and r_H values, plus it is also describe the use of a new spin, ^{195}Pt, as a diffusion probe.

Results and Discussions:

Table 2.14 shows the diffusion constants, D, and the hydrodynamic radii, r_H for the *trans*- platinum phosphine complexes, *trans*-PtX(Aryl)$(L)_2$, **38-40**, in dichloromethane solution.

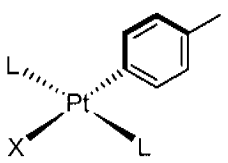

38, L = PEt_3, X = Br
39, L = PEt_3, X = Cl
40, L = PPh_3, X = Cl

Table 2.14. ^1H, ^{31}P and ^{19}F Diffusion Constants[a] and r_H Values (Å) in CD_2Cl_2.

Com	X	Aryl Y	D(^{1}H)	r_H	D(^{1}H)	r_H	D(^{31}P)	r_H
			2mM		10mM			
		L = PEt_3						
38a	Br	C_6H_5	12.01	4.5	11.86	4.5	12.09	4.4
38b	Br	C_6H_4(m-CF_3)	11.70	4.6	11.58[b]	4.6	11.76	4.5
38c	Br	C_6H_4(p-CF_3)	11.41	4.7	11.62[c]	4.6	11.76	4.5
38d	Br	C_6H_4(m-Br)	11.45	4.7	11.71	4.5	11.76	4.5
38e	Br	C_6H_4(p-Br)	11.34	4.7	11.53	4.6	11.50	4.6
38f	Br	C_6H_4(m-OCH_3)	11.39	4.7	11.56	4.6	11.62	4.6
38g	Br	C_6H_4(p-OCH_3)	11.29	4.7	11.37	4.7	11.53	4.6
38h	Br	C_6H_4(p-NMe_2)	11.15	4.8	11.16	4.7	11.33	4.7
39	Cl	C_6H_5	11.99	4.5	12.01	4.4	12.09	4.4
		L = PPh_3						
40	Cl	C_6H_5	9.12	5.8	9.12	5.8	9.16	5.8

[a] in CD_2Cl_2, x 10^{-10} m^2s^{-1}. [b] D(^{19}F) = 11.89 (10 mM), r_H = 4.4. [c] D(^{19}F) = 11.60, (10 mM), r_H = 4.5

The Table 2.14 includes both ^1H and ^{31}P data and we note that there are still almost no D-values determined using ^{31}P as a probe[25, 84]. The ^{31}P data were obtained on 10mM solutions due to the poorer sensitivity of this nucleus, however the ^1H data in Table 2.14 are for both the 2 mM and 10 mM solutions.

From these data several points are worth mentioning: (a) The change from Br^-, **38a**, to Cl^-, **39**, has little effect on the D-value. (b) Introduction of a substituent in either the *meta* or *para* position of the aryl ligand, has only a modest effect on the D-value. This is

likely to be associated with the only slightly extended size of the aryl ligand. With two *trans*-PR_3 ligands, the complex is somewhat spherical in shape and the *cis* aryl ligand may not contribute much to the overall volume. (c) Changing from L = PEt_3 to L = PPh_3 (from **39** to **40**) results in a marked decrease in D and a corresponding increase in r_H. Obviously the six P-phenyl groups are larger than the ethyl groups and offer much more resistance to translation than does the smaller two carbon fragment. (d) For the neutral complexes $PtX(Aryl)(PEt_3)_2$, the change from 2 mM to 10 mM results in only a small change (ca 1-2%) in the D-values. (e) The ^{31}P D-values do not quite agree with those D-values from the proton measurements. These latter are usually slightly smaller.

The X-ray structure of *trans*-$PtClPh(PPh_3)_2$ has been reported[92] and affords an r_H value of 6.0 Å; our r_H value of 5.8 Å is therefore reasonable.

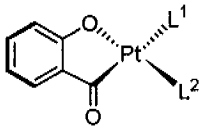

6

Table 2.15 gives diffusion data from the proton measurements for the neutral acyl complexes, $Pt(C_7H_4O_2)(L^1)(L^2)$, **41a-41m**, in dichloromethane solution.

The bis PPh_3 complex, **41a**, is of comparable molecular weight to the bis PPh_3 complex, **40** (r_H = 5.8 Å); however, for **41a**, the r_H value (6.0 Å) is larger. The structures of the complexes **41a-c**, with *cis* phosphine ligands, are presumably less spherical than **40** and seem to translate somewhat slower than **40**. Within **41**, the phenyl phosphine complexes afford the smallest D-values and thus the largest r_H values.

Extension from a P-phenyl substituent, **41a** (r_H = 6.0 Å), to a P(*p*-tolyl) substituent (r_H = 6.6 Å), **41b**, *substantially* increases the corresponding hydrodynamic radius. Complex **41b** has added six

Table 2.15. ^{1}H Diffusion Constants [a] and r_H Values (Å)

Comp	L^1	L^2	$D(^1H)$	r_H
41a	PPh_3	PPh_3	8.86	6.0
41b	$P(p\text{-Tol})_3$	$P(p\text{-Tol})_3$	8.18	6.6
41c	PPh_2Bz	PPh_2Bz	7.94	6.8
41d	$AsPh_3$	$AsPh_3$	9.30	5.8
41e	$AsPh_2Me$	$AsPh_2Me$	9.98	5.4
41f	$AsPh_2Me$	PPh_2Bz	9.28	5.8
41g	$P[OCH(CH_3)_2]_3$	$P[OCH(CH_3)_2]_3$	10.35	5.2
41h	$NH_2(CH_2)_5CH_3$	DMSO	11.79	4.5
41i[b]	$^{15}NH_2(CH_2)_5CH_3$	DMSO	11.95	4.5
41j	2-picoline	DMSO	12.18	4.4
41k	3-picoline	DMSO	12.24	4.4
41l	4-picoline	DMSO	11.94	4.5
41m	3-picoline	3-picoline	11.52	4.7

[a] in CD_2Cl_2 , x 10^{-10} m^2s^{-1}, [b] $^1J(^{15}N,^1H)$ = 72 Hz.

methyl groups to the *para* positions, thus significantly extending the radius of the molecule. This, in contrast to what we have observed for the *trans*-PEt_3 compounds, **38**, where we only add one additional substituent to the aryl group.

Substitution of PPh_3, **41a**, by PPh_2Bz, **41c**, also substantially increases the hydrodynamic radius (r_H = 6.8 Å). Presumably the benzyl groups sweep out a larger volume than the phenyl group. The nitrogen ligand/DMSO combinations afford fairly small complexes and the position of the picoline methyl group seems to be of minor importance. The $P(O\text{-}iPr)_3$ phosphite ligand has a cone angle[93] of ca 130°, smaller than that of PPh_3, ca 145°, and thus it is not surprising that complex **41g**, appears to be smaller than the tri-phenyl phosphine analogue, **41a**. Somewhat unexpected is the observation that replacement of PPh_3, **41a**, by $AsPh_3$, **41d**, affords a *smaller* hydrodynamic radius.

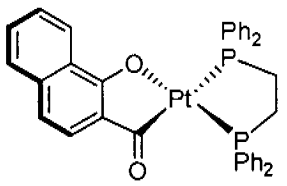

42, D = 9.32, r_H = 5.8

The related 1,2-bis-diphenylphosphinoethane chelate complex, **42**, with its smaller P-Pt-P bite angle of ca 85°[93] affords a hydrodynamic radius, 5.8 Å, which is, indeed, slightly smaller than that found for the PPh_3 complex , **41a**.

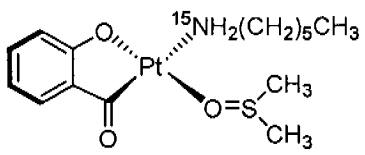

41i, $^1J(^{195}Pt,^{15}N)$ = 88Hz

The value of $^1J(^{195}Pt,^{15}N)$, for the n-hexyl amine complex, **41i**, was measured via a nitrogen, proton correlation, using the hexyl amine NH_2 resonances. A section of this spectrum is shown in Fig. 2.31. This type of measurement is well known[94, 95], especially in the chemistry of *cis*-platinum and related complexes. The relatively small value of 88 Hz is related to the strong *trans* influence of the acyl ligand[96]. Typical values of $^1J(^{195}Pt,^{15}N)$ in *cis*-platinum derivatives are of the order of 300 Hz[97].

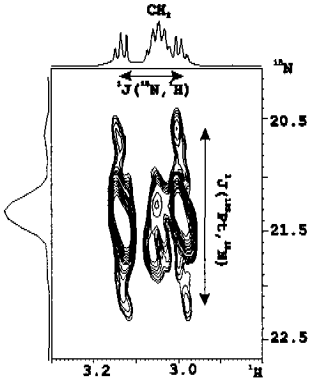

Fig. 2.31. Section of the $^{15}N,^1H$ correlation spectrum for the enriched n-hexyl amine complex, **41i**, obtained using the NH_2 amino-protons. The ^{15}N, ^1H one bond coupling constant is found to be 72 Hz and $^1J(^{195}Pt,^{15}N)$ to be 88Hz. The ^{195}Pt satellites are not resolved in the proton spectrum although they are seen as broad resonances in the nitrogen spectrum.

2.3.1 ^{195}Pt Nuclei as Diffusion Probe

Table 2.16 gives the first PGSE diffusion data obtained using ^{195}Pt (I = 1/2, 33.7% abundance). The concentrations used are fairly high due to the modest sensitivity and short relaxation characteristics[98, 99] of this nucleus. The hexachloroplatinate dianion was chosen because it is commercially available, robust, possesses relatively slow substitution kinetics and has a routine octahedral structure. Diffusion data for both Na_2PtCl_6, **43** (D = 7.13(6)) and H_2PtCl_6, **44** (D = 7.00(6)) were obtained and, in D_2O, these two complexes afford similar but not quite identical D-values. The corresponding hydrodynamic radii (from Stokes-Einstein equation described in chapter **1.3.2.3**), r_H, 3.4 Å and 3.5 Å, respectively, are reasonable (i.e., separated solvated ions) assuming a literature[39] Pt-Cl bond length of ca 2.3 - 2.4 Å and allowing for a solvation shell of ca 1 Å. On the other hand, the diffusion measurements in CD_3OD (D = 6.93 and 7.73 for **43** and **44**, respectively) reveal a different picture (see Fig. 2.32). The calculated hydrodynamic radii, r_H, 6.0 Å and 5.4 Å, for **43** and **44**, respectively, are relatively large and suggest some form of aggregation in this solvent. This may be the result of ion pairing and, possibly hydrogen bonding combined with aggregation due to the relatively high concentration employed. We also note that the ^{195}Pt chemical shift of Na_2PtCl_6 in methanol is found at higher frequency, ca 90 ppm, relative to that observed in aqueous solution. It is pertinent that Koch and co-workers[100] have recently suggested extensive ion pairing for solutions of Na_2PtCl_6 in methanol, and our findings are certainly consistent with this proposal. In any case, it is clear that the ^{195}Pt PGSE method allows us to readily distinguish between the separated ions in water and some different aggregation state in methanol. Unfortunately it was not possible to obtain, PGSE data for Na_2PtCl_4 water. This may be

due to the exchange between Na_2PtCl_4 and the aquo-complex, $Na[Pt(H_2O)Cl_3]$.[99]

Table 2.16. ^{195}Pt Diffusion Coefficients, Radius (Å)

Compound	Conc	Solvent	$D^a(^{195}Pt)$	r_H
$Na_2PtCl_6.6H_2O$	0.18	D_2O	7.13	3.4
	0.20	CD_3OD	6.93	6.0
$H_2PtCl_6.6H_2O$	0.19	D_2O	7.00	3.5
	0.19	CD_3OD	7.73	5.4

[a] $D(x\ 10^{-10}\ m^2s^{-1})$

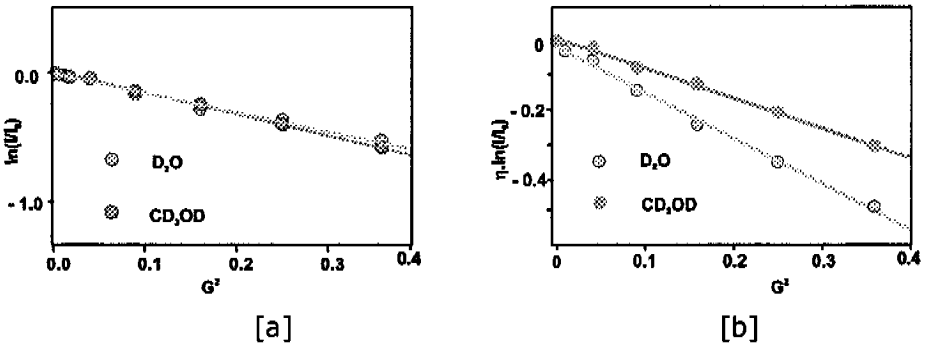

[a] [b]

Fig. 2.32. Diffusion data for $H_2PtCl_6.6H_2O$ in water (blue) and methanol (red) [a] not corrected for viscosity differences and [b] corrected for viscosity differences.

CONCLUSIONS: Diffusion data from complexes **38-42** indicate that the molecular weight is not the only important factor in determining the D and r_H values. Two large *cis* ligands may well result in an r_H value which is significantly different than that observed in an analogous *trans* geometry. The concentration dependence for the neutral complexes *trans*-PtX(Aryl)$(PEt_3)_2$, is modest. However, for salts of metals this dependence can be larger[31, 50]. ^{195}Pt PGSE measurements are possible and may well prove useful for specific problems. However, our inability to obtain data for Na_2PtCl_4 in water, together with the current concentrations required, suggest that the methodology may be limited.

2.4 Concluding Remarks

This chapter describes the synthesis, structural characterization and diffusion measurements for a modest number of catalytically relevant mono and dicationic Pd(II) BINAP complexes. Additionally, diffusion studies for a series of neutral Platinum and two cationic Rhodium carbene complexes are presented. Using these diffusion data (D values) and NOE measurements leads to set of conclusions,

1. Solvent dependent ion pairing is observed and it follows the sequence, $CHCl_3$ > THF > CH_2Cl_2 > CH_3CN.
2. Anion dependent ion pairing is follows the sequence $CF_3SO_3^-$, BF_4^-, PF_6^- > BAr_4^{F-}.
3. Anion relative position: The anions approach the positively charged centers, avoiding the region of the negatively charged ligands (supported by DFT calculations). Where hydrogen bonding is involved, the anion is in close vicinity to the cation.
4. The anion senses the change of the chirality.
5. In the cyclometallated amine complexes the chirality induces a conformational change of the amine ring.

Thus, we believe this combined diffusion/HOESY approach to ion pairing and the localization of the counterions relative to cationic organometallic fragment to be extremely promising.

2.5 Experimental section

General Comments. All air sensitive manipulations were carried out under a nitrogen atmosphere. All solvents were dried over an appropriate drying agent, and then distilled under nitrogen. Deuterated solvents were dried by distillation over molecular sieves, and stored under nitrogen. The ligands *rac*-BINAP (Strem), (R)-BINAP, (S)-BINAP (Alfa Aesar), *p*-tolyl-BINAP (Merck), (R)-(+)-N,N-dimethyl 1-phenylethylamine (Aldrich), (2R,3R)-Chiraphos, (2S,3S)-Chiraphos (Acros), 1,3 diketones 3-methyl-2,4-dione, **9,** Ethyl 2-methylacetoacetate, **10,** (E)-3-but-2-enoyloxazolidin-2-one, **11,** (Acros organics) and the silver salts (Aldrich) were purchased from commercial sources and used as received. The dichloro-metal complexes $PdCl_2L_2$, L_2 = *rac*-BINAP, the chloro-bridged metal complexes $(PdClL)_2$, L = Cyclometallated ligands (Schiffs base), (R) and (*S*) N,N-dimethyl 1-phenylethylamine (**18a-f** and **19**) and the α, β-unsaturated N-imides (**6, 7** and **8**) are synthesized according to known literature procedure[101-103]. The palladium complexes **1b, 2b, 26** and **27** were synthesized following literature procedure[2, 4, 71]. Both $Na_2PtCl_6 \cdot 6H_2O$, **43** and $H_2PtCl_6 \cdot 6H_2O$, **44** were obtained from Acros and Alpha Aesar respectively. Complex **41i** was prepared enriched in ^{15}N (>90 % ^{15}N). The Pt complexes **38-42** are all known and were prepared[96, 104, 105] in this laboratory earlier. ^{1}H, ^{13}C, ^{31}P, ^{19}F, and ^{15}N and 2D NMR spectra were recorded with Bruker DPX-250, 300, 400, 500 and 700 MHz spectrometers at room temperature unless otherwise noted. Elemental analysis and mass spectra were performed at ETH Zürich.

Diffusion measurements. All of the PGSE measurements were carried out using the stimulated echo pulse sequence and performed on a Bruker Avance spectrometer, 300 or 400 MHz,

equipped with a microprocessor-controlled gradient unit and a multinuclear inverse probe with an actively shielded Z-gradient coil. The shape of the gradient pulse was rectangular, and its length was of 1.75 ms. The gradient strength was incremented in 4 % steps from 4 % to 60 %, so that 12-15 points could be used for regression analysis. The time between midpoints of the gradients was 167.75 ms and gradient recovery time was set 100 μs for all experiments. All the diffusion ^{1}H spectra were acquired using 16K points, 16 or 32 transients, a 5 s relaxation delay and a 1.5 s acquisition time. All the ^{19}F spectra were acquired using 16K points, 16 or 8 transients, a relaxation delay of 5 times T_1 (approximately 15 - 20 s), and a 4 s acquisition time. Both the ^{1}H and ^{19}F diffusion experiments were processed using Bruker software with an exponential multiplication (EM) window function and a line broadening of 1.0 HZ. The measurements were carried out without spinning at a set temperature of 299 K or 300 K within the NMR probe. The diffusion values were measured on 2 mM in CD_2Cl_2, $CDCl_3$ and d_8-THF solutions. Cation diffusion rates were measured using the ^{1}H signal from the aromatic protons of BINAP and/or from methyl protons of chelated ligand. Anion diffusion was obtained from the ^{19}F resonances. The error in the D values is thought to be ± 0.06. The slope of the lines, m, were obtained by plotting the decrease in the natural logarithm of the signal intensity vs G^2 (see section **1.3.2.3**).

The diffusion coefficients reported were determined using the diffusion coefficient of HDO in D_2O as a reference (D_{HDO} = 1.9 x 10^{-9} m^2 s^{-1}), which afforded a slope of 2.005 x 10^{-4}. The data obtained were used to calculate the D values of the samples, according to

$$\frac{m_x}{m_H} = \left(\frac{\gamma_x}{\gamma_H}\right)^2 \left(\frac{\delta_x}{\delta_{HDO}}\right)^2 \frac{\left(\Delta - \frac{\delta}{3}\right)_x}{\left(\Delta - \frac{\delta}{3}\right)_{HDO}}$$

or

$$D = \frac{m_{obs} \times D_{HDO}}{m_{HDO}}$$

All the reported D values are derived from lines that have correlation coefficient of > 0.99. The D-values can be related to the hydrodynamic radii of the molecules via the Stokes-Einstein equation (Eq. (6), see section **1.3.2**) and this allows for a viscosity correction.

The solvent viscosities used for the calculation of r_H were 0.414, 0.534 and 0.461 at 299K for CD_2Cl_2, $CDCl_3$ and d_8-THF respectively.

NOE Measurements. The $^1H,^1H$ NOESY NMR experiments were acquired by the standard three-pulse sequence (noesyph) using a 600 ms or 1 s relaxation delay and 600 ms of mixing time on a Bruker spectrometer at a set temperature of 298 K with phse cycling by the TPPI method. Typically, 16 transients (DS 16) were acquired into 2 K data points for each of the 512 values of t_1. A QSINE weighting function was used in each dimension prior to Fourier transformation into a 2K X 1K data matrix. The $^{19}F,^1H$-HOESY NMR experiments were acquired using the standard four-pulse sequence (invhoesy) with either a 600 or 800 ms mixing time. The doubly tuned TXI probe head of the 400 MHz spectrometer was set at 298 K. Typically, 16 transients (DS 4) were acquired into 2 K data points for each of the 512 or 1 K values of t_1. A QSINE and EM (F1 and F2 dimension respectively) weighting function was used in each dimension prior to Fourier transformation into a 2K X 1K data matrix. The delay between increments was set to 1s or 2s.

[Pd(H_2O)$_2$(*rac*-BINAP)](PF_6)$_2$ (1b)

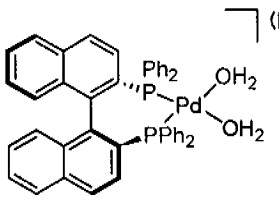

To a solution of $PdCl_2$(*rac*-BINAP) (100 mg, 0.125 mmol) in dry acetone (50 ml) were added water (0.045ml, 20eq) and $AgPF_6$ (70 mg, 2.5 mmol, 2.2 eq) at 25 °C. The reaction mixture was then stirred at 25 °C for 3 h. The precipitate of AgCl was filtered over Celite and the solvent was concentrated under vacuum. The crude product was obtained as a yellow solid. **1b.** (Yield: 192 mg, 0.182 mol, 97 %).

^{1}H NMR (THF-d_8, 400 MHz, 25 °C): δ 2.65 (br s, 4H), 6.6-8.3 (m, 32H); ^{31}P{^{1}H}-NMR (THF-d_8, 161 MHz, 25 °C): δ 34.3 (s), -144 (sept, $^1J_{FP}$ = 712 Hz); ^{19}F NMR (THF-d_8, 282 MHz, 25 °C): δ -74 (d, $^1J_{FP}$ = 712 Hz).

(ESI-MS;m/z) Pd(BINAP): 727; BINAP-PPh_2: 437; Pd(BINAP)(H_2O)$_2$: 763.

[Pd(μ-OH)(*rac*-BINAP)]$_2$(PF_6)$_2$ (2b)

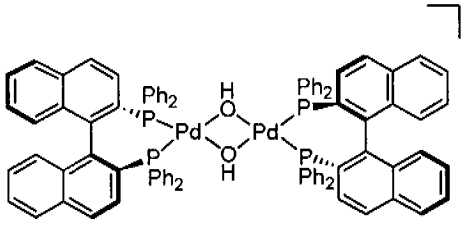

To a solution of **1b** (97 mg, 0.092 mmol) in dry acetone (15 ml) was added dried 4-Å molecular sieves (1-2 mm, 1 g). The reaction mixture was stirred at 25°C for 3 h. After filtration over Celite, the acetone was concentrated under vacuum. The crude product was obtained as an orange solid. **2b.** (Yield: 19 mg, 0.01 mol 23 %)

^{1}H NMR (CD_2Cl_2, 400 MHz, 25 °C): δ -2.9 (br s, 2H), 6.6-7.8 (m, 64H); ^{31}P {^{1}H}-NMR (CD_2Cl_2, 161 MHz, 25 °C): δ 29.3 (s), -144 (sept, $^1J_{FP}$ = 711 Hz); ^{19}F NMR (CD_2Cl_2, 282 MHz, 25 °C): δ -73 (d, $^1J_{FP}$ = 711 Hz).

(ESI-MS; m/z) M^+-PF_6-2OH: 1457; M^+- PF_6- PPh_2: 1273; M^+ - PF_6 - 2OH - BINAP + PPh_2: 1021; Pd (BINAP): 727; BINAP - PPh_2: 437

[Pd_2(μ-OH)(μ-{NH(*p*-ClC_6H_4)})(*rac*-BINAP)$_2$](CF_3SO_3)$_2$ (3a)

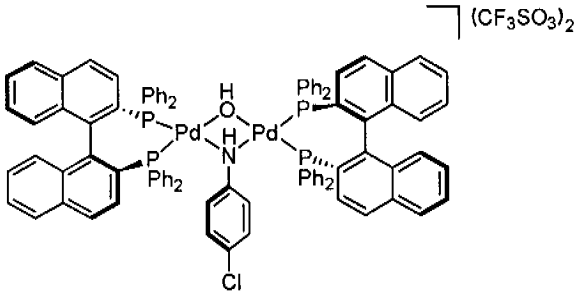

To a solution of **2a** (100 mg, 0.056 mmol) in THF (10 ml) was added *p*-chloroaniline (57 mg, 0.445 mmol). The reaction mixture was stirred at 25 °C for 3 h, during which time a clear red solution was obtained. The THF was then concentrated under vacuum. The crude solid was washed with pentane and then dried under *vacuum*. The product, **3a**, was obtained as an orange solid. (Yield: 101 mg, 0.053 mmol, 95 %) The product was recrystallized from a THF-pentane solution.

^{1}H-NMR (298K, d_8-THF): -3.74 (dd, $^3J_{HP}$ = 2.7 Hz, $^3J_{HP}$ = 2.7 Hz, OH), 6.48-7.96 (m, 69 H); ^{19}F-NMR (298K, d_8-THF): -78 (s, CF_3); ^{31}P-NMR (298K, d_8-THF): 25.0 (dd, $^2J_{PP}$ = 23.2 Hz, $^4J_{PP}$ = 5.8 Hz), 25.5 (d, $^2J_{PP}$ = 24.1 Hz), 26.3 (d, $^2J_{PP}$ = 23.1 Hz), 27.7 (dd, $^2J_{PP}$ = 24.2 Hz, $^4J_{PP}$ = 5.8 Hz); ^{15}N-NMR (213K, CD_2Cl_2) 30.0 ($NH_2C_6H_4Cl$) 55.1 (μ-NHC_6H_4Cl)

(ESI-MS) M^+: 1750; M^+ - OTf^-: 1600; Pd (BINAP)(Aniline): 856; Pd(BINAP)(OH): 744; BINAP – PPh_2:437.

[Pd_2(μ-OH)(μ-{NH(*p*-Tol)})(*rac*-BINAP)$_2$](CF_3SO_3)$_2$ (3b)

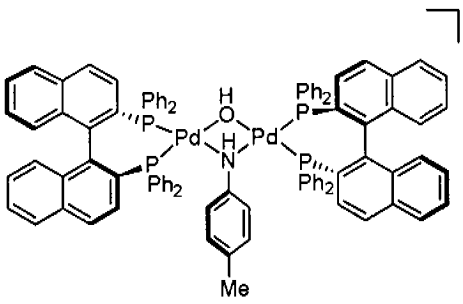

To a solution of **2a** (100 mg, 0.056 mmol) in THF (15 ml) was added *p*-Methylaniline (51.2 mg, 0.479 mmol) The reaction mixture was stirred at 25 °C for 3 h, during which time a clear red solution was obtained in THF. The THF was then concentrated under vacuum. The crude solid was washed with ether and then dried under *vacuum*. The product, **3b**, was obtained as a red solid. Yield: 49 mg, 0.026 mmol, 47 %. Red needles were obtained from recrystallisation from a THF-ether solution.

^{1}H-NMR (298K, d_8-THF): -3.86 (dd, $^3J_{HP}$ = 2.9 Hz, $^3J_{HP}$ = 2.9 Hz, OH), 6.41-7.96 (m, 69 H); ^{19}F-NMR (298K, d_8-THF): -78 (s, CF_3); ^{31}P-NMR (298K, d_8-THF): 24.6 (dd, $^2J_{PP}$ = 23.5 Hz, $^4J_{PP}$ = 5.8 Hz), 25.1 (d, $^2J_{PP}$ = 26.3 Hz), 26.5 (d, $^2J_{PP}$ = 23.6 Hz), 27.7 (dd, $^2J_{PP}$ = 26.1 Hz, $^4J_{PP}$ = 5.8 Hz).

(ESI-MS) M^+: 1729; Pd(BINAP)(Aniline): 834; Pd(BINAP)(OH): 744; BINAP – PPh_2: 437.

$[Pd_2(\mu\text{-}OH)(\mu\text{-}\{NH\text{-}(p\text{-}MeO\text{-}C_6H_4)\})(rac\text{-}BINAP)_2](CF_3SO_3)_2$ (3c)

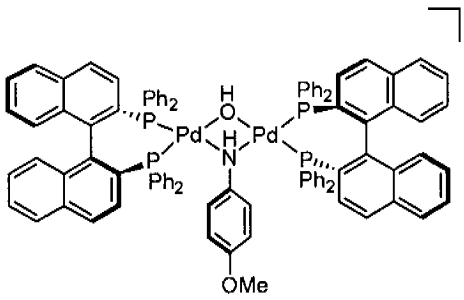

To a solution of **2a** (100 mg, 0.056 mmol) in THF (10 ml) was added *p*-Methoxyaniline (60 mg, 0.488 mmol) The reaction mixture was stirred at 25 °C for 3 h, during which time a dark red suspension was obtained in THF. The THF was then concentrated under vacuum. The crude solid was washed with ether and then dried under *vacuum*. The product, **3c**, was obtained as a dark red solid. Yield: 103 mg, 0.054 mmol, 97 %

^{1}H-NMR (298K, d_8-THF): -3.97 (dd, $^3J_{HP}$ = 2.7 Hz, $^3J_{HP}$ = 2.7 Hz, OH), 6.43-8.04 (m, 69H); ^{19}F-NMR (298 K, d_8-THF): -78 (s, CF_3); ^{31}P-NMR (298K, d_8-THF): 24.3 (dd, $^2J_{PP}$ = 25.4 Hz, $^4J_{PP}$ = 5.7 Hz), 25.1 (d, $^2J_{PP}$ = 27.6 Hz), 26.6 (d, $^2J_{PP}$ = 25.7 Hz), 27.6 (dd, $^2J_{PP}$ = 27.2 Hz, $^4J_{PP}$ = 5.7 Hz); ^{15}N-NMR (213K, CD_2Cl_2) 28.6 ($NH_2C_6H_4Cl$), 52.5 (μ-NHC_6H_4Cl)
(ESI-MS) M^+: 1746; Pd (BINAP)(Aniline): 850; Pd(BINAP)(OH): 744; BINAP – PPh_2: 437.

$[Pd(\mu\text{-}O_2PF_2)(rac\text{-}BINAP)]_2(PF_6)_2$ (4)

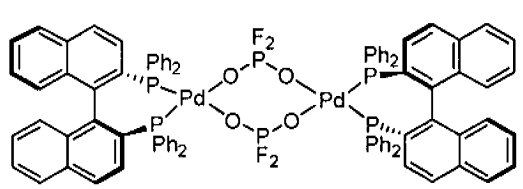

To 1 equiv of $[PdCl_2(rac\text{-}BINAP)]$ (46.5 mg, 800.01 g mol^{-1}, 58.1 x 10^{-3} mol) were added 2 equiv

of the $AgPF_6$ (30.8 6mg, 252.86 g mol^{-1}) in wet acetone. The reaction mixture was stirred at 25 °C for 3 h. After this time, the yellow solution was evaporated under reduced pressure and dried under vacuum to afford the product, **4**, as a yellow powder. (Yield: 48 mg, 0.025 mol, 84 %).

^1H NMR (CD_2Cl_2, 400 MHz, 25 °C): 6.7-7.8 (m, 64H); $^{31}P\{^1H\}$-NMR (CD_2Cl_2, 161 MHz, 25 °C): δ 33.3 (s), -15.5 (t, $^1J_{PF}$ = 962 Hz), -144.1 (sept, $^1J_{PF}$ = 707 Hz); ^{19}F NMR (CD_2Cl_2, 282 MHz, 25 °C): δ -73 (d, $^1J_{PF}$ = 707 Hz), -83 (d, J_{PF} = 962 Hz).

(ESI-MS) M^+ 930, [Pd(μ-O_2PF_2)(BINAP)]$_2$

CHN % {found (calculated)} C {54.09 (54.20)} H {3.34(3.31)}

[Pd(*rac*-BINAP)($C_{11}H_{10}NO_2$)](CF_3SO_3) (12a)

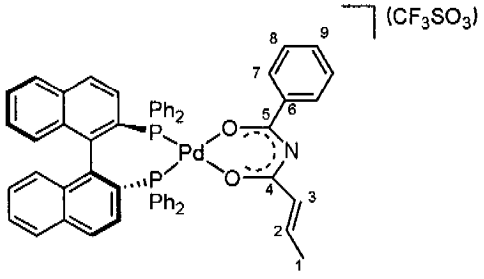

To 1 equiv of [Pd(μ-OH)(*rac*-BINAP)]$_2$[CF_3SO_3]$_2$ (99.5 mg, 1790.36 g mol^{-1}, 55.6 x 10^{-3} mol) were added 2 equiv of the $C_{11}H_{11}NO_2$ (21 mg, 189 g mol^{-1}, 111.1 x 10^{-3} mol) in dichloromethane. The reaction mixture was stirred at 25 °C for 3 h. The resulting yellow solution was reduced under *vacuum*. The resulting residue was washed with diethyl ether to afford [$C_{56}H_{42}P_2O_5NF_3PdS$] **12a.** (Yield: 100 mg, 0.094 mol 84 %).

^1H NMR (CD_2Cl_2, 400 MHz, 25 °C): δ 1.65 (d, 3H, H1, J = 6.5 Hz), 5.7-6.0 (m, 2H, H2/3), 6.7-7.9 (m, 37H); $^{31}P\{^1H\}$-NMR (CD_2Cl_2, 161 MHz, 25 °C): δ 33.5 (d, AB spin, J = 32 Hz); ^{19}F NMR (CD_2Cl_2,

282 MHz, 25 °): δ -78.8 (s); $^{13}C\{^{1}H\}$-NMR (CD_2Cl_2, 100 MHz, 25 °C): δ 18.2 (s, C1), 128.1 (s, C8), 128.8 (s, C9), 129.6 (s, C3), 130.1 (s, C7), 135.4 (s, C6), 146.5 (s, C2), 173.3 (d, C5, $^{1}J_{CN}$ = 3 Hz), 174.1 (d, C4, $^{1}J_{CN}$ = 3 Hz), 120-180 (BINAP).

(ESI-MS) M^+ 916.2, $M\text{-}C_{11}H_{10}NO_2]^+$ 729.0

CHN%{found(calculated)}[Pd(*rac*-BINAP)($C_{11}H_{10}NO_2$)][CF_3SO_3].H_2O
C {62.07 (61.95)}H {4.10 (4.03)} N {1.29 (1.29)}

[Pd(*rac*-BINAP)($C_{11}H_{10}NO_2$)](BF_4) (12b)

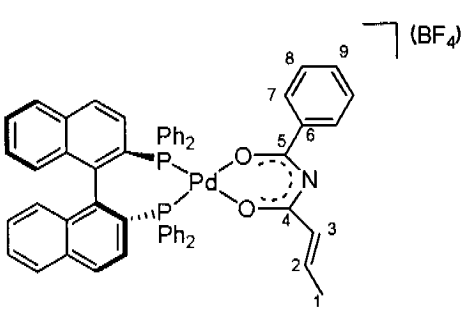

To 1 equiv of [Pd(μ-OH)(*rac*-BINAP)]$_2$[BF_4]$_2$ (33.1 mg, 1665.84 g mol^{-1}, 19.8 x 10^{-3} mol) were added 2.1 equiv of the $C_{11}H_{11}NO_2$ (6.7 mg, 189 g mol^{-1}, 35.4 x 10^{-3} mol) in dichloromethane. The reaction mixture was stirred at 25 °C for 3 h. The resulting yellow solution was reduced under *vacuum*. The resulting residue was washed with diethyl ether to afford [$C_{55}H_{42}BF_4NO_2P_2Pd$] **12b.** (Yield: 31 mg, 87 %).

^{1}H NMR (CD_2Cl_2, 400 MHz, 25 °C): δ 1.65 (d, 3H, H1, *J* = 6.8 Hz), 5.7-6.0 (m, 2H, H2/3), 6.7-7.9 (m, 37H); $^{31}P\{^{1}H\}$-NMR (CD_2Cl_2, 161 MHz, 25 °C): δ 33.5 (d, AB spin, *J* = 32 Hz); ^{19}F NMR (CD_2Cl_2, 282 MHz, 25 °): δ -153.9 (s); $^{13}C\{^{1}H\}$-NMR (CD_2Cl_2, 100 MHz, 25 °C): δ 18.0 (s, C1), 128.1 (s, C8), 128.9 (s, C9), 129.6 (s, C3), 130.1 (s, C7), 135.4 (s, C6), 146.5 (s, C2), 173.3 (d, C5, $^{1}J_{CN}$ = 3 Hz), 174.0 (d, C4, $^{1}J_{CN}$ = 3 Hz), 120-180 (BINAP).

(ESI-MS) M^+ 916.2, M-$C_{11}H_{10}NO_2]^+$ 729.0

[Pd(*rac*-BINAP)($C_{12}H_{12}NO_3$)](CF_3SO_3) (13a)

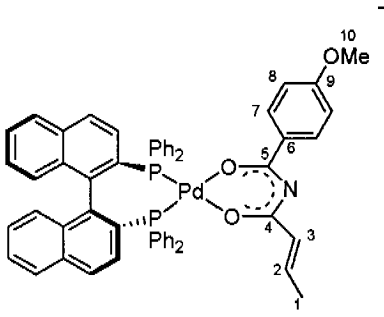

To 1 equiv of [Pd(μ-OH)(*rac*-BINAP)]$_2$[CF_3SO_3]$_2$ (2.8 mg, 1790.36 g mol^{-1}, 23.9 x 10^{-3} mol) were added 2 equiv of the $C_{12}H_{13}NO_3$ (10.6 mg, 219.2 g mol^{-1}, 48.3 x 10^{-3} mol) in dichloromethane. The reaction mixture was stirred at 25 °C for 3 h. The resulting yellow solution was reduced under *vacuum*. The resulting residue was washed with diethyl ether to afford **13a.** (Yield: 45 mg, 0.0410 mol, 85 %).

^{1}H NMR (CD_2Cl_2, 400 MHz, 25 °C): δ 1.63 (d, 3H, H1 J = 6.0 Hz), 3.8 (s, 3H, H10), 5.7-5.9 (m, 2H, H2/3), 6.6-7.9 (m, 36H); ^{31}P{^{1}H}-NMR (CD_2Cl_2, 161 MHz, 25 °C): δ 33.5 (d, AB spin, $^2J_{PP}$ = 33 Hz); ^{19}F NMR (CD_2Cl_2, 282 MHz, 25 °C): δ -78.8 (s). ^{13}C{^{1}H}-NMR (CD_2Cl_2, 100 MHz, 25 °C): δ 18.2 (s, C1), 55.6 (s, C10), 113.4 (s, C8), 127.9 (s, C6), 129.6 (s, C3), 132.5 (s, C7), 135.4 (s, C6), 145.9 (s, C2), 164.7 (s, C9), 172.8 (d, C5), 173.2 (d, C4, $^1J_{CN}$ = 3 Hz), 120-180 (BINAP).

(ESI-MS) M^+ 946.3

CHN%{found(calculated)}[Pd(*rac*-BINAP)($C_{12}H_{12}NO_3$)][CF_3SO_3].H_2O
C {61.48 (61.89)} H {4.17 (4.11)} N {1.26 (1.30)}

[Pd(*rac*-BINAP)($C_{12}H_{12}NO_3$)](BF_4)(13b)

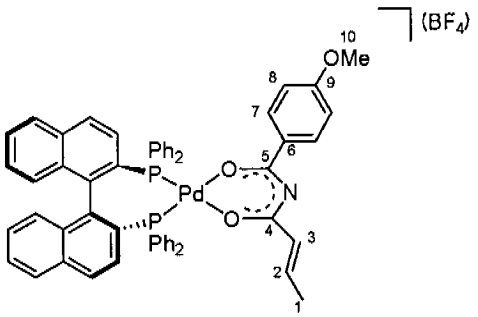

To 1 equiv of [Pd(μ-OH)(*rac*-BINAP)]$_2$[BF_4]$_2$ (51 mg, 1665.84 g mol^{-1}, 30.6 x 10^{-3} mol) were added 2 equiv of the $C_{12}H_{13}NO_3$ (13.4 mg, 219.2 g mol^{-1}, 61.1 x 10^{-3} mol) in dichloromethane. The reaction mixture was stirred at 25 °C for 3 h. The resulting yellow solution was reduced under *vacuum*. The resulting residue was washed with diethyl ether to afford **13b.** (Yield: 55 mg, 0.0410 mol, 87 %).

^{1}H NMR (CD_2Cl_2, 400 MHz, 25 °C): δ 1.63 (d, 3H, H1 J = 6.8 Hz), 3.8 (s, 3H, H10), 5.7-5.9 (m, 2H, H2/3), 6.6-7.9 (m, 36H); ^{31}P{^{1}H}-NMR (CD_2Cl_2, 161 MHz, 25 °C): δ 33.5 (d, AB spin, $^2J_{PP}$ = 33 Hz); ^{19}F NMR (CD_2Cl_2, 282 MHz, 25 °C): δ -153.9 (s); ^{13}C{^{1}H}-NMR (CD_2Cl_2, 100 MHz, 25 °C): δ 17.9 (s, C1), 55.8(s, C10), 113.4 (s, C8), 127.9 (s, C6), 129.6 (s, C3), 132.5(s, C7), 135.4 (s, C6), 145.8 (s, C2), 164.2 (s, C9), 172.8 (d, C5), 173.2 (d, C4, $^1J_{CN}$ = 3 Hz), 120-180 (BINAP).

(ESI-MS) M^+ 946.3

[Pd(*rac*-BINAP)($C_{14}H_{16}NO_2$)](CF_3SO_3) (14a)

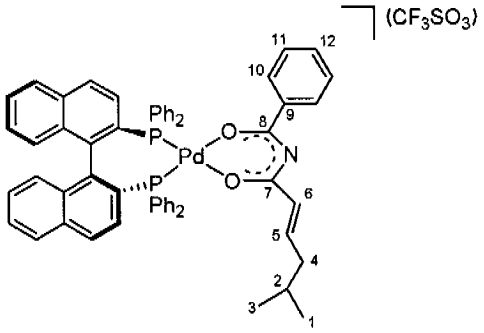

To 1 equiv of [Pd(μ-OH)(*rac*-BINAP)]$_2$[CF_3SO_3]$_2$ (35 mg, 1790.36 g mol^{-1}, 19.5 x 10^{-3} mol) were added 3 equiv of the $C_{14}H_{17}NO_2$ (13.6 mg, 231.13 g mol^{-1}, 58.8 x 10^{-3} mol) in dichloromethane. The reaction mixture was stirred at 25 °C for 3h. The resulting yellow solution was reduced under *vacuum*. The resulting residue was washed with diethyl ether to afford **14a.** (Yield: 58 mg, 89 %).

^{1}H NMR (CD_2Cl_2, 400 MHz, 25 °C): δ 0.81 (t, 6H, J = 5.2 Hz, H1,3), 1.53 (m, 1H, H2), 1.9 (m, 2H, H4), 5.3-6.0 (m, 2H, H5/6), 6.7-7.8 (m, 37H); ^{31}P{^{1}H}-NMR (CD_2Cl_2, 161 MHz, 25 °C): δ 33.6 (d, $^2J_{pp}$ = 33 Hz), 34.7 (d, $^2J_{pp}$ = 33 Hz); ^{19}F NMR (CD_2Cl_2, 282 MHz, 25 °C): δ -79.1 (s); ^{13}C{^{1}H}-NMR (CD_2Cl_2, 100 MHz, 25 °C): δ 22.4 (s, C3), 22.6 (s, C1), 28.0 (s, C4), 41.9 (s, C2), 173.3 (s, C8), 174.0 (s, C7) 120-180 (BINAP).

(ESI-MS) M^+ 860, M-$C_{14}H_{16}NO_2]^+$ 729.0

[Pd(*rac*-BINAP)($C_{14}H_{16}NO_2$)](BF_4)(14b)

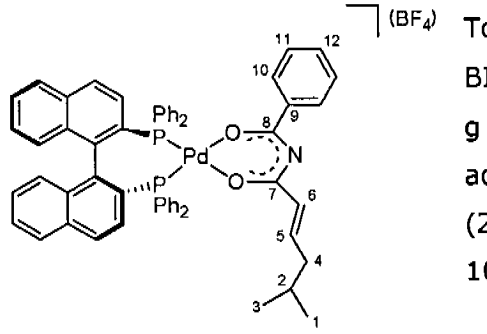

To 1 equiv of [Pd(μ-OH)(*rac*-BINAP)]$_2$[BF_4]$_2$ (52.3 mg, 1665.84 g mol^{-1}, 31.4 x 10^{-3} mol) were added 3 equiv of the $C_{14}H_{17}NO_2$ (21.8 mg 231.13 g mol^{-1}, 94.3 x 10^{-3} mol) in dichloromethane. The

reaction mixture was stirred at 25 °C for 3h. The resulting yellow solution was reduced under *vacuum*. The resulting residue was washed with diethyl ether to afford **14b.** (Yield: 54 mg, 82 %).

^{1}H NMR (CD_2Cl_2, 400 MHz, 25 °C): δ 0.81 (t, 6H, H 1/3, J = 5.2 Hz), 1.53 (m, 1H, H2), 1.9 (m, 2H, H4), 5.3-6.0 (m, 2H, H 5/6), 6.7-7.8 (m, 37H); ^{31}P{^{1}H}-NMR (CD_2Cl_2, 161 MHz, 25 °C): δ 33.6 (d, AB spin, $^2J_{PP}$ = 32 Hz); ^{19}F NMR (CD_2Cl_2, 282 MHz, 25 °C): δ -154.0 (s); ^{13}C{^{1}H}-NMR (CD_2Cl_2, 100 MHz, 25 °C): δ 22.4 (s, C3), 22.6 (s, C1), 28.0 (s, C4), 41.9 (s, C2), 173.3 (s, C8), 174.0 (s, C7) 120-180 (BINAP).

(ESI-MS) M^+ 871.2, $M\text{-}C_{14}H_{16}NO_2]^+$ 729.0

[Pd(*rac*-BINAP)($C_6H_9O_2$)](CF_3SO_3) (15a)

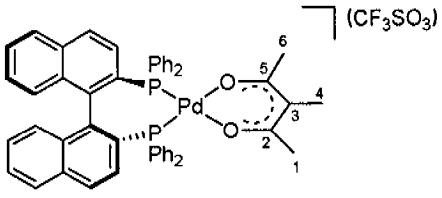

To 1 equiv of [Pd(μ-OH)(*rac*-BINAP)]$_2$[CF_3SO_3]$_2$ (50 mg, 1790.36 g mol^{-1}, 27.9 x 10^{-3} mol) were added 2 equiv of the $C_6H_{10}O_2$ (6.5 μl, 144.14 g mol^{-1}, 0.981 g cm^{-3}) in dichloromethane. The reaction mixture was stirred at 25 °C for 3h. The resulting yellow solution was reduced under *vacuum*. The resulting residue was washed with diethyl ether to afford **15a.** (Yield: 48 mg, 0.048 mol, 86 %).

^{1}H NMR (CD_2Cl_2, 400 MHz, 25 °C): δ 1.58 (s, 6H, H1,6), 1.8 (s, 3H, H4), 6.7-7.8 (m, 32H); ^{31}P{^{1}H}-NMR (CD_2Cl_2, 161 MHz, 25 °C): δ 31.9 (s); ^{19}F NMR (CD_2Cl_2, 282 MHz, 25 °C): δ -78.8 (s); ^{13}C{^{1}H}-NMR (CD_2Cl_2, 100 MHz, 25 °C): δ 16.0 (s, C4), 26.9 (t, C1/C6, J_{CP} = 5Hz), 104.3 (s, C3), 185.5 (s, C2/C5), 120-180 (BINAP).

(ESI-MS) M^+ 841.1, $M\text{-}C_6H_9O_2]^+$ 729.0.

CHN % {found (calculated)} [Pd(*rac*-BINAP)($C_6H_9O_2$)][CF_3SO_3].H_2O C {61.73 (60.86)} H {4.27 (4.23)}

[Pd(*rac*-BINAP)($C_6H_9O_2$)](BF_4) (15b)

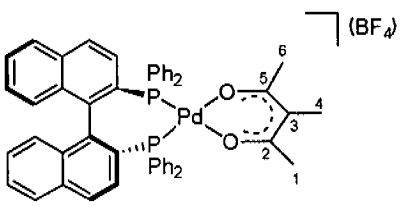

To 1 equiv of [Pd(μ-OH)(*rac*-BINAP)]$_2$[BF_4]$_2$ (54.8 mg, 1665.84 g mol^{-1}, 27.9 x 10^{-3} mol) were added 2 equivalents of the $C_6H_{10}O_2$ (7.7 µl, 144.14 g mol^{-1}, 0.981 g cm^{-3}) in dichloromethane. The reaction mixture was stirred at 25 °C for 3h. The resulting yellow solution was reduced under *vacuum*. The resulting residue was washed with diethyl ether to afford **15b.** (Yield: 50 mg, 0.053 mol, 96 %).

^{1}H NMR (CD_2Cl_2, 400 MHz, 25 °C): δ 1.57 (s, 6H, H 1/6), 1.82 (s, 3H, H4), 6.7-7.8 (m, 32H); $^{31}P\{^1H\}$-NMR (CD_2Cl_2, 161 MHz, 25 °C): δ 31.9 (s); ^{19}F NMR (CD_2Cl_2, 282 MHz, 25 °C): δ -154 (s); $^{13}C\{^1H\}$-NMR (CD_2Cl_2, 100 MHz, 25 °C): δ 15.9 (s , C4), 26.6 (t, C1/C6, J_{CP} = 5 Hz), 104.3 (s, C3), 185.3 (s, C2/C5), 120-180 (BINAP).

MS (ESI; m/z) M^+ 840.9, $M\text{-}C_6H_9O_2]^+$ 729.0

CHN % {found (calculated)} [Pd(*rac*-BINAP)($C_6H_9O_2$)][BF_4] C {63.92 (64.57)} H {4.60 (4.55)}

[Pd(*rac*-BINAP)($C_7H_{11}O_3$)](CF_3SO_3) (16a)

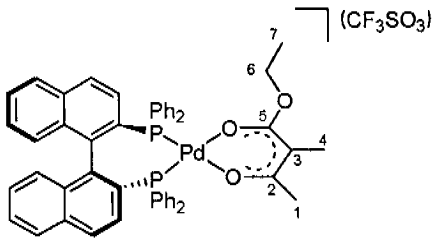

To 1 equiv of [Pd(μ-OH)(*rac*-BINAP)]$_2$[CF_3SO_3]$_2$ (40.7 mg, 1790.36 g mol^{-1}, 24.4 x 10^{-3} mol) were added 2 equiv of the $C_7H_{12}O_3$ (7.0 µl, 144.17 g mol^{-1}, 1.019 g cm^{-3}) in dichloromethane. The reaction mixture was stirred at 25 °C for 3h. The resulting yellow solution was reduced *in vacuo*. The resulting residue was washed with Et_2O to afford **16a.** (Yield: 42 mg, 0.045 mol, 89 %).

^{1}H NMR (CD_2Cl_2, 400 MHz, 25 °C): δ 0.75 (t, 3H, H7, *J* = 7.1 Hz), 1.47 (s, 3H, H1), 1.7 (s, 3H, H4), 2.7-2.9 (m, 2H, H6), 6.7-7.8 (m, 32H); ^{31}P{^{1}H}-NMR (CD_2Cl_2, 161 MHz, 25 °C): δ 30.4 ppm (d, $^2J_{pp}$ = 38 Hz), 34.7 (d, $^2J_{pp}$ = 38 Hz); ^{19}F NMR (CD_2Cl_2, 282 MHz, 25 °C): δ -154 (s); ^{13}C{^{1}H}-NMR (CD_2Cl_2, 100 MHz, 25 °C): δ 13.0 (s, C4), 14.3 (s, C7), 25.8 (s, C1), 60.9 (s, C6), 90.5 (s, C3), 169.8 (s, C2), 184.2 (s, C5), 120-180 ppm (BINAP).

MS (ESI; m/z) M^+ 871.2 , M-$C_7H_{11}O_3]^+$ 729.0

CHN % {found (calculated)} [Pd(*rac*-BINAP)($C_7H_{11}O_3$)][CF_3SO_3].H_2O
C {60.10 (60.02)} H {4.49 (4.46)}

[Pd(*rac*-BINAP)($C_7H_{11}O_3$)][BF_4] (16b)

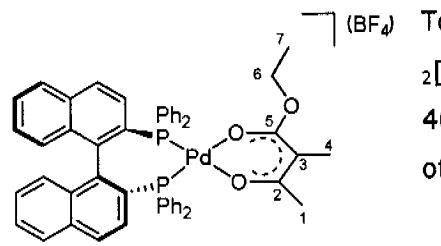

To 1 equiv of [Pd(μ-OH)(*rac*-BINAP)]$_2$[BF_4]$_2$ (67.0 mg, 1665.84 g mol^{-1}, 40.2 x 10^{-3} mol) were added 2 equiv of the $C_7H_{12}O_3$ (11.4 µl, 144.17 g

mol^{-1}, 1.019 g cm^{-3}) in dichloromethane. The reaction mixture was stirred at 25 °C for 3h. The resulting yellow solution was reduced *in vacuo*. The resulting residue was washed with Et_2O to afford **16b.** (Yield: 47 mg, 0.045 mol, 86 %).

^1H NMR (CD_2Cl_2, 400 MHz, 25 °C): δ 0.75 (t, 3H, H7, J = 7.1 Hz), 1.47 (s, 3H, H1), 1.7 (s, 3H, H4), 2.7-2.9 (m, 2H, H6), 6.7-7.8 (m, 32H); $^{31}P\{^1H\}$-NMR (CD_2Cl_2, 161 MHz, 25 °C): δ 30.4 (d, $^2J_{pp}$ = 38 Hz), 34.7 (d, $^2J_{pp}$ = 38 Hz); ^{19}F NMR (CD_2Cl_2, 282 MHz, 25 °C): δ -154 (s) $^{13}C\{^1H\}$-NMR (CD_2Cl_2, 100 MHz, 25 °C): δ 13.0 (s , C4), 14.3 (s, C7), 25.8 (s, C1), 60.9 (s, C6), 90.5 (s, C3), 169.9 (s, C2), 184.0 (s, C5), 120-180 (BINAP)

MS (ESI; m/z) M^+ 871.2, $M\text{-}C_7H_{11}O_3]^+$ 729.0

[Pd(*rac*-BINAP)($C_{15}H_{14}N$)](CF_3SO_3) (20a)

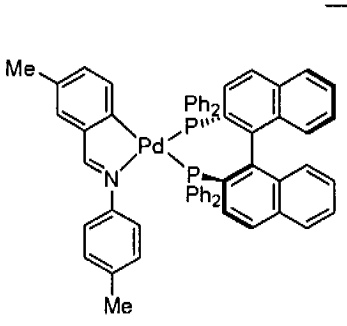

To 1 equiv of [Pd(μ-Cl)($C_{15}H_{14}N$)]$_2$ (33.4 mg, 700.3 g mol^{-1}, 47.7 x 10^{-3} mol) were added 2 equiv of the *rac*-BINAP (59.4 mg, 622.67 g mol^{-1}, 95.4x 10^{-3} mol) and 2 equiv of AgOTf (24.5 mg, 256.94 g mol^{-1}, 95.4 x 10^{-3} mol) in dichloromethane. The reaction mixture was stirred at 25 °C for 3 h. The resulting yellow solution was separated from the solid and reduced under vacuum. [$C_{60}H_{46}F_3NO_3P_2PdS$] **20a.** (Yield: 90 mg, 0.083 mol 87 %).

^1H NMR (CD_2Cl_2, 400 MHz, 25 °C): δ 1.62 (s, 3H), 2.07 (s, 3H), 6.15-7.78 (m, Aromatic), 8.06 (dd, 1H, $^4J_{HP\text{-}tras}$ = 6.4 Hz, $^4J_{HP\text{-}cis}$ =

1.0 Hz); $^{31}P\{^{1}H\}$-NMR (CD_2Cl_2, 161 MHz, 25 °C): δ 13.5 (d, AB spin, $^{2}J_{PP}$ = 47 Hz), δ 41.1 (d, AB spin, $^{2}J_{PP}$ = 47 Hz); ^{19}F NMR (CD_2Cl_2, 376.5 MHz, 25 °C): δ -79.3 (s); $^{13}C\{^{1}H\}$-NMR (CD_2Cl_2, 100 MHz, 25 °C): δ 20.6 (s, CH_3), δ 20.8 (s, Me), δ 115.4-178.0 (Aromatic), 180.0 (t, =**C**H, $^{1}J_{CP}$ = 4.2 Hz).

MS (MALDI-TOF; m/z) M^+ 938.2

CHN % {found (calculated)} [Pd(rac-BINAP)($C_{15}H_{14}N$)][CF_3SO_3].H_2O
C {65.16 (65.25)} H {4.35 (4.38)} N {1.27 (1.27)}

[Pd(*rac*-BINAP)($C_{15}H_{14}N$)](BAr^F) (20b)

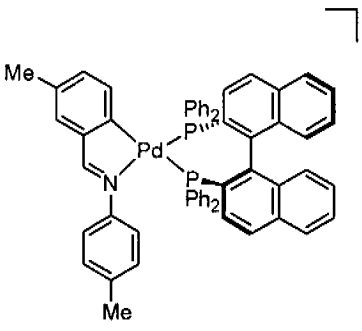

To 1 equiv of [Pd(μ-Cl)($C_{15}H_{14}N$)]$_2$ (21.5 mg, 700.3 g mol^{-1}, 30.7 x 10^{-3} mol) were added 2 equiv of the *rac*-BINAP (38.2 mg, 622.67 g mol^{-1}, 61.4 x 10^{-3} mol) and 2 equiv of $NaBAr^F$ (54.4 mg, 886.21 g mol^{-1}, 61.4 x 10^{-3} mol) in dichloromethane. The reaction mixture was stirred at 25 °C for 3 h. The resulting yellow solution was separated from the solid and reduced under *vacuum*. [$C_{91}H_{58}BF_{24}NP_2Pd$] **20b** (Yield: 104 mg, 0.0578 mol, 94 %).

^{1}H NMR (CD_2Cl_2, 400 MHz, 25 °C): δ 2.06 (s, 3H), 2.17 (s, 3H), 6.15-8.30 (m, Aromatic), 8.05 (d, 1H, $^{4}J_{HP\text{-}tras}$ = 6.9 Hz); $^{31}P\{^{1}H\}$-NMR (CD_2Cl_2, 161 MHz, 25 °C): δ 13.4 (d, AB spin, $^{2}J_{PP}$ = 48 Hz), δ 41.1 (d, AB spin, $^{2}J_{PP}$ = 48 Hz); δ ^{19}F NMR (CD_2Cl_2, 376.5 MHz, 25 °C): δ -63.3 (s); $^{13}C\{^{1}H\}$-NMR (CD_2Cl_2, 100 MHz, 25 °C): δ 20.5 (s,

CH_3), δ 20.8 (s, Me), δ 115.4-178.0 (Aromatic), 179.9 (t, =**C**H $^1J_{CP}$ = 3.5 Hz).

MS (MALDI-TOF; m/z) M^+ 938.2

CHN % {found (calculated)} [Pd(*rac*-BINAP)($C_{15}H_{14}N$)][BAr^F] C {60.98 (60.70)} H {3.43 (3.25)} N {0.79 (0.78)}

[Pd (*rac*-BINAP)($C_{14}H_{11}ClN$)](CF_3SO_3) (21a)

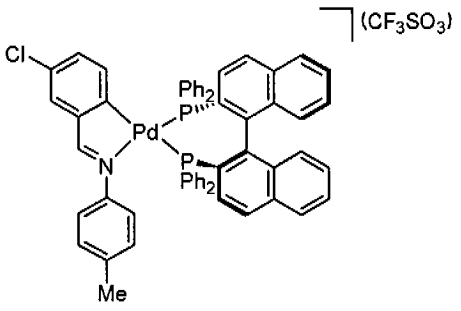

To 1 equiv of [Pd(μ-Cl)($C_{14}H_{11}ClN$)]$_2$ (28.3 mg, 741.14 g mol^{-1}, 38.2 x 10^{-3} mol) were added 2 equiv of the *rac*-BINAP (47.5 mg, 622.67 g mol^{-1}, 76.4 x 10^{-3} mol) and 2 equiv of AgOTf (19.6 mg, 256.94 g mol^{-1}, 76.4 x 10^{-3} mol) in dichloromethane. The reaction mixture was stirred at 25 °C for 3 h. The resulting yellow solution was separated from the solid and reduced under *vacuum*. [$C_{59}H_{43}ClF_3NO_3P_2PdS$] **21a.** (Yield: 80 mg, 0.072 mol 94 %).

^{1}H NMR (CD_2Cl_2, 400 MHz, 25 °C): 2.07 (s, 3H), 6.15-7.78 (m, Aromatic), 8.08 (dd, 1H, $^4J_{HP\text{-}tras}$ = 6.4 Hz, $^4J_{HP\text{-}cis}$ = 1.0 Hz); $^{31}P\{^1H\}$-NMR (CD_2Cl_2, 161 MHz, 25 °C): δ 13.7 (d, AB spin, $^2J_{PP}$ = 47 Hz), δ 40.6 (d, AB spin, $^2J_{PP}$ = 47 Hz); ^{19}F NMR (CD_2Cl_2, 376.5 MHz, 25 °C): δ -79.3 (s); $^{13}C\{^1H\}$-NMR (CD_2Cl_2, 100 MHz, 25 °C): δ 20.8 (s, CH_3), δ 115.4-178.0 (Aromatic), 178.3 (t, =**C**H, $^1J_{CP}$ = 4.1 Hz).

MS (MALDI-TOF; m/z) M^+ 958.2

CHN % {found (calculated)} [Pd(*rac*-BINAP)($C_{14}H_{11}ClN$)][CF_3SO_3] C {63.04 (64.02)} H {4.03 (3.92)} N {1.21 (1.27)}

[Pd(*rac*-BINAP)($C_{14}H_{11}ClN$)](BAr^F) (21b)

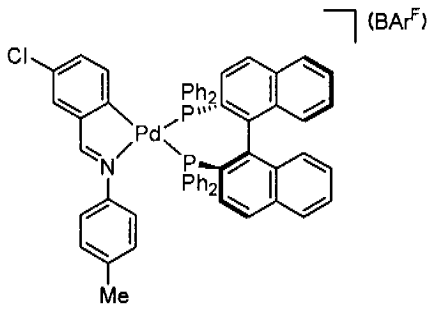

To 1 equiv of [Pd(μ-Cl)($C_{14}H_{11}ClN$)]$_2$ (19.6 mg, 741.14 g mol^{-1}, 30.7 x 10^{-3} mol) were added 2 equiv of the *rac*-BINAP (32.9 mg, 622.67 g mol^{-1}, 53.0 x 10^{-3} mol) and 2 equiv of $NaBAr^F$ (46.8 mg, 886.21 g mol^{-1}, 53.0 x 10^{-3} mol) in dichloromethane. The reaction mixture was stirred at 25 °C for 3 h. The resulting yellow solution was separated from the solid and reduced under *vacuum*. [$C_{90}H_{55}BClF_{24}NP_2Pd$] **21b** (Yield: 91 mg, 0.0499 mol, 94 %).

^{1}H NMR (CD_2Cl_2, 400 MHz, 25 °C): δ 2.07 (s, 3H), 6.15-8.30 (m, Aromatic), 8.06 (d, 1H, $^4J_{HP\text{-}tras}$ = 6.0 Hz); $^{31}P\{^1H\}$-NMR (CD_2Cl_2, 161 MHz, 25 °C): δ 13.7 (d, AB spin, $^2J_{PP}$ = 47 Hz), δ 40.8 (d, AB spin, $^2J_{PP}$ = 47 Hz); δ ^{19}F NMR (CD_2Cl_2, 376.5 MHz, 25 °C): δ -63.3 (s); $^{13}C\{^1H\}$-NMR (CD_2Cl_2, 100 MHz, 25 °C): δ 20.8 (s, CH_3), δ 115.4-178.0 (Aromatic), 178.8 (t, =**C**H $^1J_{CP}$ = 4.0 Hz).

MS (MALDI-TOF; m/z) M^+ 958.2
CHN % {found (calculated)} [Pd(*rac*-BINAP)($C_{14}H_{11}ClN$)][BAr^F] C {59.38 (59.36)} H {3.25 (3.04)} N {0.82 (0.77)}

[Pd(*rac*-BINAP)($C_{14}H_{11}N_2O_2$)](CF_3SO_3) (22a)

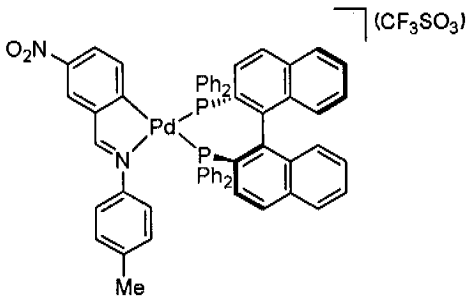

To 1 equiv of [Pd(μ-Cl)($C_{14}H_{11}N_2O_2$)]$_2$ (29.3 mg, 762.24 g mol^{-1}, 38.4 x 10^{-3} mol) were added 2 equiv of the *rac*-BINAP (47.9 mg, 622.67 g mol^{-1}, 76.9x 10^{-3} mol) and 2 equiv of AgOTf (19.8 mg, 256.94 g mol^{-1}, 76.9 x 10^{-3} mol) in dichloromethane. The reaction mixture was stirred at 25 °C for 3 h. The resulting yellow solution was separated from the solid and reduced under *vacuum*. [$C_{59}H_{43}F_3N_2O_5P_2PdS$] **22a.** (Yield: 79 mg, 0.071 mol 92 %).

^{1}H NMR (CD_2Cl_2, 400 MHz, 25 °C): 2.09 (s, 3H), 6.15-8.30 (m, Aromatic), 8.26 (dd, $^4J_{HP\text{-}tras}$ = 6.4 Hz); ^{31}P{^{1}H}-NMR (CD_2Cl_2, 161 MHz, 25 °C): δ 14.1 (d, AB spin, $^2J_{PP}$ = 47 Hz), δ 40.1 (d, AB spin, $^2J_{PP}$ = 47 Hz); ^{19}F NMR (CD_2Cl_2, 376.5 MHz, 25 °C): δ -79.3 (s); ^{13}C{^{1}H}-NMR (CD_2Cl_2, 100 MHz, 25 °C): δ 20.9 (s, CH_3), δ 115.4-178.0 (Aromatic), 178.6 (t, =**C**H, $^1J_{CP}$ = 3.7 Hz).

MS (MALDI-TOF; m/z) M^+ 969.1

CHN % {found (calculated)} [Pd(*rac*-BINAP)($C_{14}H_{11}N_2O_2$)][CF_3SO_3]
C {62.89 (63.42)} H {4.12 (3.88)} N {2.51 (2.51)}

[Pd(*rac*-BINAP)($C_{14}H_{11}N_2O_2$)](BAr^F) (22b)

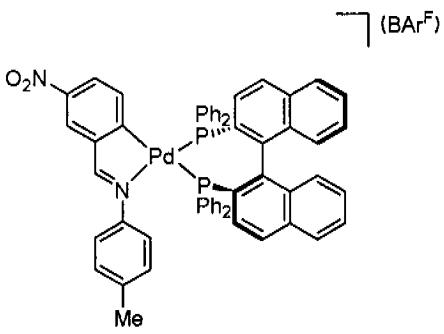

To 1 equiv of [Pd(μ-Cl)($C_{14}H_{11}N_2O_2$)]$_2$ (22.0 mg, 762.24 g mol^{-1}, 28.9 x 10^{-3} mol) were added 2 equiv of the *rac*-BINAP (35.9 mg, 622.67 g mol^{-1}, 57.7 x 10^{-3} mol) and 2 equiv of $NaBAr^F$ (51.2 mg, 886.21 g mol^{-1}, 57.7 x 10^{-3} mol) in dichloromethane. The reaction mixture was stirred at 25 °C for 3 h. The resulting yellow solution was separated from the solid and reduced under *vacuum*. [$C_{90}H_{55}BF_{24}N_2O_2P_2Pd$] **22b** (Yield: 100 mg, 0.0546 mol, 94 %).

^{1}H NMR (CD_2Cl_2, 400 MHz, 25 °C): δ 2.08 (s, 3H), 6.15-8.30 (m, Aromatic), 8.23 (d, 1H, $^4J_{HP\text{-}tras}$ = 6.8 Hz, $^4J_{HP\text{-}cis}$ = 1.2 Hz); $^{31}P\{^1H\}$-NMR (CD_2Cl_2, 161 MHz, 25 °C): δ 14.1 (d, AB spin, $^2J_{pp}$ = 47 Hz), δ 40.1 (d, AB spin, $^2J_{pp}$ = 47 Hz); δ ^{19}F NMR (CD_2Cl_2, 282 MHz, 25 °C): δ -63.3 (s); $^{13}C\{^1H\}$-NMR (CD_2Cl_2, 100 MHz, 25 °C): δ 20.8 (s, CH_3), δ 115.4-178.0 (Aromatic), 178.4 (t, =**C**H $^1J_{CP}$ = 3.9 Hz).

MS (MALDI-TOF; m/z) M^+ 969.2

CHN % {found (calculated)} [Pd(*rac*-BINAP)($C_{14}H_{11}N_2O_2$)][BAr^F] C {58.92 (59.02)} H {3.31 (3.03)} N {1.57 (1.53)}

[Pd(*rac*-BINAP)($C_{14}H_{11}N_2O_2$)](PF_6) (22c)

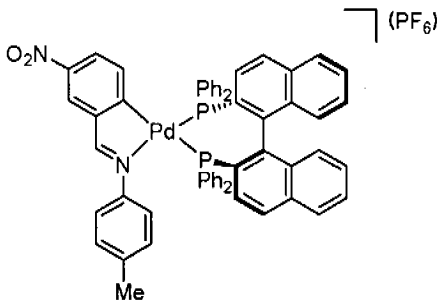

To 1 equiv of [Pd(μ-Cl)($C_{14}H_{11}N_2O_2$)]$_2$ (19.6 mg, 732.36 g mol^{-1}, 25.7 x 10^{-3} mol) were added 2 equiv of the *rac*-BINAP (32.0 mg, 622.67 g mol^{-1}, 51.4 x 10^{-3} mol) and 2 equiv of NH_4PF_6 (8.4 mg, 163 g mol^{-1}, 51.4 x 10^{-3} mol) in acetone. The reaction mixture was stirred at 25 °C for 2 h. Water was then added and the mixture stirred for a further 1h. The resulting precipitate was filtered off and dried under *vacuum*. [$C_{58}H_{43}F_6N_2O_2P_3Pd$] **22c** (Yield: 51 mg, 0.0458 mol, 89 %).

^{1}H NMR ($CDCl_3$, 400 MHz, 25 °C): δ 2.1 (s, 3H), 6.30-8.25 (m, Aromatic), 8.25 (d, 1H, $^4J_{HP\text{-}tras}$ = 6.8 Hz); ^{31}P{^{1}H}-NMR ($CDCl_3$, 161 MHz, 25 °C): δ 14.1 (d, AB spin, $^2J_{PP}$ = 46 Hz), δ 40.1 (d, AB spin, $^2J_{PP}$ = 46 Hz), δ -143.2 (sep, $^1J_{PF}$ = 713 Hz); ^{19}F NMR ($CDCl_3$, 376.5 MHz, 25 °C): δ -73.8 (d, J_{FP} = 713 Hz); ^{13}C{^{1}H}-NMR ($CDCl_3$, 100 MHz, 25 °C): δ 20.8 (s, CH_3), δ 115.4-178.0 (Aromatic), 178.5 (t, =**C**H, $^1J_{CP}$ = 3.9 Hz).

MS (MALDI-TOF; m/z) M^+ 969.1

CHN % {found (calculated)} [Pd(*rac*-BINAP)($C_{14}H_{11}N_2O_2$)][PF_6] C {62.28 (62.57)} H {3.97 (3.89)} N {2.48 (2.52)}

[Pd(*rac*-BINAP)($C_{15}H_{14}NO$)](CF_3SO_3)(23a).

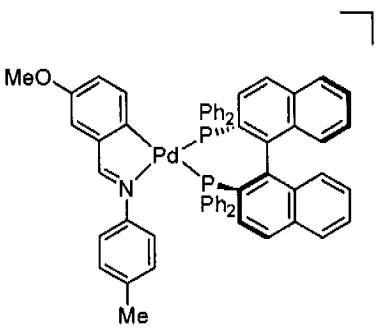

To 1 equiv of [Pd(μ-Cl)($C_{15}H_{14}NO$)]$_2$ (17.4 mg, 732.3 g mol^{-1}, 24.0 x 10^{-3} mol) were added 2 equiv of the *rac*-BINAP (29.6 mg, 622.67 g mol^{-1}, 48.0 x 10^{-3} mol) and 2 equiv of AgOTf (12.3 mg, 256.94 g mol^{-1}, 48.0 x 10^{-3} mol) in dichloromethane. The reaction mixture was stirred at 25 °C for 3 h. The resulting yellow solution was separated from the solid and reduced under *vacuum*. [$C_{60}H_{46}F_3NO_4P_2Pd$] **23a.** (Yield: 54 mg, 0.049 mol 98 %).

^{1}H NMR ($CDCl_3$, 400 MHz, 25 °C): δ 2.03 (s, 3H), 3.71 (s, 3H), 6.15-7.78 (m, Aromatic), 8.07 (d, 1H, $^4J_{HP\text{-}tras}$ = 6.4 Hz); $^{31}P\{^1H\}$-NMR ($CDCl_3$, 161 MHz, 25 °C): δ 13.6 (d, AB spin, $^2J_{PP}$ = 47 Hz), δ 41.2 (d, AB spin, $^2J_{PP}$ = 47 Hz), δ -142.9 (sep, $^1J_{PF}$ = 713 Hz); ^{19}F NMR ($CDCl_3$, 376.5 MHz, 25 °C): δ -73.8 (d, J_{FP} = 713 Hz); $^{13}C\{^1H\}$-NMR ($CDCl_3$, 100 MHz, 25 °C): δ 21.4 (s, CH_3), δ 55.8(s, OMe), δ 115.4-178.0 (Aromatic), 180.0 (t, =**C**H, $^1J_{CP}$ = 4.1 Hz).
MS (MALDI-TOF; m/z) M^+ 954.2

[Pd(*rac*-BINAP)($C_{15}H_{14}NO$)](BAr^F) (23b)

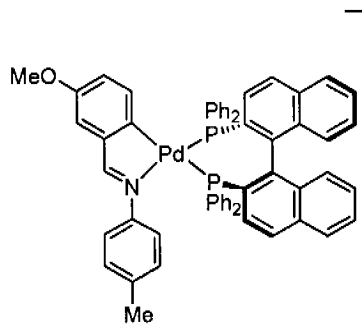

To 1 equiv of [Pd(μ-Cl)($C_{15}H_{14}NO$)]$_2$ (21.7 mg, 732.36 g mol^{-1}, 29.6 x 10^{-3} mol) were added 2 equiv of the *rac*-BINAP (36.9 mg, 622.67 g mol^{-1}, 59.3 x 10^{-3} mol) and 2 equiv of

$NaBAr^F$ (52.5 mg, 886.21 g mol^{-1}, 59.3 x 10^{-3} mol) in dichloromethane. The reaction mixture was stirred at 25 °C for 3 h. The resulting yellow solution was separated from the solid and reduced under *vacuum*. [$C_{91}H_{58}BF_{24}NOP_2Pd$] **23b** (Yield: 100 mg, 0.055 mol, 92 %).

^1H NMR ($CDCl_3$, 400 MHz, 25 °C): δ 2.03 (s, 3H), 3.70 (s, 3H) 6.15-7.78 (m, Aromatic), 7.95 (d, 1H, $^4J_{HP\text{-}tras}$ = 6.4 Hz); $^{31}P\{^1H\}$-NMR ($CDCl_3$, 161 MHz, 25 °C): δ 13.4 (d, AB spin, $^2J_{PP}$ = 47 Hz), δ 41.2 (d, AB spin, $^2J_{PP}$ = 47 Hz); δ ^{19}F NMR ($CDCl_3$, 376.5 MHz, 25 °C): δ -62.4 (s); $^{13}C\{^1H\}$-NMR ($CDCl_3$, 100 MHz, 25 °C): δ 21.4 (s, CH_3),, δ 55.8(s, OMe), δ 115.4-178.0 (Aromatic), 180.0 (t, =**C**H, $^1J_{CP}$ = 4.0 Hz).

MS (MALDI-TOF; m/z) M^+ 954.2

CHN % {found (calculated)} [Pd(*rac*-BINAP)($C_{15}H_{14}NO$)][BAr^F] C {60.17 (60.29)} H {3.22 (3.38)} N {0.77 (0.78)}

[Pd(*rac*-BINAP)($C_{15}H_{14}NO$)](PF_6) (23c)

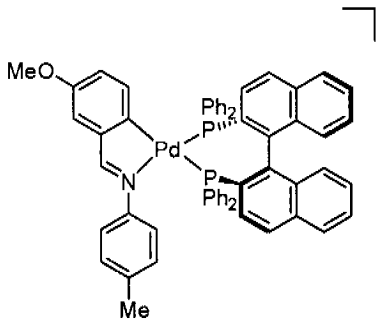

To 1 equiv of [Pd(μ-Cl)($C_{15}H_{14}NO$)]$_2$ (18.3 mg, 732.36 g mol^{-1}, 25.0 x 10^{-3} mol) were added 2 equiv of the *rac*-BINAP (31.1 mg, 622.67 g mol^{-1}, 50.0 x 10^{-3} mol) and 2 equiv of NH_4PF_6 (8.15 mg, 163 g mol^{-1}, 50.0 x 10^{-3} mol) in acetone. The reaction mixture was stirred at 25 °C for 2 h. Water was then added and the mixture stirred for a further 1h. The

resulting precipitate was filtered off and dried under *vacuum*. [$C_{59}H_{46}F_6NOP_3Pd$] **23c** (Yield: 44 mg, 0.044 mol, 80 %).

^{1}H NMR ($CDCl_3$, 400 MHz, 25 °C): δ 2.03 (s, 3H), 3.71 (s, 3H), 6.15-7.78 (m, Aromatic), 8.07 (d, 1H, $^4J_{HP\text{-}tras}$ = 6.4 Hz); $^{31}P\{^1H\}$-NMR ($CDCl_3$, 161 MHz, 25 °C): δ 13.6 (d, AB spin, $^2J_{PP}$ = 47 Hz), δ 41.2 (d, AB spin, $^2J_{PP}$ = 47 Hz), δ -142.9 (sep, $^1J_{PF}$ = 713 Hz); ^{19}F NMR ($CDCl_3$, 376.5 MHz, 25 °C): δ -73.8 (d, J_{FP} = 713 Hz); $^{13}C\{^1H\}$-NMR ($CDCl_3$, 100 MHz, 25 °C): δ 21.4 (s, CH_3), δ 55.8 (s, OMe), δ 115.4-178.0 (Aromatic), 180.0 (t, =**C**H, $^1J_{CP}$ = 4.1 Hz).

MS (MALDI-TOF; m/z) M^+ 954.2

CHN % {found (calculated)} [Pd(*rac*-BINAP)($C_{15}H_{14}NO$)][PF_6] C {64.52 (64.67)} H {4.22 (4.39)} N {1.28 (1.29)}

[Pd(*rac*-BINAP)($C_{15}H_{14}N$)](CF_3SO_3) (24a)

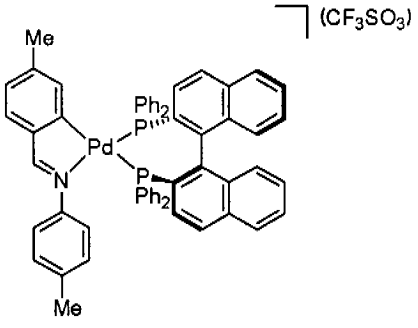

To 1 equiv of [Pd(μ-Cl)($C_{15}H_{14}N$)]$_2$ (20.1 mg, 700.3 g mol^{-1}, 28.7 x 10^{-3} mol) were added 2 equiv of the *rac*-BINAP (35.7 mg, 622.67 g mol^{-1}, 57.4 x 10^{-3} mol) and 2 equiv of AgOTf (14.7 mg, 256.94 g mol^{-1}, 57.4 x 10^{-3} mol) in dichloromethane. The reaction mixture was stirred at 25 °C for 3 h. The resulting yellow solution was separated from the solid and reduced under *vacuum*. [$C_{60}H_{46}F_3NO_3P_2Pd$] **24a.** (Yield: 112 mg, 0.103 mol 90 %).

^{1}H NMR (CD_2Cl_2, 400 MHz, 25 °C): δ 1.69 (s, 3H), 2.07 (s, 3H), 6.15-7.78 (m, Aromatic), 8.05 (dd, 1H, $^4J_{HP\text{-}tras}$ = 6.9 Hz, $^4J_{HP\text{-}cis}$ = 1.0 Hz); ^{31}P{^{1}H}-NMR (CD_2Cl_2, 161 MHz, 25 °C): δ 13.3 (d, AB spin, $^2J_{PP}$ = 48 Hz), δ 40.8 (d, AB spin, $^2J_{PP}$ = 48 Hz); ^{19}F NMR (CD_2Cl_2, 376.5 MHz, 25 °C): δ -79.3 (s); ^{13}C{^{1}H}-NMR (CD_2Cl_2, 100 MHz, 25 °C): δ 20.8 (s, CH_3), δ 21.8 (s, Me), δ 115.4-178.0 (Aromatic), 180.0 (t, =**C**H, $^1J_{CP}$ = 4.6 Hz).

MS (MALDI-TOF; m/z) M^+ 938.2

[Pd(*rac*-BINAP)($C_{15}H_{14}N$)](BAr^F) (24b)

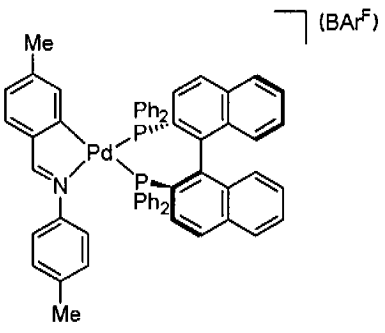

To 1 equiv of [Pd(μ-Cl)($C_{15}H_{14}N$)]$_2$ (22.3 mg, 700.3 g mol^{-1}, 31.8 x 10^{-3} mol) were added 2 equiv of the *rac*-BINAP (39.7 mg, 622.67 g mol^{-1}, 63.7 x 10^{-3} mol) and 2 equiv of NaBAr^F (56.4 mg, 886.21 g mol^{-1}, 63.7 x 10^{-3} mol) in dichloromethane. The reaction mixture was stirred at 25 °C for 3 h. The resulting yellow solution was separated from the solid and reduced under *vacuum*. [$C_{91}H_{58}BF_{24}NP_2Pd$] **24b** (Yield: 101 mg, 0.0561mol, 88 %).

^{1}H NMR (CD_2Cl_2, 400 MHz, 25 °C): δ 2.06 (s, 3H), 2.38 (s, 3H), 6.15-8.30 (m, Aromatic), 8.02 (d, 1H, $^4J_{HP\text{-}tras}$ = 6.9 Hz); ^{31}P{^{1}H}-NMR (CD_2Cl_2, 161 MHz, 25 °C): δ 13.3 (d, AB spin, $^2J_{PP}$ = 48 Hz), δ 40.8 (d, AB spin, $^2J_{PP}$ = 48 Hz); δ ^{19}F NMR (CD_2Cl_2, 376.5 MHz, 25 °C): δ -63.3 (s); ^{13}C{^{1}H}-NMR (CD_2Cl_2, 75 MHz, 25 °C): δ 20.3 (s, CH_3), δ 21.3 (s, Me), δ 115.4-178.0 (Aromatic), 179.1 (t, =**C**H $^1J_{CP}$ = 4.1 Hz).

MS (MALDI-TOF; m/z) M^+ 938.2

CHN % {found (calculated)} [Pd(*rac*-BINAP)($C_{15}H_{14}N$)][BAr^F] C {61.27 (60.70)} H {3.34 (3.25)} N {0.78 (0.78)}

[Pd(*rac*-BINAP)($C_{14}H_{11}N_2O_2$)](CF_3SO_3) (25a)

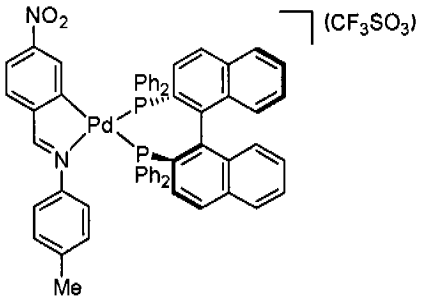

To 1 equiv of [Pd(μ-Cl)($C_{14}H_{11}N_2O_2$)]$_2$ (29.0 mg, 762.24 g mol^{-1}, 38.0 x 10^{-3} mol) were added 2 equiv of the *rac*-BINAP (47.4 mg, 622.67 g mol^{-1}, 76.0x 10^{-3} mol) and 2 equiv of AgOTf (19.6 mg, 256.94 g mol^{-1}, 76.0 x 10^{-3} mol) in dichloromethane. The reaction mixture was stirred at 25 °C for 3 h. The resulting yellow solution was separated from the solid and reduced under *vacuum*. [$C_{59}H_{43}F_3N_2O_5P_2PdS$] **25a** (Yield: 80 mg, 0.071 mol 94%).

^{1}H NMR (CD_2Cl_2, 400 MHz, 25 °C): 2.09 (s, 3H), 6.15-8.30 (m, Aromatic), 8.29 (d, 1H, $^4J_{HP\text{-}tras}$ = 6.8 Hz); $^{31}P\{^1H\}$-NMR (CD_2Cl_2, 161 MHz, 25 °C): δ 14.3 (d, AB spin, $^2J_{PP}$ = 47 Hz), δ 39.9 (d, AB spin, $^2J_{PP}$ = 47 Hz); ^{19}F NMR (CD_2Cl_2, 376.5 MHz, 25 °C): δ -79.3 (s); $^{13}C\{^1H\}$-NMR (CD_2Cl_2, 100 MHz, 25 °C): δ 20.9 (s, CH_3), δ 115.4-178.0 (Aromatic), 178.8 (t, =**C**H, $^1J_{CP}$ = 3.8 Hz).

MS (MALDI-TOF; m/z) M^+ 969.2

CHN % {found (calculated)} [Pd(*rac*-BINAP)($C_{14}H_{11}ClN$)][CF_3SO_3] C {62.80 (63.42)} H {4.04 (3.88)} N {2.54 (2.51)}

[Pd(*rac*-BINAP)($C_{14}H_{11}N_2O_2$)](BAr^F) (25b)

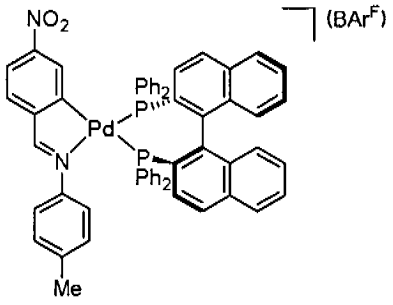

To 1 equiv of [Pd(μ-Cl)($C_{14}H_{11}N_2O_2$)]$_2$ (21.5 mg, 762.24 g mol^{-1}, 28.2 x 10^{-3} mol) were added 2 equiv of the *rac*-BINAP (35.1 mg, 622.67 g mol^{-1}, 56.4 x 10^{-3} mol) and 2 equiv of $NaBAr^F$ (50.0 mg, 886.21 g mol^{-1}, 56.4 x 10^{-3} mol) in dichloromethane. The reaction mixture was stirred at 25 °C for 3 h. The resulting yellow solution was separated from the solid and reduced under *vacuum*. [$C_{90}H_{55}BF_{24}N_2O_2P_2Pd$] **25b** (Yield: 92 mg, 0.0502 mol, 89 %).

^{1}H NMR (CD_2Cl_2, 400 MHz, 25 °C): δ 2.09 (s, 3H), 6.15-8.30 (m, Aromatic), 8.23 (d, 1H, $^4J_{HP\text{-}tras}$ = 6.8 Hz); $^{31}P\{^1H\}$-NMR (CD_2Cl_2, 161 MHz, 25 °C): δ 14.3 (d, AB spin, $^2J_{PP}$ = 46 Hz), δ 39.9 (d, AB spin, $^2J_{PP}$ = 46 Hz); ^{19}F NMR (CD_2Cl_2, 282 MHz, 25 °C): δ -63.3 (s); $^{13}C\{^1H\}$-NMR (CD_2Cl_2, 100 MHz, 25 °C): δ 20.8 (s, CH_3), δ 115.4-178.0 (Aromatic), 178.2 (t, =**C**H, $^1J_{CP}$ = 3.8 Hz).

MS (MALDI-TOF; m/z) M^+ 969.1

CHN % {found (calculated)} [Pd(*rac*-BINAP)($C_{14}H_{11}N_2O_2$)][BAr^F] C {59.29 (59.02)} H {3.08 (3.03)} N {1.60 (1.53)}

[Pd(*S*-BINAP)((*R*)-$C_{10}H_{14}N$)][CF_3SO_3] (26a)

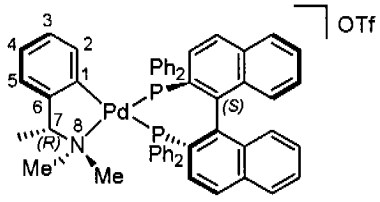

To 1 equiv of [Pd(μ-Cl)($C_{10}H_{14}N$)]$_2$ (30.3 mg, 600.35 g mol^{-1}, 50.5 x 10^{-3} mol) were added 2 equiv of the (*S*)-BINAP (62.8 mg, 622.67 g mol^{-1}, 110.9 x 10^{-3} mol) and 2 equiv of AgOTf (25.9 mg, 256.94 g mol^{-1}, 110.9 x 10^{-3} mol) in dichloromethane. The reaction mixture was stirred at 25 °C for 3 h. The resulting yellow solution was separated from the solid and reduced *in vacuo*. [$C_{55}H_{46}F_3NO_3P_2PdS$] **26a** (Yield: 102 mg, 98 %).

^{1}H NMR (CD_2Cl_2, 500 MHz, 25 °C): 1.92 (d, 3H, $^4J_{PH}$ = 2.1 Hz, NMe), 2.12 (br t, 3H, $^4J_{PH}$ = 3.5 Hz, NMe'), 2.28 (d, 2H, $^3J_{HH}$ = 6.3 Hz, Me), 3.49 (m, 1H), 6.15-8.50 (m, Aromatic); ^{31}P{^{1}H}-NMR (CD_2Cl_2, 283 MHz, 25 °C): δ 11.1 (d, AB spin, $^2J_{PP}$ = 43 Hz), δ 38.2 (d, AB spin, $^2J_{PP}$ = 43 Hz); ^{19}F NMR (CD_2Cl_2, 282.4 MHz, 25 °C): δ -78.8 (s), ^{13}C{^{1}H}-NMR (CD_2Cl_2, 125.8 MHz, 25 °C): δ 9.0 (s, CH_3), δ 25.9 (s, CH_3), δ 40.3 (s, NCH_3), δ 46.7 (s, NCH_3), δ 49.5 (s, NCH_3), δ 51.5 (s, NCH_3), δ 74.4 (m, CH), δ 79.8 (m, CH), δ 115.4-180.0 (Aromatic).

MS (MALDI; m/z) M$^+$ 876.2

[Pd(*R*-BINAP)((*R*)-$C_{10}H_{14}N$)][CF_3SO_3] (26b).

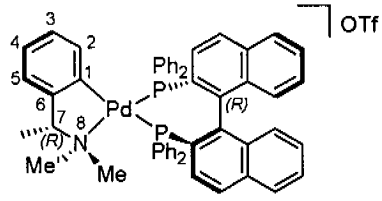

To 1 equiv of [Pd(μ-Cl)($C_{10}H_{14}N$)]$_2$ (30.0 mg, 600.35 g mol^{-1}, 49.9 x 10^{-3} mol) were added 2 equiv of the (*R*)-BINAP (62.2 mg, 622.67 g mol^{-1}, 99.9 x 10^{-3} mol) and 2 equiv of AgOTf (25.7

mg, 256.94 g mol^{-1}, 99.9 x 10^{-3} mol) in dichloromethane. The reaction mixture was stirred at 25 °C for 3 h. The resulting yellow solution was separated from the solid and reduced *in vacuo*. [$C_{55}H_{46}F_3NO_3P_2PdS$] **26b** (Yield: 100 mg, 97 %).

^1H NMR ($CDCl_3$, 400 MHz, 25 °C): 1.33 (d, 2H, $^3J_{HH}$ = 6.3 Hz, Me), 1.51 (d, 3H, $^4J_{PH}$ = 2.1 Hz, NMe'), 2.54, (br t, 3H, $^4J_{PH}$ = 3.5 Hz, NMe), 5.46 (m, 1H), 6.15-8.50 (m, Aromatic); $^{31}P\{^1H\}$-NMR ($CDCl_3$, 161.9 MHz, 25 °C): δ 11.1 (d, AB spin, $^2J_{PP}$ = 43 Hz), δ 38.2 (d, AB spin, $^2J_{PP}$ = 43 Hz); ^{19}F NMR (CD_2Cl_2, 282.4 MHz, 25 °C): δ -78.8 (s); $^{13}C\{^1H\}$-NMR (CD_2Cl_2, 125.8 MHz, 25 °C): δ 9.0 (s, CH_3), δ 40.3 (s, NCH_3), δ 49.5 (s, NCH_3), δ 74.4 (m, CH), δ 115.4-180.0 (Aromatic).

MS (MALDI; m/z) M^+ 876.2

[Pd(*rac*-BINAP)((*R*)-$C_{10}H_{14}N$)][CF_3SO_3] (26c).

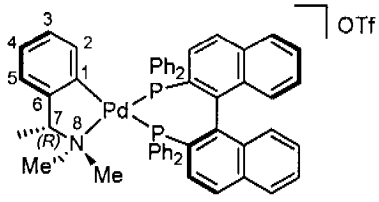

To 1 equiv of [Pd(μ-Cl)($C_{10}H_{14}N$)]$_2$ (33.6 mg, 600.35 g mol^{-1}, 55.9 x 10^{-3} mol) were added 2 equiv of the *rac*-BINAP (69.7 mg, 622.67 g mol^{-1}, 111.9 x 10^{-3} mol) and 2 equiv of AgOTf (28.8 mg, 256.94 g mol^{-1}, 111.9 x 10^{-3} mol) in dichloromethane. The reaction mixture was stirred at 25 °C for 3 h. The resulting yellow solution was separated from the solid and reduced *in vacuo*. [$C_{55}H_{46}F_3NO_3P_2PdS$] **26c** (Yield: 111 mg, 0.108 mol 96 %).

^1H NMR (CD_2Cl_2, 700 MHz, 25 °C): 1.35 (d, 2H, $^3J_{HH}$ = 6.3 Hz), 1.53 (d, 3H, $^4J_{PH}$ = 2.1 Hz), 1.92 (d, 3H, $^4J_{PH}$ = 2.1 Hz), 2.12 (br t, 3H,

$^4J_{PH}$ = 3.5 Hz), 2.28 (d, 2H, $^3J_{HH}$ = 6.3 Hz), 2.51 (br t, 3H, $^4J_{PH}$ = 3.5 Hz), 3.49 (m, 1H), 5.19 (m, 1H), 6.15 - 8.50 (m, Aromatic); $^{31}P\{^1H\}$-NMR (CD_2Cl_2, 283 MHz, 25 °C): δ 10.5 (d, AB spin, $^2J_{PP}$ = 44.2 Hz), δ 11.1 (d, AB spin, $^2J_{PP}$ = 43 Hz), δ 37.2 (d, AB spin, $^2J_{PP}$ = 44.2 Hz), δ 38.2 (d, AB spin, $^2J_{PP}$ = 43 Hz); ^{19}F NMR (CD_2Cl_2, 282.4 MHz, 25 °C): δ -78.8 (s); $^{13}C\{^1H\}$-NMR (CD_2Cl_2, 175 MHz, 25 °C): δ 25.9 (s, CH_3), δ 46.7 (s, NCH_3), δ 51.5 (s, NCH_3), δ 79.8 (m, CH), δ 115.4-180.0 (Aromatic). MS

(MALDI; m/z) M^+ 876.2

[Pd(2*S*,3*S*)-Chiraphos)((*R*)-$C_{10}H_{14}N$)][CF_3SO_3] (27a).

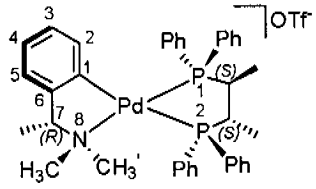

To 1 equiv of [Pd(μ-Cl)($C_{10}H_{14}N$)]$_2$ (28.7 mg, 600.35 g mol^{-1}, 47.8 x 10^{-3} mol) were added 2 equiv of the (2*S*,3*S*)-Chiraphos (40.8 mg, 426.47 g mol^{-1}, 95.6 x 10^{-3} mol) and 2 equiv of AgOTf (24.6 mg, 256.94 g mol^{-1}, 95.6 x 10^{-3} mol) in dichloromethane. The reaction mixture was stirred at 25 °C for 3 h. The resulting colorless solution was separated from the solid and reduced *in vacuo*. [$C_{39}H_{42}F_3NO_3P_2PdS$] **27a** (Yield: 80 mg, 98 %).

^1H NMR ($CDCl_3$, 400 MHz, 25 °C): 1.05 (dd, 3H, $^3J_{HH}$ = 6.4 Hz, $^3J_{PH}$ = 2.4 Hz), 1.07 (d, 3H, $^3J_{HH}$ = 6.4 Hz), 1.69 (d, 3H, $^3J_{HH}$ = 6.4 Hz, 7Me), 2.22 (m, 1H), 2.28 (d, 3H, $^4J_{PH}$ = 1.2 Hz, NMe), 2.31 (m, 1H) 2.50 (t, 3H, $^4J_{PH}$ = 3.6 Hz, NMe') 3.55 (m, 1H) 6.50 - 8.20 (m, Aromatic); $^{31}P\{^1H\}$-NMR ($CDCl_3$, 161.9 MHz, 25 °C): δ 45.2 (d, AB spin, $^2J_{PP}$ = 40 Hz), δ 63.3 (d, AB spin, $^2J_{PP}$ = 40 Hz); ^{19}F NMR ($CDCl_3$, 376.5 MHz, 25 °C): δ -78.4 (s); $^{13}C\{^1H\}$-NMR ($CDCl_3$, 100 MHz, 25 °C): δ 13.9 (dd, CH_3, $^2J_{CP}$ = 17.1 Hz, $^3J_{CP}$ = 6.1 Hz), δ 15.4 (dd, CH_3, $^2J_{CP}$ = 18.6 Hz, $^3J_{CP}$ = 5.5 Hz), δ 26.6 (s, CH_3), δ 38.4 (dd,

CH, $^{1}J_{CP}$ = 26.8 Hz, $^{2}J_{CP}$ = 13.4 Hz), δ 39.9 (dd, CH, $^{1}J_{CP}$ = 33.3 Hz, $^{2}J_{CP}$ = 22 Hz), δ 50.4 (d, NCH_3, $^{3}J_{CP}$ = 5.2 Hz), δ 51.7 (d, NCH_3, $^{3}J_{CP}$ = 2.4 Hz), δ 78.8 (br t, CH), δ 115.4-180.0 (Aromatic).

MS (MALDI; m/z) M^+ 680.2

[Pd(2*R*,3*R*)-Chiraphos)((*R*)-$C_{10}H_{14}N$)][CF_3SO_3] (27b).

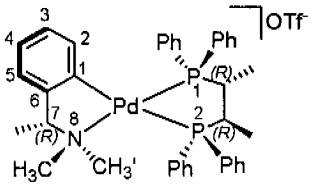

To 1 equiv of [Pd(μ-Cl)($C_{10}H_{14}N$)]$_2$ (30.5 mg, 600.35 g mol^{-1}, 50.8 x 10^{-3} mol) were added 2 equiv of the (2*R*,3*R*)-Chiraphos (43.3 mg, 426.47 g mol^{-1}, 101.6 x 10^{-3} mol) and 2 equiv of AgOTf (26.1 mg, 256.94 g mol^{-1}, 101.6 x 10^{-3} mol) in dichloromethane. The reaction mixture was stirred at 25 °C for 3 h. The resulting colorless solution was separated from solid and reduced *in vacuo*. [$C_{39}H_{42}F_3NO_3P_2PdS$] **27b** (Yield: 80 mg, 95 %).

^{1}H NMR ($CDCl_3$, 300 MHz, 25 °C): 1.04 (dd, 3H, $^{3}J_{HH}$ = 6.8 Hz, $^{3}J_{PH}$ = 2.9 Hz), 1.08 (d, 3H, $^{3}J_{HH}$ = 6.7 Hz), 1.41 (d, 3H, $^{3}J_{HH}$ = 6.7 Hz, 7Me), 2.09 (d, 3H, $^{4}J_{PH}$ = 1.6 Hz, NMe'), 2.22 (m, 1H), 2.35 (m, 1H), 2.78 (t, 3H, $^{4}J_{PH}$ = 2.5 Hz, NMe), 4.31 (m, 1H), 6.50 - 8.20 (m, Aromatic); $^{31}P\{^{1}H\}$-NMR ($CDCl_3$, 121.5 MHz, 25 °C): δ 43.3 (d, AB spin, $^{2}J_{PP}$ = 40.5 Hz), δ 62.5 (d, AB spin, $^{2}J_{PP}$ = 40.5 Hz); ^{19}F NMR ($CDCl_3$, 376.5 MHz, 25 °C): δ -78.5 (s); $^{13}C\{^{1}H\}$-NMR ($CDCl_3$, 100 MHz, 25 °C): δ 14.1 (dd, CH_3, $^{2}J_{CP}$ = 16.2 Hz, $^{3}J_{CP}$ = 6.0 Hz), δ 15.4 (dd, CH_3, $^{2}J_{CP}$ = 17.8 Hz, $^{3}J_{CP}$ = 5.2 Hz), δ 16.6 (s, CH_3), δ 38.6 (dd, CH, $^{1}J_{CP}$ = 26.5 Hz, $^{2}J_{CP}$ = 12.7 Hz), δ 40.8 (dd, CH, $^{1}J_{CP}$ = 33.1 Hz, $^{2}J_{CP}$ = 21.5 Hz), δ 45.7 (s, NCH_3), δ 52.1 (s, NCH_3), δ 75.4 (t, CH, $^{3}J_{CP}$ = 3.2 Hz), δ 115.4-180.0 (Aromatic).
MS (MALDI; m/z) M^+ 680.3

Crystallography:

[Pd(μ-OH)(*rac*-BINAP)](CF$_3$SO$_3$)$_2$ (2a)

Organometallics,**2007**

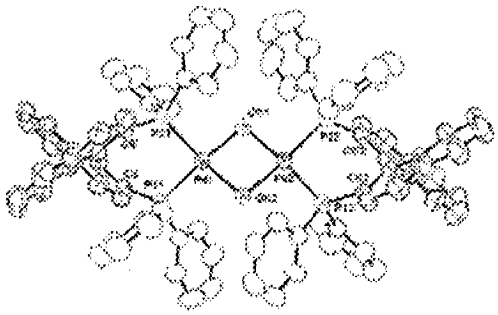

Table E1. Crystal data and structure refinement for **2a**.

Empirical formula	$C_{90}H_{68}F_6O_8P_4Pd_2S_2$
Formula weight	1800.24
Temperature	293(2) K
Wavelength	0.71073 A
Crystal system, space group	Monoclinic, $P2_1/c$
Unit cell dimensions	a = 20.0621(5) A
	alpha = 90 deg.
	b = 18.7386(4) A
	beta = 96.572(1) deg.
	c = 23.2203(5) A
	gamma = 90 deg.
Volume	8672.0(3) A3
Z, Calculated density	4, 1.379 Mg/m^3
Absorption coefficient	0.604 mm^{-1}
F(000)	3656
Theta range for data collection	1.49 to 26.09 deg.
Limiting indices	-24<=h<=24, -23<=k<=23,

	-28<=l<=28
Reflections collected / unique	79935 / 17073 [R(int) = 0.0506]
Completeness to theta = 26.09	99.3 %
Refinement method	Full-matrix least-squares on F^2
Data / restraints / parameters	17073 / 3 / 978
Goodness-of-fit on F^2	1.031
Final R indices [I>2sigma(I)]	R1 = 0.0616, wR2 = 0.1705
R indices (all data)	R1 = 0.0881, wR2 = 0.1957
Largest diff. peak and hole	1.093 and -1.592 $e.A^{-3}$

Table E1.1. Few Bond lengths [Å] and Bond angles [°] for Bridged Aniline complex **2a**.

Pd(1)-OH1	2.060(3)	Pd(1)-OH2	2.080(3)
Pd(1)-P(21)	2.2252(12)	Pd(1)-P(11)	2.2329(12)
Pd(1)-Pd(2)	3.1378(5)	Pd(2)-OH1	2.062(3)
Pd(2)-OH2	2.076(3)	Pd(2)-P(22)	2.2264(12)
Pd(2)-P(12)	2.2322(12)	OH1-Pd(1)-OH2	79.70(14)

OH1-Pd(1)-P(21)	93.34(10)	OH2-Pd(1)-P(21)	171.29(10)
OH1-Pd(1)-P(11)	170.78(14)	OH2-Pd(1)-P(11)	95.08(10)
P(21)-Pd(1)-P(11)	92.49(5)	OH1-Pd(1)-Pd(2)	40.44(10)
OH2-Pd(1)-Pd(2)	40.92(9)	P(21)-Pd(1)-Pd(2)	130.99(3)
P(11)-Pd(1)-Pd(2)	135.70(3)	OH1-Pd(2)-OH2	79.77(14)
OH1-Pd(2)-P(22)	94.96(10)	OH2-Pd(2)-P(22)	171.18(13)
OH1-Pd(2)-P(12)	171.07(11)	OH2-Pd(2)-P(12)	92.17(10)
P(22)-Pd(2)-P(12)	93.51(5)	OH1-Pd(2)-Pd(1)	40.41(10)
OH2-Pd(2)-Pd(1)	41.02(9)	P(22)-Pd(2)-Pd(1)	135.00(4)
P(12)-Pd(2)-Pd(1)	130.82(3)	Pd(1)-OH1-Pd(2)	99.15(15)
Pd(2)-OH2-Pd(1)	98.05(14)		

[Pd_2(μ-OH)(μ-{NH(*p*-Tol)})(*rac*-BINAP)$_2$](CF_3SO_3)$_2$ (3b)

Organometallics,**2006**,25,4596-4604

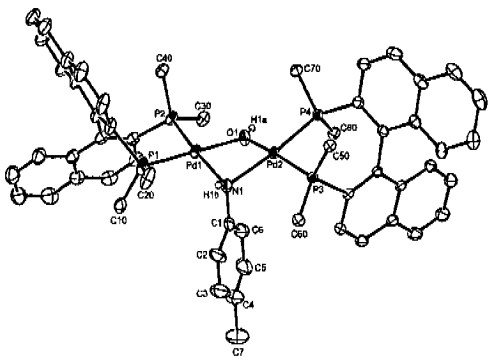

Table E2. Crystal data and structure refinement for Bridged Aniline complex **3b**.

Empirical formula	$C_{105}H_{89}F_6NO_9P_4Pd_2S_2$
Formula weight	2023.57
Temperature	200(2) K
Wavelength	71.073 pm
Unit cell dimensions	a = 1263.36(9) pm
	alpha = 80.1980(10)
	b = 1310.83(9) pm
	beta = 83.5970(10)
	c = 3038.9(2) pm
	gamma = 75.7990(10)
Volume, Z	4.7947(6) nm, 2
Calculated density	1.402 Mg/m^3
Absorption coefficient	1 0.555 mm^{-1}
F(000)	2072
Crystal size	0.53 x 0.33 x 0.18 mm
Theta range for data collection	0.68 to 26.37

Limiting indices	-15 < h < 15, -16 < k < 16, -37 < l < 37
Reflections collected / unique	43118 /19526 (R(int) = 0.0395)
Completeness to theta = 26.37	99.5 %
Max. and min. Transmission	0.9067 and 0.7574
Refinement method	Full-matrix Least-Squares on F^2
Data / Restraints / Parameters	19526 / 32 / 1106
Goodness-of-Fit on F^2	1.058
Final R -indices [I>2Gs(I)]	R1 = 0.0761, wR2 = 0.2149
R-indices (all data)	R1 = 0.0992, wR2 = 0.2328
Largest Maximum and Minimum	3330 and -859 e.nm^{-3}

Table E2.1. Few Bond lengths [pm] and Bond angles [°] for Bridged Aniline complex **3b**.

Pd1–P1 223.5(2), Pd1–P2 226.2(1), Pd1–O1 204.9(4), Pd1–N1 211.9(4), Pd1···Pd2 311.45(5), Pd2–P3 222.9(1), Pd2–P4 226.9(1), Pd2–O1 205.9(4), Pd2–N1 211.1(4), N1–C1 142.8(8), Pd1–N1–Pd2 94.8(2), N1–Pd1–O1 79.3(2), N1–Pd2–O1 79.3(2), Pd1–O1–Pd2 98.6(2), N1–Pd1–P1 96.9(1), N1–Pd1–P2 169.4(1), O1–Pd1–P2 91.8(1), O1–Pd1–P1 174.9(1), N1–Pd2–P3 102.2(1), N1–Pd2–P4 166.7(1), O1–Pd2–P4 87.5(1), O1–Pd2–P3 169.9(1), P1–Pd1–P2 92.32(5), P3–Pd2–P4 90.56(5); ϕ^1 = 6.5°, ϕ^2 = 10.3°; θ = 156.0°; $\phi^{1,2}$ is the intersection of the planes described by 1) P1, Pd1, P2 and O1, Pd1, N1 and 2) P3, Pd2, P4 and O1, Pd2, N1. θ is the intersection of the two L_4-coodination spheres around Pd1 and Pd2.

[Pd(*rac*-BINAP)($C_6H_9O_2$)](BF_4) (15b)

Organometallics,**2007**

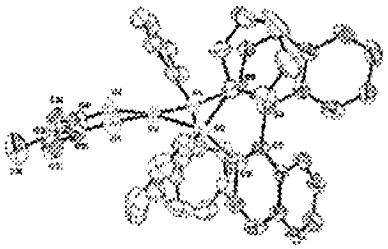

Table E3. Crystal data and structure refinement for **15b**.

Empirical formula	$C_{50}H_{41}BF_4O_2P_2Pd$
Formula weight	928.98
Temperature	296(2) K
Wavelength	0.71069 A
Crystal system, space group	Orthorombic, $Pna2_1$ (33)
Unit cell dimensions	a = 19.879(5) A
	alpha = 90.000(5) deg.
	b = 16.824(5) A
	beta = 90.000(5) deg.
	c = 12.510(5) A
	gamma = 90.000(5) deg.
Volume	4184(2) A^3
Z, Calculated density	4, 1.475 Mg/m^3
Absorption coefficient	0.579 mm^{-1}
F(000)	1896
Theta range for data collection	2.03 to 21.39 deg.
Limiting indices	-20<=h<=20,
	-17<=k<=17,
	-12<=l<=12
Reflections collected / unique	27830 / 4721
	[R(int) =0.0575]

Completeness to theta = 21.39	99.7 %
Refinement method	Full-matrix least-squares on F^2
Data / restraints / parameters	4721 / 1 / 516
Goodness-of-fit on F^2	1.006
Final R indices [I>2sigma(I)]	R1 = 0.0379, wR2 = 0.0958
R indices (all data)	R1 = 0.0461, wR2 = 0.1023
Absolute structure parameter	-0.04(4)
Largest diff. peak and hole	0.755 and -0.507 $e.A^{-3}$

Table E3.1. Few Bond lengths [Å] and Bond angles [°] for **15b**.

Pd-O(2)	2.012(5)	Pd-O(1)	2.024(5)
Pd-P(1)	2.2480(19)	Pd-P(2)	2.251(2)
O(2)-Pd-O(1)	88.5(2)	O(2)-Pd-P(1)	88.60(16)
O(1)-Pd-P(1)	177.08(15)	O(2)-Pd-P(2)	171.47(16)
O(1)-Pd-P(2)	90.66(15)	P(1)-Pd-P(2)	92.21(7)

[Pd(*rac*-BINAP)($C_6H_9O_2$)](BF_4) (15b.CH_2Cl_2)

Organometallics,**2007**

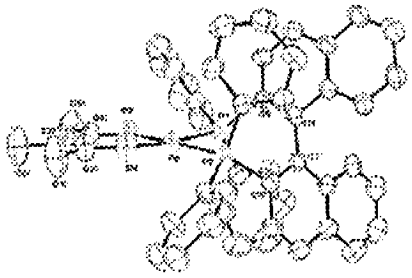

Table E4. Crystal data and structure refinement for **15b.CH_2Cl_2**.

Empirical formula	$C_{51}H_{43}BCl_2F_4O_2P_2Pd$
Formula weight	1013.90
Temperature	296(2) K
Wavelength	0.71069 A
Crystal system, space group	Triclinic, P-1 (2)
Unit cell dimensions	a = 11.560(5) A
	alpha = 8.198(5) deg.
	b = 11.609(5) A
	beta = 75.174(5) deg.
	c = 18.806(5) A
	gamma = 73.210(5) deg.
Volume	2312.4(15) A^3
Z, Calculated density	2, 2.671 Mg/m^3
Absorption coefficient	1.048 mm^{-1}
F(000)	1900
Theta range for data collection	1.13 to 25.99 deg.
Limiting indices	-14<=h<=14, -14<=k<=14,
	-22<=l<=23
Reflections collected / unique	20752 / 9002 [R(int) = 0.0376]
Completeness to theta = 25.99	99.3 %
Refinement method	Full-matrix
	least-squares on F^2
Data / restraints / parameters	9002 / 0 / 545
Goodness-of-fit on F^2	0.912
Final R indices [I>2sigma(I)]	R1 = 0.0621, wR2 = 0.1801
R indices (all data)	R1 = 0.0773, wR2 = 0.1988
Largest diff. peak and hole	1.725 and -1.409 $e.A^{-3}$

Table E4.1. Few Bond lengths [Å] and Bond angles [°] for **15b.CH_2Cl_2**

Pd-O(2)	2.026(3)	Pd-O(1)	2.031(4)
Pd-P(1)	2.2592(15)	Pd-P(2)	2.2649(13)
O(2)-Pd-O(1)	89.15(15)	O(2)-Pd-P(1)	89.14(11)
O(1)-Pd-P(1)	174.34(13)	O(2)-Pd-P(2)	177.38(12)
O(1)-Pd-P(2)	90.35(11)	P(1)-Pd-P(2)	91.60(4)

[Pd(*rac*-BINAP)($C_{15}H_{14}N$)](CF_3SO_3) (20a)

Organometallics,**2007**

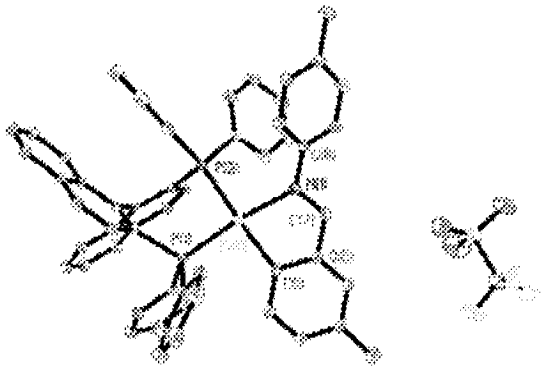

Table E5. Crystal data and structure refinement for **20a**.

Empirical formula	$C_{63}H_{50}C_{15}F_3NO_3P_2PdS$
Formula weight	1303.69
Temperature	200(2) K
Wavelength	0.71073 A
Crystal system, space group	Triclinic, P -1
Unit cell dimensions	a = 11.3820(11) A
	alpha = 71.786(2) deg.
	b = 15.5502(14) A
	beta = 84.497(2) deg.
	c = 17.1910(16) A

	gamma = 79.695(2) deg.
Volume	2841.0(5) A^3
Z, Calculated density	2, 1.524 Mg/m^3
Absorption coefficient	0.713 mm^{-1}
F(000)	1326
Crystal size	0.49 x 0.27 x 0.19 mm
Data collection	Siemens SMART PLATFORM with CCD Detector Graphite monochromator
Detector distance	50 mm
Method; exposure time/frame	omega-scans; t = sec
	Solution by direct methods
Refinement method	full matrix least-squares on F^2, SHELXTL
Theta range for data collection	1.57 to 26.02 deg.
Limiting indices	-14<=h<=14, -19<=k<=19, -21<=l<=21
Reflections collected / unique	25009 / 11160 [R(int) = 0.0246]
Completeness to theta = 26.02	99.6 %
Absorption correction	Empirical
Max. and min. transmission	0.8764 and 0.7209
Refinement method	Full-matrix least-squares on F^2
Data / restraints / parameters	11160 / 0 / 712
Goodness-of-fit on F^2	1.034
Final R indices [I>2sigma(I)]	R1 = 0.0572, wR2 = 0.1462
R indices (all data)	R1 = 0.0639, wR2 = 0.1538
Largest diff. peak and hole	2.956 and -2.584 $e.A^{-3}$

Table E5.1. Few Bond lengths [Å] and Bond angles [°] for **20a**.

Pd(1)-C(1)	2.065(4)	Pd(1)-N(1)	2.124(3)
Pd(1)-P(1)	2.2601(10)	Pd(1)-P(2)	2.3876(10)
C(1)-Pd(1)-N(1)	80.11(14)	C(1)-Pd(1)-P(1)	92.16(11)
N(1)-Pd(1)-P(1)	166.94(9)	C(1)-Pd(1)-P(2)	160.27(11)
N(1)-Pd(1)-P(2)	98.50(9)	P(1)-Pd(1)-P(2)	92.31(3)

[Pd(*rac*-BINAP)($C_{14}H_{11}N_2O_2$)](CF_3SO_3) (22a)

Organometallics,**2007**

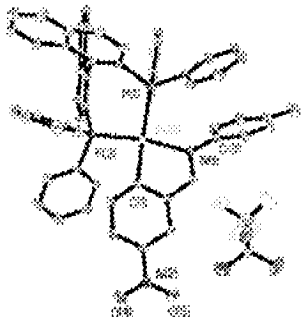

Table E6. Crystal data and structure refinement for **22a**.

Empirical formula	$C_{62}H_{49}Cl_6F_3N_2O_5P_2PdS$
Formula weight	1372.13
Temperature	200(2) K
Wavelength	0.71073 A
Crystal system, space group	Triclinic, P -1
Unit cell dimensions	a = 13.2269(5) A
	alpha = 75.4480(10) deg.
	b = 14.3139(6) A
	beta = 82.3430(10) deg.
	c = 16.4955(7) A

	gamma = 85.9830(10) deg.
Volume	2993.7(2) A^3
Z, Calculated density	2, 1.522 Mg/m^3
Absorption coefficient	0.727 mm^{-1}
F(000)	1392
Crystal size	0.54 x 0.28 x 0.27 mm
Data collection	Siemens SMART PLATFORM
	with CCD Detector
	Graphite monochromator
Detector distance	50 mm
Method; exposure time/frame	omega-scans; t = 3 sec
Solution by	direct methods
Refinement method	full matrix least-squares on F^2,
	SHELXTL
Theta range for data collection	1.47 to 28.36 deg.
Limiting indices	-17<=h<=17, -19<=k<=19, -
	22<=l<=22
Reflections collected / unique	55615 / 14874
	[R(int) = 0.0361]
Completeness to theta = 28.36	99.5 %
Absorption correction	Empirical
Max. and min. transmission	0.8279 and 0.6949
Refinement method	Full-matrix least-squares on F^2
Data / restraints / parameters	14874 / 0 / 739
Goodness-of-fit on F^2	1.040
Final R indices [I>2sigma(I)]	R1 = 0.0465, wR2 = 0.1241
R indices (all data)	R1 = 0.0540, wR2 = 0.1306
Largest diff. peak and hole	1.785 and -1.123 $e.A^{-3}$

Table E6.1. Few Bond lengths [Å] and Bond angles [°] for **22a.**

Pd(1)-C(1)	2.069(2)	Pd(1)-N(1)	2.134(2)
Pd(1)-P(2)	2.2670(6)	Pd(1)-P(1)	2.3643(6)
C(1)-Pd(1)N(1)	80.39(9)	C(1)-Pd(1)-P(2)	92.96(7)
N(1)-Pd(1)-P(2)	167.86(6)	C(1)-Pd(1)-P(1)	166.13(7)
N(1)-Pd(1)-P(1)	96.97(6)	P(2)-Pd(1)-P(1)	91.86(2)

[Pd(*R*-BINAP)((*R*)-$C_{10}H_{14}N$)][CF_3SO_3] (26b)

Organometallics,**2007**

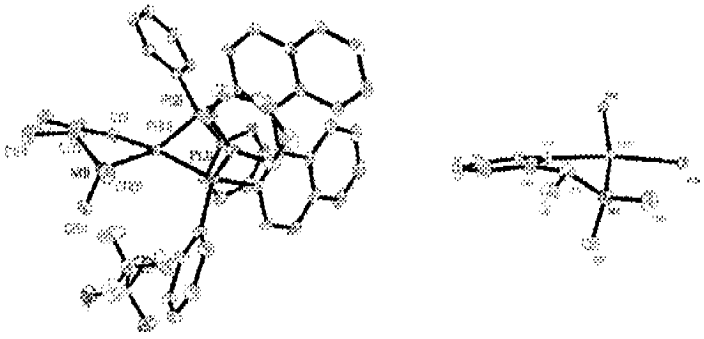

Table E7. Crystal data and structure refinement for **26b**.

Empirical formula	$C_{57}H_{47}Cl_6F_3NO_3P_2PdS$
Formula weight	1264.06
Temperature	200(2) K
Wavelength	0.71073 A
Crystal system, space group	Orthorhombic, P 21 21 21
Unit cell dimensions	a = 11.8308(10) A
	alpha = 90 deg.
	b = 12.8673(10) A
	beta = 90 deg.
	c = 36.642(3) A
	gamma = 90 deg.

Volume	5578.0(8) A^3
Z, Calculated density	4, 1.505 Mg/m^3
Absorption coefficient	0.770 mm^{-1}
F(000)	2564
Crystal size	0.51 x 0.48 x 0.28 mm
Data collection	Siemens SMART PLATFORM
	with CCD Detector
	Graphite monochromator
Detector distance	70 mm
Method; exposure time/frame	omega-scans; t = 2 sec
Solution by	direct methods
Refinement method	full matrix least-squares on F^2,
	SHELXTL
Theta range for data collection	1.68 to 28.33 deg.
Limiting indices	-15<=h<=15,
	-17<=k<=17, -48<=l<=48
Reflections collected / unique	58341 / 13866
	[R(int) = 0.0345]
Completeness to theta = 28.33	99.8 %
Absorption correction	Empirical
Max. and min. transmission	0.8133 and 0.6948
Refinement method	Full-matrix least-squares
	on F^2
Data / restraints / parameters	13866 / 0 / 687
Goodness-of-fit on F^2	1.078
Final R indices [I>2sigma(I)]	R1 = 0.0371, wR2 = 0.0918
R indices (all data)	R1 = 0.0394, wR2 = 0.0930
Absolute structure parameter	0.007(16)
Largest diff. peak and hole	0.882 and -0.598 $e.A^{-3}$

Table E7.1. Few Bond lengths [Å] and Bond angles [°] for **26b.**

Pd(1)-C(1)	2.026(3)	Pd(1)-N(1)	2.192(2)
Pd(1)-P(2)	2.2616(6)	Pd(1)-P(3)	2.4182(7)
C(1)-Pd(1)-N(1)	78.74(10)	C(1)-Pd(1)-P(2)	90.39(8)
N(1)-Pd(1)-P(2)	162.77(7)	C(1)-Pd(1)-P(3)	171.30(9)
N(1)-Pd(1)-P(3)	101.46(7)	P(2)-Pd(1)-P(3)	91.31(2)

[Pd(*rac*-BINAP)((*R*)-$C_{10}H_{14}N$)][CF_3SO_3] (26c).
Organometallics, **2007**

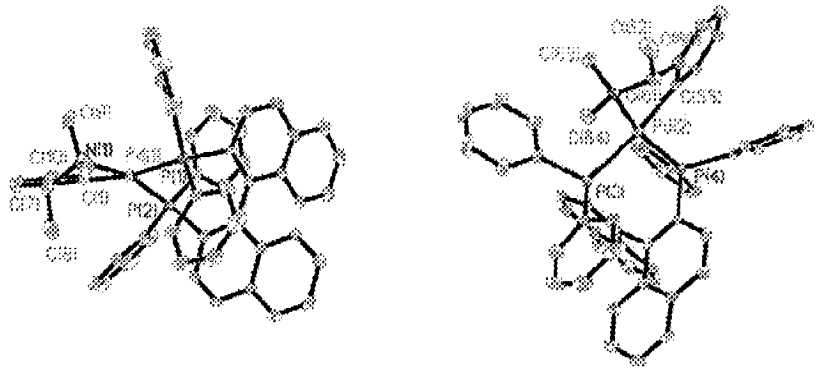

Table E8. Crystal data and structure refinement for **26c.**

Empirical formula	$C_{110}H_{92}F_6N_2O_6P_4Pd_2S_2$
Formula weight	2052.66
Temperature	200(2) K
Wavelength	0.71073 A
Crystal system, space group	Monoclinic, P 21
Unit cell dimensions	a = 17.6911(10) A
	alpha = 90 deg.
	b = 11.5190(6) A
	beta = 90.8320(10) deg.
	C = 23.0571(13) A

	gamma = 90 deg.
Volume	4698.2(4) A^3
Z, Calculated density	2, 1.451 Mg/m^3
Absorption coefficient	0.566 mm^{-1}
F(000)	2104
Crystal size	0.51 x 0.46 x 0.40 mm
Data collection	Siemens SMART PLATFORM
	with CCD Detector
	Graphite monochromator
Detector distance	50 mm
Method; exposure time/frame	omega-scans; t = sec
Solution by	direct methods
Refinement method	full matrix least-squares on F^2,
	SHELXTL
Theta range for data collection	0.88 to 28.33 deg.
Limiting indices	-23<=h<=23, -15<=k<=15,
	-30<=l<=29
Reflections collected / unique	49277 / 23207
	[R(int) = 0.0342]
Completeness to theta = 28.33	99.8 %
Absorption correction	Empirical
Max. and min. transmission	0.8066 and 0.7605
Refinement method	Full-matrix least-squares on F^2
Data / restraints / parameters	23207 / 1 / 1189
Goodness-of-fit on F^2	1.042
Final R indices [I>2sigma(I)]	R1 = 0.0515, wR2 = 0.1193
R indices (all data)	R1 = 0.0587, wR2 = 0.1241
Absolute structure parameter	-0.018(17)
Largest diff. peak and hole	1.598 and -0.821 $e.A^{-3}$

Table E8.1. Few Bond lengths [Å] and Bond angles [°] for **26c**

Pd(1)-C(1)	2.042(4)	Pd(2)-C(55)	2.035(4)
Pd(1)-N(1)	2.182(4)	Pd(2)-N(2)	2.187(3)
Pd(1)-P(2)	2.2658(10)	Pd(2)-P(4)	2.2531(10)
Pd(1)-P(1)	2.4102(10)	Pd(2)-P(3)	2.3968(10)
C(1)-Pd(1)-N(1)	79.33(16)	C(55)-Pd(2)-N(2)	78.69(14)
C(1)-Pd(1)-P(2)	92.84(12)	C(55)-Pd(2)-P(4)	91.36(11)
N(1)-Pd(1)-P(2)	164.47(11)	N(2)-Pd(2)-P(4)	159.46(10)
C(1)-Pd(1)-P(1)	170.73(11)	C(55)-Pd(2)-P(3)	170.27(11)
N(1)-Pd(1)-P(1)	97.97(10)	N(2)-Pd(2)-P(3)	100.29(9)
P(2)-Pd(1)-P(1)	91.76(4)	P(4)-Pd(2)-P(3)	92.48(3)

2.6 Bibliography

[1] Y. Hamashima and M. Sodeoka, *Chem. Rec.* **2004**, *4*, 231-242.

[2] A. Fujii, E. Hagiwara and M. Sodeoka, *J. Am.Chem. Soc.* **1999**, *121*, 5450-5458.

[3] J. Christoffers and A. Baro, *Angew. Chem.-Int. Edit.* **2003**, *42*, 1688-1690.

[4] A. Miyashita, H. Takaya, T. Souchi and R. Noyori, *Tetrahedron* **1984**, *40*, 1245-1253.

[5] S. F. O. Kirsch, L. E. *J. Am. Chem. Soc.* **2005**, *127*, 2866-2867; Overman, L. E.; Remarchuk, *J. Am. Chem. Soc* **2005**, *127*, 2866.

[6] E. P. Mas-Marzá, M.; Sanaú, M.; Peris, E., *Inorg. Chem* **2004**, 2213.

[7] A. R. Chianese and R. H. Crabtree, *Oranometallics* **2005**, 4432.

[8] J. M. Brown, D. I. Hulmes and P. J. Guiry, *Tetrahedron* **1994**, *50*, 4493-4506.

[9] B. M. Trost and M. L. Crawley, *Chem. Revs.* **2003**, *103*, 2921-2943.

[10] P. S. Pregosin and R. Salzmann, *Coord. Chem. Revs.* **1996**, *155*, 35-68.

[11] M. Hatano and K. Mikami, *J. Am.Chem. Soc.* **2003**, *125*, 4704-4705.

[12] A. Fujii and M. Sodeoka, *Tetrahedron Lett.* **1999**, *40*, 8011-8014.

[13] K. L. Li and K. K. Hii, *Chem. Commun.* **2003**, 1132-1133.

[14] K. L. Li, X. H. Cheng and K. K. Hii, *Eur. J. Org. Chem.* **2004**, 959-964.

[15] P. H. Phua, A. J. P. White, J. G. de Vries and K. K. Hii, *Advanced Synthesis & Catalysis* **2006**, *348*, 587-592.

[16] W. Zhuang, R. G. Hazell and K. A. Jørgensen, *Chem. Commun.* **2001**, 1240-1241.

[17] D. A. Evans, R. J. Thomson and F. Franco, *J. Am.Chem. Soc.* **2005**, *127*, 10816-10817.

[18] P. H. Phua, J. G. de Vries and K. K. Hii, *Advanced Synthesis & Catalysis* **2005**, *347*, 1775-1780.

[19] K. Fagnou and M. Lautens, *Angew. Chem. Int. Ed. Engl.* **2002**, *41*, 27-47.

[20] I. Krossing and I. Raabe, *Angew. Chem. Int. Ed. Engl.* **2004**, *43*, 2066-2090.

[21] D. Drago, P. S. Pregosin and A. Pfaltz, *Chem. Commun.* **2002**, 286-287.

[22] M. A. Firestone, P. G. Rickert, S. Seifert and M. L. Dietz, *Inorg. Chim. Acta* **2004**, *357*, 3991-3998.

[23] N. L. Lancaster and T. Welton, *J. Org. Chem.* **2004**, *69*, 5986-5992.

[24] J. W. Faller and P. P. Fontaine, *Organometallics* **2005**, *24*, 4132-4138.

[25] I. Fernández, E. Martínez-Viviente and P. S. Pregosin, *Inorg. Chem.* **2004**, *43*, 4555-4557.

[26] P. J. Stang, D. H. Cao, G. T. Poulter and A. M. Arif, *Oranometallics* **1995**, *14*, 1110-1114.

[27] G. Trabesinger, A. Albinati, N. Feiken, R. W. Kunz, P. S. Pregosin and M. Tschoerner, *J. Am.Chem. Soc.* **1997**, *119*, 6315.

[28] P. Barbaro, P. S. Pregosin, R. Salzmann, A. Albinati and R. W. Kunz, *Organometallics* **1995**, *14*, 5160.

[29] P. Dotta, P. G. A. Kumar, P. S. Pregosin, A. Albinati and S. Rizzato, *Organometallics* **2004**, *23*, 2295-2304.

[30] A. Magistrato, P. S. Pregosin, A. Albinati and U. Rothlisberger, *Organometallics* **2001**, *20*, 4178-4184.

[31] M. Valentini, H. Ruegger and P. S. Pregosin, *Helv. Chim. Acta* **2001**, *84*, 2833-2853.

[32] R. G. Parr and W. Yang, *Density Functional Theory of Atoms and Molecules*, Oxford University Press, New York, **1989**, p.

[33] F. H. Allen, *Acta Crystallogr. Sect. C-Cryst. Struct. Commun.* **2002**, *58*, 380-388.

[34] J. E. Carpenter and F. Weinhold, *(Theochem) J. Mol. Struct.* **1988**, *46*, 41-62.

[35] F. Weinhold and J. E. Carpenter, *The Structure of Small Molecules and Ions*, New York, **1988**, p. 227.

[36] A. E. Reed, L. A. Curtiss and F. Weinhold, *Chem. Revs.* **1988**, *88*, 899-926.

[37] P. G. A. Kumar, P. S. Pregosin, T. M. Schmid and G. Consiglio, *Magn. Reson. Chem.* **2004**, *42*, 795-800.

[38] P. G. A. Kumar, P. S. Pregosin, J. M. Goicoechea and M. K. Whittlesey, *Organometallics* **2003**, *22*, 2956-2960.

[39] A. G. Orpen, L. Brammer, F. H. Allen, O. Kennard, D. G. Watson and R. Taylor, *J. Chem. Soc.-Dalton Trans.* **1989**, S1-S83.

[40] K. Mashima, K. Kusano, T. Ohta, r. Noyori and H. Takaya, *J. Chem. Soc., Chem. Commun.* **1989**, 1208.

[41] T. Ohkuma, M. Koizumi, K. Muniz, G. Hilt, C. Kabuto and R. Noyori, *J. Am. Chem. Soc.* **2002**, *124*, 6508-6509.

[42] J. A. Wiles and S. H. Bergens, *Organometallics* **1999**, *18*, 3709-3714.

[43] S. Kannan, A. J. James and P. R. Sharp, *Inorg. Chim. Acta* **2003**, *345*, 8-14.

[44] D. Drago and P. S. Pregosin, *Organometallics* **2002**, *21*, 1208-1215.

[45] C. White, S. J. Thompson and P. M. Maitlis, *J. Organomet. Chem.* **1977**, *134*, 319-325.

[46] N. G. Connelly, T. Einig, G. G. Herbosa, P. M. Hopkins, C. Mealli, A. G. Orpen, G. M. Rosair and f. Figuri, *J. Chem Soc. Dalton Trans* **1994**, 2025.

[47] C. J. Ammann, P. S. Pregosin, H. Ruegger, A. Albinati, F. Lianza and R. W. Kunz, *J. Organomet. Chem.* **1992**, *423*, 415-430.

[48] X. Y. Zhang, K. Mashima, K. Koyano, N. Sayo, H. Kumobayashi, S. Akutagawa and H. Takaya, *Journal of the Chemical Scociety Perkin Transactions* **1994**, 2309-2322.

[49] M. Oestreich, P. R. Dennison, J. J. Kodanko and L. E. Overman, *Angew. Chem. Int. Ed. Engl.* **2001**, *40*, 1439-1442.

[50] P. S. Pregosin, E. Martinez-Viviente and P. G. A. Kumar, *Dalton Transactions* **2003**, 4007-4014.

[51] D. Nama, D. Schott, P. S. Pregosin, L. F. Veiros and M. J. Calhorda, *Organometallics* **2006**, *25*, 4596-4604.

[52] P. S. Pregosin, P. G. A. Kumar and I. Fernandez, *Chem. Revs.* **2005**, *105*, 2977-2998.

[53] D. Zuccaccia and A. Macchioni, *Organometallics* **2005**, *24*, 3476-3486.

[54] M. Althaus, C. Bonaccorsi, A. Mezzetti and F. Santoro, *Organometallics* **2006**, *25*, 3108-3110.

[55] J. Dehand and M. Pfeffer, *Coord. Chem. Revs.* **1976**, *18*, 327-352.

[56] A. D. Ryabov, I. K. Sakodinskaya and A. K. Yatsimirsky, *J. Chem. Soc. Dalton Trans.* **1985**, 2629-2637.

[57] A. D. Ryabov, *Chem Rev* **1990**, *90*, 403.

[58] P. E. Espinet, M. A.; Oro, L. A.; Serrano, J. L.; Sola, *Coord. Chem. Rev.* **1992**, *15*, 215.

[59] A. Albinati, S. Affolter and P. S. Pregosin, *Organometallics* **1990**, *9*, 379-387.

[60] Y. T. Li, G.-K.; Koh, L. L.; Vittal, J. J.; Leung, P. H., *Inorg. Chem* **2005**, *44*, 9874.

[61] Y. L. Qin, H.; Vittal, J. J.; Tan, G.-K.; Selvaratnam, S.; White, A. J. P.;Williams, D. J.; Leung, P.-H, *Oranometallics* **2003**, 3944.

[62] B. E. Mann and B. F. Taylor, *^{13}C NMR Data for Organometallic Compounds*, Academic Press, London, **1981**, p.

[63] M. Tschoerner, R. W. Kunz and P. S. Pregosin, *Magn. Reson. Chem* **1999**, *37*, 91-97.

[64] M. Tschoerner and P. S. Pregosin, *Inorg. Chim. Acta* **1999**, *290*, 95-99.

[65] E. Martinez-Viviente, P. S. Pregosin and M. Tschoerner, *Magn. Reson. Chem.* **2000**, *38*, 23-28.

[66] A. G. B. Orpen, L.; Allen, F. H.; Kennard, O.; Watson, D. G.; Taylor, R, *j. Am. Chem. Soc. Dalton* **1989**, S1-S83.

[67] T. Ohta, T. H. and R. Noyori, *Inorg. Chem.* **1988**, *27*, 566-569.

[68] J. A. Wiles, C. E. Lee, R. McDonald and S. Bergens, H., *Organometallics* **1996**, *15*, 3782-3784.

[69] H. Ruegger, R. W. Kunz, C. J. Ammann and P. S. Pregosin, *Magn. Reson. Chem.* **1991**, *29*, 197-203.

[70] D. Drago, P. S. Pregosin, M. Tschoerner and A. Albinati, *J. Chem. Soc. Dalton Trans.* **1999**, 2279-2280.

[71] W. McFarlane, J. D. Swarbrick and J. L. Bookham, *J. Chem. Soc., Daltton Trans* **1998**, 3233-3238.

[72] O. R. Jiang, H.; Venanzi, L. M., *J. Organomet. Chem.* **1995**, 233-240.

[73] P. S. Pregosin, *Prog. Nucl. Magn. Reson. Spectrosc.* **2006**, 261-288.

[74] S. P. Smidt, N. Zimmermann, M. Studer and A. Pfaltz, *Chem.-Eur. J.* **2004**, *10*, 4685-4693.

[75] A. Macchioni, *Chem. Revs.* **2005**, *105*, 2039-2073.

[76] S. Burling, S. Douglas, M. F. Mahon, D. Nama, P. S. Pregosin and M. K. Whittlesey, *Organometallics* **2006**, *25*, 2642-2648.

[77] D. Schott, P. S. Pregosin, N. Jacques, M. Chavarot, F. Rose-Munch and E. Rose, *Inorg. Chem.* **2005**, *44*, 5941-5948.

[78] D. Schott, P. S. Pregosin, L. F. Veiros and M. J. Calhorda, *Organometallics* **2005**, *24*, 5710-5717.

[79] P. Stilbs, *Prog. Nucl. Magn. Reson. Spectrosc.* **1987**, *19*, 1.

[80] M. Kadi, S. V. Dvinskikh, I. Furo and M. Almgren, *Langmuir* **2002**, *18*, 5015-5018.

[81] M. Ludwig, R. Kadyrov, H. Fiedler, K. Haage and R. Selke, *Chem.-Eur. J.* **2001**, *7*, 3298-3304.

[82] R. K. Harris, K. A. Kinnear, G. A. Morris, M. J. Stchedroff and A. Samadi-Maybadi, *Chem. Commun.* **2001**, 2422-2423.

[83] S. V. Dvinskikh, I. Furo, D. Sandstrom, A. Maliniak and H. Zimmermann, *J. Mag. Res.* **2001**, *153*, 83-91.

[84] E. Martinez-Viviente, H. Ruegger, P. S. Pregosin and J. Lopez-Serrano, *Organometallics* **2002**, *21*, 5841-5846.

[85] E. J. Cabrita, S. Berger, P. Brauer and J. Karger, *J. Mag. Res.* **2002**, *157*, 124-131.

[86] N. E. Schlorer, E. J. Cabrita and S. Berger, *Angew. Chem.-Int. Edit.* **2002**, *41*, 107-109.

[87] K. Hayamizu and W. S. Price, *J.Mag. Res.* **2004**, *167*, 328-333.

[88] K. Hayamizu, E. Akiba, T. Bando, Y. Aihara and W. S. Price, *Macromolecules* **2003**, *36*, 2785-2792.

[89] E. Martinez-Viviente, P. S. Pregosin, L. Vial, C. Herse and J. Lacour, *Chem.-Eur. J.* **2004**, *10*, 2912-2918.

[90] E. Martinez-Viviente and P. S. Pregosin, *Inorg. Chem.* **2003**, *42*, 2209-2214.

[91] C. Zuccaccia, N. G. Stahl, A. Macchioni, M. C. Chen, J. A. Roberts and T. J. Marks, *J. Am.Chem. Soc.* **2004**, *126*, 1448-1464.

[92] W. Conzelmann, J. D. Koola, U. Kunze and J. Strahle, *Inorg. Chim. Acta* **1984**, *89*, 147-149.

[93] C. A. Tolman, *Chem. Revs.* **1977**, *77*, 313.

[94] N. A. Kratochwil, J. A. Parkinson, C. Sacht, P. D. Murdoch, T. Brown and P. J. Sadler, *Eur. J. Inorg. Chem.* **2001**, 2743-2746.

[95] A. Habtemariam, B. Watchman, B. S. Potter, R. Palmer, S. Parsons, A. Parkin and P. J. Sadler, *Dalton Transactions* **2001**, 1306-1318.

[96] H. J. Ruegger, P. S. Pregosin, A. Scrivanti, L. Toniolo and C. Botteghi, *J. Organomet. Chem.* **1986**, *316*, 233-241.

[97] T. G. Appleton, *Coord. Chem. Revs.* **1997**, *166*, 313-359.

[98] R. Benn, R. D. Reinhardt and A. Rufinski, *Magn. Rewon. Chem.* **1985**, *23*, 259.

[99] P. S. Pregosin in *Platinum NMR Spectroscopy, Vol. 17* ('Ed.'^'Eds.' W. G.), Academic Press, London, **1986**, p.^pp. 285-349.

[100] K. J. Naidoo, A. S. Lopis, A. N. Westra, D. J. Robinson and K. R. Koch, *J. Am.Chem. Soc,* **2003**, *125*, 13330-13331.

[101] J. K. Myers and E. N. Jacobsen, *J. Am.Chem. Soc.* **1999**, *121*, 8959-8960.

[102] A. Albinati, P. S. Pregosin and R. Ruedi, *Helv. Chim. Acta* **1985**, *68*, 2046-2061.

[103] A. C. Cope and Friedric.Ec, *J. Am.Chem. Soc.* **1968**, *90*, 909-&.

[104] C. Anklin, P. S. Pregosin, F. Bachechi, P. Mura and L. Zambonelli, *J. Organomet. Chem.* **1981**, *222*, 175-185.

[105] A. Albinati, U. Von Gunten, P. S. Pregosin and H. J. Ruegg, *J. Organomet. Chem.* **1985**, *295*, 239-256.

Chapter 3

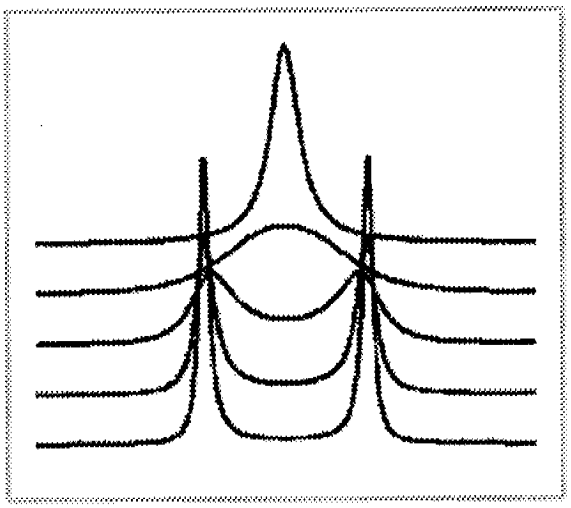

NHC-Exchange and Dynamics

3. N-Heterocyclic Carbene Complexes- Exchange and Dynamics.

Overview:

In this chapter, the sections **3.2** and **3.3** describe the structure and, inter- and intra- molecular dynamics of Ru (**3a**, **4** and **5**) and Rh N-heterocyclic carbene complexes (**6** and **7**). These complexes are known to be catalytically useful in tandem reactions involving C-C bond formation from alcohols[1].

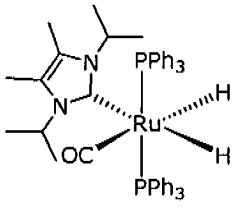

3a

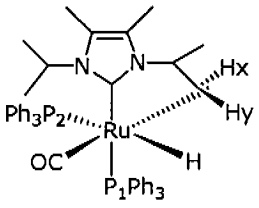

4

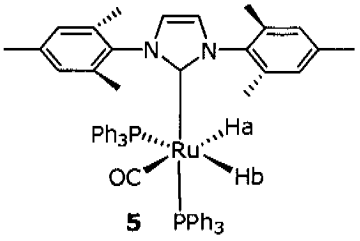

5

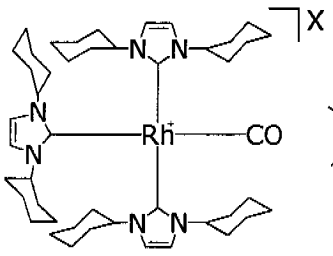

6

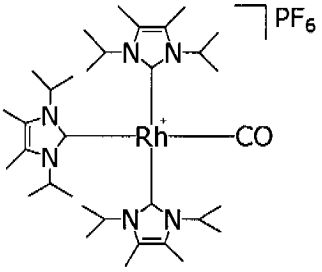

7

X = PF_6, BAr^F

The exchange experiments carried out prove that PPh_3 can dissociate. The resulting new products have been characterized by 1D and 2D NMR spectroscopy.

Section **3.4** describes the structure and reactivity of Ru N-heterocyclic HF complexes (**8** and **9**).

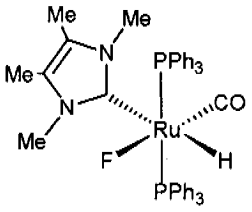

8

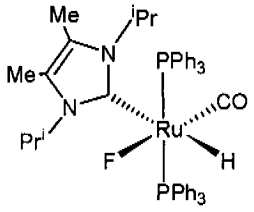

9

Both homo and hetero nuclear NMR measurements on these N-heterocyclic HF complexes prove that, isomerization and disproporationation reactions are occurring in solution.

Finally, the chapter ends with a set of conclusions, with respect to showing how variable temperature and NMR techniques helped to analyze the structure, molecular dynamics in solution.

3.1 Introduction

There are relatively few homogeneous transition metal catalysts where both steric and electronic effects can be finely controlled by small changes of ligand structure within the series. Phosphines have been the most widely used in this connection, aided by the availability of the Tolman map of electronic and steric effects.[2] N-heterocyclic carbenes (NHCs), derived from the replacement of the proton at C-2 in an imidazolium salt by a metal, have been known for many years[3-5], but interest was dormant until Arduengo's[6], isolation of the free imidazol-2-ylidene carbene in 1991. The first catalytic applications of NHC complexes, described by Hermann in 1995, together with the recognition that NHCs are excellent stabilizing ligands for a variety of homogeneous catalysts[7], prompted many research groups to prepare a large number of NHC-based catalysts for a wide variety of reactions.

3.1.1 N-Heterocyclic Carbene Complexes

N-heterocyclic carbenes (NHCs) based on imidazolium ions and related heterocycles have emerged as an alternative to phosphines in the design of new organometallic catalysts for homogeneous catalytic reactions. Spectroscopic studies suggested NHCs were principally sigma-donors and only poor pi-acceptors, like alkyl phosphines, so an analogy between the two classes of ligands developed[8-10].

Further it has been shown that the two ligand classes are distinct in electronic properties, NHCs being stronger donors than even the most basic phosphines[11-13]. The fan-shaped steric profile of NHCs is also different from the cone shape of PR_3 (see Fig. 3.1) but this has yet to be fully exploited. Based on the accepted analogy

between NHCs and trialkylphosphines many metal complexes have been synthesized and targeted as a catalyst for various catalytic reactions.

The attractivity of N-heterocyclic carbenes as ligands for transition metal catalysis is a result of the following features.

(a) Electronic Character

N-Heterocyclic carbenes are thought to be very electron rich, neutral σ- donor ligands. The degree of π- acceptor character of N-heterocyclic carbenes is still disputed and unclear. Experimental and theoretical results range from no π-back-bonding at all, to up to 30% of the complexes overall orbital interaction energies being a result of π-back-bonding. Clear-cut conclusions are hampered by the dependency on the metal, the co-ligands relative to the metal[14-17].

The electron-donating property can be semi-quantified by a comparison of the stretching frequencies of the CO ligands of the complexes $LRh(CO)_2Cl$[18], $LIr(CO)_2Cl$[18] or $LNi(CO)_3$[19] with L = NHC or PR_3. From these studies it is clear that NHCs are slightly better σ-donor ligands than even the most basic trialkyl phosphines (Table 3.1).

Table 3.1. IR values for the carbonyl stretching frequencies in $LNi(CO)_3$ measured in CH_2Cl_2[2, 19]

Ligand	ν_{CO} (A_1)[cm^{-1}]	ν_{CO} (E) [cm^{-1}]
IMes	2050.7	1969.8
SIMes	2051.5	1970.6
IPr	2051.5	1970.0
SIPr	2052.2	1971.3
ICy	2049.6	1964.6
PPh_3	2068.9	1990
PCy_3	2056.4	1973
P^tBu_3	2056.1	1971

From these IR data, it is evident that NHCs have very similar levels of electron-donating ability, whereas phosphines span a much wider electronic range on going from alkyl to aryl phosphines. Clearly for NHCs, only substituents on the periphery of the ligand are exchanged, whereas for phosphines the different substituents are directly attached to the donor atom itself. Furthermore, as a consequence of their strong electron-donor property, NHCs are considered to be higher ligand field as well as higher *trans* effect ligands than phophines[20].

(b) Complex Stability

N-Heterocyclic carbenes form stable bonds with the majority of transition metals[17, 21, 22]. Whereas for saturated and unsaturated NHCs of comparable steric demand, very similar bond dissociation energies have been observed, phosphines generally form much weaker bonds (Table 3.2)[17]. As a result, the equilibrium constant for the carbene metal complex is larger than for the analogous phosphines (Scheme 3.1). This minimizes the amount of free NHC in solution and thus increases the life time of the complex as well as its robustness against heat, air and moisture. It has to be kept in mind that NHCs, while they can be isolated and stored, are still very sensitive and reactive towards many electrophilic compounds.

The resulting extraordinary stability of NHC-metal complexes has been utilized in many applications. However, an increasing number of publications report that the metal-carbene bond is not inert[23, 24]. For example, the migratory insertion of an NHC into a ruthenium-carbon double bond[25], the reductive elimination of alkylimidazolium salts from NHC alkyl complexes[26] or the ligand substitution of NHC ligands by phosphines[27, 28] have all been described. In addition, the formation of palladium black is frequently

observed in applications of palladium NHC complexes, also pointing at decomposition pathways.

Scheme 3.1

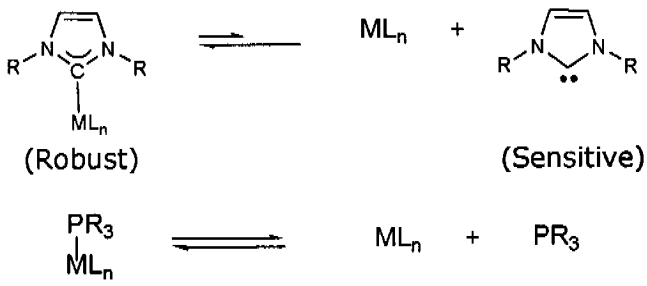

Table 3.2. Steric demand and bond strength of some important ligands[17, 29]

Ligand	BDE [Kcal/mol](theoretical) For L in $Ni(CO)_3L$
IMes	41.1
SIMes	40.2
IAd	20.4
I^tBu	24.0
PPh_3	26.7

(c) Steric Effects

Despite the fact that NHCs have often been used as phosphine mimics, their shape is very different (Fig. 3.1). For phosphine complexes, the substituents R on the phosphrous point away from the metal, resulting in the formation of a cone. The steric demand of these ligands can easily be described using Tolman's ingenious cone angle descriptors[2]. The topology of NHCs is different from this and it is more complicated to define parameters measuring the steric demand of these ligands. The R substituents on the nitrogen atoms have a strong impact on the ligand's shape. NHCs have been described as fence- or fan-like[30], the substituents pointing toward

the metal, thereby "wrapping" it to some extent and forming a pocket (Fig. 3.1). In addition, the NHC ligands are anisotropic and a rotation around the metal-carbene bond can substantially change the steric and electronic interactions.

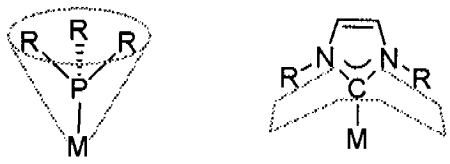

Fig. 3.1. Shape of phosphines and NHC

3.1.2 C-H Activation in Carbene Complexes

Over the past 30 years or so, a number of carbon-hydrogen bond activation reactions catalysed by transition metals have appeared in the literature[31, 32]. This work took on greater significance in 1982, when Bergman reported a reaction in which a "simple" oxidative addition of cyclohexane to a photochemically generated reactive Ir^{I} fragment had occurred[33]. Since then, many other transition metal complexes that can activate alkane C-H bonds by a variety of mechanisms to give products with metal-carbon bonds have been discovered. In examining the reactions of homogeneous metal complexes with hydrocarbons, the various examples can be classified according to four general types of reaction. These types are shown in Fig. 3.2. Reaction 3.2a represents the most common type, in which a metal with a vacant coordination site undergoes oxidative addition (formation of two new bonds, using 2e– from the metal + 2e– from the C–H bond) to the metal center. Reaction 3.2b shows a homolytic or radical process that is quite rare, but nonetheless has been observed. Reaction 3.2c represents the use of an electrophilic metal center to break the C–H bond, and there is debate as to whether this

mechanism is concerted or actually proceeds via an oxidative addition pathway. Finally, reaction 3.2d shows the reversible addition of a C–H bond to a M=X bond where X can be either a heteroatom containing ligand or an alkylidene.

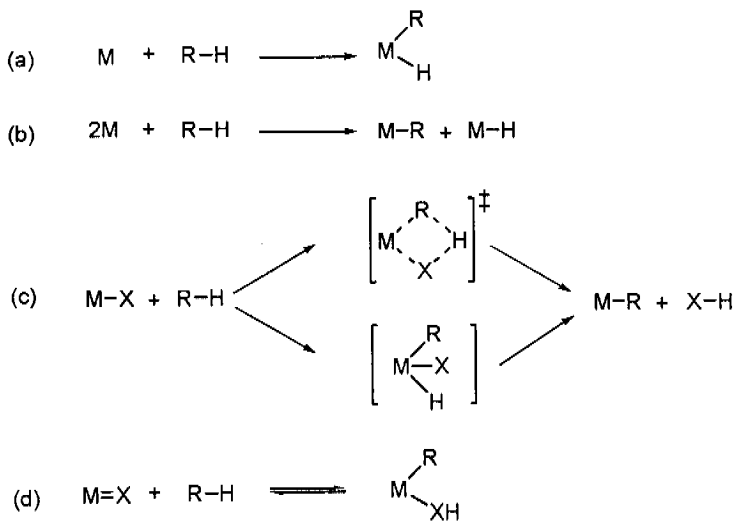

Fig. 3.2. Mechanisms for C–H activation by transition metal complexes.

It is now apparent that N-heterocyclic carbenes are not necessarily innocent, inert ligands that simply help to stabilize reactive and potentially catalytically useful metal complexes[26, 34, 35]. In a number of cases with late transition metals, NHCs have been found to undergo facile intermolecular C-H bond activation reactions[36-38] and, in some cases C-C bond activation[24] under more forcing conditions. The selective activation and functionalization of CH bonds has attracted increased attention in recent years[39]. The facility of this reaction using carbene complex can be explained by the increased electron density on the metal as a result of the strongly electron donating carbene and the fact that

C-H and C-C bonds are forced into close contact with the metal because of the steric bulk of the NHC.

As an examples, Lappert et al have reported that activation of an aromatic CH bonds at an N-heterocyclic carbene, forming an orthometalated Ir(III) complex.[40] Hermann[41] has reported the C-H bond cleavage of 1,3-bis(cyclohexyl)imidazole-2-ylidene (ICy) by $[(\eta^5\text{-}C_5Me_5)IrCl_2]_2$ (the direct activation product was not observed, since rapid β-hydrogen elimination afforded a 1-(2-cyclohexyl)-3-cyclohexylimidazol-2-ylidene ligand in the ultimate product), while Nolan and co-workers have very recently described double C-H activation of 1,3-bis(tert-butyl)imidazole-2-ylidene (I^tBu) at rhodium.[42] Whittlesey[43, 44] and co-workers have shown C-H activation of the carbene in $[Ru(IMes)(PPh_3)_2(CO)H_2]$ at room temperature in the presence of hydrogen acceptor (vinyltrimethylsilane). Later the same group have shown an unexpected intramolecular C-H bond activation of an alkyl NHC IEt_2Me_2 (1,3-bis(ethyl)-4,5-dimethylimidazol-2-ylidene) in $Ru(IEt_2Me_2)(PPh_3)_2(CO)H_2$, which generates a stable and fully characterized product resulting from NCH_2CH_2-H activation.

The N-heterocyclic carbene complexes reported in the following sections have been donated by Professor Michael K. Whittlesey group for which author is indebted; the NMR studies have been carried out by the author.

3.2 C-H Activation and Phosphine Exchange in Ru(II) Hydrido NHC Complexes.

Ruthenium complexes have played a pivotal role in the elevation of N-heterocyclic carbene (NHC) ligands to the ubiquitous position that they now occupy in organometallic chemistry, most spectacularly in their applications in metathesis reactions[45, 46]. Several groups[38, 47-49] have been involved in the synthesis and development of these molecules as catalysts, and it is now recognized that these are relatively bulky directing ligands, in that, apart from the steric aspects, the carbene-ligand possesses a substantial *trans* effect. Moreover, N-heterocyclic carbenes (NHCs) are not necessarily innocent, inert ligands. Recently, Crudden and co-workers[50] have shown that $Rh(IMes)(PPh_3)_2Cl$ (IMes = 1,3-bis(2,4,6-trimethylphenyl)imidazol-2-ylidene) not only undergoes slower intermolecular phosphine exchange than the parent phosphine species $Rh(PPh_3)_3Cl$, but surprisingly, dissociates IMes irreversibly in chlorinated solvents in the presence of excess phosphine[50].

Results and Discussion

In several earlier studies, Whittlesey and co - workers have shown that complexes such as **1**, are capable of affording new cyclometallated Ru-derivatives, **2**, via an intra-molecular C,H activation reaction (see Scheme 3.2). The studies, which follow, report on several new derivatives of **1** and **2**, and suggest, as a consequence of a number of NMR measurements, that this reaction proceeds, in part, via a combination of dissociation and isomerization reactions.

Scheme 3.2

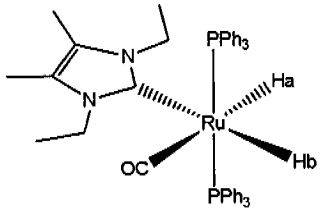

1

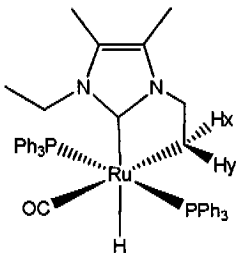

2

3.2.1 Ru(II) isopropyl-substituted Carbene $I^iPr_2Me_2$ (1,3-bis-isopropyl-4,5-dimethlyimidazol-2-ylidene) Complexes

The new Ru carbene complexes can be readily identified via multinuclear NMR measurements, for example, ^{31}P, ^{1}H hydride and ^{13}C carbene resonances. Throughout this discussion use will be made on the empiricism that $^{2}J(P,H)$ trans is usually much larger (often one order of magnitude) than $^{2}J(P,H)$ cis.

Phosphine Exchange experiments. The ^{1}H, ^{13}C and ^{31}P NMR characteristics of complex **3a** clearly reveal the two non-equivalent hydride ligands, the expected high frequency position of the ^{13}C carbene and CO resonances and the two equivalent ^{31}P spins, respectively.

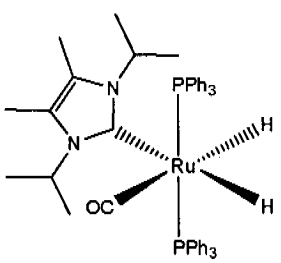

3a

As it is often the case that six-co-ordinate complexes can dissociate a bulky neutral ligand (ex: PPh_3). We have added one equivalent of P(*p*-Tol)$_3$ to a solution of **3a** in THF solution and allowed these to react at 40°C for 30′ (Without warming we do not observe exchange, see Fig. 3.3, lower trace). After cooling to RT, the ^{31}P spectrum of the resulting solution is shown as the middle trace of Fig. 3.3. Clearly several new complexes, **3b-3d**, are formed. One of these, **3c**, shows a typical AB spin system, ^{2}J(P,P) = 255 Hz, consistent with a structure containing non-equivalent *trans* phosphine donors. Whereas complex **3b** and **3d**, shows two doublets and singlet respectively. All four complexes **3a-3d** have non equivalent hydride ligands. If this solution is allowed to stand for 20h, component **3c** is shown to increase in intensity (Fig. 3.3).

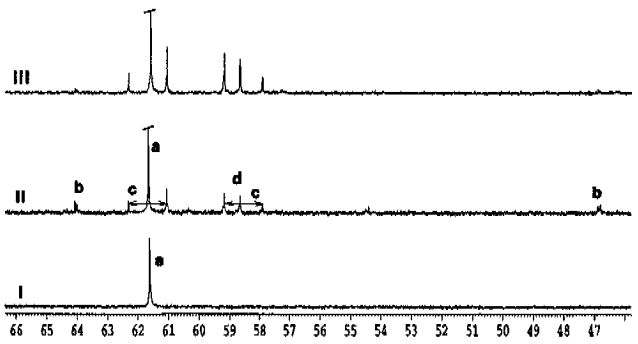

Fig. 3.3. $^{31}P\{^{1}H\}$ spectrum of (I) complex **3a** at RT. (II) Complex **3a** and 1eq.P(p-tol)$_3$ warming for 30 min at 40° C and measured at RT. (III) Complex **3a** and 1eq.P(*p*-tol)$_3$ after 20 hours at RT. THF solution.

Based on the ^{31}P (and ^{1}H) data we suggest in Scheme 3.3 that the solution now contains the following complexes. Obviously, there is facile exchange between PPh_3 and P(*p*-Tol)$_3$.

Scheme 3.3

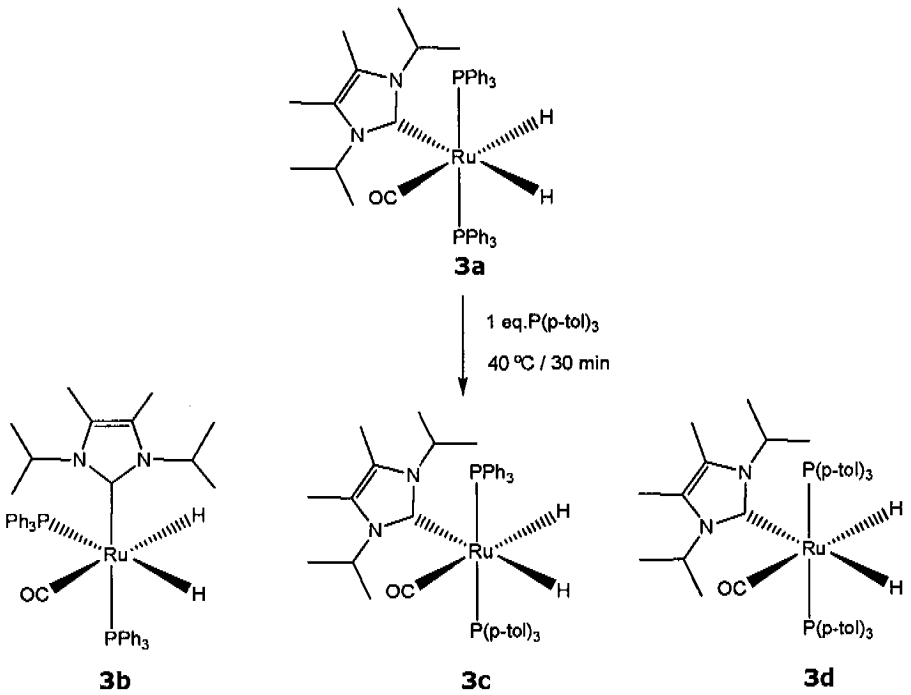

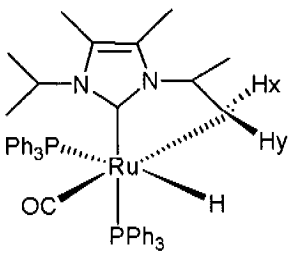

4

Given the observed dynamics for complex **3**, it was interesting to study Complex **4**. A THF solution of the new cyclometallated cis-complex **4**, was then treated with one equivlent of P(*p*-Tol)$_3$. It was not thought to be necessary to warm this THF solution as, in contrast to **3a**, both the carbene and hydride ligands are thought to possess relatively large *trans* effects, i.e., ligand dissociation should be facile. Fig. 3.4 gives the ^{31}P spectra of the pure material and the solution which results, whereas Fig. 3.5 shows the hydride section of the ^{31}P,^{1}H-correlation for the same solution. The four isomeric complexes observed (see Scheme 3.4) possess non-equivalent *cis* phosphine ligands (based on the

observed ^{2}J(P,P) values). Fig. 3.5 proves that each of the eight ^{31}P signals in the upper trace of Fig. 3.4 correlates to a ^{1}H hydride resonance (one of which is *trans* to a P-donor). For each isomer one expects four ^{1}H hydride absorptions [$^{2}J_{PH}$ trans and $^{2}J_{PH}$ cis] and one observes 16 hydride signals from the four isomers. With a modest amount of effort all four of these isomers can be properly assigned. Obviously, there is phosphine exchange both *trans* to the carbene and *trans* to one of the two hydrides.

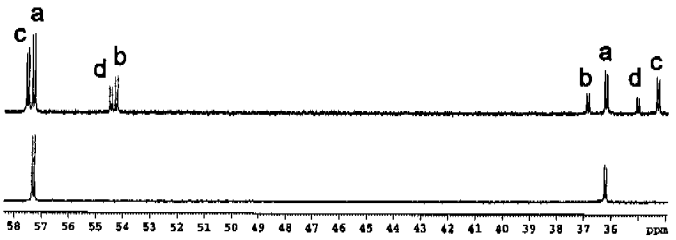

Fig. 3.4. ^{31}P {^{1}H} spectrum in THF solution showing four isomers formed after adding one equivalent of P(p-tol)$_3$ to complex **4**.

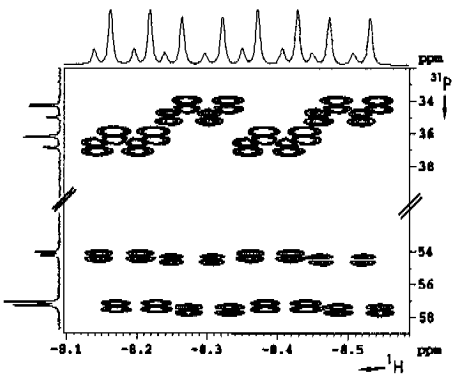

Fig. 3.5. Section of the PH COSY of Complex **4** in the presence of 1eq of P(p-tol)$_3$ showing four different isomers.

Scheme 3.4

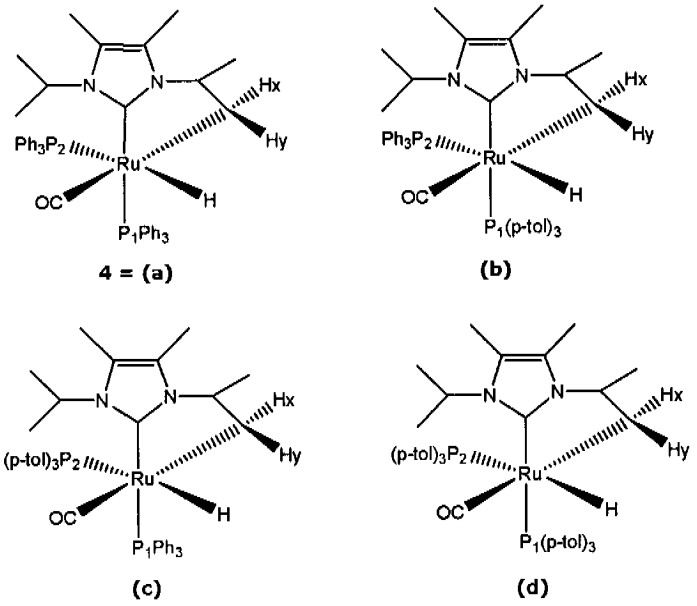

3.2.2 Ru(II) IMes Carbene Complex (1,3-(2,4,6-trimethylphenyl)imidazol-2-ylidene)

A similar exchange reaction with P(*p*-Tol)$_3$ was carried out starting from the *cis*-complex **5**, which contains the well-known larger carbene ligand, IMes.

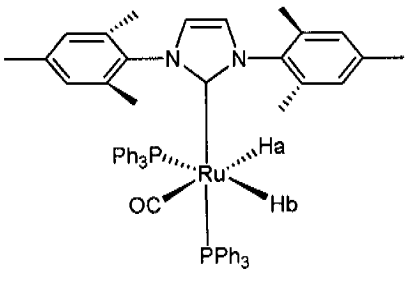

5

Fig. 3.6 shows the analogous ^{31}P spectra of the pure material and the solution which results upon addition of the tolyl phosphine, whereas Fig. 3.7 shows the hydride section of the ^{31}P,^{1}H-correlation. The structures assigned to the isomers are given in Scheme 3.5 and once again the exchange chemistry results in the P(*p*-Tol)$_3$ ligands taking up positions both *trans* to the carbene and *trans* to a hydride.

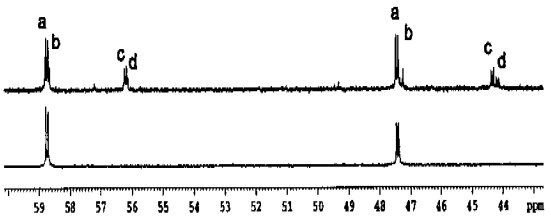

Fig. 3.6. $^{31}P\{^{1}H\}$ spectrum in THF solution showing the four different isomers after adding one equivalent of P(p-tol)$_3$ to complex **5.**

Scheme 3.5

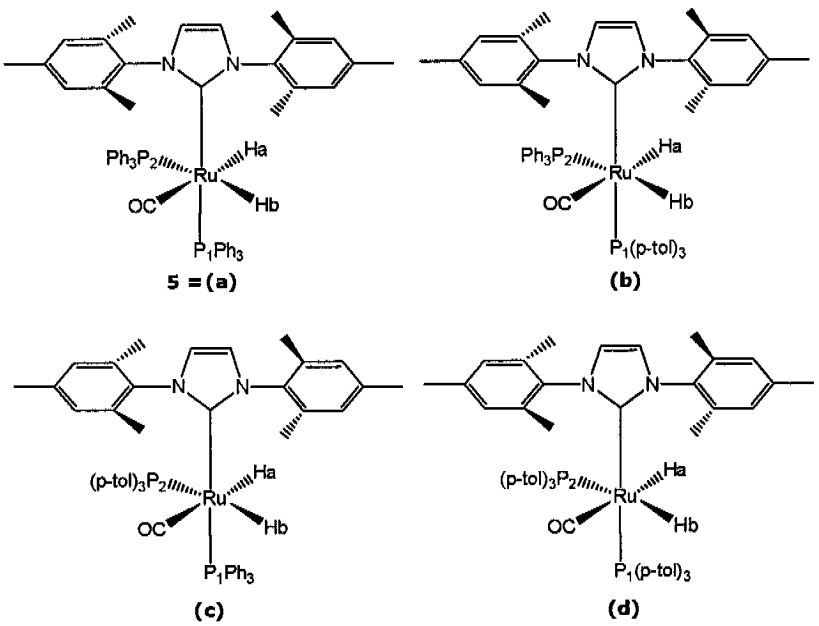

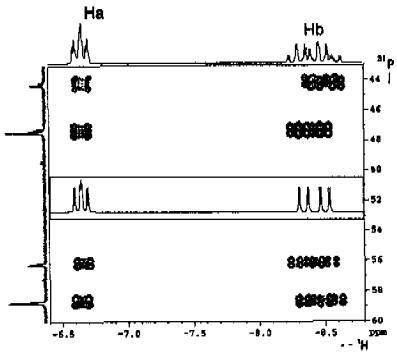

Fig. 3.7. Section of ^{31}P-^{1}H COSY spectrum showing four isomers. Each ^{31}P resonance correlates to two ^{1}H sigansl. The ^{1}H spectrum for the hydride region of pure complex **5** is displayed in the center. Ha is is cis to two cis ^{31}P spins whereas Hb is trans to one of the two ^{31}P spins and cis to the other.

Addition of one equivalent of PBu$^{n}_3$ (a stronger donor) to the *cis*-

bis phosphine complex **5**, immediately affords only three of the possible four analogous isomers, a-c, in almost, but not quite, equal proportions shown in Fig. 3.8 (middle row). The fourth isomer, d, is observed only after approximately 24 hours. Clearly, the exchange proceeds smoothly for a different type of donor as well.

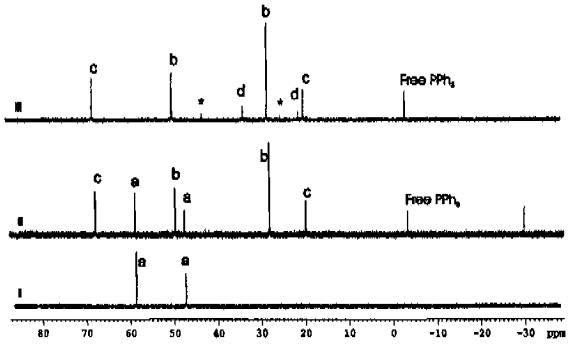

Fig. 3.8. $^{31}P\{^{1}H\}$ spectrum of (I) complex **5** in THF at RT. (II) Complex **5** and 1eq. PBu^{n}_{3} measured at RT. (III) Complex **5** and 1eq. PBu^{n}_{3} after 24 hours at RT.

Given that a presumed dissociative exchange is active, it was interesting to consider the reaction arising from a THF solution of *trans* complex **3a**, in the presence of the olefin $Me_3Si\text{-}CH{=}CH_2$, the reagent used by Whittlesey in his previous study to promote hydride insertion and subsequent cyclometallation chemistry. Fig. 3.9 shows a set of ^{31}P spectra and Scheme 3.6 the presumed reaction sequence. The lower trace corresponds to the starting material. The center trace shows the products from addition of one equivalent of silane after 3h, and the upper trace the result of addition of an additional 10 equivalents of the silane, after the 3h period, followed by immediate measurement. The new *cis* mono hydride cyclometallated complex, **4a**, is now readily recognized via its ^{1}H spectrum (not shown); however, more interesting is the detection of **3b**, the cis isomer of the starting material, indicated in the

middle trace. This *cis*-isomer, whose concentration decreases as the reaction progresses, is relevant as we know from the studies described above, that it will readily exchange a tertiary phosphine ligand, without warming, thus opening a coordination position. These results prompt us to consider the mechanism given in Scheme 3.6 for the cyclometallation of **3a**.

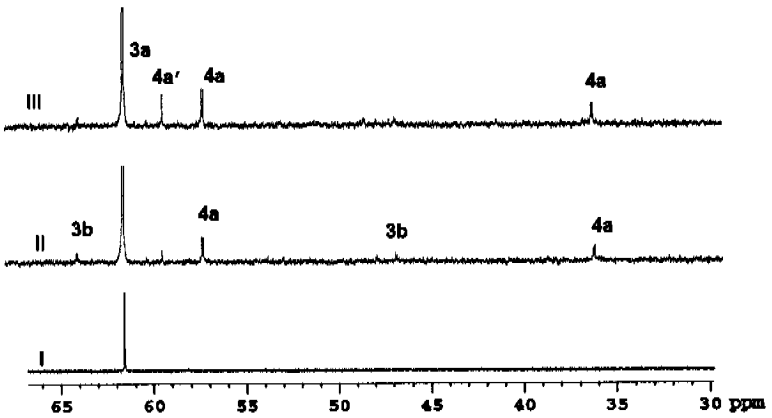

Fig. 3.9. (I) $^{31}P\{^{1}H\}$ spectrum of complex **3a** in THF solution. (II) Complex **3a** and one equivalent of trimethyl vinylsilane (TMVS) after 3 hours. (III) complex **3a** and 10 additional equivalents of TMVS.

The loss of phosphine allows for the silane olefin complexation. Insertion and reductive elimination afford the ethylsilane in the THF solution. This product, $EtSiMe_3$, was identified via a $^{29}Si,^{1}H$ correlation, see Fig. 3.10. The new presumed Ru(0) species which results in an oxidative addition reaction then readily adds the proximate iso-propyl C,H bond to afford the two isomeric cyclometallated products shown. At the moment we cannot be certain that the phosphine loss occurs only from one position within the coordination sphere.

Scheme 3.6

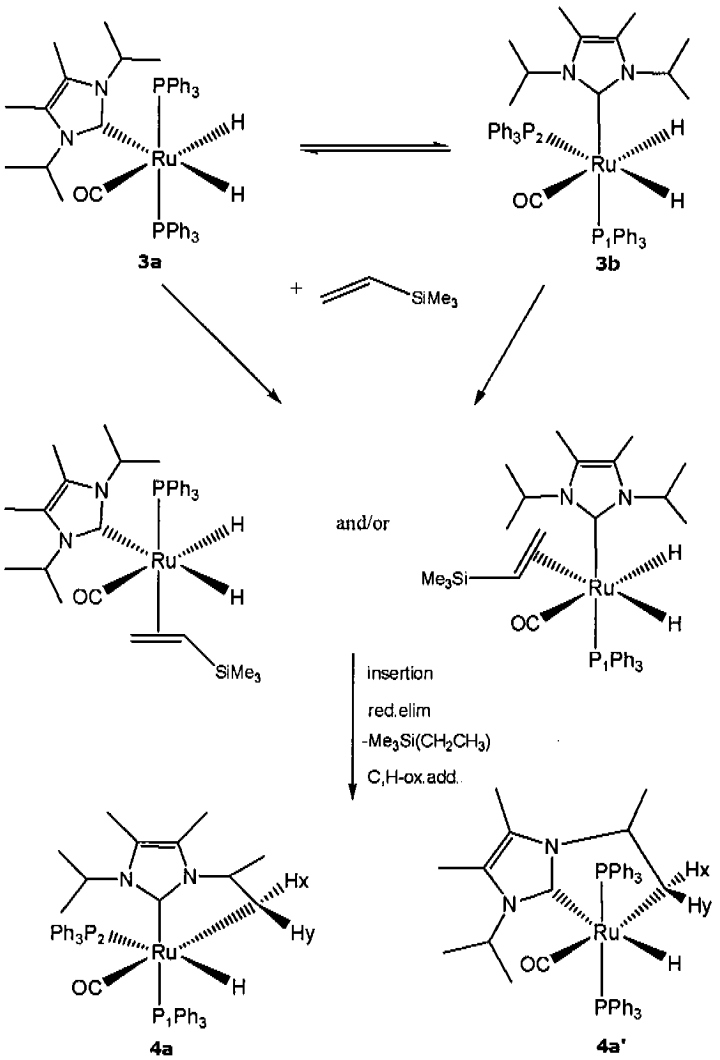

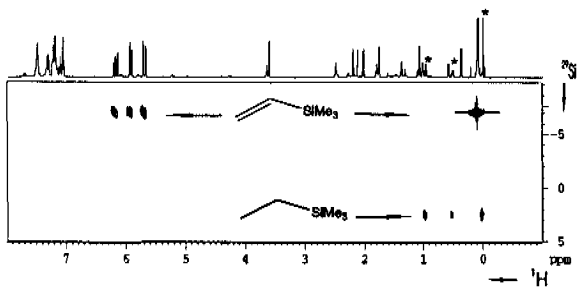

Fig. 3.10. ^{29}Si-^{1}H HMQC showing the three cross peaks for the product ethyltrimethylsilane in the presence of excess trimethyl vinylsilane (TMVS) in a mixture of complex **3a** + 11 equivalent of TMVS.

Conclusions: The phosphine exchange experiments carried out on Ru(II) hydrido NHC complexes **3**, **5** and cyclometallated cis-complex **4** to results in a mixture containing starting material and the three new products. The structures of the new products were identified by NMR to show that phosphine exchange occurs both trans to the carbene and trans to the hydride.

3.3 Dynamics

Diversified dynamic processes occur in molecules of different heteroorganic compounds (HOC) and, in particular, organometallic compounds (OMC), due to structural changes in the mutual arrangement of various groups in HOC molecules (rotation, small-amplitude oscillation, inversion, etc.). Generally, these processes are degenerate and occur rather rapidly. Occasionally these are suitable for study by dynamic NMR spectroscopy[51]. Studies of dynamics by NMR have often been carried out using detailed calculations of the line shapes that vary with temperature[52]; nevertheless, magnetization transfer[53, 54] and newer two-dimensional (2D) methods can often provide more comprehensive information[55, 56].

Examination of DNMR spectra allows the determination of rates and subsequently the elucidation of mechanisms. This approach was first applied to intramolecular rearrangements of organometallics 40 years ago in a series of measurements on "stereochemically non-rigid organometallic compounds." [57-59] The compounds were designated as fluxional[60] in situations where equivalent structures of these non-rigid compounds inter converted via a series of bond angle changes, rotations of ligands, or bond-breaking and bond-making reactions.

Transition metal complexes with N-heterocyclic carbenes have proven to be very efficient catalysts[61]. The efficiency of NHCs is attributed to both their strong sigma donor properties and sterically demanding structure. These very large ligands, in the presence of further bulky donors such as PPh_3, may well no longer freely rotate around the M-C(carbene) bond. Using classical temperature

dependent and 2-D NMR exchange techniques, aspects of the dynamics (restricted rotation features) of few carbene complexes are discussed in the following sections.

3.3.1 Restricted Rotation in Ru(II) Carbene Complexes

^{1}H NMR studies reveal that the two *iso*-propyl groups of the *trans* isomer **3a** are non-equivalent in THF solution at ambient temperature. This suggests that the plane defined by the three atoms, N-C(carbene)-N, does not eclipse the P-Ru-P axis, but rather lies rotated at some angle away from the two phosphine ligands, thus placing the two iso-propyl groups in different local environments. Sections of the phase sensitive 2-D NOESY exchange spectrum for this complex are shown in Fig. 3.11, and reveal that the two alkyl groups exchange with one another. i.e., there is rotation around the Ru-C(carbene) bond, but it is not rapid.

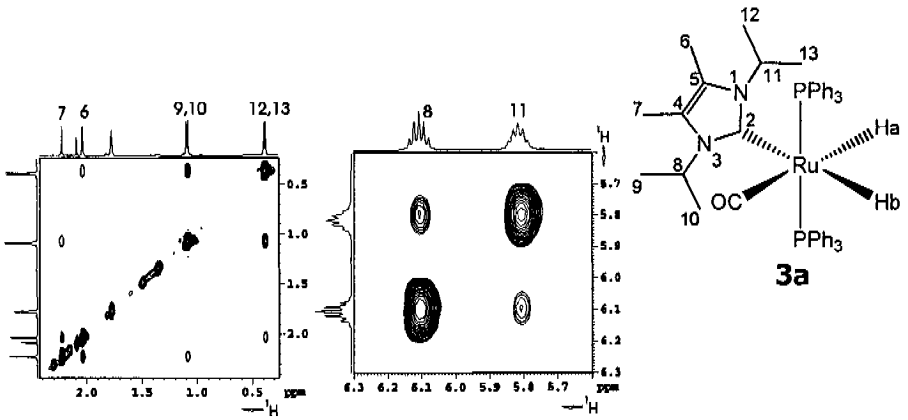

Fig. 3.11. Sections of ^{1}H, ^{1}H NOESY for **3a** in THF solution. The left section shows the exchange from the isopropyl methyl resonances (top right) and the right section shows the exchange between two methine signals.

In contrast to **3a**, the ambient temperature ^{1}H spectrum for **5** shows only two poorly resolved methyl signals (see Fig. 3.12). A series of variable temperature spectra eventually afford a ^{1}H

spectrum at 233K that contains six non-equivalent methyl resonances. This result is consistent with restricted rotation around both the Ru-C(carbene) and N-C(mesityl) bonds as indicated by the arrows in the structure beside. One of the two *p*-mesityl methyl groups is found at relatively low frequency, ca 1.2 ppm, and we assign this to a methyl group which is close to one or more of the phenyl groups of a PPh_3 ligand (i.e., local anisotropic effects).

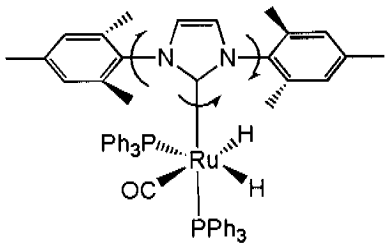

5

A line shape analysis using the data from Fig. 3.12 gives the following kinetic data: $\Delta H^{\ddagger}$ = 52.3 kJ/mol, $\Delta S^{\ddagger}$ = -3.6 J/K•mol and $\Delta G^{\ddagger}$ = 51.2 kJ/mol. Most likely, the difference in size between the IMes and iso-propyl carbene ligands is responsible for the differing dynamics associated with the restricted rotation.

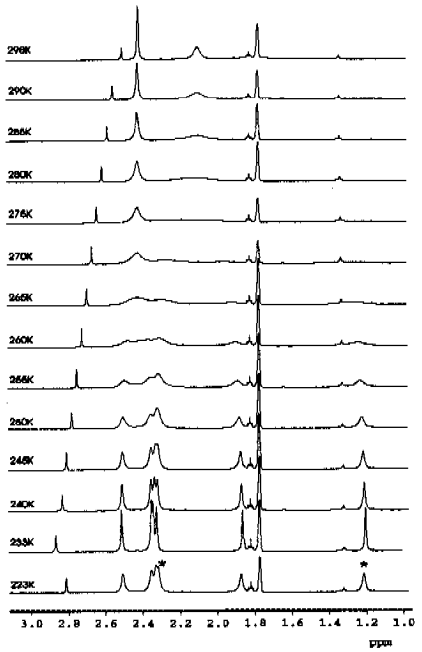

Fig. 3.12 ^1H NMR spectra (methyl region) of complex **5** at different temperatures. (*p*-mesityl methyl groups are indicated as stars).

It is observed that, between 240K and 255K, the CH_3-signals at ca 2.5 ppm, ca 1.8 ppm and ca 1.2 ppm all appear to broaden at the same rate, even though these represent rather different methyl signals. Consequently, it is tempting to think that there is a single mechanism contributing to these exchange processes. One possibility involves loss of phosphine, e.g., *trans* to the hydride ligand, followed by rapid rotation around both of the Ru-C(carbene) and N-C(mesityl) bonds due to the release of the steric pressure due to the PPh_3 ligand.

Again, in contrast to the observations for **3a**, the ambient temperature ^1H NOESY for **5** in the hydride region indicates exchange between the hydride ligands (see Fig. 3.13). This exchange might well be coupled to the phosphine loss in that perhaps the five-coordinate complex favors a rapid equilibrium between the di-hydride and the η^2 dihydrogen form. In any case, the IMes complex **5** seems to have rather different NMR characteristics than either of the *cis* isomers of **3** and **4**.

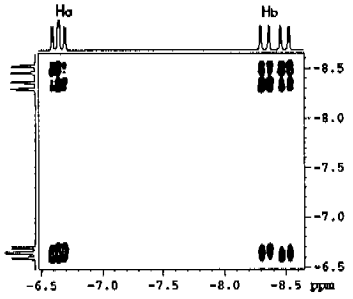

Fig. 3.13. Hydride region of ^1H, ^1H NOESY showing exchange between Ha and Hb

3.3.2 Restricted Rotation in Mono Cationic Rh(I) Carbene Complexes.

A variety of carbene complexes in a square planar (rather than an octahedral) environment are well known. The room temperature ^{1}H NMR spectrum of the Rh - carbene complex **6**[PF_6] reveals a number of broad signals in the aliphatic region for the Cy-substituents and two signals, in the ratio 2:1, for the NCH=CHN protons. Further, one of the two observable methine resonances of the Cy groups, at ca. 4.5 ppm, is extremely broad suggesting some form of fluxional behaviour. A set of variable temperature ^{1}H spectra for **6**[PF_6] was measured and these are shown in Fig. 3.14.

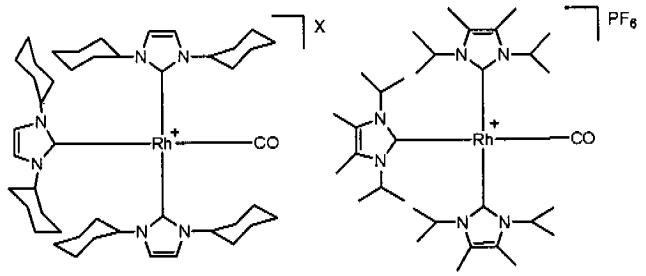

X = PF_6, BAr^F

6 **7**

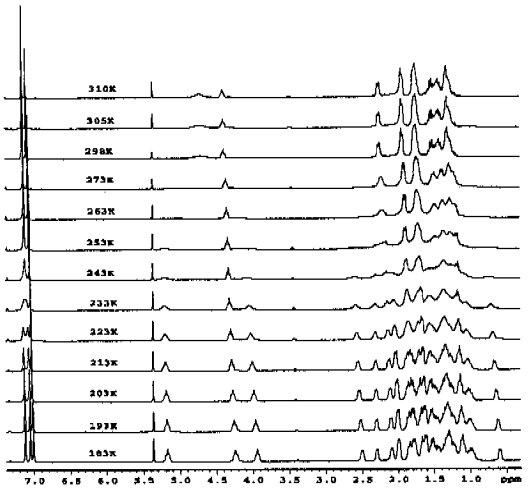

Fig. 3.14. ^{1}H NMR spectra (500 MHz) of [Rh(ICy)$_3$(CO)][PF_6], (**6**[PF_6]) in CD_2Cl_2 as a function of temperature.

At 203 K, all of the signals are relatively sharp and reveal three non-equivalent signals, in the ratio 1:1:1, for both the Cy-methine groups and the NCH=CHN backbone protons. A line shape analysis[62] of the data from Fig. 3.14 affords an energy of activation of 35 (±1) kJ/mol for the two *trans* positioned Rh-C_{NHC} bonds.

A similar set of NMR spectra were recorded for salt **7**[PF_6] (Fig. 3.15), and, at 203 K, gave three non-equivalent signals for the ^{i}Pr-methine resonances as well as three signals for the NCMe=CMeN protons. The relative integrals within each group are again 1:1:1. For **7**[PF_6], at 203 K one finds six non-equivalent i-Pr methyl signals due to the three different sets of diastereotopic CH_3 protons. Analysis of the various line shapes afforded an energy of activation of 40 (±1) kJ/mol for the two mutually *trans* NHC ligands. The variable temperature study for **6**[BAr^{F-}] salt (see Fig. 3.16) resulted in an activation energy of 38 (±1) kJ/mol. We do not observe any significant difference between the NMR spectra for **6**[PF_6] and **6**[BAr^{F-}] in the regions of the carbene resonances and we attribute the differences in the calculated energies to the experimental error[62].

The observed temperature dependences in the salts **6**[PF_6] and **7**[PF_6] are a consequence of restricted rotation associated with the three Rh-C(carbene) bonds.

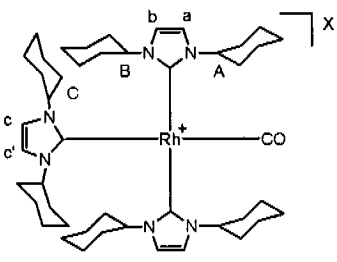

X = PF_6, BAr^F

At low temperature the three different sites are assigned as A-C for the Cy-methine protons and a-c for the three NCH=CHN protons, as indicated in the structure beside. The two *trans* carbene ligands are not exactly perpendicular to

the C-Rh-C plane defined by the OC-Rh-C(trans-carbene) fragment, with the result that the two N-substituents on the carbene reside in two different environments, i.e. one closer to the CO, the other proximate to the *trans* carbene ligand. Sections of the ROESY spectra[63] for **6**[PF_6] and **7**[PF_6] are shown in Fig. 3.17 and reveal that, even at 203 K, there is slow exchange, e.g. in **6**[PF_6] between sites A and B.

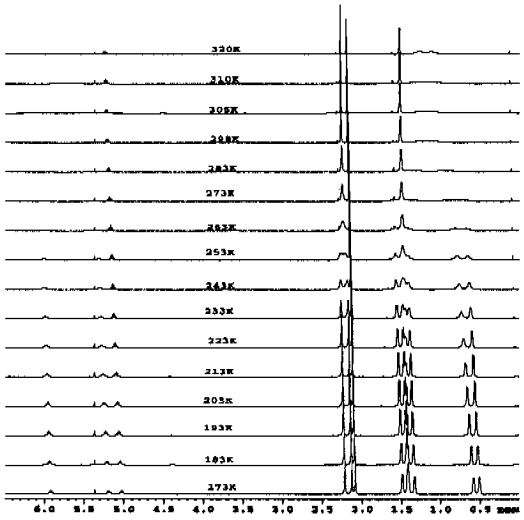

Fig. 3.15. ^{1}H NMR spectra (500 MHz) of [Rh($I^iPr_2Me_2$)$_3$(CO)][PF_6], **7**[PF_6], in CD_2Cl_2 as a function of temperature.

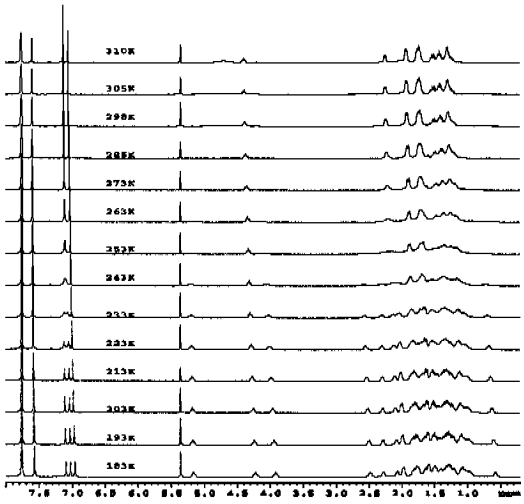

Fig. 3.16. ^{1}H NMR spectra (500 MHz) of [Rh(ICy)$_3$(CO)][BAr^{F-}], (**6**[BAr^{F-}]) in CD_2Cl_2 as a function of temperature.

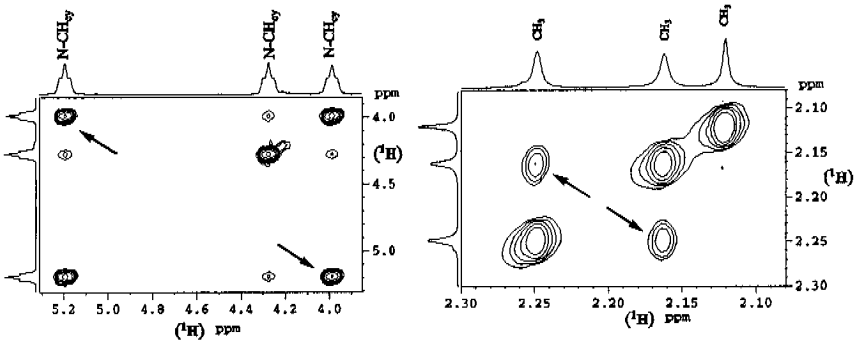

Fig. 3.17. Sections of the ROESY spectra at 203 K for (left) the methine region of **6**[PF_6] and (right) the heterocyclic ring methyl groups for **7**[PF_6]. In both, the cross-peaks due to the exchange between the two sides of the *trans* carbene ligands are indicated with arrows (CD_2Cl_2, 500 MHz).

We believe that the sites c and c' are also in exchange and that the entire process is concerted, i.e. all three carbene rings are rotating together. However, rotation of the imidazole ring in the NHC *trans* to the CO ligand moves the N-substituents into equivalent NMR environments, so that this exchange is not immediately recognized. However, a hint with respect to the rotation of this third ligand comes from the observed exchange between the diastereotopic ^{i}Pr methyl groups within the ring *trans* to the CO of **7**[PF_6]. These two methyl resonances, indicated as "x" and "y", are well resolved (δ 0.52 and 1.33) and are also in slow exchange at 203 K based on the ROESY data. We believe that this exchange process develops from the rotation indicated in cartoon below.

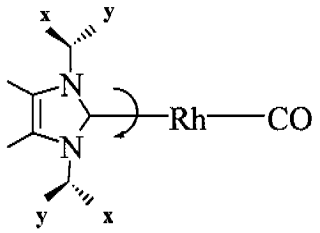

3.4. N-Heterocyclic Carbene HF Complexes

Fluoride complexes of the platinum group metals form a largely neglected class of compounds, which have long been considered as being too unstable and/or too reactive to be of any value. This is primarily because of the supposed incompatibility of the soft late metal center with the small, hard, electronegative fluoride ligand[64-66]. However, the development over the last 5-10 years of more widely applicable synthetic routes allowing fluoride to be introduced into the coordination sphere of a metal (e.g. AgF metathesis[67], C-F bond activation[68-72], development of mild HF sources such as $Et_3N{\cdot}3HF$[67, 73], oxidative addition of XeF_2[74, 75]) has made M-F complexes more common. As a consequence, a better understanding of the fundamental bonding interactions that can help to stabilise M-F complexes has also developed[76, 77], such that there is now a range of synthetic as well as catalytic applications[71, 74, 78, 79].

In the majority of M-F complexes, one or more tertiary phosphines are present as ancillary ligands, although not always in an innocent capacity[80]. One could ask the question, how stability and reactivity might be affected upon replacing PR_3 by an N-heterocyclic carbene (NHC), especially as NHCs are known to be significantly better donor ligands[20]. For example, while reductive elimination of imidazolium chloride from NHC-M-Cl complexes is well established[81], loss of imidazolium fluoride has not been investigated. This is to be expected given that only three fully characterized late M-F complexes carrying NHC ligands have been reported, one by Whittlesey et al. (Ru)[82] and two by Radius and co-workers (Ni)[83].

Given the interest in both Ru-carbene complexes and the still fairly scarce number of Ru-F complexes, an NMR study on the carbene fluoro-complexes **8** and **9** was undertaken.

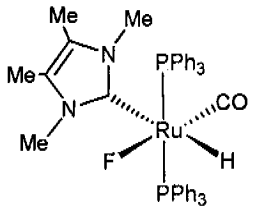

8

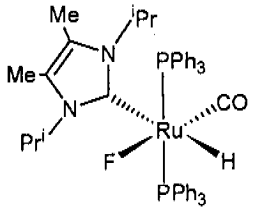

9

The ^{1}H NMR spectrum of complex **8** reveals the expected hydride signal as a triplet centered at δ -5.08 (in C_6D_6) plus four non-equivalent carbene methyl resonances. Two of these are found at relative high frequency (δ 3.34, δ 3.14) and are assigned to the N-Me absorptions. The appearance of four methyl signals is again indicative of restricted rotation about the Ru-C(carbene) bond. The N- C(carbene)-N plane is not parallel to the P-Ru-P axis and consequently, one of the two N-methyl resonances is closer to

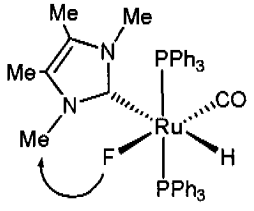

the F-atom (see above). As a consequence of this structure, the 2-D $^{1}H,^{19}F$ HOESY (Fig. 3.18) spectrum affords a selective NOE contact from the fluoride ligand to this methyl group and, therefore, since each N-methyl resonance shows a selective NOESY cross-peak to its proximate C-methyl partner, all four of the methyl signals can be assigned. Interestingly, one finds a selective,

through-space spin-spin interaction from the ^{19}F spin to the proximate methyl group and this is confirmed via a selective $^{1}H\{^{19}F\}$ decoupling experiment (see Fig. 3.19). There are no exchange peaks in the phase sensitive proton 2-D NOESY map so that there is a significant barrier to the rotation. The ^{31}P spectrum shows equivalent P-atoms at δ 44.75 and the ^{19}F resonance is observed at δ -353.30

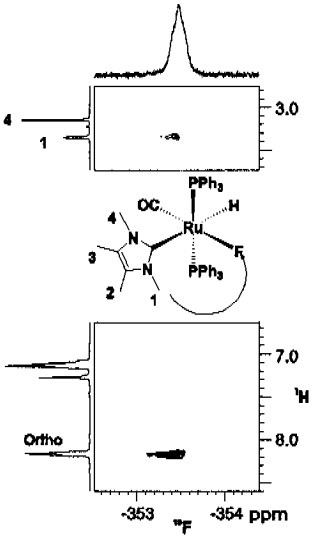

Fig. 3.18. $^{1}H,^{19}F$ HOESY spectrum of complex **8** showing selective NOE contact to the methyl group and *ortho* protons of the triphenyl phosphine (C_6D_6, 400 MHz, 298 K).

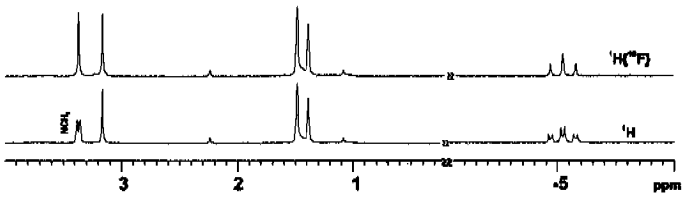

Fig. 3.19. Section of the ^{1}H (lower trace) and $^{1}H\{^{19}F\}$ (upper trace) NMR spectra of complex **8** (d_8-THF, 200 MHz, 298 K).

These results are somewhat in contrast to what one finds in solution for the i-Pr analog **9** (see Scheme 3.7). Initially, the NMR spectra are consistent with **9**. The hydride appears as a doublet of triplets, δ -5.94, ^{2}J(P,H) = 25.6 Hz and J(H,F) = 4.8 Hz. The ^{31}P spectrum shows equivalent P-atoms at δ 40.50 with ^{2}J(P,F) = 28 Hz.

Scheme 3.7.

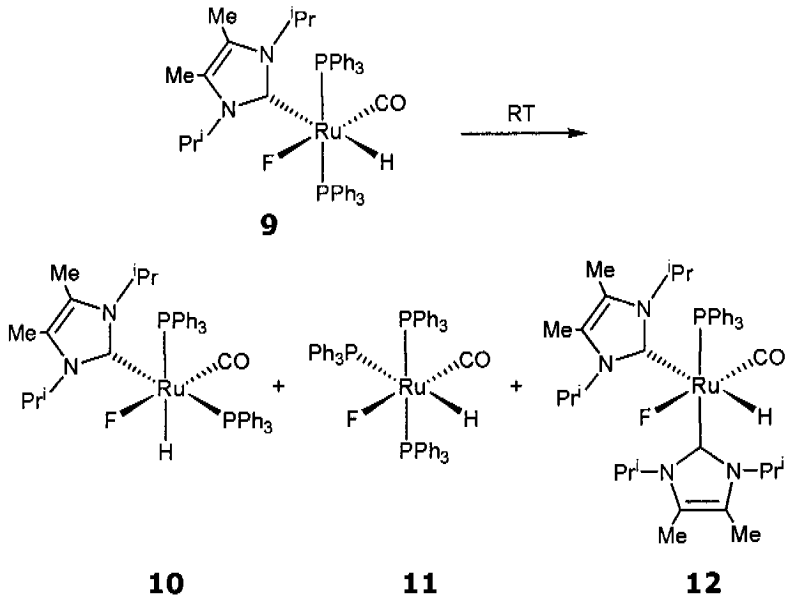

The ^{19}F resonance is observed at δ -355.6 as a poorly resolved multiplet. The two N-i-Pr (and C-Me) groups are non-equivalent and, again, the 2-D $^{1}H,^{19}F$ HOESY spectrum shows a selective contact to one of the two i-Pr methine protons, δ 6.29 (see Fig. 3.20), thereby facilitating the assignment of all of the aliphatic protons.

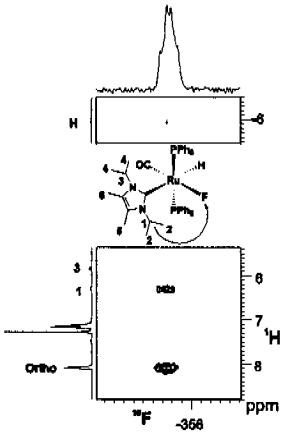

Fig. 3.20. $^{1}H,^{19}F$ HOESY spectrum of complex **9** showing selective NOE contact to one of the two isopropyl methine protons and the *ortho* protons of the triphenyl phosphine (C_6D_6, 400 MHz, 298 K).

However, the triplet hydride resonance slowly diminishes in intensity and three new groups of resonances appear in the hydride region (see Fig. 3.21) that can be assigned to structures **10-12**. After several hours, the relative intensities of these four Ru-species are ca 1:1:3:4 for **9-12**, respectively, i.e., **9** and **10** are now the minor components. Phase sensitive 2-D NOESY spectroscopy reveals that these complexes are not in equilibrium on the NMR time scale (see Fig. 3.22).

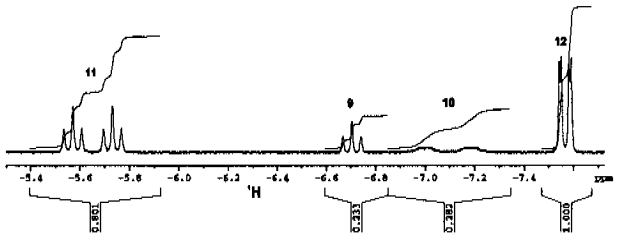

Fig. 3.21. ^{1}H spectrum of complex **9** after several hours showing the relative intensities of four Ru-species (**9**, **10**, **11** and **12**) are approximately 1:1:3:4 ratios. (d_8-THF, 700 MHz, 298 K).

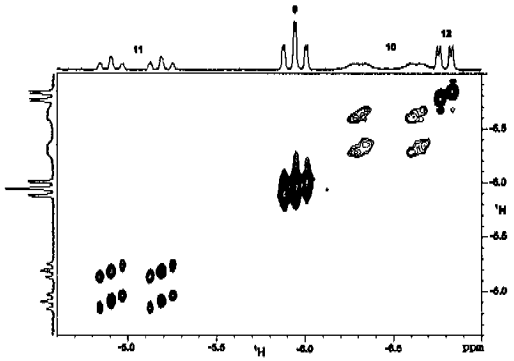

Fig. 3.22. Section of Hydride region of the NOESY spectrum for **9** at ambient temperature revealing no exchange between the species **10**, **11** and **12** (C_6D_6, 400 NMR).

Complex **10**, which gives broad NMR resonances at ambient temperature, can be shown (via low temperature measurements, in d_8-THF, see Fig. 3.23) to be the *cis* bis-phosphine isomer of **9**. In addition to the non-equivalent ^{31}P signals, δ 40.39 and δ 19.50 and

a broad ^{19}F signal at δ -320.0, one finds that the hydride resonance for **10** now appears as a doublet of doublets with the expected relative large $^{2}J(P,H)$ trans coupling of 131 Hz.

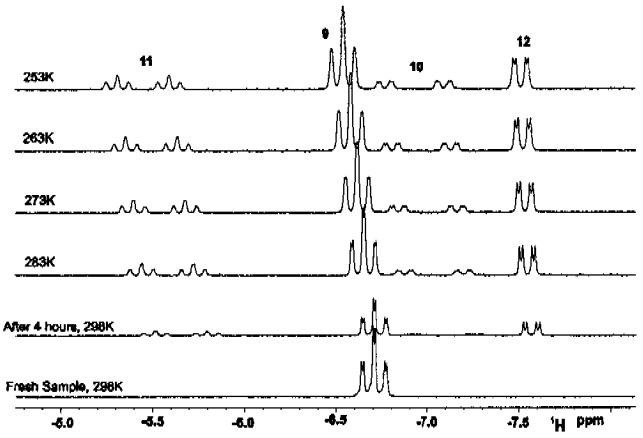

Fig. 3.23. Variable-temperature NMR study of complex **10** showing doublet of doublets at below 283K (d_8-THF, 400 MHz).

The major components, complexes **11** and **12**, arise due to a disproportionation reaction. The new tris-phosphine complex, **11**, reveals a hydride signal, δ -5.65 composed of two triplets separated by the expected relatively large $^{2}J(P,H)$ trans coupling of 112 Hz. There is a further small splitting of ca 3.5 Hz from the ^{19}F atom in benzene solution, but this is no longer visible in THF solution. One finds the expected A_2X ^{31}P spectrum, and a quartet ^{19}F signal at δ -385.1, $^{2}J(P,F)$ = 23 Hz.

The bis-carbene complex, **12**, reveals a sharp doublet of doublets for its hydride resonance at δ - 7.57. The two bond interactions, 28 Hz and 7 Hz, are assigned to $^{2}J(P,H)$ and $^{2}J(F, H)$, respectively. Further, one finds a sharp doublet at 44.6 ppm in the $^{31}P\{^{1}H\}$ NMR spectrum, $^{2}J(P,F)$ = 41.4 Hz and a broad ^{19}F signal at ca δ - 344. The two carbene ligands are non-equivalent and a $^{13}C\{^{1}H\}$-^{1}H HMBC correlation from the hydride resonance at -7.57, shows three correlations: one each to the two carbene carbons, ca δ 184 and δ 192, and one to the ruthenium carbonyl carbon, at ca δ 204 (see

Fig. 3.24). These cross-peaks stem from two-bond proton-carbon interactions and it was not obvious that these would be large enough to be analytically useful.

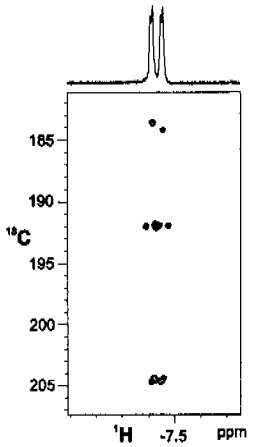

Fig. 3.24. Section of the ^{13}C, ^{1}H HMBC spectrum for **12** at ambient temperature showing correlations to one each of to the two carbene carbons and one to the carbonyl carbon.(d_8-THF, 700 MHz).

The obvious difference in stability between **8** and **9** is undoubtedly related to the sterically bulky i-Pr groups in **9** and suggestions that conclusions with respect to the catalytic properties of **9** will require a consideration of possible disproportionation products.

Conclusions: The NMR measurements on N-heterocyclic carbene HF complexes (**8** and **9**) concern themselves with the structure and reactivity. The relatively large carbene ligands induce interesting isomerization and disproporationation reactions.

3.5 Concluding Remarks

This chapter describes a modest number of N-Heterocyclic carbene complexes which have been characterized by 1D and 2D NMR spectroscopy. Variable- temperature ^{1}H NMR and / or NOE studies reveal that there is restricted rotation about the M-C_{NHC} bond in several of these complexes. Line shape analysis from the NMR studies afford activation barriers for selected carbene complexes (**5, 6** and **7**). In specific complexes (**3a, 4** and **5**) the phosphine exchange, monitored via NMR spectroscopy, proves that the coordination positions both trans to carbene and trans to hydride are quite labile. In complexes **8** and **9** the relatively large carbene ligands induce interesting isomerization and disproporationation reactions.

3.6 Experimental Part

^{1}H, ^{31}P, ^{13}C and ^{19}F NMR spectra were recorded with Bruker DPX-200, 300, 400, 500 and 700 MHz spectrometers at room temperature unless otherwise noted. The T_1 values were measured using standard inversion recovery pulse sequence: [For complex **4b,** THF, Hydride signal, 895 ms, Aromatic, 1.48 s], [For complex **3a,** THF, Hydride signal, 845 ms, Aromatic, 1.34 s], [For complex **8,** C_6D_6, Hydride signal, 550 ms, N-Methyl, 890 ms, Aromatic, 1.4s]. [For complex **9,** C_6D_6, Hydride signal, 552 ms, Methyl, 690 ms, Aromatic, 1.1 s]. The ^{1}H, ^{13}C-HMBC was acquired using a 0.6 s relaxation delay and coupling constant of 135 Hz (d2 = 3.7 ms).The $^{1}H,^{1}H$ NOESY spectra were acquired using a 0.6 s relaxation delay and 600ms of mixing time. $^{1}H,^{1}H$ ROESY was performed using standard Bruker pulse sequence keeping a mixing time of 250 ms at a set temperature of 203 K within the NMR probe. $^{19}F,^{1}H$-HOESY NMR experiments were acquired using the standard four-pulse sequence and carried out using a doubly tuned TXI probe. A mixing time of 800 ms was used and 16 or 32 scans were taken for each of the 1024 t_1 increments recorded. The delay between increments was set to 2 s.

The rate constants derived from variable-temperature data are extracted by fitting the calculated line shape to the experiment. This was done by manual iteration and visual comparison. The iterative program, MEXICO (version 3) was used[84]. Line shape analysis over the temperature range 298 K to 203 K gave a set of rate constants, and resulting plot of ln (k) vs. 1/T revealed the activation parameter E_A from the Arrhenius equation (**a**)

$$\ln(k) = -E_A / RT + \ln A \quad \text{.....(a)}$$

Where, E_A, Energy of activation and A, the pre-exponential or frequency factor.

T (K)	k(s^{-1})
223	1.5
233	5.7
237	10.0
240	13.3
245	23.0
250	41.0
255	70.0
260	123.0
265	209.0
270	303.0
280	700.0
285	950.0
290	1500
298	2200

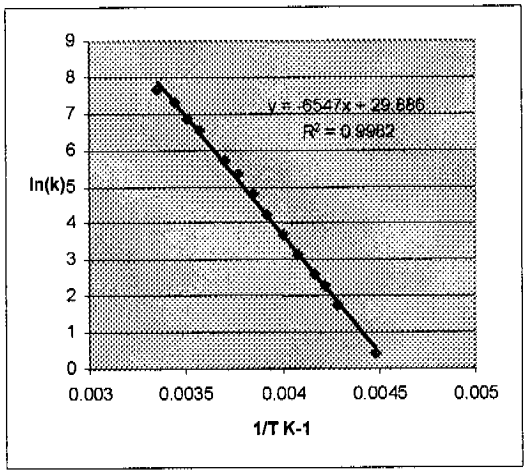

Fig. E1. Rate constants for the internal exchange of the *p*-mesityl methyl of IMes ligand in Ru(IMes)(PPh_3)$_2$(CO)(H)$_2$ (**5**) as a function of temperature and graph showing ln(k) vs. 1/T for the same.

$\ln(k) = -E_a / RT + \ln A$

Slope = m = $- E_a / R = -6547$

$E_a = 54.4$ kJ mol^{-1}

T (K)	k(s^{-1})
203	6
213	14
223	33
233	80
243	175
253	370
263	640
273	1200

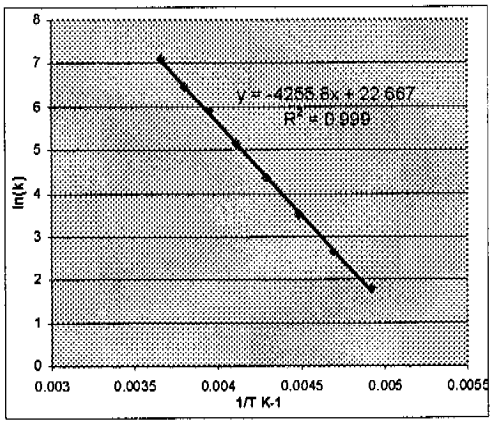

Fig. E2. Rate constants for the Methine protons of ICy ligand in [Rh(ICy)$_3$CO] PF_6 (**6**) as a function of temperature and graph showing ln(k) vs. 1/T for the same

$\ln(k) = -E_a / RT + \ln A$

Slope = m = $- E_a / R = -4255.8$

$E_a = 35.4$ kJ mol^{-1}

T (K)	k(s^{-1})
213	10
223	23
233	54
243	118
253	255
263	560
273	1100
285	2100
298	4150

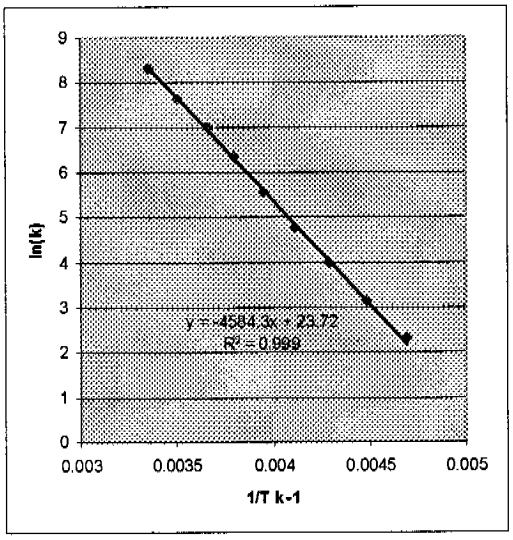

Fig. E3. Rate constants for the Methine protons of ICy ligand in $[Rh(ICy)_3CO]$ BArF (**6**) as a function of temperature and graph showing ln(k) vs. 1/T for the same

$$\ln(k) = -E_a / RT + \ln A$$

Slope = m = $- E_a / R = -4584.3$

$E_a = 38.1$ kJ mol^{-1}

T (K)	k(s^{-1})
228	10.5
233	16.5
238	23.5
243	36
248	53
253	79
258	122
263	168
268	235
273	337
278	453
283	655
288	846
298	1423

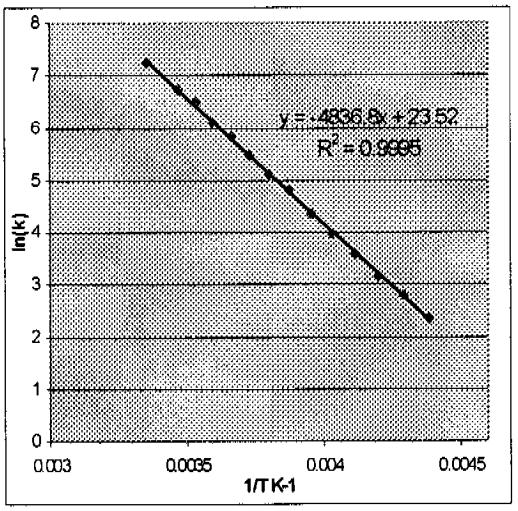

Fig. E4. Rate constants for the Methyl protons of IPr_2Me_2 ligand in $[Rh(IPr_2Me_2)_3CO]$ PF_6 (**7**) as a function of temperature and graph showing ln(k) vs. 1/T for the same.

$$\ln(k) = -E_a / RT + \ln A$$

Slope = m = $- E_a / R = -4836.8$

$E_a = 40.2$ kJ mol^{-1}

3.7 Bibliography

[1] S. Burling, B. M. Paine, D. Nama, V. S. Brown, M. F. Mahon, T. J. Prior, P. S. Pregosin, M. K. Whittlesey and J. M. J. Williams, *J. Am. Chem. Soc* **2007**, *129*, 1987-1995.

[2] C. A. Tolman, *Chem. Revs.* **1977**, *77*, 313.

[3] K. Ofele, *J. Organomet. Chem.* **1968**, *12*, P42-&.

[4] H. W. Wanzlick and Schonher.Hj, *Angew. Chem.-Int. Edit.* **1968**, *7*, 141-&.

[5] D. J. Cardin, Cetinkay.B, Cetinkay.E, M. F. Lappert, E. W. Randall and Rosenber.E, *J. Chem. Soc.-Dalton Trans.* **1973**, 1982-1985.

[6] A. J. Arduengo, R. L. Harlow and M. Kline, *J. Am.Chem. Soc.* **1991**, *113*, 361-363.

[7] W. A. Herrmann, M. Elison, J. Fischer, C. Kocher and G. R. J. Artus, *Angewandte Chemie-International Edition in English* **1995**, *34*, 2371-2374.

[8] K. Ofele, W. A. Herrmann, D. Mihalios, M. Elison, E. Herdtweck, T. Priermeier and P. Kiprof, **1995**, *498*, 1-14.

[9] W. A. Herrmann, D. Mihalios, K. Ofele, P. Kiprof and F. Belmedjahed, *Chemische Berichte-Recueil* **1992**, *125*, 1795-1799.

[10] K. Ofele, W. A. Herrmann, D. Mihalios, M. Elison, E. Herdtweck, W. Scherer and J. Mink, **1993**, *459*, 177-184.

[11] W. A. Herrmann, M. Elison, J. Fischer, C. Kocher and G. R. J. Artus, *Chem.-Eur. J.* **1996**, *2*, 772-780.

[12] L. Perrin, E. Clot, O. Eisenstein, J. Loch and R. H. Crabtree, *Inorg. Chem.* **2001**, *40*, 5806-5811.

[13] J. K. Huang, E. D. Stevens, S. P. Nolan and J. L. Petersen, *J. Am.Chem. Soc.* **1999**, *121*, 2674-2678.

[14] A. T. Termaten, M. Schakel, A. W. Ehlers, M. Lutz, A. L. Spek and K. Lammertsma, *Chem.-Eur. J.* **2003**, *9*, 3577-3582.

[15] M. T. Lee and C. H. Hu, *Organometallics* **2004**, *23*, 976-983.

[16] X. L. Hu, I. Castro-Rodriguez and K. Meyer, *J. Am.Chem. Soc.* **2004**, *126*, 13464-13473.

[17] L. Cavallo, A. Correa, C. Costabile and H. Jacobsen, *J. Organomet. Chem.* **2005**, *690*, 5407-5413.

[18] A. R. Chianese, X. W. Li, M. C. Janzen, J. W. Faller and R. H. Crabtree, *Organometallics* **2003**, *22*, 1663-1667.

[19] R. Dorta, E. D. Stevens, N. M. Scott, C. Costabile, L. Cavallo, C. D. Hoff and S. P. Nolan, *J. Am.Chem. Soc.* **2005**, *127*, 2485-2495.

[20] S. P. Nolan, *N-Heterocyclic Carbenes in Synthesis*, Wiley-VCH, Weinheim, **2006**, p.

[21] W. A. Herrmann, *Angew. Chem.-Int. Edit.* **2002**, *41*, 1291-+.

[22] R. Dorta, E. D. Stevens, C. D. Hoff and S. P. Nolan, *J. Am.Chem. Soc.* **2003**, *125*, 10490-10491.

[23] E. Becker, V. Stingl, G. Dazinger, M. Puchberger, K. Mereiter and K. Kirchner, *J. Am.Chem. Soc.* **2006**, *128*, 6572-6573.

[24] R. F. R. Jazzar, S. A. Macgregor, M. F. Mahon, S. P. Richards and M. K. Whittlesey, *Journal of the American Chemical Society* **2002**, *124*, 4944-4945.

[25] E. Becker, V. Stingl, G. Dazinger, M. Puchberger, K. Mereiter and K. Kirchner, **2006**, *128*, 6572-6573.

[26] D. S. McGuinness, N. Saendig, B. F. Yates and K. J. Cavell, *J. Am.Chem. Soc.* **2001**, *123*, 4029-4040.

[27] L. R. Titcomb, S. Caddick, F. G. N. Cloke, D. J. Wilson and D. McKerrecher, *Chem. Commun.* **2001**, 1388-1389.

[28] R. W. Simms, M. J. Drewitt and M. C. Baird, *Organometallics* **2002**, *21*, 2958-2963.

[29] A. C. Hillier, W. J. Sommer, B. S. Yong, J. L. Petersen, L. Cavallo and S. P. Nolan, *Organometallics* **2003**, *22*, 4322-4326.

[30] J. K. Huang, H. J. Schanz, E. D. Stevens and S. P. Nolan, *Organometallics* **1999**, *18*, 2370-2375.

[31] S. Murai, *Activation of Unreactive Bonds and Organic Synthesis*, Springer-Verlag, Berlin a.o., **1999**, p.

[32] R. H. Crabtree, *Chem. Revs.* **1995**, *95*, 987-1007.

[33] A. H. Janowicz and R. G. Bergman, *J. Am.Chem. Soc.* **1982**, *104*, 352-354.

[34] A. A. Danopoulos, N. Tsoureas, J. C. Green and M. B. Hursthouse, *Chem. Commun.* **2003**, 756-757.

[35] V. K. Dioumaev, D. J. Szalda, J. Hanson, J. A. Franz and R. M. Bullock, *Chem. Commun.* **2003**, 1670-1671.

[36] P. B. Hitchcock, M. F. Lappert and P. L. Pye, *J. Chem. Soc.-Chem. Commun.* **1976**, 644-646.

[37] M. J. Chilvers, R. F. R. Jazzar, M. F. Mahon and M. K. Whittlesey, *Advanced Synthesis & Catalysis* **2003**, *345*, 1111-1114.

[38] K. Abdur-Rashid, T. Fedorkiw, A. J. Lough and R. H. Morris, *Organometallics* **2004**, *23*, 86-94.

[39] A. E. Shilov and G. B. Shul'pin, *Chem. Revs.* **1997**, *97*, 2879-2932.

[40] P. B. Hitchcock, M. F. Lappert and P. Terreros, *J. Organomet. Chem.* **1982**, *239*, C26-C30.

[41] M. Prinz, M. Grosche, E. Herdtweck and W. A. Herrmann, *Organometallics* **2000**, *19*, 1692-1694.

[42] R. Dorta, E. D. Stevens and S. P. Nolan, *J. Am.Chem. Soc.* **2004**, *126*, 5054-5055.

[43] M. G. Edwards, R. F. R. Jazzar, B. M. Paine, D. J. Shermer, M. K. Whittlesey, J. M. J. Williams and D. D. Edney, *Chem. Commun.* **2004**, 90-91.

[44] S. Burling, M. F. Mahon, B. M. Paine, M. K. Whittlesey and J. M. J. Williams, *Organometallics* **2004**, *23*, 4537-4539.

[45] R. H. Grubbs, *Tetrahedron* **2004**, *60*, 7117-7140.

[46] R. H. Grubbs, S. J. Miller and G. C. Fu, *Acc. Chem. Res.* **1995**, *28*, 446.

[47] H. M. Lee, D. C. Smith, Z. J. He, E. D. Stevens, C. S. Yi and S. P. Nolan, *Organometallics* **2001**, *20*, 794-797.

[48] U. L. Dharmasena, H. M. Foucault, E. N. dos Santos, D. E. Fogg and S. P. Nolan, *Organometallics* **2005**, *24*, 1056-1058.

[49] D. Giunta, M. Holscher, C. W. Lehmann, R. Mynott, C. Wirtz and W. Leitner, *Advanced Synthesis & Catalysis* **2003**, *345*, 1139-1145.

[50] D. P. Allen, C. M. Crudden, L. A. Calhoun and R. Y. Wang, *J. Organomet. Chem.* **2004**, *689*, 3203-3209.

[51] M. Gielen, R. Willem and B. Wrackmeyer in *Advanced Applications of NMR to Organometallic Chemistry, Vol.* ('Ed.'^'Eds.' Joh wiley and Sons, Chichester, England, **1996**, p.^pp.

[52] G. Binsch and H. Kessler, *Angewandte Chemie-International Edition in English* **1980**, *19*, 411-428.

[53] K. G. Orrell in *Dynamic NMR spectroscopy in inorganic and organometallic chemistry, Vol. 37* ('Ed.'^'Eds.' **1999**, p.^pp. 1-74.

[54] D. R. Muhandiram and R. E. D. McClung, *J. Mag. Res.* **1987**, *71*, 187-192.

[55] C. L. Perrin and T. J. Dwyer, *Chem. Revs.* **1990**, *90*, 935-967.

[56] A. D. Bain, *Prog. Nucl. Magn. Reson. Spectrosc.* **2003**, *43*, 63-103.

[57] F. A. Cotton, A. Davison and J. W. Faller, *J. Am.Chem. Soc.* **1966**, *88*, 4507-&.

[58] J. W. Faller and A. Davison, *Inorg. Chem.* **1967**, *6*, 182-&.

[59] W. K. Bratton, F. A. Cotton, A. Davison, A. Musco and J. W. Faller, *Proc. Natl. Acad. Sci. U. S. A.* **1967**, *58*, 1324-&.

[60] W. E. V. Doering and W. R. Roth, *Angew. Chem.-Int. Edit.* **1963**, *75*, 27-&.

[61] W. A. Herrmann and C. Kocher, *Angewandte Chemie-International Edition in English* **1997**, *36*, 2163-2187.

[62] J. Sandstrom, *Dynamic NMR Spectroscopy*, Academic Press, London, **1982**, p.

[63] W. E. Hull, *Two-Dimensional NMR Spectroscopy. Applications for Chemists and Biochemists.*, VCH, New York, **1987**, p. 153.

[64] V. V. Grushin, *Chem.-Eur. J.* **2002**, *8*, 1006-1014.

[65] N. M. Doherty and N. W. Hoffman, *Chem. Revs.* **1991**, *91*, 553-573.

[66] E. F. Murphy, R. Murugavel and H. W. Roesky, *Chem. Revs.* **1997**, *97*, 3425-3468.

[67] V. V. Grushin and W. J. Marshall, *Angewandte Chemie-International Edition in English* **2002**, *41*, 4476-+.

[68] H. Torrens, *Coord. Chem. Revs.* **2005**, *249*, 1957-1985.

[69] J. L. Kiplinger, T. G. Richmond and C. E. Osterberg, *Chem. Revs.* **1994**, *94*, 373-431.

[70] T. Braun, S. P. Foxon, R. N. Perutz and P. H. Walton, *Angewandte Chemie-International Edition in English* **1999**, *38*, 3326-3329.

[71] T. Braun and R. N. Perutz, *Chem. Commun.* **2002**, 2749-2757.

[72] M. S. Kirkham, M. F. Mahon and M. K. Whittlesey, *Chem. Commun.* **2001**, 813-814.

[73] M. K. Whittlesey, R. N. Perutz, B. Greener and M. H. Moore, *Chem. Commun.* **1997**, 187-188.

[74] J. H. Holloway and E. G. Hope, *Journal of Fluorine Chemistry* **1996**, *76*, 209-212.

[75] A. Yahav, I. Goldberg and A. Vigalok, *Inorg. Chem.* **2005**, *44*, 1547-1553.

[76] K. G. Caulton, *New J. Chem.* **1994**, *18*, 25-41.

[77] C. Becker, I. Kieltsch, D. Broggini and A. Mezzetti, *Inorg. Chem.* **2003**, *42*, 8417-8429.

[78] P. Barthazy, R. M. Stoop, M. Worle, A. Togni and A. Mezzetti, *Organometallics* **2000**, *19*, 2844-2852.

[79] S. Kuhl, R. Schneider and Y. Fort, *Advanced Synthesis & Catalysis* **2003**, *345*, 341-344.

[80] S. A. Macgregor, D. C. Roe, W. J. Marshall, K. M. Bloch, V. I. Bakhmutov and V. V. Grushin, *J. Am.Chem. Soc.* **2005**, *127*, 15304-15321.

[81] W. J. Marshall and V. V. Grushin, *Organometallics* **2003**, *22*, 1591-1593.

[82] S. L. Chatwin, M. G. Davidson, C. Doherty, S. M. Donald, R. F. R. Jazzar, S. A. Macgregor, G. J. McIntyre, M. F. Mahon and M. K. Whittlesey, *Organometallics* **2006**, *25*, 99-110.

[83] T. Schaub and U. Radius, *Chem.-Eur. J.* **2005**, *11*, 5024-5030.

[84] A.D.Bain in *The McMaster program for exchange line shape calculations, version 3, Vol.* ('Ed.'^'Eds.' **2002**, p.^pp.

Appendices

Introduction

The use of ionic liquids as alternative solvent, especially in biphasic catalysis, continues to attract interest in the chemical community[1-4]. Many catalysts are efficiently immobilised in these liquids, allowing for facile catalyst recycling[5, 6]. Addition of co-solvents may, however, be required for a number of purposes: (i) to help dissolve a catalyst (ii) to decrease the viscosity (iii) to induce phase separation between the ionic liquid and the substrates/products and (iv) facilitate catalyst activation[7]. While many physical properties of ionic liquids including *e.g.* gas solubility, viscosity, and temperature effects have been studied in recent years[8, 9], a detailed understanding of how ionic liquids behave in the presence of a co-solvent is still lacking. From ESI-MS studies it is known, that dilute ionic liquids can form oligomeric cation-anion aggregates with their size depending on the concentration of the solution[10, 11]. However, in concentration regimes usually encountered in synthesis, aggregation states and cation-anion interactions in ionic liquid solutions remain unknown.

Ion effects and ion-pairing are now well established in homogeneous catalysis[12]. An influence of the nature of the ionic liquid anion on the catalytic activity is also known, although in this case such effects can often be attributed to either the presence of halide impurities or decomposition (*e.g.,* hydrolysis of PF_6^-).

We have chosen to study the diffusion and HOESY characteristics of the BF_4^- and $N(OTf)_2$ (and to a lesser extent PF_6^-) anions as 1-butyl-3-methylimidazolium salts, $[C_4C_1im][BF_4]$, $[C_4C_1im][PF_6]$, and $[C_4C_1im][N(OTf)_2]$.

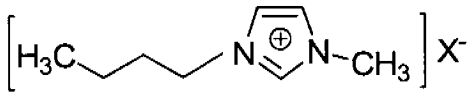

X= BF_4, PF_6, $(CF_3SO)_2N$

Diffusion and HOESY NMR techniques are becoming increasingly used to study inter-ionic interactions in a variety of main-group and transition metal salts[13-19]. Recently, Wang[15] and Watanabe and co-workers[16] have used this approach to study the temperature dependencies of the self-diffusion coefficient, viscosity and ionic conductivity for several ionic liquids. We present here NMR data, which support marked effects of the co-solvent on the structure of the ionic liquid.

Results and Discussion

Fig. 1 shows a $^1H,^{19}F$-HOESY spectra for the neat ionic liquid $[C_4C_1im]BF_4$, (A) as well as six additional spectra for the various dilutions in methanol, (B-D) and dichloromethane, (E-G). In pure $[C_4C_1im]BF_4$, there are strong contacts from the BF_4^- *to all of the cation protons*, and thus there is no selectivity. The anion "sees" all of the various protons more or less equally. ^1H, ^1H NOESY experiments reveal contacts from the N=CH-N proton, δ 8.4, to the two non-equivalent olefinic protons, δ 7.28 and 7.33, as well as NOE contacts between the two side-chains. These NOE results are in keeping with *inter*-rather than intra-molecular contacts, i.e., an individual cation is surrounded by more than one anion. Similar results are found for $[C_4C_1im][N(OTf)_2]$, see Fig. 2. On dilution in methanol (B-D), Fig. 1 shows (a) the ^1H, ^{19}F-HOESY selectivity increases and (b) all of the $^1H,^{19}F$ cross-peak intensities decrease. These observations are consistent with strong solvation by methanol and thus reduced anion-cation contacts.

Sections (E)-(G), in Figure 1, show the effects of dilution with CD_2Cl_2. At an ionic liquid/solvent volume ratio of 1:5 (spectrum F) the cross peaks to all of the protons are clearly visible. Even at the maximum dilution, 1:59 (spectrum G), almost all of the cross-peaks are still visible. These results are consistent with strong ion pairing. A similar HOESY result, i.e., contacts from the anion to *all* of the protons of the cation, was also found for $[C_4C_1im][N(OTf)_2]$ (ionic liquid/ CD_2Cl_2 volume ratio of 1:5, entry 13).

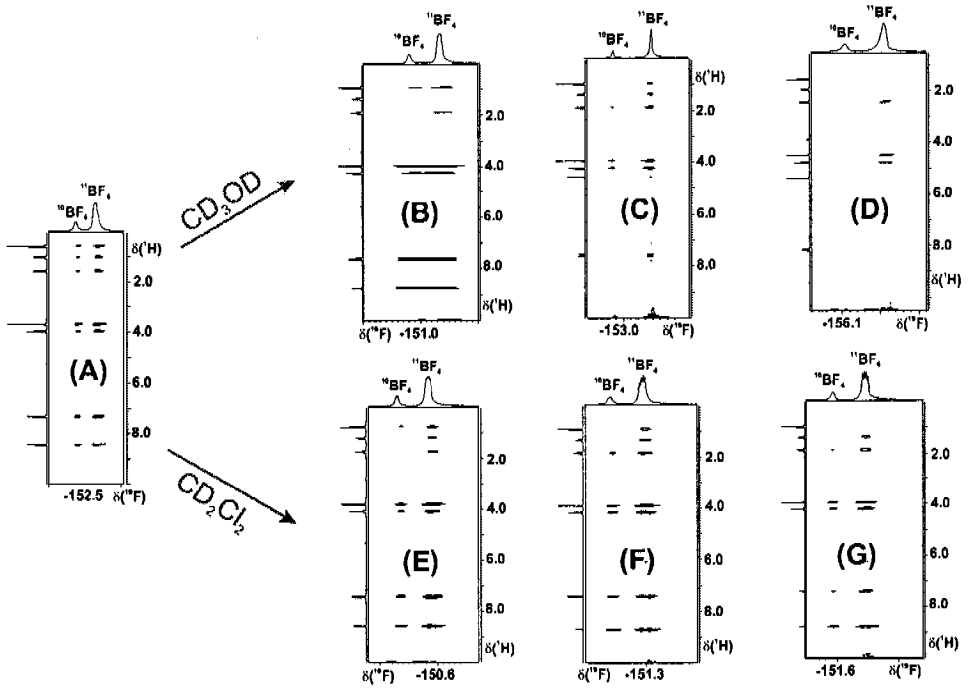

Figure 1. Series of ^1H, ^{19}F- HOESY spectra under differing conditions: (A) Neat ionic liquid (IL) $[C_4C_1im]BF_4$ (B) 0.55 ml IL + 0.05 ml CD_3OD (C) 0.1 ml IL + 0.5 ml CD_3OD (D) 0.01 ml IL + 0.59 ml CD_3OD (E) 0.55 ml IL + 0.05 ml CD_2Cl_2 (F) 0.1 ml IL + 0.5 ml CD_2Cl_2 (G) 0.01 ml IL + 0.59 ml CD_2Cl_2

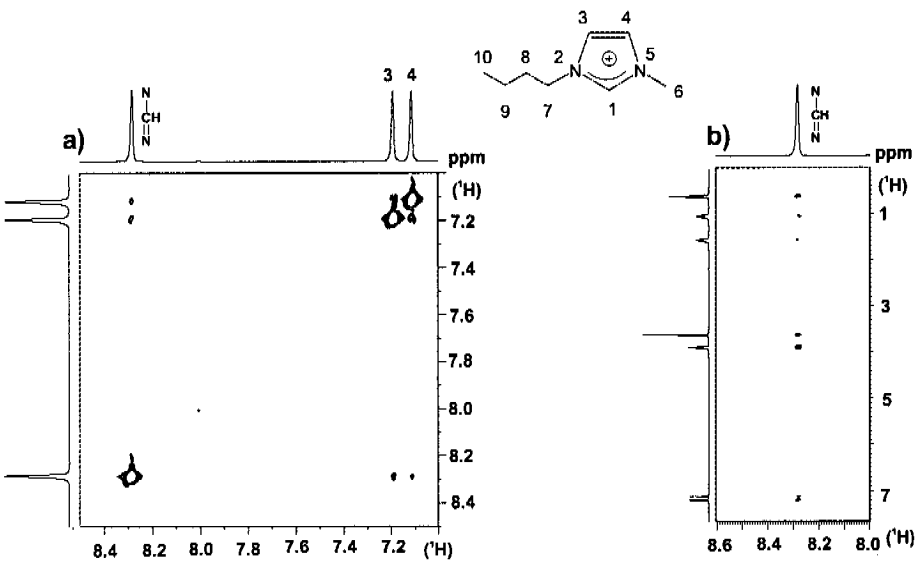

Figure 2. Section of the ^{1}H-^{1}H NOESY (800 ms mixing time) spectrum of the neat ionic liquid (IL) $[C_4C_1im]$ $[N(OTf)_2]$ showing NOE contacts from the N=C**H**-N proton to (a) the non-equivalent olefinic protons (labeled as 3 and 4) and (b) to the two side chains that is N-CH_3 (labeled as 6) and N-CH_2-CH_2-CH_2-CH_3 (labeled as 7-10) suggesting inter-molecular contacts.

It has been suggested that in the solid-state, that anion-cation hydrogen bonding forces are involved[20, 21]. However, in the neat ionic liquid and in dichloromethane solution the HOESY contacts to the N=C**H**-N proton (the site suggested for the H-bonding) are approximately equivalent to those arising from the two olefinic, N-methyl and N-methylene protons (see (A) and (F)). Consequently, we discount *selective* hydrogen bonding as being the only major contributor, under these conditions, and conclude that ionic interactions are primarily responsible for the observed HOESY effects. Accordingly, in dichloromethane solution we tentatively assign a structural motif, **A,** to $[C_4C_1im]BF_4$ in which the BF_4^- anion straddles the imidazolium plane. We cannot exclude a structure in which the anion "floats" around the cation, but remains quite close.

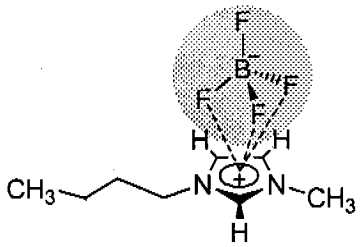

A

We note that, in deuterated methanol, the intensity of the imine proton (δ 8.4) slowly decreases due to slow exchange with the CD_3OD proton from the co-solvent and such exchange is well established[22].

Scheme 1 and table 1 shows ^1H chemical shift data and the self-diffusion coefficient values, D, for the cations (via ^1H) and anions (via ^{19}F) in the neat ionic liquids, $[C_4C_1im]BF_4$, $[C_4C_1im]PF_6$, and $[C_4C_1im][N(OTf)_2]$ as well as the diffusion data arising (primarily) from dilution of $[C_4C_1im]BF_4$ in either CD_3OD or CD_2Cl_2. The measured D-values for the neat ionic liquid $[C_4C_1im]BF_4$, 0.158 and 0.146, for the cation and anion, respectively, are similar and relatively small. The diffusion constants for the neat $[C_4C_1im][N(OTf)_2]$ salt, 0.282 and 0.216, for the cation and anion, respectively, are again, relatively small, but somewhat different. We suggest that these small D-values arise from the relatively large measured viscosities of these ionic liquids [23].

Scheme 1 (Proton chemical shifts, in ppm for the neat IL as BF_4 salt)

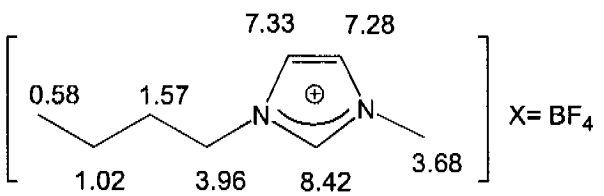

Table 1. PGSE Data for the ionic liquids.

Salt			D [d]	r_H(Å)[b]	η (cp)
1. X = BF_4	neat	Cation	0.158	1.34	104.0
		Anion	0.146	1.45	
2. (0.55ml)	CD_3OD	Cation	1.108	0.32 (0.48)	62.3
	(0.05ml)	Anion	1.340	0.26 (0.39)	
3. (0.1ml)	CD_3OD	Cation	7.441	3.4 (5.0)	0.88
	(0.5ml)	Anion	8.550	2.9 (4.4)	
4. (0.01ml)	CD_3OD	Cation	11.379	3.0 (4.4)	0.65
	(0.59ml)	Anion	13.189	2.6 (3.8)	
5. (0.55ml)	CD_2Cl_2	Cation	0.698	0.43 (0.7)	72.8
	(0.05ml)	Anion	0.770	0.39 (0.6)	
6. (0.1ml)	CD_2Cl_2	Cation	5.814	4.0 (6.0)	0.94
	(0.5ml)	Anion	5.965	3.9 (5.9)	
7. (0.01ml)	CD_2Cl_2	Cation	8.957	4.6 (6.9)	0.53
	(0.59ml)	Anion	9.042	4.6 (6.9)	
8. X = PF_6	neat	Cation	0.071	0.95	326.0
		Anion	0.054	1.25	
9. (0.1ml)	CD_3OD	Cation	7.535	3.2 (4.9)	0.90
	(0.5ml)	Anion	8.105	3.0 (4.5)	
10. X = $(CF_3SO)_2N$	neat	Cation	0.282	1.3	58.8
		Anion	0.216	1.7	
11. (0.55ml)	CD_2Cl_2	Cation	0.472	1.6(2.4)	29.7
	(0.05ml)	Anion	0.381	1.9(2.9)	
12. (0.55ml)[c]	CD_2Cl_2+ CH_2Cl_2	Cation	0.638		
	(0.05ml) (0.05ml)	Anion	0.493		
13. (0.1ml)	CD_2Cl_2	Cation	6.07	3.1(4.6)	1.17
	(0.5ml)	Anion	6.23	3.0(4.5)	
14. (0.55ml)	CD_3OD	Cation	0.392	1.7(2.6)	32.1
	(0.05ml)	Anion	0.304	2.3(3.4)	

[b] The r_H value in parenthesis was calculated using a factor of 4 (not 6) in the Stokes-Einstein relation. [c] CH_2Cl_2 D value = 3.02; one observes a HOESY contact to the CH_2Cl_2.[d] D values (x 10^{-10} m^2s^{-1})

It is known from the PGSE literature[18, 24-28] that methanol successfully solvates the ions of many salts, and that for BF_4^-, a typical hydrodynamic radius (as calculated from the Stokes-Einstein

equation) would be ca 2.6 Å. Addition of methanol as a co-solvent, results in a marked increase in the D-values (partially due to decreasing viscosity), until, at a ca 1:5 volume ratio the D (and hydrodynamic radius, r_H)-values of the cation, and anion, correspond to a more or less completely solvated salt[18, 19, 27, 29, 30]. Further dilution seems to have only a minimal effect on the sizes of the solvated ionic fragments.

For $[C_4C_1im]BF_4$ and $[C_4C_1im][N(OTf)_2]$ the addition of dichloromethane as solvent results in a modified picture. At a 1:5 volume ratio the D (and, r_H)-values of the cation, and anion are almost identical and this situation corresponds to strong ion pairing, in keeping with the data from the Overhauser spectroscopy, noted above. Obviously, the two solvents, methanol and dichloromethane, affect the ionic liquid differently.

We note that entries 1, 2, 5, 8, 10 and 11 afford unrealistic r_H values. We believe that traces of impurities, due to sample handling and preparation, (mostly water) acquired before the NMR experiments, but after the viscosity measurements, affect the viscosity of the mixtures, and thus the calculated r_H values[31].

Summarizing, the HOESY results reveal that, contrary to results from X-ray crystallography[20, 21], the anion does not occupy a specific position in this salt. Moreover, in dichloromethane, where the PGSE data show almost complete ion pairing, there are strong, non-selective NOE contacts between the cation and anion. This eliminates hydrogen bonding as the primary source of the interaction between the cation and anion, as this would lead to selectivity in the HOESY contacts. These NMR data provide a new

picture of both the structure of this salt and the function of the co-solvent.

Two additional important implications may be derived from this study. First, the absence of selective contacts might find its expression in the often unexpectedly low melting points of ionic liquids. If on the one hand (diffuse) charge attraction is the dominant factor, but on the other hand, anions and cations cannot form a close packed structure due to their different size and shape, the crystallization energy will remain relatively low. Second, biphasic catalysis often suffers from slower reaction rates due to mass transfer limitations. As shown above, one needs only a relatively small amount of co-solvent to dramatically reduce potential aggregation within the ionic liquid. This might find its expression in significantly higher reaction rates.

Bibliography

[1] J. Dupont, R. F. de Souza and P. A. Z. Suarez, *Chem. Revs.* **2002**, *102*, 3667-3691.

[2] P. J. Dyson, *Applied Organometallic Chemistry* **2002**, *16*, 495-500.

[3] M. Picquet, D. Poinsot, S. Stutzmann, I. Tkatchenko, I. Tommasi, P. Wasserscheid and J. Zimmermann, *Topics in Catalysis* **2004**, *29*, 139-143.

[4] C. E. Song, *Chem Commun.* **2004**, 1033-1043.

[5] Z. Li and C. G. Xia, *J. Mol. Catal. A-Chem.* **2004**, *214*, 95-101.

[6] D. B. Zhao, Z. F. Fei, T. J. Geldbach, R. Scopelliti and P. J. Dyson, *J. Am.Chem. Soc.* **2004**, *126*, 15876-15882.

[7] C. Daguenet and P. J. Dyson, *Organometallics* **2004**, *23*, 6080-6083.

[8] P. Wasserscheid and T. Welton, *Ionic Liquids in Synthesis*, Wiley-VCH, Weinheim, **2002**, p.

[9] K. S. Kim, B. K. Shin and H. Lee, *Korean Journal of Chemical Engineering* **2004**, *21*, 1010-1014.

[10] P. J. Dyson, J. S. McIndoe and D. B. Zhao, *Chem. Commun.* **2003**, 508-509.

[11] S. Dorbritz, W. Ruth and U. Kragl, *Advanced Synthesis & Catalysis* **2005**, *347*, 1273-1279.

[12] A. Macchioni, *Chem. Revs.* **2005**, *105*, 2039-2073.

[13] W. S. Price, *Concepts Magn. Resonance* **1997**, *9*, 299-336.

[14] W. S. Price, *Concepts Magn. Resonance* **1998**, *10*, 197-237.

[15] J. F. Huang, P. Y. Chen, I. W. Sun and S. P. Wang, *Spectroscopy Letters* **2001**, *34*, 591-603.

[16] A. Noda, K. Hayamizu and M. Watanabe, *J. Phys. Chem. B* **2001**, *105*, 4603-4610.

[17] P. S. Pregosin, P. G. A. Kumar and I. Fernandez, *Chem. Revs.* **2005**, *105*, 2977-2998.

[18] M. Valentini, H. Ruegger and P. S. Pregosin, *Helv. Chim. Acta* **2001**, *84*, 2833-2853.

[19] D. Nama, P. G. Anil Kumar and P. S. Pregosin, *Magn. Reson. Chem.* **2005**, *43*, 246.250.

[20] S. Saha, S. Hayashi, A. Kobayashi and H. Hamaguchi, *Chem. Lett.* **2003**, *32*, 740-741.

[21] P. Kolle and R. Dronskowski, *Inorg. Chem. Commun.* **2004**, *43*, 2803-2809.

[22] S. A. Katsyuba, P. J. Dyson, E. E. Vandyukova, A. V. Chernova and A. Vidis, *Helv. Chim. Acta* **2004**, *87*, 2556-2565.

[23] M. L. Connolly, *J. Mol. Graphics* **1993**, *11*.

[24] J. M. Goicoechea, M. F. Mahon, M. K. Whittlesey, P. G. A. Kumar and P. S. Pregosin, *Dalton Transactions* **2005**, 588-597.

[25] A. Macchioni, *Eur. J.Inorg. Chem.* **2003**, 195-205.

[26] P. G. A. Kumar, P. S. Pregosin, M. Vallet, G. Bernardinelli, R. F. Jazzar, F. Viton and E. P. Kundig, *Organometallics* **2004**, *23*, 5410-5418.

[27] E. Martinez-Viviente, H. Ruegger, P. S. Pregosin and J. Lopez-Serrano, *Organometallics* **2002**, *21*, 5841-5846.

[28] D. Zuccaccia, S. Sabatini, G. Bellachiom, G. Cardaci, E. Clot and A. Macchioni, *Inorg. Chem.* **2003**, *42*, 5465-5467.

[29] P. S. Pregosin, E. Martinez-Viviente and P. G. A. Kumar, *Dalton Transactions* **2003**, 4007-4014.

[30] E. Martinez-Viviente and P. S. Pregosin, *Inorg. Chem.* **2003**, *42*, 2209-2214.

[31] J. A. Widegren, A. Laesecke and J. W. Magee, *Chem. Commun.* **2005**, 1610-1612.

Curriculum Vitae

Devendra Babu Nama

I was born in Chintaparthy, Andhra Pradesh (India) on 05th of October 1977. I had my primary, secondary and pre university education during the period 1983-1995.

06/95 - 06/98	B.Sc degree in Physics, Chemistry and Maths P.E.S College, Bangalore University, India.
07/98 - 06/00	M.Sc degree in Inorganic Chemistry Central College, Bangalore University, India.
07/00 - 08/01	Analytical Chemist Shiva Analytical (INDIA) Ltd, Bangalore, India
09/01 - 10/02	NMR Project Assistant S.I.F department, IISc, Bangalore, India
11/02 - 03/04	Science Associate Aurigene Discovery Technologies Ltd, Bangalore, India
04/04 - 04/07	Ph.D thesis at the ETH Zurich, Switzerland under the supervision of Professor Paul S. Pregosin on *"Synthesis, PGSE Diffusion and Multidimensional NMR Studies on Transition Metal Organometallic Species: Applications in Coordination Chemistry and Homogeneous Catalysis."*